Exergy and Exergoeconomic Analyses and Optimization of Thermal Management Systems in Electric and Hybrid Electric Vehicles

By

HALIL S. HAMUT

A Thesis Submitted in Partial Fulfillment
of the Requirements for the degree of Doctor of Philosophy
in
Mechanical Engineering

Faculty of Engineering and Applied Science
University of Ontario Institute of Technology

Oshawa, Ontario, Canada, 2012

Exergy and Exergoeconomic Analyses and Optimization of Thermal Management Systems in Electric and Hybrid Electric Vehicles

By

HALIL S. HAMUT

Supervisory Committee

1. **Dr. Ibrahim Dincer**, Supervisor (Faculty of Engineering and Applied Science, University of Ontario Institute of Technology)

2. **Dr. Greg Naterer**, Co-supervisor (Faculty of Engineering and Applied Science, University of Ontario Institute of Technology, Faculty of Engineering and Applied Science, Memorial University of Newfoundland)

3. **Dr. Yuping He**, Associate Professor (Faculty of Engineering and Applied Science, University of Ontario Institute of Technology)

4**. Dr. Martin Angelin-Chaab**, Assistant Professor (Faculty of Engineering and Applied Science, University of Ontario Institute of Technology)

5. **Dr. Pietro-Luciano Buono**, University Examiner (Faculty of Science, University of Ontario Institute of Technology)

6. **Dr. Alan S. Fung**, External Examiner (Faculty of Engineering and Architectural Science, Ryerson University)

7. **Dr. Ali Grami**, Chair (Faculty of Engineering and Applied Science, University of Ontario Institute of Technology)

Abstract

With the recent improvements in battery technologies, in terms of energy density, cost and size, the electric (EV) and hybrid electric vehicle (HEV) technologies have shown that they can compete with conventional vehicles in many areas. Although EVs and HEVs offer potential solutions for many key issues related to conventional vehicles, they still face considerable challenges that prevent the widespread commercialization of these technologies, such as thermal management of batteries and electrification.

In this PhD thesis, a liquid thermal management system (TMS) for hybrid electric vehicles is investigated and evaluated against alternative thermal management systems, and optimal parameters are selected to maximize the system efficiency. In order to achieve this goal, a model of the liquid thermal management system is established to determine the irreversibilities and second-law efficiencies associated with the overall system and its components. Furthermore, the effects of different configurations, refrigerants and operating conditions are analyzed with respect to conventional exergy analyses. In addition, advanced exergy analyses are also conducted in order to better identify critical relationships between the TMS components and determine where the system improvement efforts should be concentrated. Moreover, investment costs are calculated and cost formation of the system is developed in order to evaluate the TMS with respect to exergoeconomic principles and provide corresponding recommendations. Environmental impact correlations are developed, along with a cradle-to-grave life cycle assessment (LCA), to highlight components causing significant environmental impact, and to suggest trends and possibilities for improvement based on the exergoenvironmental variables. Finally, the TMS is optimized using multi-objective evolutionary algorithm which considers exergetic and exergoeconomic as well as exergetic and exergoenvironmental objectives simultaneously with respect to the decision variables and constraints.

Based on the conducted research for the studied system under the baseline conditions, the exergy efficiency, total cost rate and environmental impact rate are determined to be 0.29, ¢28/h and 77.3 mPts/h, respectively. The exergy destruction associated with each component is split into endogenous/exogenous and avoidable/unavoidable parts, where the exogenous exergy destruction is determined to be relatively small but significant portion of the total exergy

destruction in each component (up to 40%), indicating a moderate level of interdependencies among the components of the TMS. Furthermore, it is determined that up to 70% of the exergy destruction calculated within the components could potentially be avoided.

According to the analyses, electric battery is determined to have the highest exergoeconomic and exergoenvironmental importance in the system, with cost rate of ¢3.5/h and environmental impact value of 37.72 mPts/h, due to the high production cost of lithium ion batteries and the use of copper and gold in the battery pack. From an exergoeconomic viewpoint, it is determined that the investment costs of the condenser and evaporator should be reduced to improve the cost-effectiveness of the system. On the other hand, from an exergoenvironmental viewpoint, all the component efficiencies (except for the battery) should be improved in order to reduce the total environmental impact even if it increases the environmental impact during production of the components. In addition, it is determined that the coolant pump and the thermal expansion valve before the chiller are relatively insignificant from exergoeconomic and exergoenvironmental perspectives.

Subsequently, objective functions are defined and decision variables are selected, along with their respective system constraints, in order to conduct single and multiple objective optimizations for the system. Based on the single objective optimizations, it is determined that the exergy efficiency could be increased by up to 27% using exergy-based optimization, the cost can be reduced by up to 10% using cost-based optimization and the environmental impact can be reduced by up to 19% using environmental impact-based optimization, at the expense of the non-optimized objectives.

Moreover, multi-objective optimizations are conducted in order to provide the respective Pareto optimal curve for the system and to identify the necessary trade-offs within the optimized objectives. Based on the exergoeconomic optimization, it is concluded that 14% higher exergy efficiency and 5% lower cost can be achieved, compared to baseline parameters at an expense of 14% increase in the environmental impact. Furthermore, based on the exergoenvironmental optimization, 13% higher exergy efficiency and 5% lower environmental impact can be achieved at the expense of 27% increase in the total cost.

Acknowledgements

I would like to express my deep and sincere gratitude to my supervisors, Dr. Ibrahim Dincer and Dr. Greg Naterer, for their resourceful guidance and never-ending support.

I would like to thank all my committee members, Dr. Yuping He, Dr. Martin Angelin-Chaab, Dr. Pietro-Luciano Buono, Dr. Alan S. Fung and Dr. Ali Grami for their valuable time in reading and providing their comments to improve the content of my thesis. I also would like to thank Dr. Greg Rohrauer for providing me with the direction and help I needed to undertake this project. In addition, I would like to thank General Motors for providing the opportunity that made this research possible, especially Mike Kobylecky, who was extremely helpful and supportive throughout the project.

Moreover, I would like to thank my friends, Nader Javani, Ahmet Ozbilen, Mehmet Kursat Cohce, Hadi Ganjeie, Mehdi Hosseini, Pouria Ahmadi and Stephen Petryna for their support throughout my time in the University.

Furthermore, the financial support from Automotive Partnerships Canada and the Natural Sciences and Engineering Research Council of Canada is gratefully acknowledged.

Last but not least, I would like to thank my parents Huseyin and Zuhal Hamut and my sisters Ebru Hamut and Deniz Ongun for their understanding and encouragement throughout my education.

Table of Contents

List of Tables

List of Figures

Nomenclature

A	area (m^2)
$\dot{B}$	environmental impact rate (mPoints/s)
c	cost per unit of exergy ($/kJ)
$\dot{C}$	cost rate associated with exergy ($/h)
C	specific heat capacity (J/kgK)
C_{CO_2}	imposed cost of carbon dioxide per year ($/year)
C_p	specific heat capacity (J/kgK)
C_{pump}	pump coefficient
C_{txv}	valve flow coefficient
D	diameter (m)
en	specific energy (kJ/kg)
ex	specific exergy (kJ/kg)
$\dot{E}n$	energy rate (kW)
$\dot{E}x$	exergy rate (kW)
f	friction factor
f_b	exergoenvironmental factor
f_k	exergoeconomic factor
f_k^*	advanced exergoeconomic factor
h	specific enthalpy (kJ/kg)
$\bar{h}$	heat transfer coefficient (W/m^2K)
i	interest rate
I	current (A)
k	thermal conductivity (W/m^oC)
k_A	TXV characteristic parameter
K	energy storage capacity (kW)
$\dot{m}$	mass flow rate (kg/s or L/min)
N	annual number of operation hours (h)

P	pressure (kPa)
Pr	Prandtl number
$\dot{Q}$	heat transfer rate (kW)
r_b	relative difference of exergy-related environmental impacts
r_k	relative difference of exergy-related cost
R	resistance (mΩ)
Ra	Rayleigh Number
Re	Reynolds number
s	specific entropy (kJ/kgK)
t	time (s)
T	temperature (K or ºC)
U	overall heat transfer coefficient (W/m^{2}K)
$\dot{W}$	work rate or power (kW)
x_{CO_2}	amount of carbon dioxide released per year (tCO_2/year)
V	velocity (m/s)
v	specific volume (m^3/kg)
$\dot{Y}$	component-related environmental impact rate associated with LCA (mPoints/h)
ε	exergy destruction ratio (%)
Z	height (m)
$\dot{Z}$	cost rate associated with the sum of capital investment ($/h)

Greek letters

β	coefficient of thermal expansion (1/ºC)
Δ	change in variable
δ	thickness (m)
ε	effectiveness
η	efficiency
η_o	finned heat transfer surface efficiency
θ	pressure ratio
μ	dynamic viscosity (kg/ms)

ρ	density (kg/m^3)
φ	maintenance factor
γ	specific heat ratio

Superscripts

AV	avoidable
EN	endogenous
EX	exogenous
n	equipment lifetime (years)
UN	unavoidable

Subscripts

0	ambient
act	actual
b, bat	battery
$comp$	compressor
$cool$	coolant
$chil$	chiller
$comp$	compressor
$ctxv$	thermal expansion valve before chiller
$c, cond$	condenser
cool	coolant
$crit$	critical
D	destruction
dis	discharge
e	exit
$elect$	electricity
en	energy
$etxv$	thermal expansion valve before evaporator
ex	exergy
$evap$	evaporator

f	final
F	fuel
g	gas
gen	generation
H	high
i, in	in
k	component
L	low
max	maximum
min	minimum
o, out	outlet or outside
P	product
q	heat
ref	refrigerant
s	isentopic
sc	subcooling
sh	superheating
tot	total
txv	thermal expansion valve
w	work
wg	water/glycol mix

Acronyms

AACS	automotive air conditioning system
BMS	battery management system
CAN	controller area network
CD	charge depleting
CFC	choloro-fluoro-carbon
CHCM	coolant heating control module
COP	coefficients of performance
CRF	capital recovery factor

CS	charge sustaining
CV	conventional vehicle
DME	dimethyl ether
DOD	depth of discharge
EA	evolutionary algorithm
EES	engineering equation solver
EV	electric vehicle
EXCEM	exergy, cost, energy, mass
GA	generic algorithm
GHG	greenhouse gases
GWP	global warming potential
HEV	hybrid electric vehicle
ICE	internal combustion engine
LCA	life cycle assessment
LINMAP	linear programming technique for multidimensional analysis of preference
LMTD	logarithmic mean temperature difference
NBP	normal boiling point
NTU	number of transfer units
ODP	ozone depleting potential
PCM	phase change material
PHEV	plug-in hybrid electric vehicle
SOC	state of charge
TMS	thermal management system
TPIM	traction power inventor module
TRR	total revenue requirement
TXV	thermal expansion valve
VOC	volatile organic compound

Chapter 1: Introduction

1.1 Energy Aspects

Energy is used in all aspects of life and makes the existence of ecosystems, human civilization and life itself possible. Thus, energy related issues are one of the most important problems we face in the 21th century. With the advent of industrialization and globalization, the demand for energy has increased exponentially over the past decades. Especially with a population growth of faster than 2% in most countries, along with improvements on lifestyles that are linked to energy demand, the need for energy is ever increasing (Dincer, 2000). Based on the current global energy consumption pattern, it is predicted that the world energy consumption will increase by over 50% before 2030 (Toklu et al., 2010; Sugathi and Samuel, 2012). Thus, based on this pervasive use of global energy resources, energy sustainability is becoming a global necessity and is directly linked to the broader concept of sustainability and affects most of the civilization (Rosen, 2009).

Currently, the world relies heavily on fossil fuels, such as oil, gas and coal which provide almost 80% of the global energy demands, to meet its energy requirements. It is estimated that most of large scale energy production and consumption of energy causes degradation of the environment as they are generated from these sources. Climatic changes driven by human activities (especially greenhouse gas emissions) have significant direct negative effects on the environment and contribute over 160,000 deaths per year from side-effects associated with climate change which is estimated to double by 2020 (Asif and Muneer, 2007). Moreover, the nominal price of retail gasoline have increased approximately five times between the years of 1949 and 2005 (Shafiee and Topal, 2006).

These aforementioned reasons lead people into looking for more efficient, cheaper and ecofriendly options for energy usage. As transportation sector being a major contributor to this problem, several alternatives to conventional vehicles are developed which can be competitive in many aspects while being significantly more efficient and environmentally benign. Among those, electric and hybrid electric vehicles are one of the leading candidates to replace conventional vehicles in the future.

1.2 Motivation

Over the last few decades, concern over the dependence and ever-increasing prices of imported oil as well as environmental pollution and global warming have led to active research on vehicles with alternative energy sources. Today, approximately 15 million barrels of crude oil is used in the United States (US) per day (EPA, 2008). About 50% of this crude oil is used in the transportation sector, a sector where 95% of the energy supply comes from liquid fossil fuels (Kristoffersen et al., 2011). Moreover, the increasing demand and relatively static supply for petroleum and stricter pollutant regulations have caused an increase and instability in crude oil prices, where the retail gasoline nominal price increased approximately five times between the years of 1949 and 2005 (Shafiee and Topal, 2006). Furthermore, since the majority of the crude oil reserves are located in a few countries, some of which have highly volatile political and social situations, it presents a problem for diversified energy supply and potential cause for political conflict (DOE, 2009). In addition, the conventional vehicles using these fossil fuels cause excessive atmospheric concentrations of greenhouse gasses (GHG), where the transportation sector is the largest contributor in the US with over a quarter of the total GHG emissions (Kristoffersen et al., 2011).

Fortunately, the electric vehicle (EV) and hybrid electric vehicle (HEV) technologies have improved significantly, due to recent enhancements in battery technology, and they now compete with conventional vehicles in many areas. They offer solutions to key issues related to today's conventional vehicles by diversification of energy resources, load equalization of power, improved sustainability, quite operation as well as lower operating costs and considerably lower emissions during operation (virtually zero emissions for EVs during operation) without significant extra costs (Chau and Wong, 2002). Especially with plug-in hybrid electric vehicles (PHEVs), it became possible to achieve further energy consumption and emission reductions as well as potential applications for performing ancillary services (such as vehicle to grid) by being able to draw and store energy from the electric grid and utilizing it in the most efficient operational modes for both the engine (high speed cruising) and the motor (low speed driving and acceleration) (Weiller, 2011; Diamond, 2008). These vehicles in all-electric range can reduce the gasoline consumption by more than one half and reduce the environmental impact up to 75% based on the electricity production mix used (EPRI, 2007).

Even though EVs and HEVs have considerable advantages, they still have certain shortcomings such as relatively long charging times, limited range, and lower efficiencies under extreme temperatures that prevent the widespread commercialization of these vehicles. When the current EV and HEV technology is examined, the main difficulty comes from achieving the most ideal battery performance which is inherently linked to determining the most compatible batteries for corresponding applications and reducing the discrepancy between the optimum and operating conditions of the selected batteries. Since the battery characteristics, performance and efficiency directly affect the vehicle performance, reliability, safety and life cycle cost (Pesaran et al., 2003), considerable attention needs to be given to selecting the appropriate battery technology and keeping it at ideal conditions.

Although no battery technology would meet all the needs of the vehicles, certain trade-offs need to be made to optimize the vehicle performance. The selected battery technology should be able to provide sufficient energy for acceleration in various operating and ambient conditions, operate over long periods of time, have a low cost and be environmentally friendly as well as being lightweight and charging fast. Currently, only a limited number of battery technologies, such as lead-acid (Pb-acid), nickel-cadmium (NiCd), nickel-metal hydride (NiMH) and lithium ion (Li-ion) are good candidates for electric and hybrid electric vehicles.

In order to achieve the most ideal battery performance, the discrepancy between the optimum and operating conditions of the batteries need to be reduced significantly by implementing thermal management systems (TMS) in EVs and HEVs. These systems are utilized to improve the battery efficiency, by keeping the battery temperature at the ideal operating ranges, and prevent the electrochemical systems in the battery from freezing, which can reduce the power capability, as well as prevent them from overheating, which can lead to a reduction in charge/discharge capacity and premature aging of the battery (Noboru S., 2001; Pesaran et al., 2009; Kuper et al., 2009). Moreover, TMSs are also responsible for preventing temperature non-uniformity among the cells in the battery pack, which leads to thermal runaway that can have catastrophic outcomes. Based on the battery characteristics, vehicle applications, drive cycle, size and weight limitations and cost along with environmental impact, several types of TMSs are currently used in EVs and HEVs. These thermal management systems vary in their objectives

(cooling vs. cooling and heating), method, (passive vs. active), heat transfer medium (air vs. liquid) and application (series vs. parallel or direct vs. indirect). Moreover, alternative TMSs such as phase change materials are also having a significant role in the future of thermal management systems.

In the EV and HEV thermal management systems, the system should be designed in order to have high performance and operate as efficiently as possible for given economic limitations and environmental restrictions under a wide range of operating conditions. Designing of these TMSs are normally performed by conventional methods based on experimental data and practical experience (Selbaş et al, 2006). Thus, most of these systems are often operating outside of their optimum parameters which result in inefficient use of resources, increasing production costs and adverse environmental impact. Therefore, EV and HEV thermal management systems should be analyzed in a systematic way in order to improve the system efficiency, reduce investment and operating costs and corresponding environmental impact.

1.3 Scope of Research and Objectives

Today EVs and HEVs offer solutions for many key issues related to conventional vehicles, however they still face considerable challenges that prevent the widespread commercialization of these technologies. Among these, batteries have a significant role, since the vehicle performance, range, cost and safety are highly linked to the battery characteristics and efficiency. Currently, the most important battery issues are related to battery efficiency as well as temperature distribution and uniformity of the battery packs.

In the absence of any thermal management, the cells in the battery pack can heat beyond efficient temperature ranges, decreasing the charge/discharge capacity and cycle life and even cause prematurely failure by thermal runaway. Moreover, among the analyzed TMSs, cabin air and refrigerant based systems are usually either insufficient or uneconomical for removing the battery heat or providing cabin cooling under demanding drive cycles and severe ambient conditions. Thus, a more effective TMS is needed in order to limit the temperature range and non-uniformity in the battery packs and provide sufficient cooling into the cabin. Liquid thermal management systems (refrigerant and coolant) can successfully reduce the discrepancy between

the optimum and operating conditions of the batteries by having a higher heat capacity and thermal conductivity than air and refrigerant based TMSs. Moreover, they tend to have high efficiencies and low operating costs. However, even though these systems have significant advantages over the compared TMSs, they still have certain shortcomings that reduce the overall performance and efficiency of the system which needs to be studied extensively.

Currently, there is no study in the literature that examines the thermal management system of an electric or hybrid electric vehicle based on a second-law analysis. Thus, in this PhD thesis, a new analysis was conducted on the HEV liquid thermal management system in order to determine the efficiency, cost and environmental impact of the system and its associated components with the use of a second-law analysis, investigate the areas of irreversibilities and their corresponding effects, and recommend ways to improve and optimize the overall thermal management performance based on thermodynamic, economic and environmental criteria.

These analyses were conducted using Engineering Equation Solver (EES) software package to determine the properties of the associated refrigerant and coolant at each stage. The performance of each component will be determined and evaluated under various parameters and operating conditions and the outputs will be used to guide the experiments in the thermal management system test bench. In addition, the results will be compared against the original baseline liquid thermal management system to show the improvements achieved by the modifications.

This PhD thesis consists of four main objectives as follows:

1. To develop a mathematical model of the TMS, conduct associated exergy analysis, and comment on its significance and potential challenges on the baseline system.
    - To determine the properties of the refrigerant and coolant medium in each stage of the TMS.
    - To calculate the energy and exergy efficiencies of the system under current configurations.
    - To use numerical analysis in order to improve the computational model.

- To conduct advanced exergy analysis along with exergoeconomic and exergoenvironmental analyses of the system.

2. To correlate and verify the model through experimental studies with the HEV thermal management test bench setup.
    - To have a thermal management test bench in fully operational condition.
    - To place all the sensors and gages on the test bench and obtain experimental data for the analysis.
    - To conduct various studies on the bench in order to gain a better understanding of the key variables of the system and it associated components.
    - To predict the output parameters and system efficiency using the TMS model.
3. To conduct various experimental studies based on different operating parameters and make recommendations using the model as a predictive tool.
    - To use the computational models and software analysis in order to guide the experimental parameters.
    - To conduct parametric studies using the model and the test bench based on various inputs.
    - To optimize the system parameters and make recommendations with respect to:
        - Exergy analysis to improve the system efficiency;
        - Exergoeconomic analysis to reduce the associated cost;
        - Exergoenvironmental analysis to reduce the environmental impact.
    - To compare the exergy efficiency results with cabin air and refrigerant based TMSs models as well as baseline liquid thermal management systems.
4. To compile source codes of the model and prepare a vehicle level experimentation
    - To fully instrument the production vehicle for experimentations and perform a vehicle level experimentation based on the conducted analysis.
    - To provide software source codes with a user friendly capability of altering the inputs and operating parameters.

1.4 Summary of Approach and Rationale

In this research, the effects of liquid thermal management systems in hybrid electric vehicles (using Li-ion batteries) are analyzed and areas of inefficiencies; their magnitude, causes and locations are determined; methods of improvements are suggested in order to reduce the energy requirement of the system, and/or increase the associated performance with respect to conventional exergy analysis. In addition, and advanced exergy analysis is also conducted where the exergy destruction is split into endogenous/exogenous and avoidable/unavoidable parts in order to advance our understanding of the interactions among the TMS components, establish priorities on which components should be improved first and assist in further optimization of the overall system.

Moreover, investment and exergy destruction costs associated with the TMS are calculated and cost formation of the system is provided in order to evaluate the TMS with respect to exergoeconomic variables. Furthermore, an environmental analysis is also conducted using a cradle to grave life cycle assessment (with Eco-indicator 99) using Sima Pro 7 as well as by creating environmental impact correlations from the literature in order to point out the components causing the highest environmental impact and suggest possibilities and trends for improvement based on the exergoenvironmental variables. Finally, the TMS is optimized in Matlab using a multi-objective evolutionary algorithm which considers exergetic, exergoeconomic and exergoenvironmental objectives with respect to the decision variables and constraints. A Pareto frontier is obtained for the system and a single desirable optimal solution is selected based on a linear programming technique for multidimensional analysis of preference (LINMAP) decision making processes.

Furthermore, a TMS test bench is assembled and a production vehicle (Chevrolet Volt Gen 1) is fully instrumented in order to develop a vehicle level demonstration of the study. The experimental results are then used to validate the numerical model outcomes. Finally, conclusions and recommendations are provided based on the conducted research.

1.5 Thesis Outline

This thesis is organized in 7 chapters as described below;

Chapter 2 presents an introduction associated with current energy problems, their ties to conventional vehicles and identification of alternative technologies to mitigate the problem introduced.

Chapter 3 provides a literature review on the electric and hybrid electric vehicles and battery technologies as well as their proposed thermal management systems and provides information on all the exergy analyses conducted on various TMS applications along with key gaps on the current state of knowledge.

Chapter 4 illustrates the experimental setup and instrumentation of the test bench and production vehicle along with the descriptions of tools and methods used to gather data as well as brief explanations of the provided outputs.

Chapter 5 describes the studied thermal management system layout and the conducted energy and exergy analyses as well as exergoeconomic and exergoenvironmental analyses in the system along with the associated multi-objective optimization.

Chapter 6 presents the numerical results based on the developed models and the conducted analyses on the system and their verification through the simulation outputs and experimental results.

Chapter 7 summarizes the conclusions and provides recommendations for future research.

Chapter 2: Background

2.2 Electric and Hybrid Electric Vehicles

Electric and hybrid electric vehicles have significant advantages over conventional vehicles in terms of energy efficiency, energy source options and corresponding environmental impact. Electric vehicles can be powered either directly from an external power station, or through stored electricity (that is acquired originally from an external power source), and by an on-board electrical generator, such as an engine (in HEVs) (Faiz et al., 1996). Pure electric vehicles have the advantage of having full capacity withdrawn at each cycle, but they have a limited range. HEVs on the other hand, have significantly higher ranges, as well as the option of operating in electric only mode, and therefore they will be the main focus of the analysis.

Hybrid electric vehicles take advantage of having two discrete power sources; usually primary being the heat engine (such as diesel or turbine, or a small scale ICE) and the auxiliary power source is usually a battery. Their drivetrains are generally more fuel efficient than conventional vehicles since the auxiliary source either shares the power output allowing the engine to operate mostly under efficient conditions such as high power for acceleration and battery recharging (dual mode), or the auxiliary sources furnish and absorb high and short bursts of current on demand (power assist). Moreover, in both architectures, the current is drawn from the power source for acceleration and hill-climbing, and the energy from braking is charged back into the HEV battery for reuse which increases the overall efficiency of the HEVs (Nelson, 2000). In plug-in hybrid electric vehicles (PHEVs), the power can also be drawn from the grid instead of the use of the fossil fuels alone. Since the vehicle has an alternative energy unit and a battery that can be charged from the grid, the mass of the battery is significantly smaller than EVs, thus enabling the PHEVs to operate more efficiently in electric-only mode (due to the reduction in power required to propel the vehicle) than similar EVs (Doucette and McCulloch, 2011). PHEV chargers must be light-weight, compact and highly efficient in order to maximize the effectiveness of the electric energy from the grid. They are designed to use either inductive or conductive chargers. Inductive chargers have preexisting infrastructure and are intrinsically safer. Conductive chargers are lighter, more compact and allow bidirectional power, thus achieve

higher efficiencies. By utilizing the stored multi-source electrical energy from the grid and stored chemical energy in the fuel tank together or separately, PHEVs can achieve even better driving performance, higher energy efficiencies, lower environmental impact and lower cost than conventional HEVs, mainly depending on the driving behavior and energy mix of the electricity generation (Bradley and Frank, 2009)

2.2.1 HEV Configurations

In all hybrid electric vehicles, the arrangement between the primary and secondary power sources can be categorized as parallel, series or split parallel/series configuration. The parallel and series hybrid vehicles configurations can be seen in Figure 2.1.

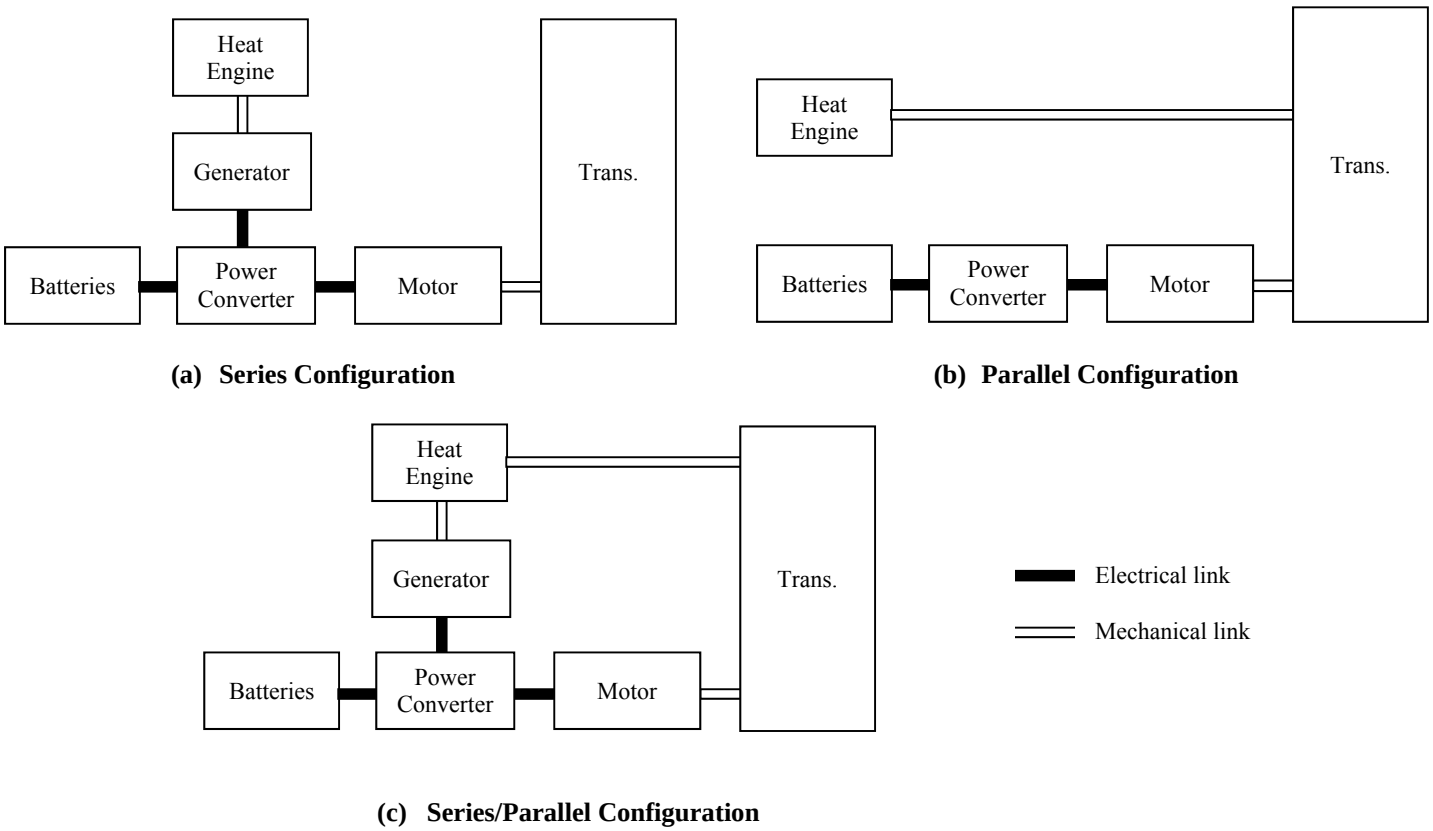

(a) Series Configuration

(b) Parallel Configuration

(c) Series/Parallel Configuration

Figure 2.1: Hybrid vehicles configurations in (a) Series, (b) Parallel and (c) Series/Parallel (adapted from Chau and Wong, 2002).

In a series configuration (such as GM Volt), the engine provides the electrical power through a generator to charge the battery and power the motor, where only the motor provides torque to the wheels. Conceptually, it is an engine-assisted EV which extends the driving range in order for it to be comparable with conventional vehicles (Chau and Wong, 2002). In this configuration, the output of the heat engine is converted to electrical energy that, along with the battery, powers the drivetrain. The main advantage of this configuration is the ability to size the engine for average rather than peak energy needs and therefore having it operate in its most efficient zone. Moreover, due to a relatively simplistic structure and the absence of clutches, it has the flexibility of locating the engine-generator set. On the other hand, relatively larger batteries and motors are needed to satisfy the peak power requirements and significant energy losses occur due to energy conversion from mechanical to electrical and back to mechanical again. In a parallel configuration (such as Honda Civic and Accord hybrids), both the engine and motor provide torque to the wheels, hence much more power and torque can be delivered to the vehicle's transmission. Conceptually, it is an electric assisted conventional vehicle for attaining lower emissions and fuel consumption. In this configuration, the engine shaft provides power directly to the drivetrain and the battery is parallel to the engine, providing additional power when there is an excess demand beyond the engine's capability. Since the engine provides torque to the wheels, the battery and motors can be sized smaller but the engine is not free to operate in its most efficient zone. In general, the initial configuration has worse fuel economy (due to power conversion) as well as cost (due to extra generator), but has a flexible component selection and lower emissions (due to the engine working more efficiently). Finally, in a split parallel/series powertrain (such as Toyota Prius), a planetary gear system power split device is used as well as a separate motor and generator in order to allow the engine to provide torque to the wheels and and/or charge the battery through the generator. This configuration has the benefits of both the parallel and series configurations in the expense of utilizing additional components (Nelson, 2000; Shiau, 2009; Yap and Karri, 2010). However, the advantages of each configuration are solely based on the ambient conditions, drive style and length, electricity production mix as well as the overall cost.

Unlike EVs that can have their full capacity withdrawn at each cycle, an HEV battery has a capacity draw that ranges around 10% of the nominal operating level (which is 50% state of

charge) in order to deal with charge/discharge current surges without going into overcharge above 75% and deep discharge below 25% state of charge (SOC). Thus, only half of the battery capacity is being used in HEVs (Gutmann, 2009). For this reason, after charging PHEVs through conventional electrical outlets, they operate in charge-depleting mode (CD-mode) as they drive until the battery is depleted to the target state of charge, which is generally around SOC of 35%. At this point, the vehicle switches to charge-sustaining mode (CS-mode) by utilizing the ICE engine to maintain the current SOC. PHEVs can be further categorized based on their functions in CS-mode. Range-extended PHEVs act as a pure EV in CD-mode using only the electric motor, whereas blended PHEVs use the electric motor primarily with the occasional help of the engine to provide additional power. Finally, after CS-mode, if the vehicle is still driving, it enters the engine-only mode where the operation of the electric traction system does not provide tractive power to the vehicle (Bradley and Frank, 2009).

2.2.2 HEV Emissions

EVs, conventional HEVs and PHEVs provide significant reduction in emissions compared to conventional vehicles (CVs) with ICEs, while having competitive pricing due to government incentives, increasing oil prices, and high carbon taxes combined with low-carbon electricity generation (Shiau et al, 2009). The emissions of CVs increase significantly for short distance travels due to the inefficiencies of the current emissions control systems during cold starting of the gasoline vehicles (Ross 1994). It is estimated that vehicles travelling fewer than 50 km per day are responsible for more than 60% of daily passenger vehicle kilometers travelled in the US (US Department of Transportation, 2001). Powering this distance with electricity would reduce gasoline use significantly and yield a considerable reduction of emissions. Even when traveling with the use of gasoline in HEVs and PHEVs, the efficiency of the ICE is significantly higher than the ICE of CVs. However, the reduction in fuel and emissions depends primarily on the energy generation mix used to produce the electricity. The balance of the 2006 US electricity mix is composed of coal (49%), nuclear (20%), natural gas (20%), hydroelectric (7%), renewable (3%) and other (1%) (EIA, 2008a). Therefore, for the US average GHG intensity of electricity, PHEVs can reduce the GHG emissions by 7-12% compared to HEVs. This reduction is negligible under high-carbon scenarios of electricity production and 30-47% under the low-

carbon scenarios. When PHEVs are compared against CVs, the reduction in GHG emissions is about 40% for the average scenarios, 32% for high cases and between 51-63% for low-carbon based scenarios (Samaras and Meisterling, 2008). The detailed life cycle GHG emissions (g CO_2-eq/km) for CVs, HEVs and PHEVs under various scenarios are shown in Figure 2.2. The number after PHEV (PHEV30 or PHEV90) represents the all-electric range of the vehicle in km.

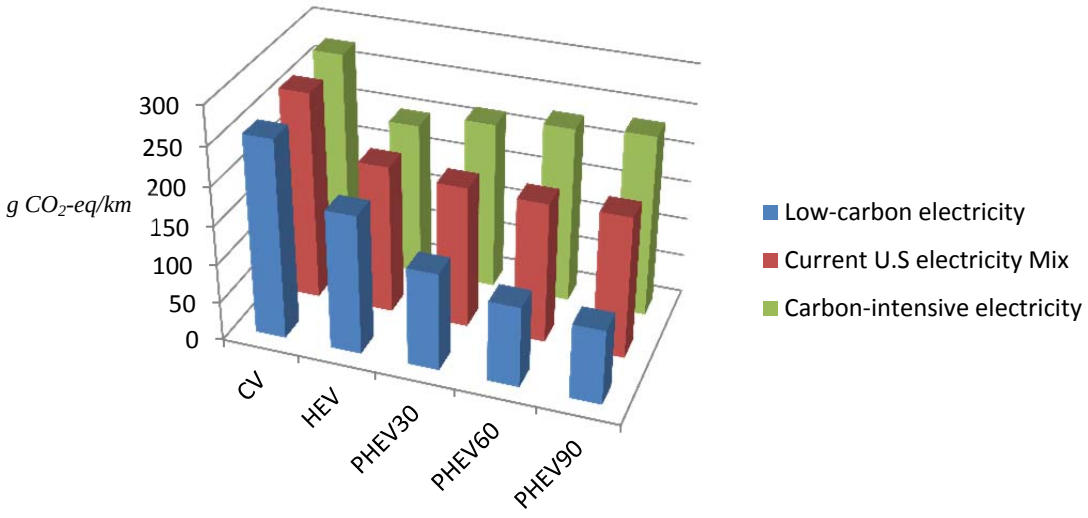

Figure 2.2: Life cycle GHG emissions sensitivity of CVs, HEVs, PHEV30 and PHEV90 under different carbon intensity scenarios (data taken from Samaras and Meisterling, 2008).

When the emissions for PHEVs are examined, the majority of emissions come from the operational stage as shown in Figure 2.2. A large portion is due to the gasoline used for traveling, followed by electricity used for traveling based on the carbon-intensity of the electricity generation source. When the emissions from the electric power increase significantly under a high-carbon scenario (coal-based generation capacity), the reduction in volatile organic compounds (VOCs) and CO are offset by a dramatic increase in SO_x and slight increase particulate emissions (PM10). However, the total GHG emissions are still lower compared to CVs since the increase in upstream emissions has a lower magnitude than the decrease in tailpipe emissions (Bradley and Frank, 2009). The GHGs associated with most battery materials and production generates a relatively small portion of the emissions and accounts for 2-5% of the life cycle emission from PHEVs (Samaras and Meisterling, 2008). Moreover, the GHG emissions from the vehicle end-of-life are not shown since they are relatively negligible (Schmidt et al.,

2004). The reduced fuel use and GHG emissions for PHEVs depend significantly on vehicle and battery characteristics, as well as the recharging frequency. Using PHEVs also has a significant impact on the operating costs of the vehicle. PHEVs in all-electric mode can reduce the gasoline consumption by half, by shifting 45-77% of the miles from gasoline to electricity, which would reduce the operating costs assuming the electricity cost per mile is significantly less than the gasoline cost (Yeh, 2009). Battery life also has a significant role on the cost associated with PHEVs since replacing the battery would increase the life cycle cost of a PHEV by between 33% and 84% (Wood and Bradley, 2011). However, the overall cost savings would be based on the overall cost of the vehicle, range and driving behavior, as well as economic incentives such as taxes on carbon emissions and gasoline.

Even though EVs and HEVs compete with conventional vehicles in terms of performance and cost with much less environmental impact, their benefits depend mainly on the battery technology utilized in these vehicles. Even though many battery technologies are currently being analyzed for EVs and HEVs, the main focus is mainly lead-acid, NiCd, NiMH and Li-ion battery technologies. Thus, in order to understand the effects of EVs and HEVs, further analysis is needed for these battery technologies based on various criteria.

2.3 Battery Technologies

Selection of the appropriate battery technology for the right application is crucial in EVs and HEVs. Even though no battery technology would meet all needs of the vehicle, trade-offs need to be made to optimize the battery utilization. Current battery technologies are evaluated based on their capacity to provide sufficient energy and power for acceleration under various operating and ambient conditions while being compact, long lasting, low cost and environmentally friendly. Today, only a limited number of battery technologies for electric and hybrid electric vehicles, such as lead-acid, NiCd, NiMH and Li-ion, are suitable based on these factors. Therefore, comparisons among these batteries are provided with respect to various criteria as shown in Table 2.1.

Table 2.1: Battery characteristics for today's most common battery technologies[1].

Battery	Specific Energy (Wh/kg)	Specific Power (W/kg)	Operating Temp. Range (ºC)	Cycle Life	Cost ($/kWh)	Environmental Impact[2] (mPts)
Pb-acid	30 – 40	80 – 300	-30 – 60	200-300	150	503
NiCd	50 – 60	200 – 500	-20 – 50	500	400 – 500	544
NiMH	60 – 70	200 – 1500	-20 – 50	500	500	491
Li-ion	60 – 150	800 – 2000	-20 – 55	1000	500 – 800	278

[1]Data taken from Nelson et al., 2002; Cooper and Moseley, 2009; Khateeb, 2004; Bossche, 2006; Conte 2006; Matheys et al., 2009.
[2]Based on eco-indicator 99.

2.3.1 Battery Performance Characteristics

The battery technologies to be analyzed have various performance characteristics based on the limitations of their chemical structure. Lead-acid battery technology is the oldest commercially available battery technology and significant progress has been made on the battery in terms of achieving higher performance. However, although lead-acid batteries have good energy-power balance, they have the lowest specific energy and power among the analyzed batteries. Even though this is suitable for providing energy for smaller devices (such as laptops), it requires significant extra mass for EVs and HEVs. NiCd batteries have adequate specific power and good specific energy (still significantly larger than lead-acid batteries) and very good low temperature performance (Nelson, 2000). NiMH has good power capability but lower specific energy than Li-ion. Even though it does not excel in any of the performance characteristics, it does not have any major weaknesses either. Finally, Li-ion has the highest energy density among the compared batteries making it highly compatible with EVs and HEVs without increasing the overall mass of the vehicle significantly (Patil, 2008).

When the operating temperature ranges for the battery technologies are analyzed, lead-acid has very good high temperature operation, but the electrolytes would freeze when operated at low temperatures at 50% state of charge level. The battery can be brought to a full state of charge at the expense of reduced battery life. For NiCd and NiMH, discharge performance at the lower limit would be poor. At the upper limit, the charge acceptance is minimal and can suffer permanent capacity loss when fully discharged at high temperatures. Li-ion cannot operate at low temperatures (below -20ºC) due to significant reduction in cell conductivity as a result of freezing of the electrolytes. It can operate up to 45ºC with significant efficiency, after which

electrolytes may become unstable, resulting in an exothermic electrolyte oxidation which can lead to thermal runaway (Tichy, 2009).

Based on cycle life, lead acid batteries have the lowest longevity among the compared battery technologies with 200-300 cycles when cycled to 80% of initial capacity. It is followed by NiCd and NiMH with up to 500 cycles and Li-ion where 1,000+ cycles can be achieved. However, the lifecycle assessments of these batteries are relative to their tested conditions since they mainly depend on the operating state of charge (SOC), depth of discharge (DOD), overcharge, associated drive cycle and temperature. Thus, results based on EPRI/SCE preliminary tests for NiMH and Li-ion batteries on PHEVs show that less than 5% capacity and power degradation can be achieved at more than 1,500 large SOC excursion cycles at their tested conditions, where above 20% degradation signifies end-of-life of the battery (Bradley and Frank, 2009).

2.3.2 Battery Cost

Aside from the battery characteristics, production costs have a significant role in selecting the most appropriate battery technology for the application. However, due to relatively recent commercialization and widespread usage of these battery technologies in EV and HEV applications and current low production numbers, it is difficult to compare the costs associated with these battery technologies. The cost corresponding to each kWh of the associated battery technology is estimated in Table 2.1. Even though the total costs of these batteries are significantly higher than the cost of the ICEs, they are predicted to be reduced significantly when these vehicles are produced commercially in large quantities. Lead-acid batteries are cheapest to produce among the other analyzed batteries, and they are being recycled extensively which also reduces the overall cost of the technology. The cost associated with NiCd batteries is significantly higher than the cost of lead-acid batteries mainly due to the recycling cost of the materials, especially cadmium, which is an environmental hazardous substance that is highly toxic to all higher forms of life. However, it has a remarkable cycle-life performance which reduces the total cost over time. The cost associated with NiMH batteries is relatively lower than NiCd based on a higher capacity and lower amounts of toxic materials. However, they may require additional maintenance which may increase the operating costs. In future large-scale

applications, on the other hand, the overall costs can be reduced to 220 $/kWh^{-1}. The costs of Li-ion batteries are the highest among the aforementioned batteries since it incorporates thermal management and packaging costs (based on their considerable thermal management needs). However it is likely to be heavily funded for EV and HEV development due to its significantly high specific energy and power values. By 2020, General Motors is targeting to have the cost of Li-ion batteries drop to 200 – 300 $/kWh for their extended range EV batteries (Brooke, 2010).

2.3.3 Battery Environmental Impacts

Environmental impact also has a significant role in advancing the battery technologies based on customer behavior, regulatory limitations and cost (such as carbon tax and government incentives). Even though the substitution of battery technologies with conventional energy sources in the transportation industry reduces the associated environmental impact, the content and magnitude of this impact depends heavily on the electricity mix, battery technologies and the operating conditions. Life cycle assessment (LCA) has been performed in order to assess the overall environmental impact of the different battery technologies in various stages of their life (Matheys et al., 2009; Majeau-Bettez et al., 2011). The environmental impact of the study based on eco-indicator 99 under a European electricity mix can be seen in Figure 1.3. It should be noted that the energy losses due to efficiency as well as the mass of the battery have a significant effects on the environmental impact.

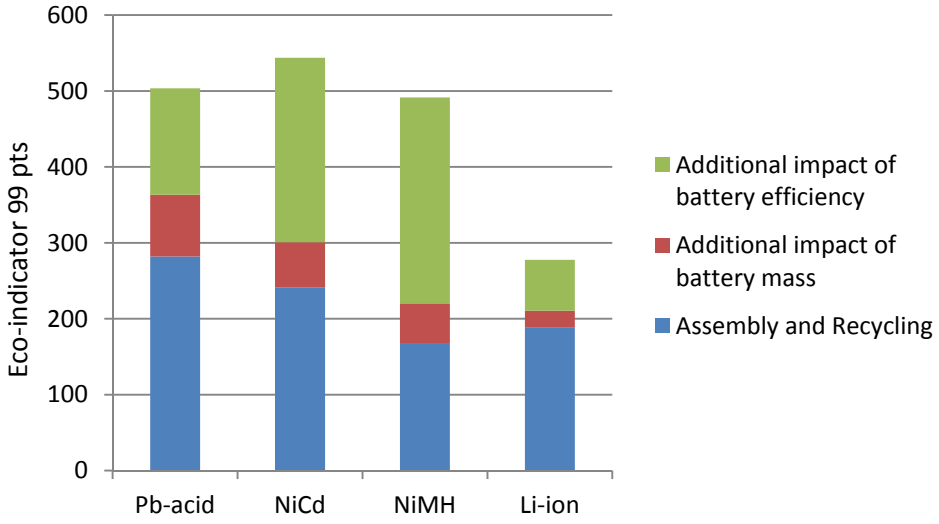

Figure 2.3: Environmental impact of the evaluated technologies based on Eco-indicator 99 (data taken from Bossche et al., 2006).

Among the analyzed battery technologies, NiCd has the most environmental impact mainly due to the presence of the environmentally hazardous material cadmium. This is followed by lead-acid based on its energy storage capacity, rather than the chemical content of the battery. The high environmental impact during the production stage is reduced by the excess recyclability since this battery technology has been utilized the longest. However, since lead-acid has the lowest specific energy density among the analyzed batteries, it may require additional mass and/or multiple charging to cover the same range with other batteries, producing more environmental impact. NiMH has relatively lower impact than the previous batteries since it has a significantly higher energy density than lead-acid and better recyclability than NiCd technologies. This environmental impact is only reduced further with Li-ion (Bossche et al., 2006) since it can store 2-3 times more energy than NiMH in its lifetime and has an order of magnitude less nickel and an insignificant amount of rare earth metals (Majeau-Bettez et al., 2011). However, these predictions are very sensitive to the battery characteristics and even a 5% change in battery efficiency can lead up to 23% change in global warming potential (GWP) and reduction of life-time can increase the impact in all categories by up to 45%.

In the environmental assessments, the impact associated with the operating phase is determined to contribute up to 40% of the global warming potential and 27-45% of eutrophication for the currently used battery technologies (based on the European electricity mix) (Majeau-Bettez et al., 2011). However, this impact is very sensitive to the content of the electricity mix and would increase by 10-16% for GWP and 10-29% for particulate matter for the Chinese electricity mix. The remainder is associated with assembly and recycling, which is based on the emissions with respect to the energy and materials used to assemble the batteries as well as the likelihood of recycling.

In conclusion, various battery technologies exist today for EV and HEV applications, each with their competitive advantages and limitations based on their physical properties, chemistry and operating conditions. Among the aforementioned batteries, lead-acid is one of the oldest commercially used battery technologies. It is the least expensive and requires the least thermal management, but it has low cycle-life and energy density. Moreover, when used under large depth of discharge (DOD), its lifetime reduces even further. NiCd has nearly twice the specific

energy of lead-acid batteries, a good power to energy ratio, high cycle life, low internal resistance and the best low temperature performance among the batteries studied, but it has very poor round-trip energy efficiency even at moderately elevated temperatures. Furthermore, there are considerable environmental concerns associated with the presence of cadmium in the battery. NiMH has better power capability and less toxicity than NiCd with reduced weight and volume, but lower energy density than Li-ion which can add considerable mass and volume to the vehicle. Li-ion is more compact and lightweight than the other considered battery technologies and it has outstanding specific energy and power. Compared to NiMH batteries, Li-ion cells can pack up to three times as much power in a much smaller package. Moreover, they are more configurable and prone to less discharge when not in use. However, Li-ion technology still faces safety, aging and cycle life challenges and requires effective thermal management. Furthermore, even though it has the most potential to be lower cost in the future, currently it is the most expensive choice. Moreover, the cycle life for these batteries varies based on battery temperature and utilization. Therefore, the most appropriate battery technology needs to be selected with respect to the corresponding application, operating temperature, driving behavior, cost and other criteria considered in EVs and HEVs.

Even though different battery technologies have varying characteristics, the battery performance for all of them depends heavily on the operating temperatures. As previously mentioned, batteries operate efficiently over a narrow temperature range (20℃ to 45℃ for most commonly used batteries) and uniformity (usually less than 5℃ non-uniformity) which is generally difficult to maintain due to different ambient temperatures and operating conditions. Operating outside of the specified temperature range affects the round trip efficiency, charge acceptance and power and energy capability of the battery (Pesaran, 2002). Since the battery performance and efficiency directly affect the vehicle performance, such as range, power for acceleration and fuel economy, as well as reliability, safety and life cycle cost (Pesaran et al., 2003), considerable focus has been given on keeping the battery at ideal conditions. In order to achieve this objective, several types of thermal management systems (TMSs) are currently used in EVs and HEVs.

2.4 Thermal Management Systems

Thermal issues associated with EV and HEV battery packs and under hood electronics can significantly affect the performance and life cycle of the battery and the associated system. In order to keep the battery operating at the ideal parameter ranges, the discrepancy between the optimum and operating conditions of the batteries need to be reduced significantly by implementing thermal management systems (TMS) in EVs and HEVs. These systems are utilized to improve the battery efficiency, by keeping the battery temperature within desired ranges. Thus, freezing and overheating of the electrochemical systems in the battery can be averted which can prevent any reduction in power capability, charge/discharge capacity and premature aging of the battery (Noboru S., 2001; Pesaran et al., 2009; Kuper et al., 2009).

Most electric and hybrid electric vehicle thermal management systems consist of four different cycles to keep the associated components in their ideal temperate range in order to operate safely and efficiently. Even though the components and structure of these loops may vary from vehicle to vehicle, their purposes are usually the same; creating an efficient and robust system that is not adversely affected by internal and ambient temperature variations. Generally, the overall vehicle thermal TMS is composed of the radiator coolant loop, power electronics coolant loop, drive unit coolant loop, and air-conditioning (A/C) and battery loop. A brief description of these loops is provided below.

2.4.1 Radiator Circuit

In the radiator loop, the engine is kept cool by the mixture of water and anti-freeze pumped into the engine block to absorb the excess heat and draw it away from the crucial areas. When this superheated engine coolant leaves the engine block, it returns to the radiator. The radiator has a very large surface area through the internal chambers where the excess heat of the coolant is drawn out through the walls of the radiator. As the vehicle moves, the front of the radiator is also cooled by the ambient air flowing through the car's grill. The loop also includes a surge tank, which acts as a storage reservoir for providing extra coolant during brief drops in pressure, as well as to absorb sudden rises of pressure. Next, a coolant pump is used for moving the coolant back and forth to the radiator. When the ICE is off, the coolant heating control module is used to

provide heat to the coolant. A portion of the heat in this loop is also transferred to the passenger cabin with help of the heater core.

2.4.2 Power Electronics Circuit

The power electronics coolant loop is mainly dedicated to cooling the battery charger and the power inverter module to ensure the main under-hood electronics do not overheat during usage. The power inverter module converts direct current (DC) from the high-voltage battery into 3-phase alternating current (AC) motor drive signals for the motor generator units. The module is also responsible for converting AC to DC for charging operations during regenerative braking. In these operations, a large amount of heat is generated in the system. In order to prevent overheating, the loop incorporates a high flow electric pump to produce and control the coolant flow which passes through the plug-in battery charger assembly, the radiator, and the power inverter module before it flows back to the pump. This loop also includes a coolant pump for the circulation of the coolant and an air separator to ensure that the coolant does not have any air bubbles that would affect the cooling performance before traveling through the major electronic parts.

2.4.3 Drive Unit Circuit

The drive unit loop is designed to cool the two motor generator units and electronics within the drive unit transaxle that are used to propel the vehicle using electric power (in addition to generating electricity to maintain high voltage battery state of charge). It provides lubrication for the various associated parts. Significant heat is generated in these parts due to high power levels during normal operation. The drive unit uses a system of pressurized automatic transmission fluid to cool the electronics in the loop, especially the motor generator units to prevent overheating (GM-Volt LLC, 2011).

2.4.4 A/C Circuit

Even though all of the circuits mentioned above have significant roles in enabling the vehicle to operate as robustly, efficiently and safely as possible, in EVs and HEVs, a majority of the focus is given to A/C and battery cooling loops due to its direct effect on the battery performance,

which has significant impact on the overall vehicle performance, safety and cost. For this reason, various studies are conducted in this cooling loop to optimize their operating conditions of the associated components, the cabin and the battery. Thus, different cooling systems and configurations will be analyzed based on various criteria and operating conditions.

The main goal of the A/C cycle is to keep the battery pack at an optimum temperature range, based on the cycle life and performance trade-off, in a wide spectrum of climates and operating conditions as well as keeping even temperature distributions with minimal variations within cells, while keeping the vehicle cabin at desired temperatures. Meanwhile, the system should also consider trade-offs between functionality, mass, volume, cost, maintenance and safety (Pesaran, 2001).

Since the main focus will be the A/C and battery loops, they will be called the thermal management systems (TMSs) for the rest of the analysis. They will be categorized based on their objective (providing only cooling vs. cooling and heating), method (passive where only the ambient environment is used vs. active cooling where a built-in source is utilized for heating/cooling), and heat transfer medium (air distributed in series/parallel or liquid via direct/indirect contact) (Pesaran, 2001).

A passive cabin air cooling system utilizes the conditioned air to cool the battery in warm ambient conditions. It was used on early EV and HEV battery packs (Honda Insight, Toyota Prius and Nissan Leaf) mainly due to cost, mass and space considerations. This is a very effective cooling method for the battery at mild temperatures (10℃ to 30℃) without the use of any active components designated for battery cooling. It is highly efficient since it utilizes the heat from the vehicle air conditioning. The ideal battery operating temperature (for Li-ion) is approximately 20℃ on the low end, which is highly compatible with the cabin temperature. However, air conditioning systems are limited by the cabin comfort levels and noise consideration, as well as dust and other contaminants that might get into the battery, especially when air is taken from outside. Certain precautions should be taken in this system to prevent toxic gases from entering the vehicle cabin at all situations. In independent air cooling, the cool air is drawn from a separate micro air conditioning unit (instead of the vehicle cabin) with the use of the available refrigerant. Even though this may provide more adequate cooling to the

battery, the energy consumption as well as cost and space requirements associated with installation of the blower and the micro air conditioning unit increases significantly (Behr, 2012). The rate of heat transfer between the fluid and the battery module depends on various factors such as the thermal conductivity, viscosity, density and velocity of the fluid. Cooling rates can be increased by optimizing the design of air channels; however it is limited by the packaging efficiency due to larger spacing between the cells. Air can flow through the channel in both serial and parallel fashions, depending on whether the air flow rate splits during the cooling process. In series cooling, the same air is exposed to the modules since the air enters from one end of the pack and leaves from the other. In parallel cooling however, the same air flow rate is split into equal portions where each portion flows over a single module. In general, parallel airflow provides a more uniform temperature distribution than series (Pesaran et al., 1999).

Refrigerant cooling is a compact way of cooling the battery, with more flexibility compared to a fan with ducts, by connecting the battery evaporator parallel to the evaporator in the cooling loop. Heat generated by the battery is transferred to the evaporating refrigerant. This system only requires two additional refrigerant lines, namely suction and pressure lines. The battery evaporator uses some portion of the compressor output that was reserved for the air conditioning, and thus this might cause conflict in some conditions. However, the compressor work needed to cool the battery is usually considerably lower than the air conditioning evaporator need.

Liquid cooling utilizes the previous cooling method with the incorporation of an additional liquid cooling loop specifically for the battery that connects to the refrigerant. This additional cooling loop usually has water or a 50/50 water-glycol mixture and it is kept cool via different procedures depending on the cooling load and ambient conditions. The coolant can be cooled either by ambient air through the battery cooler (if the ambient temperature is low enough) or by transferring the heat to the refrigerant through the chiller. Both methods increase the efficiency of the system since the additional compressor work (that is used in refrigerant cooling) is no longer needed.

In addition, battery cooling can also be done with phase change materials (PCM) integrated cooling systems. PCMs have significant advantages over the aforementioned TMSs, due to their

simple design, light weight and compact size, safety and relatively low cost, especially when the integration is considered from the outset and it is improved with the addition of aluminum foam and fins (Khateeb et al., 2004). PCMs are capable of keeping the magnitude and uniformity of the cell temperatures under stressful operating conditions without the need of a complicated system or fan power. Moreover, the heat transfer associated with adding PCMs to a cell can prevent the propagation of thermal runaway, when the cell temperature reaches critical levels. Furthermore, PCMs can be used to have both an active and passive role (complementary/secondary) in thermal management of the battery packs which can reduce the complexity and cost of the system (Kizilel et al., 2009; Sabbah et al., 2008).

Chapter 3: Literature Review

In past literature, there have been various studies associated with thermal management systems for electric and hybrid electric vehicles. Due to the environmental concerns and technological developments in the last decade, both the need and capability of producing EVs and HEVs have grown significantly. This resulted in a significant increase in the amount of studies conducted on this subject in various scientific disciplines. The related papers, their aims, methods of analysis and brief conclusions are presented in this section. These studies examine different kinds of EVs and HEVs and their impacts, the associated battery technologies, the thermal management systems utilized in batteries, and analysis of associated exergy models for the corresponding cycles.

3.1 EVs and HEVs

Electric and hybrid electric vehicles are undertaking to meet the needs caused by conventional vehicles due to increasing costs of fuel and environmental impact. Even though the current technology allows EVs and HEVs to outperform CVs in these aspects, they have various shortcomings that need to be resolved before they can be a permanent solution. In the literature, many studies have been conducted with respect to the need for EVs and HEVs, their various applications and configurations as well as their associated operating costs and environmental impact.

Nelson (2000) reviewed the specifications and operational requirements imposed on the batteries for various hybrid electric vehicle designs and applications as defined by the Department of Energy Partnership for New Generation of Vehicles (DOE PNGV) Program. Moreover, he evaluated each battery technology advantages and shortcomings in order to assess the compatibility with the proposed systems and recommended designs for major projected HEV applications. He concluded that even though most of the DOE / PVNG goals are very difficult to achieve, significant improvements have been achieved in this field and it is not too far before these targets can be met.

Weiller (2011) explored the effects of different charging behaviors of PHEVs in the United States on electricity demand profiles and energy use. By using 2003 National Household Travel Survey (NHTS) load profiles and average the US electricity production mix, he calculated that PHEVs with all-electric ranges up to 40 miles allow drivers in the US to cut their gasoline consumption by more than half by shifting 45-77% of miles traveled from gasoline electricity. This also corresponds to a $0.09 per kWh reduction of energy cost and 53% to 58% reduction in environmental impact. He also concluded that the reduction of environmental impact can be even further with the use of electricity produced from renewable energy sources.

Doucette and McCulloch (2001) and Samaras and Meisterling (2008) studied the CO_2 emissions from EVs, PHEVs and compared them with respect CVs with ICEs. They expressed the emissions in terms of CO_2 intensity, defined by "the average amount of CO_2 emitted per unit of electrical energy generated by all the power production processes in a mix weighted by the amount of power obtained from each of those processes". They concluded that the emissions over the entire driving range were lowest for EVs on low and mid-range CO_2 intensity (such as France and US electricity production mix respectively), but lowest for PHEVs for high CO_2 intensity. In all scenarios, EVs and PHEVs had significantly lower emissions than CVs with ICEs.

Shiau et al. (2009) developed PHEV simulation models to determine the effects of additional battery weight on fuel consumption, cost, and GHG emissions for a variety of charging frequencies. They used a structural weight multiplier to account for the additional weight needed to support the extra battery weight and calculated the emissions based on the average U.S electricity mix. In conclusion, they determined that among PHEVs, HEVs and EVs, small capacity PHEVs provide the lowest lifetime cost and emissions when charged frequently (under 20 miles). When charged between 20 to 100 miles on the other hand, HEVs provide the lower costs. However, they determined that the impact of PHEVs and HEVs, even with increased battery specific energy or carbon taxes, would only have limited impact without decarburization of the electricity grid.

3.2 Battery Technology

There are also various studies evaluating the most compatible battery technologies for plug-in as well as regular hybrid electric vehicle applications. These batteries are examined mainly based on their performance, temperature range, cycle life, cost and environmental impact. There are various analyses that elaborate on the specific issues associated with the chemistry of each battery technology and how these affect the overall hybrid electric vehicle performance.

Conte (2006) pointed out the advantages and drawbacks for each battery technology relevant for HEV applications. The energy storage devices for HEVs are selected as lead-acid, NiMH, Li-ion, and the electric double layer capacitor (EDLC), to a certain extent. Even though there is no "perfect" battery with high power, capacity and eternal life, among the compared batteries, Li-ion technology is most likely be the pathway for the HEV's future.

Bossche et al. (2006) and Matheys et al. (2009) also added sodium-nickel chloride (NaNiCl) batteries to the list and evaluated their impact to determine the most environmentally friendly battery technology for electrically propelled vehicles. Based on using an LCA with Eco-indicator 99 and European (EU-25) electricity production mix, they determined that Li-ion technology has a better score than all the compared batteries, except for NaNiCl. Furthermore, Bossche et al. (2006) concluded that lead-acid, NiCd and NiMH technologies have a higher environmental burden than Li-ion and NaNiCl batteries, due to lower energy storage capacities that may require multiple charging to cover the same distance.

Majeau-Bettez et al. (2011) conducted a life cycle assessment of NiMH and two Li-ion batteries, namely nickel cobalt manganese lithium-ion (NCM) and iron phosphate lithium-ion (LFP), for PHEVs and full performance battery EVs. In the paper, it is reported that NiMH performs significantly worse than the two Li-ion batteries for all except the ozone depletion potential category and concluded that a shift from NiMH to Li-ion battery technology may be viewed positively based on environmental criteria. They rationalized this by Li-ion's higher phase efficiency and its ability to store considerably more energy in its lifetime for the same mass as well as consisting of less environmentally intensive materials compared to NiMH. In addition,

they have determined the overall global warming impact of the batteries to be 35 gCO_{2-eq}, 19 $gCO_{2-eq}$and 14 gCO_{2-eq} for NiMH, NCM and LFP respectively over their life time for the average European electricity mix. Over 40% of the GWP and fossil depleting impacts and between 27-45% of the eutophication impacts were attributed to the electricity consumed for the battery during the operating stage, which can be reduced considerably by shifting into a cleaner (with renewable energy) electricity production mix.

Nelson (2000) evaluated the different battery technology based specifications and operational requirements imposed on the batteries as defined by the DOE/PNGV program for the HEVs. VRLA, NiCd, NiMH, Ni-Zn, Li-ion and Li-polymer are selected as potential candidates for HEV applications and a thorough comparison was made based on numerous battery characteristics including size, power/energy balance, round-trip efficiency, cycle life and cost. The study concluded that even though the current battery technologies do not completely meet all of the DOE/PNGV goals, especially in weight, life cycle and cost (in the year 2000), these battery characteristics will improve considerably in the future as the technologies mature and large-scale production becomes possible. The paper also stated the importance of preventing extreme temperature variations in the battery for the various technologies in order to have a desirable performance and long cycle life. At the targeted DOE/PNGV temperatures ranges (-40℃ to +52℃), the electrolytes in lead-acid batteries would freeze at the low temperature end at 50% SOC, which could be prevented by bringing the battery to a full state of charge, however at the expense of reducing the cycle life. For NiCd and NiMH batteries, discharge performance at the low end would be poor and the charge acceptance at the high end would be minimal. The life cycle of these batteries can be halved by going from 30℃ to 40℃. Li-ion batteries would not even operate at the low end due to high cell impedance and low conductivity of the organic solvent/electrolyte system. At temperatures over 45℃, on the other hand, the cycle life decreases drastically. Therefore, in the paper it is recommended that all of the analyzed battery technologies require a certain thermal management system to have optimum performance and a long life time.

3.3 Thermal Management Systems

After analyzing hybrid electric vehicles and associated battery technologies, the next step is to evaluate the most compatible thermal management systems for the chosen battery technology since the main vehicle performance problems are related to the batteries operating in non-ideal temperature ranges. In this regard, there are various studies in the literature describing and comparing various TMSs with respect to their capability for the desired applications. These TMSs are categorized with respect to providing cooling vs. heating, passive vs. active, using air vs. liquid or having configurations in parallel vs. serial. The main criteria are based on the corresponding temperature distribution and uniformity of the battery packs that is associated with each TMS as well as the performance characteristics of the TMS and its individual components under various system parameters and operating conditions.

Bhatti (1999) analyzed automotive air conditioning systems (AACSs) using R134a to find potential improvements in order to increase the performance and reduce the associated global warming impact of the system. He identified the several effective augmentation strategies and investigates their effects on the coefficient of performance (COP) of the system. He also compared the performance of the real system with the idealized one to provide an upper bound on the maximum possible augmentation on the system. Moreover, the paper provided comparison on the total equivalent warming impact of the improved R134a system with several proposed systems that incorporates refrigerants such as R0145a, R290, R717, R-744 and R729.

Lee and Yoo (2000) assessed the performance of individual components in a conventional AACS under different operating conditions. They used computer simulations to asses and compare the experimentally derived overall heat transfer coefficient and pressure drop associated with heat exchangers, as well as the overall performance of the condenser. Moreover, they discussed the effects of condenser size and refrigerant charge on the performance of the studied AACS. In the paper, it is concluded that 10% overcharge is highly effective for various operating conditions and that the COP of the system reduces when charged over this value.

Jabardo et al. (2002) performed a steady state experimental study for the refrigeration circuit of an AACS and compared it against their numerical analyses. They predicted the effects of various parameters on the system. The COP was calculated within 20% error with respect to the experimental results. Moreover, they determined that the refrigeration capacity is significantly affected by the evaporator return air temperature and that refrigeration capacity, mass flow rate and COP vary linearly with condensing and return air temperatures and compressor speed.

Kaynakli and Horuz (2006) investigated the performance of an AACS with respect to various cooling loads, compressor power consumption as well as refrigerant mass flow rates by using an experimental vapor compression refrigeration system. They concluded that the cooling capacity increases with increasing condensing temperature and compressor speed. Moreover, they determined that the refrigerant flow rate is affected slightly by the changes in the condenser, the evaporator and the ambient temperatures and drastically by the changes in the compressor speed. They calculated a mass flow rate change from 0.016 kg/s to 0.030 kg/s by increasing the compressor speed from 1750 rpm to 3150 rpm.

Wang and Gu (2004) conducted an experimental study of an AACS with two-phase flow measurements. They evaluated the system performance characteristics with respect to the evaporator and condenser temperatures and refrigerant charge. They determined that the total mass flow rate increases with the increase of the refrigerant charge, evaporator air inlet temperature, condenser water temperature, and compressor speed. Moreover they concluded that the COP of the system decreases with the increase of the refrigerant charge, condenser water temperature and compressor speed.

Hosoz and Direk (2006) examined the performance characteristics of an R134a AACS capable of operating as an air-to-air heat pump using ambient air as a heat source. The system was evaluated with respect to the associated COP and exergy destruction in the system. They concluded that the heat pump operation provides adequate heating only in mild weather conditions. However, it has the capability of yielding higher COPs and a lower rate of exergy destruction per unit capacity.

Pesaran (2001) compared various thermal management systems based on cooling vs. heating, passive vs. active, parallel vs. serial and air vs. liquid for VRLA, NiMH and Li-ion batteries. He compared the heat generation for these batteries and their behavior with respect to different temperature and cycles. Based on the thermal management medium used in the system, the average heat transfer coefficient is determined to be 57 W/m^2K for oil, about 2.3 times higher than air (25 W/m^2K), and indirect cooling water with 390 W/m^2K under the same mass flow rates and atmospheric conditions for the systems analyzed in the paper. He concluded that the passive TMS is less complicated, though less effective, and it can be used for relatively small battery packs (especially for parallel HEVs); however, the ambient air must be between 10ºC and 35ºC for the thermal management to work for passive systems, otherwise the battery pack can suffer in extreme temperature ranges. Outside these conditions, active components might be needed to provide adequate thermal management. On the other hand, for EVs and series HEVs, more elaborate liquid-based systems may be required for optimum thermal performance. He also suggested that it is imperative for Li-ion batteries to have a good TMS due to their safety and low temperature performance concerns.

Keller and Whitehead (1991) studied the effects of batteries under extreme temperatures and their associated effects on the vehicle characteristics, especially range, on the Griffon Electric Vehicle equipped with a CMP 3ET205 lead-acid battery. Initially they conducted tests on the vehicle with no TMS and compared their results with the same vehicle that has an air and liquid TMS. In the absence of any TMS, high ambient temperatures and heat spread across the battery pack can reduce the vehicle range significantly and can cause the seasonal driving variability and premature cell failure. Based on the experiments, they determined that the vehicle can achieve up to 20% greater mileage with TMS. Moreover, the temperature spread can be reduced or eliminated significantly with the use of TMS, where they achieved a 4.0ºC and 2.3ºC temperature spread in the pack for a circulating-air and circulating-liquid TMS respectively compared to 11.6ºC for the non-managed pack.

Pesaran et al. (1999) and Kim et al. (2006) developed a computational fluid dynamics (CFD) model simulation for a typical parallel cell cooling system with various cooling media (air, mineral oil and water/glycol), mass flow rates and coolant channel hydraulic diameters taken as

system control parameters. Based on the analysis, they determined that even though the rate of heat removal from cell to coolant is the same for air and water/glycol systems, air flow is rapidly heated and the coolant temperature and cell surface temperature difference is larger for the air system due to air having a smaller heat capacity and heat coefficient, respectively. Thus, both the maximum temperature and temperature non-uniformity inside the cells is larger for air cooling than the water/glycol cooling system. In addition, they have determined that the mineral oil liquid cooling system would significantly outperform an air cooling system based on the heat transfer rate and battery cell temperature increase.

Kuper et al. (2009) presented heat generation in the battery cells as well as different types of active cooling systems with air, liquid and refrigerant cooling mediums. They formulated the increase in battery temperature over time based on internal heating and cooling rates. They recommended maintaining maximum and minimum cell temperatures within a 3 – 5 K range since it can lead to 25% acceleration of the aging kinetics and up to 50% variance in power capability (in a high temperature power degradation range). They also recommended keeping the inlet and outlet coolant temperature difference to be less than 3 K to keep the cell temperatures sufficiently uniform.

Mi et al. (2007) evaluated the TMS of a Li-ion battery pack designed for HEV applications, including estimating the thermal loss, predicting the temperature rise and modeling the gradients of the battery pack under various operating conditions. They calculated the heat generation to be 2.0 kW with respect to the battery impedance and charge rate. In addition, based on the scenario of the vehicle parked under the sun (vehicle compartment temperature of 55℃), they calculated it would take approximately 16 minutes to cool the battery below the threshold temperature of 40℃.

Kizilel et al. (2008) compared the temperature increase and capacity degrading of the battery pack as well as uniformity among the packs with and without the use of phase change materials (PCM) under room temperatures. A wax with wax volume to pack volume of 80% and a melting temperature range of 42 - 45℃ is used on the tested battery. They determined that when the PCM was used, the rate of temperature increase in the battery was slower in the wax melting range

since filling the gaps between the cells with PCMs enabled high heat conduction. Thus, the temperature difference between the cell in the center of the pack and the surface temperature of the cell at the corner of the pack is reduced from 10℃ to 4℃. Moreover, the capacity fading for operating temperatures under 45℃ is reduced significantly from 10.7, 13.4 and 12.2 mAh/cycle without PCMs to 5.5, 5.3 and 5.7 mAh/cycle with PCMs for cycles from 1-50, 51-96 and 97-300, respectively. As a result, they concluded that the use of PCMs can have significant advantages over active cooling systems due to their effectiveness, low mass and simplified and economic design.

Pesaran et al. (1998) analyzed the effects of ambient temperature ranges on the battery packs by passing air into the battery module operating under the federal urban driving schedule profile. They concluded that the capacity and performance of the batteries is reduced significantly with internal battery temperatures over 60ºC. Moreover, Al-Hallaj and Selman (2002) analyzed the effects of high temperature on Li-ion batteries through both theoretical (thermal modeling) and experimental analysis and compared active thermal management systems with PCM-based passive cooling. They found that the PCM-based system is more reliable and effective than active TMS.

Siddique et al. (2004) studied the effects of using phase change materials for a Li-ion battery in an electric scooter and compared them to cooling the cells via air. Li-ion cells were modeled as unsteady-state two-dimensional systems with air flowing in between with natural convection and a heat transfer coefficient of 5 W/m^2K. For forced air cooling, the Li-ion cell temperature (at the center) rose to 45℃, while the cell exposed to cooling rose to 35℃, creating a temperature gradient of 10℃ in between. A temperature gradient of 20℃ is also determined between air at the center of the module and air exposed to forced air-draft convection at the outer location. For PCM cooling, 216 grams of PCM was used (12 grams for each of the 18 cells) and 10% additional volume is added to the battery pack to compensate for volume expansion upon solidification of the material. The study showed that employing PCMs alone to the battery module is ineffective due to the poor thermal conductivity. However, the thermal conductivity was improved by an order of magnitude by adding aluminum foam to PCM, which reduced to temperature of the battery module to 25℃. On the other hand, the PCM still failed to provide

adequate cooling due to the material being completely melted during the second cycle (in a three cycle experiment). Thus, aluminum fins were also added to the existing battery module to overcome this problem. As a result of this analysis, they concluded that PCMs can be a simple and cost effective solution for Li-ion battery applications including HEVs, especially in the cases where passive air cooling fails.

Even though the aforementioned studies evaluated different thermal management systems under various operating conditions and compared them with respect to temperature distribution and uniformity, they do not provide any information on the efficiency of the system, causes/sources of inefficiencies and the steps needed to be taken in order to improve the system performance. Thus, various exergy based analyses are conducted in this thesis in order to evaluate the efficiency of the studied thermal management system and provide recommendations for improvement in system as well as component level.

3.4 Exergy Models

Currently, there is no exergy model in the literature for EV/HEV thermal management systems. However, there are several exergy models for various other HVAC applications. Since the vehicle thermal management system incorporates a vapor-compression cycle, various studies regarding these cycles have been examined in many applications from oil refineries and chemical processing plants to large public buildings. Even though the configurations and components of the cycles might vary, the main idea behind the system is to remove heat from the targeted space and transfer it elsewhere. Moreover, there are no studies currently available conducting exergy based economic and environmental analysis for EV/HEV TMSs. However, there are various studies conducted in the literature based on different refrigerant and cooling mediums as well as operating and ambient temperatures where the exergy based efficiency, economy and/or environmental impact of the systems is calculated for various applications.

Nikolaidis and Probert (1992) assessed the exergy loses occurring in a single-stage, vapor-compression refrigerant plant and associated cold-storage room. They determined that the compressor had the greatest rate of exergy loss followed by the condenser. The exergy losses can be reduced by using a compressor with higher isentropic efficiency or implementing multi-stage

compound compression for the compressor and by reducing the mean temperature difference between the condenser and ambient temperatures for the condenser. Moreover, they suggested that the exergy loss can be reduced by subcooling the refrigerant at the exit from the condenser for the throttling process, and by reducing the temperature difference between the cold room and the evaporating refrigerant for the evaporator.

Hosoz and Direk (2006) studied the performance characteristics of an R134a automotive air conditioning and air-to-air heat pump system with an ambient air heat source. Two groups of tests were conducted, with respect to the maximum outdoor fan speed and the constant condensing temperature tests. They determined that the cooling/heating capacities increase with increasing compressor speed while COPs for both cases decrease with it. Moreover, for the same compressor speed and condensing/evaporating temperatures, the heat pump operation yielded lower compressor discharge temperatures. Furthermore, in both operation modes, the ratio of the rate of total exergy destruction to the capacity increased with compressor speed while the heating mode operation resulted in lower ratios. Finally, even though the heat pump operation provided sufficient heat at mild weather conditions, the heating capacity dropped significantly at severe conditions due to both decreasing evaporator temperatures and activation of the capacity control systems. Thus, they suggested that the air-to-air heat pump should be considered only as a supplementary heating method to be used in automobiles lacking waste heat.

Bilgen and Takahashi (2002) conducted an exergy analysis of heat pump-air conditioner systems and developed a simulation program to simulate and evaluate experimental systems based on this exergy analysis. The experiment system was a Matsushita room air conditioner with R410a refrigerant. The COP and exergy efficiency of the system varied as an inverse function of load from 7.40 to 3.85 and 0.35 to 0.22, respectively. The study also determined that the percentage of exergy used to run the heat pump system varied from 39.7℃ to 62.1℃ with respect to design and off-design conditions and that COP may be improved by 20% to 30% when optimum design is achieved.

Yumrutas et al. (2002) presented a computational model based on an exergy analysis for investigating the effects of evaporating and condensing temperatures on the pressure and exergy

losses, exergy efficiency and COP of the vapor compression cycle. Ammonia is used as refrigerant, and compact heat exchangers are used as the condenser and evaporator in the study. The cold room and ambient air temperatures are assumed to be 0℃ and 20℃, respectively, and the isentropic compressor efficiency is taken as 0.85. They used the effectiveness-NTU method to determine the evaporator and condenser matrix dimensions and heat transfer rates. They determined that most of the exergy losses occurred in the compressor, followed by the condenser, expansion valve and evaporator. They also concluded that evaporating and condensing temperatures have strong effects on the exergy losses in the evaporator and condenser as well as the exergy efficiency of the overall cycle, while having very little effects on the other components. Moreover, they determined that the total exergy loss decreases with a decreasing temperature difference between the evaporator and the refrigerated space and between the condenser and outside air.

Kabul et al. (2008) performed energy and exergy analyses for a vapor compression refrigeration system with a heat exchanger using isobutene (R600a). In the analysis, a refrigeration capacity of 1 kW, cold chamber temperature of 0℃, and evaporator and condenser temperatures of -10℃ and 40℃ are used. They determined the highest irreversibility in the system occurred in the compressor, due to various associated inefficiencies, accounting for half of the total irreversibility. This is followed by the condenser, since at the end of compression process the vapor becomes super-heated, and the expansion valve as a result of the pressure drop in the component. They also conducted various parametric studies where they showed that as the evaporator temperature increases, the values of COP, efficiency ratio and exergy efficiency also increase, whereas the total irreversibility rate decreases. On the other hand, the exact opposite trend is observed for the condenser temperature increase.

Shilliday et al. (2009) conducted a detailed energy and exergy analysis of the low global warming potential refrigerants, R744 and R290, against the commercial refrigerant R404a. Moreover, they also compared the results of this analysis against a two-stage vapor-compression cycle of R744 with an internal heat exchanger. In the analysis, an evaporation temperature of -10℃ and condensing/gas cooling temperature of 40℃ are used. They concluded that the specified operating conditions, both R404 and R290, exhibit higher COPs then R744. Moreover,

the COP of the systems also increases with increasing evaporating and decreasing condensing temperatures for all refrigerants. Furthermore, at a 25℃ condensing temperature, the component with the highest exergy destruction ratio is determined to be the expansion valve for R744 and compressor for R404a and R290. In addition, the total cycle exergy ratio of R744 is decreased by an average of 4% with the implementation of two-stage compression and 12% by also adding an internal heat exchanger.

Arora and Kaushik (2008) used a computational model to present a detailed exergy analysis of an actual vapor-compression refrigerant cycle with R502, R404a and R507a refrigerants. The analysis is conducted in the temperature ranges of -50℃ to 0℃ and 40℃ to 55℃ for the evaporator and condenser, respectively. They concluded that the COP and exergetic efficiency for R507 are better than that of R404a but lower than R502 in the specified condenser temperature range. Moreover, the worst components in the system based on irreversibilities are determined to be the condenser, followed by the compressor, throttle valve and evaporator; whereas the most efficient component is determined to be the liquid vapor heat exchanger. In addition, decreasing the pressure drop in the evaporator and condenser, subcooling as well as increasing the dead state temperature had positive effects on the exergetic efficiency of the systems. Based on the analysis, they concluded that R507a is a better alternate to R502 than R404a.

Arcaklioglu et al. (2005) studied the rational efficiency and component based irreversibility ratios of a cooling system based on the exergy analysis using HFC and HC based pure and mixed refrigerants. They suggested that a general trend of increase of efficiency is parallel to increasing the temperatures of both the condenser and evaporator. Moreover, in the analysis, the highest irreversibility is calculated in the condenser (40 - 55% of the total irreversibility of the system), followed by the compressor, evaporator, expansion valve and suction line heat exchanger. Finally, they calculated that the exergy efficiency of the cooling system varies between 40% and 44% based on the refrigerants used in the system.

Stegou-Sagia and Paignigiannus (2005) compared the performance values of various working fluid mixtures in a vapor compression refrigerating cycle based on the exergy analysis. The

analysis was conducted based on an ambient temperature of 20℃, isentropic compression efficiency of 0.75 and compressor motor efficiency of 1 and temperature difference between the cold space and evaporator of 2℃. They determined that the compressor has the highest irreversibility in the system for all refrigerants, followed by the condenser, evaporator and expansion valves. Moreover, they presented that the exergy efficiency increases with an increase in pressure drop for the evaporator and condenser, isentropic compression efficiency, use of subcooling and suction of superheated vapor to a certain point.

Zubair et al. (1996) analyzed an HFC-134a vapor compression cycle based on both the first and second law of thermodynamics with respect to two-stage and mechanical-subcooling refrigerant cycles. In the analysis, the compressor inlet temperature was 20℃, compressor efficiency of 0.65, temperature of the liquid subcooling in the condenser to be 3℃ and the pressure drop in the condenser, evaporator and suction lines were 5% each. They determined that, in these operating conditions, most of the losses are associated with low efficiency of the compressor, followed by irreversibilities of expansion valves and condensers.

Arora et al. (2007) conducted parametric investigations of actual vapor compression refrigeration cycles in terms for COP, exergy destruction and exergetic efficiency for R-22, R407C and R-410A by using EES software package. Condenser and evaporator temperatures were varied between 40℃ and 60℃ and 7℃ and -38℃ respectively, and a refrigerant flow rate of 1 kg/s were used in the analysis. They determined the optimum evaporator temperature for a minimum exergy destruction ratio at various condenser temperatures. They also determined that the COP increases with increasing evaporator temperatures and decreasing condenser temperatures. Moreover, they calculated that the exergy efficiency increases as the dead-state temperature increases. Furthermore, they checked their work against the experimental results obtained by Aprea and Renno (2004) and found that their COP and exergetic efficiency values are only 3% and 6% higher respectively.

Şencan et al. (2005) presented a computer-based first and second law analysis of vapor-compression refrigerant systems for determining subcooling and superheating effects of R134a, R407c abd R410a. They have simulated the thermodynamic properties of the refrigerants using

an artificial neural network (ANN) methodology. They determined that the COP increases with decreasing condensing and increasing evaporating and subcooling temperatures, as well as compressor efficiency. Increasing the superheating temperature increased the COP for R134a and R407c, but reduced the COP for R410a. Moreover, the exergy efficiencies followed the same trends with COP for all refrigerants. They determined that R134a had the highest efficiency rate whereas R410a has the lowest.

Joudi et al. (2003) presented a computational model with the objective of simulating the performance of an ideal automotive air conditioning system that works with various refrigerants in order to find the most suitable alternative to R-12 refrigerants. R-12, R-134a, R-290, R-600a and a mixture of propane and isobutene (62/38 molar percentage) were analyzed under various evaporating / condensing temperatures and compressor rotational speeds. They concluded that R290/R600a exhibits higher COP values than R-12 and would be the most appropriate substitute.

Somchai et al. (2005) conducted an experimental study on applications of various hydrocarbon mixtures involving propane, butane and isobutene to replace R134a in automotive air conditioners. Based on the refrigeration capacity, compressor power and the coefficient of performance (COP), they concluded that a propane/butane/isobutene mix of 50%/40%/10% is the most promising alternative refrigerant to replace R134a. Furthermore, Park et al. (2007) analyzed the performance of two pure hydrocarbons (propane and propylene) and seven mixtures composed of propylene, propane, HFC152a and dimethylether to replace R22 in residential air conditioners and heat pumps. They determined that a propylene/propane/dimethylether mix of 45%/40%/15% provides the highest COP, which is 5.7% higher than R22.

Yoo and Lee (2009) conducted an experimental study comparing R134a with R152a at the bench level with an experimental apparatus simulating a real automotive air conditioning system consisting of a cabin and engine room structure. They evaluated the refrigerants based on the cooling and condensing capacity, coefficient of performance (COP) and power consumption characteristics with respect to different air mass flow rates and compressor rotation speeds. They concluded that R152a performs better than R134a in an automotive air conditioning system.

Dalkilic and Wongwises (2010) conducted a theoretical performance study on a traditional vapour-compression system with various refrigerant mixes comprised of HFC134a, HFC152a, HF32, HC290, HC1270, HC600 and HC600a and compared them with CFC12, CFC22 and HFC134a. They investigated the effect of certain parameters such as refrigerant type, degree of superheating and subcooling, coefficient of performance (COP) and volumetric refrigeration capacity in the analysis. They found that all refrigerant mixtures have slightly lower COPs than CFC12, CFC22 and HFC134a under the range of condensation and evaporation temperatures. Among the refrigerant mixtures, HC290/HC600a (40/60 by weight%) and HC290/HC1270 (20/80 by weight%) were found to be the most suitable alternatives to CFC12 and CFC22, respectively, based on COP, pressure ratios and ozone depleting potential (ODP) and global warming potential (GWP).

Reasor et al. (2010) and Zilio et al. (2011) performed simulations to compare the refrigerant R1234yf with R134a in order to evaluate their performance under various input parameters and assess R1234yf's corresponding drop-in potential for systems designed for R134a. They concluded that even though the thermodynamic properties of R1234yf are very similar to R134a for outlet refrigerant temperatures and heat loads, R1234yf would have a lower COP and significantly different pressure drops which would require changes in the heat exchanger design and piping.

Hepbasli (2007) conducted a thermoeconomic analysis of household refrigerators based on the exergy cost energy and mass (EXCEM) method using R134a as the refrigerant for the reference state temperatures between 0℃ and 20℃. The greatest irreversibility (exergy destruction) is calculated to occur in the compressor, followed by the condenser, capillary tube, evaporator, and superheating coil. The exergy efficiency of the system is also determined to be increasing as the reference state temperature increases. Moreover, the loss-to-capital ratios based on energy for the overall system as well as the compromising devices are determined to vary significantly more than those based on exergy. Furthermore, the correlations are developed for estimating exergy efficiencies and ratios of exergy loss rate-to-capital cost as a function of the reference state temperature.

Ozgener et al. (2005) developed an exergoeconomic model of a vertical ground-source heat pump (GSHP) residential heating system. They calculated the ratio of thermodynamic loss rate to capital cost values to be in the range from 0.18 to 0.43 and provided a linear correlation between the value of this parameter and ambient temperatures. They have also drawn attention to the compressor as the component where the most availability destroyed.

Ozgener and Hepbasli (2005) presented an EXCEM analysis for a solar assisted ground-source heat pump greenhouse heating system with a 50 meter vertical and 32 millimeter nominal diameter U-bend ground heat exchanger. They determined that the total exergy loss values were between 0.010 kW and 0.480 kW and found the largest energy and exergy losses in the greenhouse compressor. Moreover, they have calculated the ratio of thermodynamic loss rate to capital cost values to be in the range of 0.035 to 1.125.

Bakan et al. (2008) conducted an exergoeconomic analysis of glycol thermal management storage with a storage tank of 350,000 kg capacity and a water solution based on ethylene glycol as the storage medium. They calculated the ratio of thermodynamic loss to capital for the overall system to be between 0.00233 and 0.00225 $kW\$^{-1}$.

D'Accadia and Rossi (1998) presented a thermoeconomic optimization of a conventional refrigeration plant based on a simplified cost minimization methodology. They demonstrated the systematic equations for calculating exergetic and economic costs and provided the cost balance equations associated with each component. Furthermore they obtained a reduction of about 1.8% for the overall operating and amortization cost of the analyzed plant by means of greater investment of the plants, mainly with regards to an electric motor and evaporator.

Dingeç and Ileri (1999) formulated a thermoeconomic optimization of refrigerators and applied them to a specific domestic refrigerator case. The independent variables are selected as the condenser and evaporator areas and the compressor efficiency. By conducting the thermoeconomic optimization, they calculated that the annual cost of operation of an actual system is 74% higher than an optimum system. Moreover, the COP of the optimum system is determined to be 1.26 compared the COP of the actual system which is 1.08.

Selbaş et al. (2006) and Ozkaymak et al. (2008) conducted an exergy-based thermoeconomic optimization application with independent variables of condenser and evaporator areas to a subcooled and superheated vapor compression system based on various working fluids. They calculated the optimization results based on various condensing, evaporating, superheating and subcooling values.

Wall (1991) presented an application of thermoeconomics to the optimization of a heat-pump. He chose the efficiencies of the compressor, condenser, evaporator and electric motor as the variable to be optimized, developed cost relations in terms of their efficiencies and conducted parametric studies based on the price of electricity and the temperature of the heat input. He concluded that the electric motor costs approximately 2.4 times as much at 91% efficiency than at 75% efficiency and is the most critical component to improve. He also calculated that the COP of the system increases from 2.69 to 3.63 when the parameters are optimized.

D'Accadia and Rossi (1998) applied thermoeconomic optimization to a conventional refrigeration plant in order to minimize the overall operation and amortization costs. They used a theory of exergetic unit costs to evaluate the economic cost of all internal flows and products. They presented a case study where the overall operation and amortization costs were reduced 1.8% with respect to the base case and concluded that a design configuration not far from the real global optimum can be obtained my means of sequential, local optimization of the system. This would have acceptable accuracy when compared to conventional and more complex optimization methods.

Caliskan et al. (2012) conducted an energy, exergy, environmental, exergoeconomic and enviroeconomic analyses of the Maisotsenko cycle based novel air cooler with respect to nine different dead state temperatures that varies from 0℃ to 37.77℃. They calculated the electrical energy consumption cost of the system to be 59.85 $/year (based on 8 hours a day for 125 days a year). Moreover they have calculated the exergetic cost rate to be 0.0228 kWh/$-year at the dead state temperature of 37.77℃. Furthermore, based on the environmental cost analysis, the dollar

value of the amount of carbon dioxide released to the atmosphere in a year is determined to be 6.96 $\$CO_2$.

Al-Otaibi et al. (2004) studied thermoeconomic optimization of vapor compression refrigeration systems and verified their model with an illustrative example for an actual system using R134a as a refrigerant. They have selected compressor, condenser, evaporator and electric motor as the decision variables and have selected the condenser temperatures to be between 25℃ and 60℃ and the evaporator temperatures between -5℃ and -20℃ for the analysis. They concluded that increasing the refrigerant flow rate requires more compressor work input and therefore increases the corresponding overall cost.

Sanaye and Malekmohammadi (2004) presented a thermal and economic optimum design of an air conditioning unit with a vapour compression refrigeration system that includes a compressor, condenser, and evaporator along with centrifugal and axial fans. They chose heat exchanger temperatures, their heating surface areas as well as fan and compressor powers among the design variables and studied the performance of the system under various situations, then implemented an optimization procedure. They selected the objective function for optimization as the total cost per unit cooling load of the system including capital investment for components as well as the required electricity cost.

Frangopolous and Caralis (1997) developed enviroeconomic method which considers the environmental aspects by internalizing external costs caused by pollutants for energy-intensive systems. They presented main classes of economic approaches for environmental protection through assessing the unit cost of reducing pollutants by abatement technologies. They have concluded that the introduction of environmental technologies will result in a considerable reduction of the energy system cost effectiveness. Moreover they have determined that the pollution charges will affect the economic stability of the energy systems and that the incentives for environmental investment would be provided as the economic viability improves.

Valero (1998) and Sciubba (1999) built on this analysis with exergoecological analysis and extended exergy accounting by introducing additional concepts such as the pyhsico-

mathematical reasoning which underpins the theory of cost allocation through conceptual studies. In the exergoecological analysis, they include the calculation for exergy of natural resources starting from a reference environment through its life cycle along with the exergetic cost of the replacement with currently available technology of the materials used.

Meyer et al. (2009) and Petrakopoulou et al. (2011) conducted exergoenvironmental analysis by taking life cycle of components into account through a cradle to grave environmental impact assessment (using Eco-indicator 99) for energy conversion systems. They calculated various exergoenvironmental variables and provided recommendation on the system designs based on these variables. They used case studies including a high temperature solid oxide fuel cell integrated with an allothermal biomass gasification process, and combined cycle power plant with chemical looping technologies respectively.

Tsatsaronis and Morosuk (2008a, 2008b) introduced so called advanced exergoenvironmental analysis (analogous to advanced exergoeconomic analysis) by splitting the exergy destruction and the component related environmental impact into avoidable/unavoidable and endogenous/exogenous parts and demonstrated the concepts through basic case studies. Boyano et al. (2012) applied both conventional and advanced exergoenvironmental analyses on a steam methane reforming reactor for hydrogen production and suggested design improvements based on the environmental impacts associated with the avoidable parts of exergy destruction. They determined that the chemical reaction in the combustion chamber is the most significant source of exergy destruction, which can be reduced by reducing the percentage access air and by preheating the reactants. They also calculated that the real potential for improving the component-related pollutant formation within the reformer to be only 2% based on the corresponding avoidable environmental impacts for the component.

Tsatsaronis (2011) compiled a book chapter on exergoeconomic and exergoenvironmental analysis where the he described the methodology for conducting both of the analyses in detail with descriptions and used them on a compression refrigeration machines case study. He introduced the exergoeconomic and exergoenvironmental models using annual total revenue (as total product costs) and LCA (as eco-indicator points) and described how they could be used to

evaluate the system accordingly. He also included advanced exergetic analysis, where the exergy destruction is split for each component into endogenous/exogenous and avoidable/unavoidable parts in order to determined where the design improvements should be focused the most in order to reduce the overall exergy destruction and investment costs. Subsequently, the advanced exergetic analysis is used to determine the avoidable endogenous, avoidable exogenous, unavoidable endogenous and unavoidable exogenous costs.

Lazaretto and Toffolo (2004) compared a single-objective thermo-economic optimization with two-objective energetic and economic optimization for thermal system designs using energy, economy and environment as separate objectives. They analyzed a test case plant of the CGAM problem with respect to three-objective approach. The environmental impact objective function was defined with respect to weight of carbon dioxide and nitrogen oxide emissions and an evolutionary algorithm was used to find the surface of the optimal solutions based on the three objective functions. They determined the Pareto optimal curve for the multi-objective optimization and discussed possible points on the curve based on the trade-off between the total cost and environmental impact.

Berhane et al. (2009) proposed a systematic method based on mathematical programming for the design of environmentally conscious absorption cooling systems with respect to a multi-objective formulation that simultaneously accounts for the minimization of cost and environmental impact at the design stage. The environmental impact criterion was measured by the Eco-indicator 99 methodology, which follows the principles of life cycle assessment (LCA). They used bi-criteria nonlinear programming problem and the solution of which is defined by a set of Pareto points. They picked three points on the Pareto optimal curve that represents the minimum Eco-indicator solution (A), minimum total cost solution (B) and a possible trade-off solution between the two points (C). They have calculated that by switching from solution B to solution C, the total Eco-indicator 99 value is reduced by 3.8% at the expense of 4.8% increase in the total cost.

Saayaadi and Nejatolahi (2011) analyzed cooling tower assisted vapor compression refrigeration machines with respect to total exergy destruction and total product cost objective functions. They

used energy and exergy analyses for the thermodynamic model and incorporated Total Revenue Requirement (TRR) for the economic model. They have optimized the system with respect to single-objective thermodynamic, single-objective economic and multi-objective criteria. For the multi-objective optimization, they selected final solutions from the Pareto frontier curve. Finally, they compared the results obtained from the three optimizations and calculated that the percentage deviation from ideal results for thermodynamic and economic criteria are 0.00% and 40.09% for thermodynamically optimized system, 82.46% and 0.00% for economically optimized system and 22.51% and 10.37% for the multi-objective optimized system and therefore determined that the multi-objective optimization satisfies the generalized engineering criteria more than the other two single-objective optimized designs.

Ahmadi et al. (2011) conducted a comprehensive exergy, exergoeconomic and environmental impact analysis and a multi-objective optimization for combined cycle power plants (CCPPs) with respect to the exergy efficiency, total cost rate and CO_2 emissions of the overall plant. They determined that the largest exergy destructions occurred in the CCPP combustion chamber and that increasing the gas turbine inlet air temperatures decreases the CCPP cost of exergy destruction. They derived the expression for the Pareto optimal point curves for the determined exergy efficiency range and concluded that the increase in total cost per unit exergy efficiency is considerably high after exergy efficiencies over 57% and therefore a point below this should be chosen on the Pareto optimal curve.

Sayyaadi and Babaelahi (2011) analyzed a liquefied natural gas re-liquefaction plant with respect to multi-objective approach which simultaneously considers exergy and exergoeconomic objectives. They used MATLAB multi-objective optimization algorithm of NSGA-II, which is based on the Genetic Algorithm, and obtained Pareto optimal frontier to find the Pareto optimal solutions. They compared the final optimal system with the base case and exergoeconomic single-objective optimized system and found that the exergetic efficiency in the multi-objective optimum design is 11.11% higher than that of the exergoeconomic optimized system, while the total product cost of the multi-objective optimal design is 16.7 higher than that of the exergoeconomic optimal system.

Even though there are several studies in the literature that utilizes exergy analysis to evaluate the system efficiencies, they are not currently used in any EV and HEV thermal management system applications. Moreover, even most of the studies conducted on conventional vehicle air conditioning systems do not provide any information on the interdependencies of the components used in the system and the portion of the system inefficiencies that could be avoided. Furthermore, the exergy analysis is mostly used to evaluate the efficiencies of the system and suggest recommendations without any information on the cost and environmental impact it would require for implementing these enhancements. Therefore, a conventional and advanced exergetic and exergoeconomic analyses along with exergoenvironmental analysis are conducted in this thesis, where the component level irreversibilities are divided into endogenous/exogenous and avoidable/unavoidable portions to provide more in depth information of the inefficiencies, their causes and relationships among the system components as well as creating optimization studies where the efficiency, cost and environmental impact are evaluated for the system with respect to various system parameters.

Chapter 4: Experimental Apparatus for Thermal Management System

In order to understand the EV and HEV thermal management systems, gather data and validate the numerical models, experimentations are conducted under various conditions using both a TMS test bench and a full size vehicle. The experimental setup and process, instrumentations utilized along with the gathered data are described in this chapter.

4.1 Test Bench

Initially, a test bench of Chevrolet Volt thermal management system provided from General Motors was assembled and utilized to examine the components of the system and the relationships within different circuits. The test bench was composed of the full TMS with refrigerant and coolant loops, and the effects of battery and engine is simulated through an auxiliary bench. The components and instrumentation for the main refrigerant loop is provided in Figure 4.1.

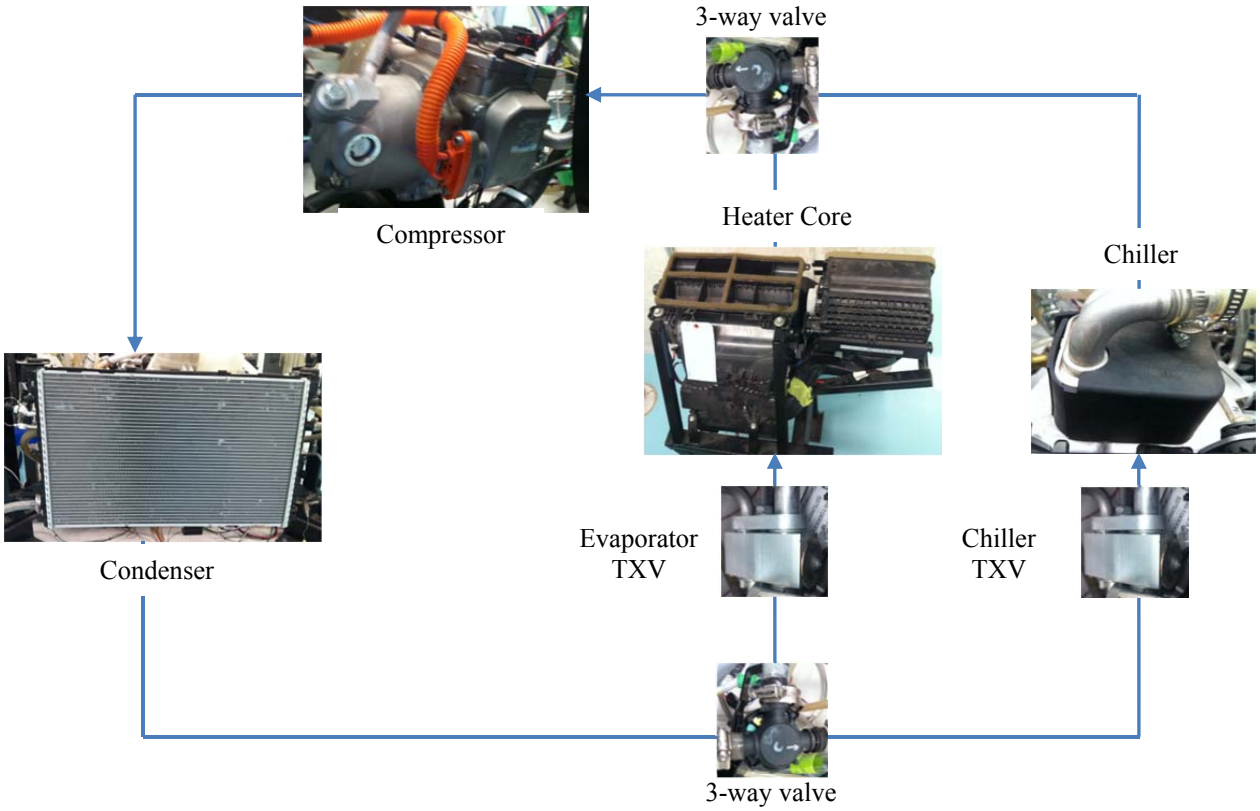

Figure 4.1: Schematic of the test bench refrigerant loop used.

The system components are received and assembled in University of Ontario Institute of Technology (UOIT) facilities, plumbing is inspected for leaks and filled with cooling media (DEX-Cool). Temperature sensors and pressure gauges were placed at critical locations and mass flow rates were measured in points where there is a significant change in the flow. The test bench unit was then connected to the complex engineering bench in order to acquire data and power the electronics used in the test bench. The schematic of the experimental setup is provided in Figure 4.2.

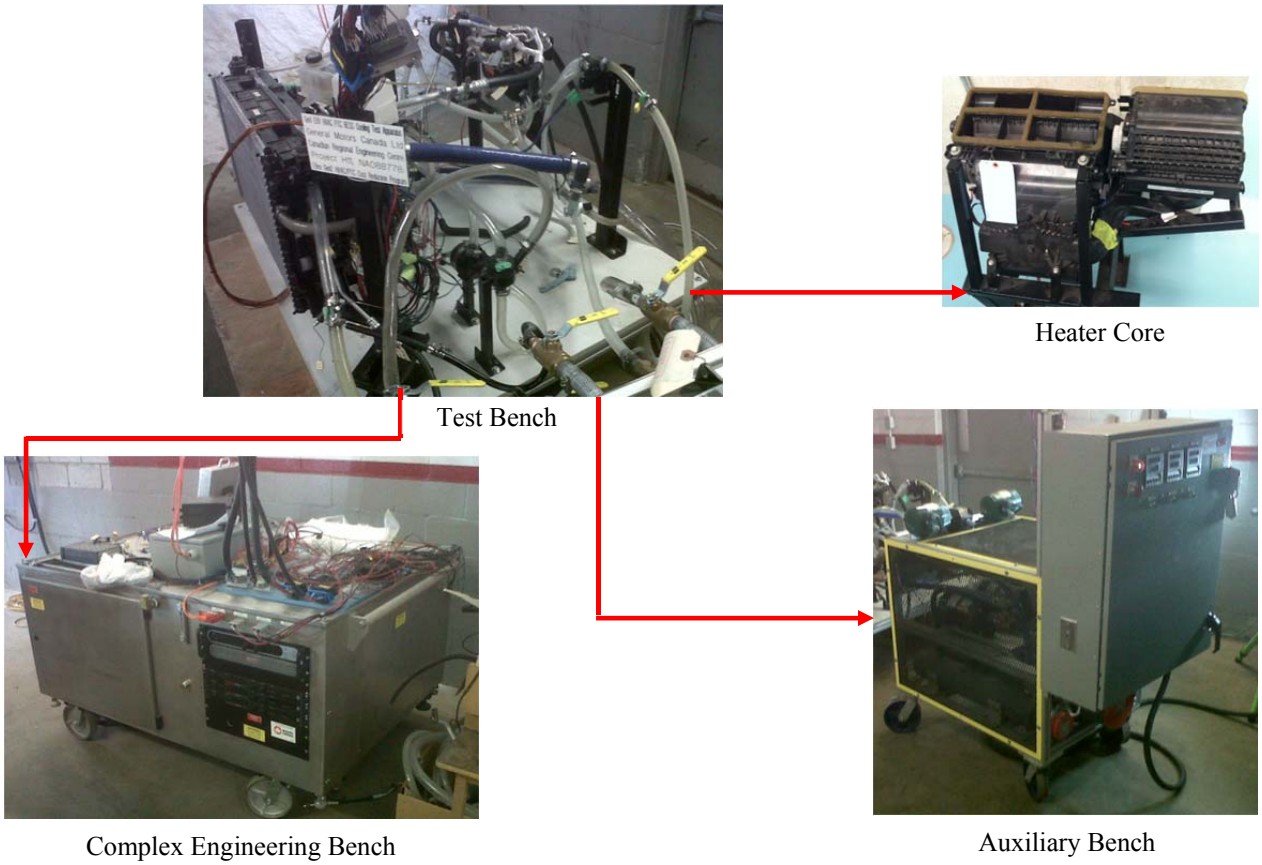

Figure 4.2: Schematic of the experimental setup.

The test bench is then used to obtain data on the system and gain a more profound understanding of the key parameters associated with the TMS. A sample data acquired from the test bench for a scenario where the electric battery is fully drained using the auxiliary bench is provided in Section 6.2.3.

4.2 Production Vehicle

Aside from the test bench, a production vehicle (Chevrolet Volt Gen 1) was also provided by General Motors along with an IPETRONIK data acquisition system and numerous sensor and gauges. The vehicle provided was a 2011 5-door hatchback hybrid electric vehicle (in series configuration) with 1.4L 84 HP internal combustion engine and 16 kW-h (9.4 kW usable) lithium-ion electric battery. The vehicle electric two-wheel and front drive types and had 111 kW drive motor and 54 kW generator motor. It provides 40 – 80 km range in charge-depleting mode. A picture of the vehicle is shown in Figure 4.3.

Figure 4.3: Vehicle used in the experimental analyses.

The lithium-ion battery used was a 198 kg and 1.7 meter long T-shaped battery with glass-filled polyester structural composite with aluminum thermal radiation shield and steel as casing located under the rear seats. It incorporated 288 individual prismatic lithium-ion manganese-spinel ($LiMn_2O_4$) cells arranged in 9 modules, where each cell is less than 6.35 mm thick and measure approximately 127x178 mm with less than 0.45 kg weight. The battery takes approximately 4 hours to charge using 240 V and has maximum and minimum state of charge levels of 85% and 30% respectively. A picture of the battery is provided in Figure 4.4.

Figure 4.4: Battery used in the experimental analyses (courtesy of General Motors).

The test vehicle used a liquid active thermal management system (described in Section 2.4.4) using DEX-Cool (50/50 water glycol mix) on the battery coolant loop to keep the battery operating within the ideal temperature range. In the refrigerant loop, R134a was used to provide air conditioning to the cabin and remove the heat from the coolant loop when necessary. Moreover, an engine loop is used to keep the engine cool by the mixture of water and anti-freeze pumped into the engine block in order to draw the excess heat away from the crucial areas. In addition, a power electronics loop was used for cooling the battery charger and the power inverter module to ensure the main under-hood electronics do not overheat during usage. The schematic of the thermal management system loop in the vehicle are provided in Figure 4.5.

In the figure, the numbers represent the locations where the temperature sensors (℃), pressure gauges (kPa) or anemometers and flow meters (kg/s) are placed. Moreover, voltages (V) and currents (A) are measured where the power output was necessary.

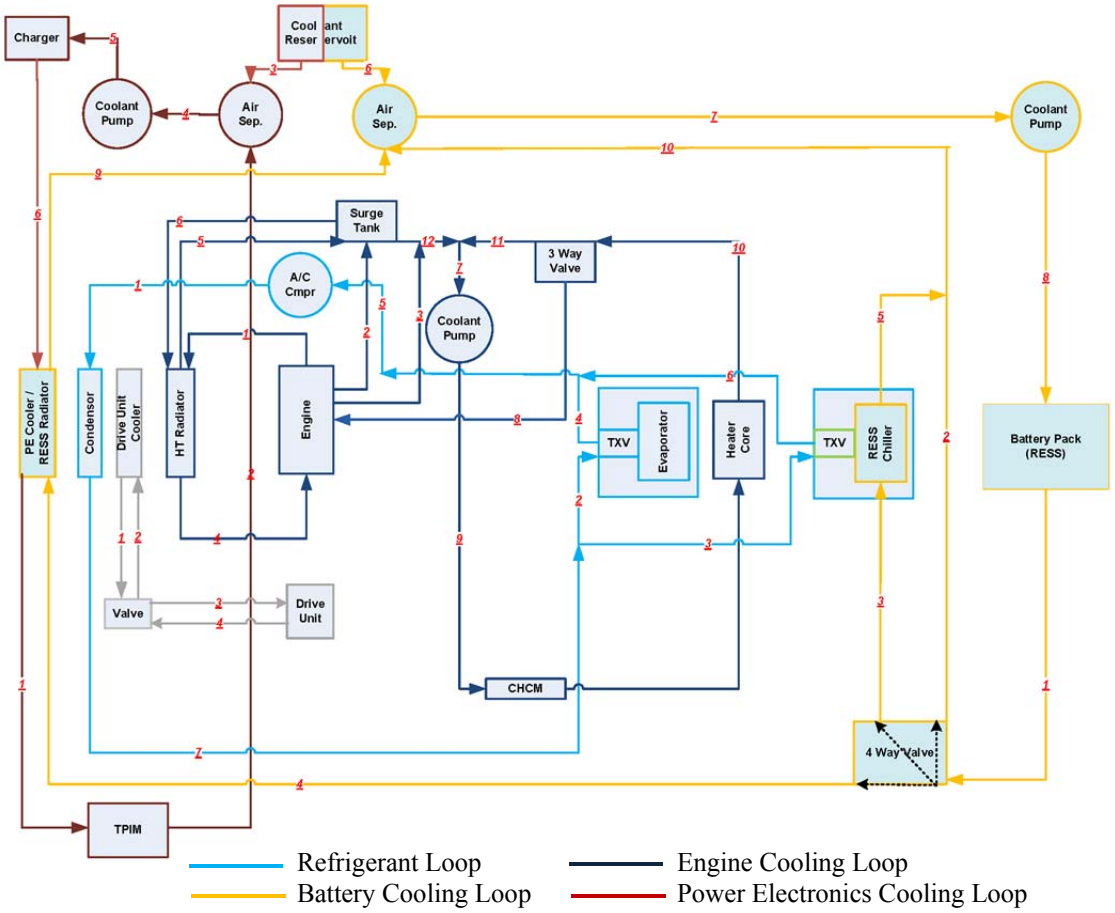

Figure 4.5: Experimental setup of the electric vehicle thermal management system.

In order to gather data, IPETRONIK data acquisition system is used for the experimentations. The simplified schematics on how the IPETRONIK work is shown in Figure 4.6.

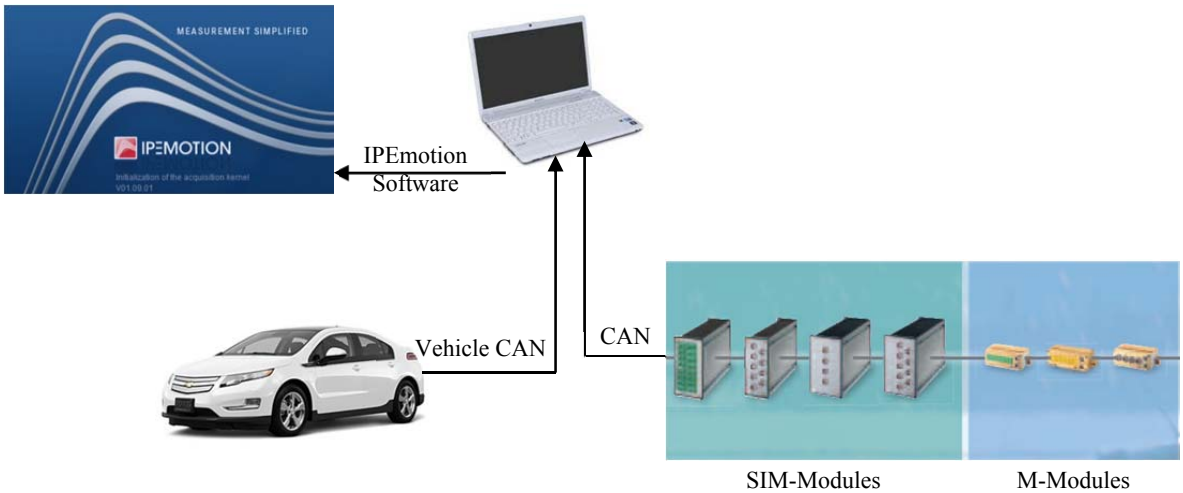

Figure 4.6: Application of IPETRONIK in the vehicle (modified from IPETRONIK catalogue).

In the IPETRONIK system, M-Series hardware is used for the measurements which include M-THERMO, M-SENS and M-FRQ. This modular system is placed in the trunk of the vehicle and is powered by a 12 V power supply which draws its power form the vehicle. All the sensors, gauges and flow meters that are placed in the thermal management system are wired through the vehicle to the trunk and are labeled with respect to their type and position. The IPETRONIK system in the vehicle can be seen in Figure 4.7.

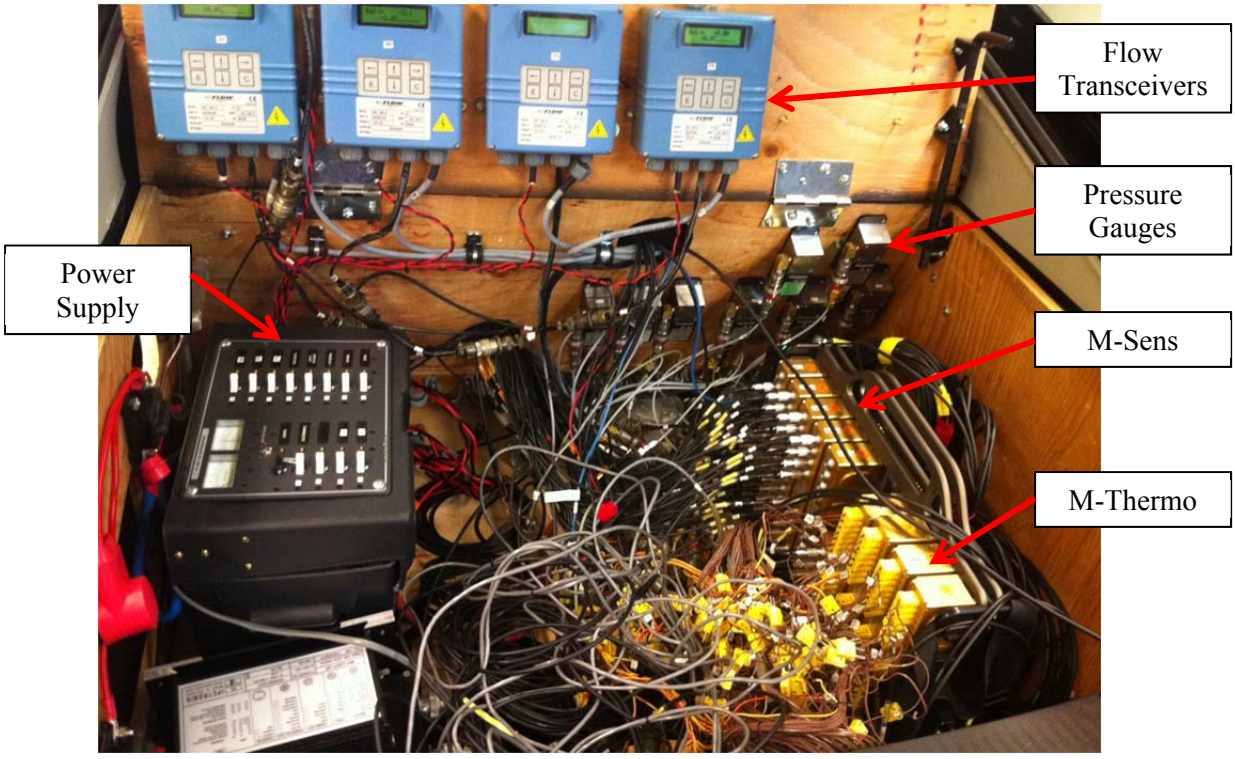

Figure 4.7: IPETRONIK data acquisition system installed in the trunk of production Chevrolet Volt.

In the TMS, 82 M-THERMO K-type (16 Channel ANSI) thermocouples are used for measuring the temperature before and after every major component in the vehicle. These thermocouples have 16-bit analog converter and can measure as low as -60℃. In addition, 12 Validyne P2 pressure transducers are used in the TMS lines in order to determine the associated pressure values in the system along with the pressure drop through the components. These pressure transducers have 0.25% accuracy and temperature compensation and can operate between -20℃ and 80℃ temperature ranges, which cover the majority of the temperatures reached in the experimentation. The accuracy of the transducers decreases as they deviate from these temperature ranges. Moreover, 4 M-Sens 8 (8 channel) voltage/current sensors are utilized in the

experimentation in order to determine the corresponding mass flow rates associated with the refrigerant and coolant in the system. These sensors have 11 voltage 2 current measuring ranges and work on a high speed CANbus. Furthermore, 12 M-FRQs are used which have 4 signal inputs with adjustable ON and OFF threshold and anemometers are placed on the condenser to determine the amount of air flow to the system. They have the measurement modes of frequency from period duration, plus duration, pause duration and duty cycle and can measure data output to CANbus (high speed). The M-FRQ's have 4 inputs with the ranges of 1±4 V in 250 mV steps and 1±40 V in 200 mV steps (IPETRONIK catalog, 2009). The IPETRONIK sensors used are provided in Figure 4.8.

M-Thermo M-Sens Pressure Transducers

Figure 4.8: Sensors used in the IPETRONIK system.

Furthermore, in order to record the flow rate in the system, 5 Flow Technology electromagnetic transmitters (MC106A) were placed in the vehicle. The electromagnetic flow meter (EL 4000 series) with 3/4" line size was installed to the vehicle, the sensor and converter is grounded and isolated from any source of vibrational and magnetic noise for the system to operate correctly. When started, the measured lines are completely filled with the associated cooling media and ensured that there is no flow in order to calibrate the equipment and ensured a compatible sample rate is selected for each device. The flow readings were being read through the flow transmitter as well as the IPEmotion software package. The picture of one of the flow transceivers used is shown in Figure 4.9.

Figure 4.9: Picture of one of the five flow transceivers used in the experimentation.

In the vehicle, these sensors and gauges are placed at every crucial location of the thermal management system in order to gather reliable data of the temperature, pressure and mass flow rates. The list of the sensors and their locations is provided in Table 4.1.

Table 4.1: Instrumentation details of the experimented Chevrolet Volt.

Channel Name	Channel Description
RadInCool	Radiator Inlet Coolant - ℃
RadOutCool	Radiator Outlet Coolant - ℃
TrnAuxOilCoolAI	Transmission Aux Oil Cooler Air Inlet - ℃
TrnAuxOilCoolAO	Transmission Aux Oil Cooler Air Outlet - ℃
TrnAuxOilCoolFl	Transmission Aux Oil Cooler Air Fluid - ℃
TrnAuxOilCoolFO	Transmission Aux Oil Cooler Air Fluid - ℃
GrilleOATSens	Grille at AOT Sensor - ℃
CowlAI	Cowl Inlet Air - ℃
FrtBlwrAO	Front Blower Outlet Air - ℃
CompOut	Compressor Outlet Stinger - ℃
CondOut	Condenser Outlet Stinger - ℃
FrtEvapInPipe	Front Evaporator Inlet Pipe Stinger - ℃
FrtEvapOutlet	Front Evaporator Outlet Stinger - ℃
CompIn	Compressor Inlet Stinger- ℃

RrEvapLnPipe	Rear Chiller / Evaporator Inlet Pipe Stinger- ℃
RrEvapout	Rear Chiller / Evaporator Outlet Stinger- ℃
FrtHtCorFl	Front Heater Core Inlet Fluid - ℃
FrtHtCorFO	Front Heater Core Outlet Fluid - ℃
Cond_Aln_Grid_1 through 12	Condenser Air In Grid #1 - #12 ℃
Cond_AOutGrid_1 through 12	Condenser Air Out Grid #1 - #12 ℃
Rad_AlnGrid_1 through 5	Radiator Air In Grid #1- #5 ℃
Rad_AlnGrid_1 through 5	Radiator Air Out Grid #1- #5 ℃
FrtEvapInGrid_1 through 9	Front Evaporator Air In Grid #1 - #9 ℃
FrtEvapAOGrid_1 through 9	Front Evaporator Out Grid #1 - #9 ℃
FtHtrCoreAlGrd_1 through 6	Front Heater Core Air in Grid #1 - #6 ℃
FtHtrCoreAOGrd_1 through 6	Front Heater Core Air out Grid #1 - #6 ℃
Comp_Out_P	Compressor Outlet (0-500 psig) kPa
Cond_Out_P	Condenser Outler (0-500 psig) kPa
Evap_Frt_In_P	Front Evaporator Inlet (0-1000 psig) kPa
Evap_Frt_Out_P	Front Evaporator Outlet (0-100 psig) kPa
Comp_In_P	Compressor Inlet (0-100 psig) kPa
Evap_Rr_In_P	Rear Chiller/Evaporator Inlet (0-100 psig) kPa
Evap_Rr_Out_P	Rear Chiller/ Evaporator Outlet (0-1000 psig) kPa
TransCoolIn_P	Transmission Cooler Inlet – kPa
TransCoolOut_P	Transmission Cooler Outler – kPa
Rad_In_P	Radiator Inlet – kPa
Rad_Out_P	Radiator Outlet – kPa
FrHeatCoreIn_P	Front Heater Core Inlet – kPa
FrHeatCoreOut_P	Front Heater Core Outlet – kPa
Frt_Blower_V	Left/Main Cooling Fan – V
CoolingFan_Lt_A	Left/Main Cooling Fan – A
CoolingFan_Rt_V	Right Cooling Fan – V
CoolingFan_rt_A	Right Cooling Fan – A
TransOilCool_lpm	Transmission Oil Cooler (3/4” Turbine) – lpm
Radiator_lpm	Radiator – (1 - 1/2” Magnetic) lpm
TPIM_lpm	TPIM_Coolant – (3/4” Magnetic) lpm
FrtHeatCore_Return_lpm	Front Heater Core Return to Engine (3/4” Magnetic) – lpm
Cond_Fan_Freq_1 through 12	Condenser Anemometer #1 - #12 FREQ

In order to acquire data shown above from IPETRONIK, IPEmotion Developer Version 01.03 is used. IPEmotion is software package for configuring, displaying, measuring and storing acquisition data (IPEmotion manual, 2010). The signals are acquired by using manufacturer application layer which is a plug-in component made of several dynamic link library files along with description files in XML format.

In the software, the configuration is defined using the project properties. For all the signals, sampling rates of 5 Hz is used as it is the recommended sampling rate (due to its optimal accuracy and frequency) for this particular application based on the IPETRONIK manual. Subsequently, the corresponding units are selected for the channels. Next, the maximum and minimum displaying ranges of the acquisition value are defined. Using the scaling calculator, the voltages are being able to accurately converted to the corresponding measurement units for the setup. The limits for each value is determined and logged in to the software. The limit violations are recorded and are reset by the software when the signal returns to the set range by passing a hysteresis of 2%.

The data manager main navigation tab is used to manage and analyze the acquired data. Loaded acquisition data sets are then converted to excel format through the export function. Finally, the analysis tab is used to visualize the data by using the software charts as shown in Figure 4.10. Once the data is acquired and stored using IPEmotion, it is used to evaluate the vehicle performance.

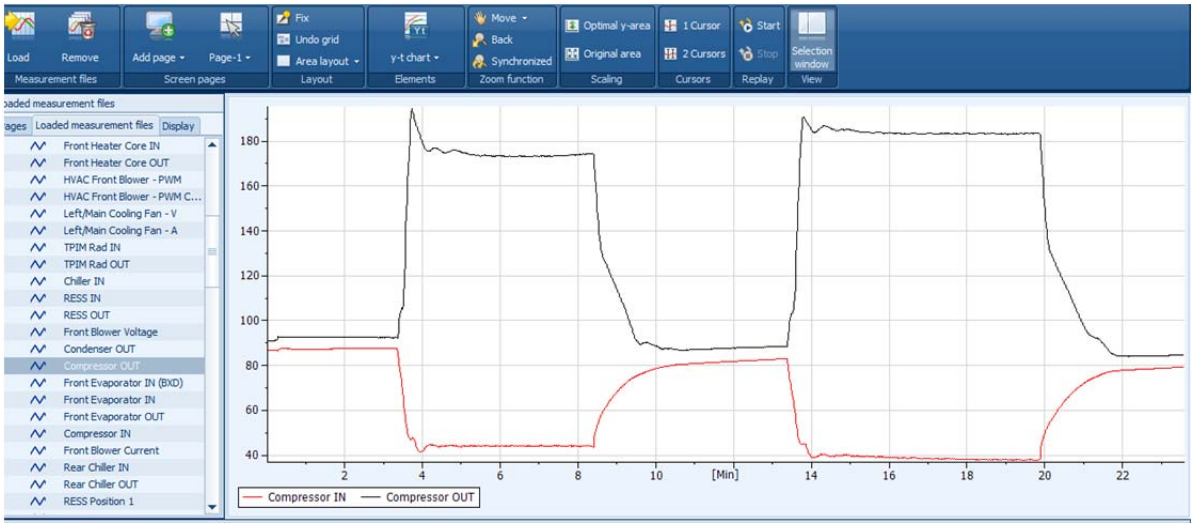

Figure 4.10: IPEMotion main tab.

Moreover, neoVI RED device with Vehicle Spy 3 software package (NeoVI, 2006) is used to monitor the high speed and medium speed controller area network (CAN) busses in the vehicle in order to log the associated signals. The list of obtained data is given in Table 4.2.

Table 4.2: List of medium speed CAN bus signals received from the vehicle.

Channel Name	Channel Description
OAT	Outside Ambient Temperature - ℃
HVBat_Max_Temp	Battery Maximum Temperature - ℃
HVBat_Min_Temp	Battery Minimum Temperature - ℃
RadInCool	Compressor High Side Pressure – kPa
HVBat_SOC	Battery State of Charge - %
HVBat_Proc_Voltage	Battery Processed Voltage – V
HVBat_Proc_Current	Battery Processed Voltage – A
Comp_Volt	Compressor Voltage – V
Comp_Current	Compressor Current – A
Comp_Pwr	Compressor Power – kW
Comp_Speed	Compressor Speed – RPM

Finally, numerous experiments under different scenarios are conducted in order to gather a wide range of data of the vehicle thermal management system from both CAN Busses. The experimentation procedure is defined similar to the ones set by GM and experimental analyses conducted in the literature for ease of comparison. Key parameters are varied systematically in order to record the associated changes in the system and new tests are conducted once the system reaches back to its steady state. These obtained data were used to re-validate the numerical analysis and further improve it by creating a more accurate representation of the actual vehicle system. A portion of the recorded sample data set is provided in Section 6.2.3 for reference and is obtained through the following scenario.

- The vehicle is turned on and data acquisition started.
- The heater and fan are fully turned on for t_1 seconds.
- The heater and fan are turned off until the parameters return to the initial state.
- The air conditioner and fans are fully turned on for t_2 seconds.
- The air conditioner and fans are turned off until the parameters are returned to the initial state.
- The data acquisition system is stopped.

Chapter 5: Model Development

5.1 Introduction

The efficiency of the thermal management systems in EVs and HEVs has great importance due to the limited supply of available energy onboard as well as the overall impact on vehicle performance, operational cost and the environmental impact. Thus, it is imperative to have a good understanding of the efficiencies associated with the system and its components. In this regard, energy-based efficiencies may lead to inadequate and misleading conclusions, since all energy forms are taken to be equal and the ambient environment is not taken into consideration. The second law of thermodynamics defines the energy conversion limits of this available energy based on irregularities between different forms of energies. The quality of the energy is highly correlated to the reference environment as well as the success level of this conversion capacity, and needs to be considered to prevent any incomplete and/or incorrect results. An analysis for examining the work potentials of the initial and final stages of a system can give an evaluation criterion for the quality of the energy. Such analysis is called "exergy analysis", which represents the amount of energy that may be totally converted to work (Arcaklioglu et al., 2005; Ozkaymak et al., 2008).

Exergy (also called available energy or availability) of a system is the "maximum shaft work that can be done by the composite of the system and a specified reference environment" (Dincer and Rosen, 2007). In every thermal management system, heat transfer within the system, or between the system and surrounding environment, occurs at a finite temperature difference, which is a key contributor to irreversibilities for the system. All real processes, including natural events are irreversible and the system performance degrades as a result of these irreversibilities in each individual thermodynamic process that makes up the system. The work potential is reduced by the irreversibilities and the corresponding amount of energy becomes unusable (Arcaklioğlu et al., 2005). Entropy generation measures the effect of these irreversibilities in a system during a process and helps compare each component in the system based on how much they contribute to the operation inefficiencies of the overall system. Therefore, entropy generation associated with

each process needs to be evaluated to determine the overall system efficiency. Even though energy analysis is the most commonly used method for examining thermal systems, it is only concerned with the conservation of energy, which neither takes the corresponding environmental conditions into account, nor provides how, where and why the system performance degrades. Consequently, the energy analysis only measures the quantity of energy and does not reveal the full efficiencies of the system (Yumrutas et al., 2002). Thus, in this research, the thermal management system will be examined with respect to exergy analysis in order to better understand the true efficiencies of the components by determining the irreversibilities in each cycle, as well as the overall system and how nearly the respective performances approach ideal conditions. By analyzing both the quality (usefulness) and the quantity of the energy, the true magnitude of losses, and their causes and locations are identified by investigating the sites of exergy destruction in order to improve the individual components and overall system (Dincer and Rosen, 2007; Yumrutas et al., 2002).

Before conducting any analysis on the studied thermal management system, the system configuration is first needed to be introduced and the system parameters are needed to be properly defined. The description of the studied thermal management system is provided in the following section.

5.2 System Configuration

Hybrid electric vehicle thermal management systems (HEV TMSs) are significantly different systems with unique requirements with respect to their commercial and industrial counterparts such as conventional vehicle and residential building air conditioning systems. The TMS needs to handle significant thermal load variations and provide comfort under highly fluctuating conditions, as well as be compact and efficient, and last several years without any significant maintenance. Moreover, the airflow volume, velocity and temperature must be adjustable over a wide range of ambient temperatures and drive cycles without having a significant impact on the all-electric vehicle performance characteristics. Furthermore, due to the limited time spent in the vehicles compared to buildings, along with the competing energy requirements between the cabin and the battery, the thermal management systems must be capable of conditioning the air in the passenger cabin quickly and quietly, while keeping the vehicle components operating

under ideal operating temperature ranges (especially the electric battery) to prolong their lifetime, increase the fuel efficiency and all electric range. Thus, special attention needs to be given to hybrid electric vehicle TMSs (Jabardo et al., 2002; Wang et al., 2005).

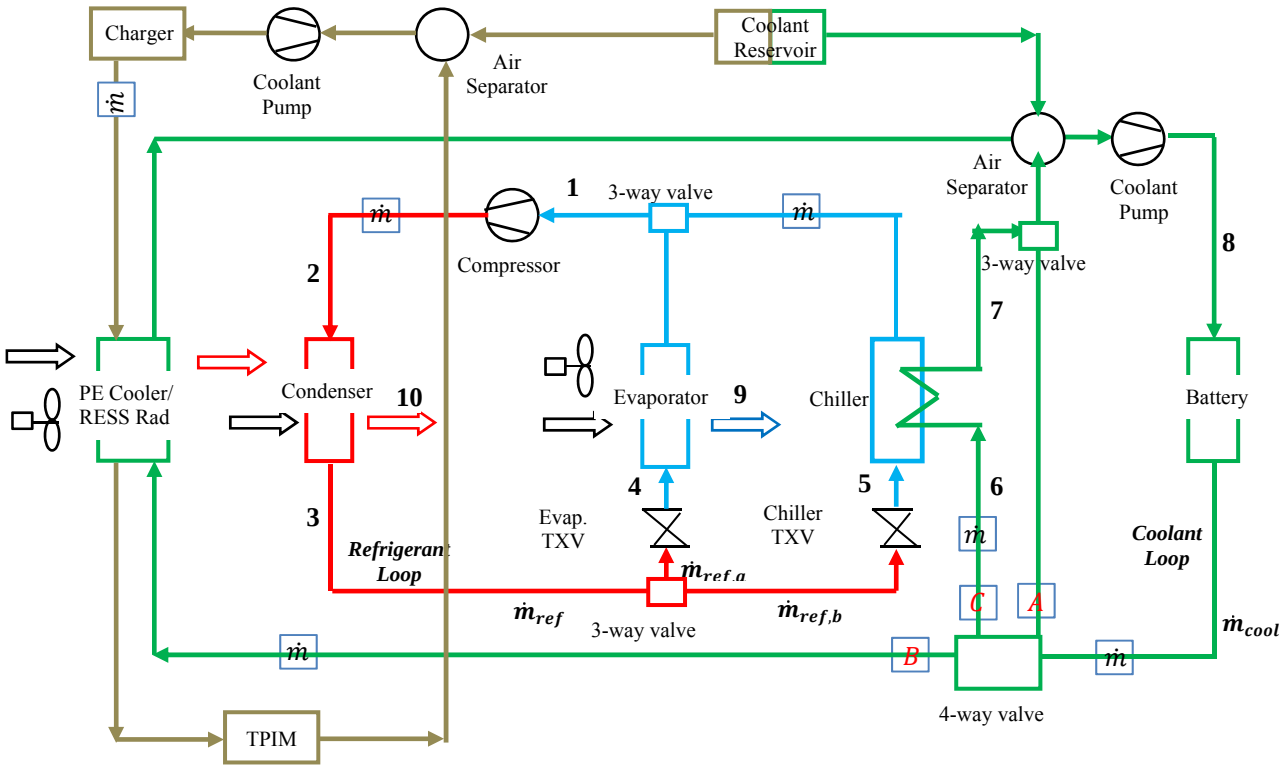

Figure 5.1: Simplified representation of the hybrid electric vehicle thermal management system.

A simplified thermal management system of an electric vehicle with liquid battery cooling is considered in Figure 5.1. The system is composed of two loops, namely a refrigerant and battery coolant loop. The refrigerant loop enables air conditioning of the vehicle cabin, while the coolant loop keeps the electric battery operating within its ideal temperature range. These two loops are connected via a chiller, which enables heat exchange among the loops to provide supercooling to the battery cooling as it passes through the chiller unit. This increases the efficiency of the system significantly since cooling via refrigeration circuit would consume more energy than operating the battery coolant circuit due to the need of the air compressor in the first case (Behr, 2012).

The thermal management system incorporates the advantages of both the air cooling and refrigerant based cooling with the help of the additional battery cooler and chiller. The additional cooling loop is kept cool via different procedures depending on the cooling load and ambient conditions. If the battery coolant circuit has stable temperatures within the ideal range, then it bypasses the thermal management systems and only re-circulates before getting pumped into the battery (Route A as shown in Figure 5.1). This loop permits temperature stability by controlling cell temperatures through pump control. When the battery temperature is high and the ambient temperature is lower than the desired temperature of the battery, the ambient air flow in the battery cooler is used to keep this coolant circuit cool (Route B). If the battery temperature is significantly higher and the ambient temperature is higher than the desired battery temperature, then by operating the electric air conditioning (A/C) compressor, R134a refrigerant is throttled by the thermal expansion valve (TXV) to permit super-cooling of the battery coolant as it passes through the chiller unit (Route C). This increases the efficiency of the system significantly since cooling via a cooling circuit would consume more energy than operating the battery coolant circuit due to the need of the air compressor in the first case (Behr, 2012).

The system includes three cooling media – an R134a refrigerant is used in the refrigerant cycle, water/glycol mixture of 50/50 by weight is used in the battery coolant cycle, and ambient air is utilized in the evaporator and condensers in the system. In the baseline model, ambient air conditions of 35ºC and 1 ATM are used to study the effects of the TMS on the battery. The refrigerant mass flow rates are determined from thermal expansion valve correlations and the cooling capacity is calculated accordingly. For the baseline model, the temperature of the passenger cabin is set at 20ºC. Temperatures of 5ºC and 55ºC are used for evaporating and condensing temperatures along with 5ºC superheating and subcooling in the evaporator and condenser, respectively. The refrigerant mass flow rate in the chiller is determined with respect to the amount of battery heat transferred from the water/glycol mix in the coolant circuit to the refrigerant circuit via the chiller. In the refrigerant cycle, the refrigerant flow in the evaporator and chiller is combined in the system before it is compressed to the condenser. For the coolant circuit, the battery coolant temperature is assumed to be 19ºC (since it operates in a temperature range of 19ºC to 25ºC) before entering the battery, and the heat generated by the battery is considered to be 0.35 kW (Kobylecky, 2011), where the mass flow rate of the battery coolant is

determined accordingly. When the system is subdivided into its components, it is mainly composed of a compressor, heat exchangers, thermal expansion valves, pump and the battery. These components are described in more detail below. The coolant pump is not described further due to its relatively negligible impact on the overall system.

5.1.1 Major Components

5.1.1.1 Compressor

The compressor is a main component of the air conditioning system. A magnetic clutch is located at the front of the compressor and used to engage it when power is provided to the system (Kaynakli and Horuz, 2003). In the analysis, a scroll type compressor is used and modeled with respect to the isentropic efficiency correlation as follows (Brown et al., 2002):

$$\eta_s = 0.85 - 0.046667\,\theta \tag{5.1}$$

Moreover, by using the ideal polytrophic equation for adiabatic and isentropic compression and with the assumption of ideal behavior for the compressor suction port gas, the following relationship can be obtained between the discharge and suction temperatures (Bhatti, 1999).

$$\frac{T_{discharge}}{T_{suction}} = 1 + \frac{1}{\eta_s}\left[\theta^{1-(1/\gamma)} - 1\right] \tag{5.2}$$

The above equations show that the refrigerants with lower pressure ratios ultimately result in a higher compression efficiency which then increases the COP of the system. Also, for a given pressure ratio, higher isentropic efficiencies lead to a lower compressor discharge temperature which results in lower compressor work, and consequently higher COP of the system.

5.1.1.2 Heat Exchangers

There are three heat exchangers in the TMS, namely the condenser, evaporator and chiller. The condenser is located in front of the radiator and the evaporator is located adjacent to the passenger compartment to condition the cabin. The chiller is placed between the air conditioner

and battery loops and has coolant on one side and the refrigerant on the other. For the analysis, the following assumptions will be made to determine the heat transfer coefficients and pressure drops:

- The heat exchangers operate under steady-state conditions.
- The heat losses to surroundings are negligible.
- The changes in kinetic and potential energies of the fluid stream are negligible.
- There is no fouling.
- The temperature of the fluid is uniform over the flow cross section.
- There are no thermal energy sources and sinks in the heat exchanger walls or fluids.
- The velocity and temperature at the entrance of the heat exchanger on each fluid side are uniform.
- The overall heat exchanger surface efficiency is assumed uniform and constant.

The overall heat transfer coefficient is determined as follows:

$$\frac{1}{UA} = \frac{1}{\eta_i A_i \bar{h}_i} + \frac{\delta_w}{k_w A_w} + \frac{1}{\eta_o \bar{h}_o A_o} \tag{5.3}$$

Since the wall thickness of the tube is small and the thermal conductivity of the tube material is high, the thermal resistance of the tube is negligible and therefore the equation can be simplified as follows:

$$\frac{1}{U} = \frac{A_o}{\eta_i A_i \bar{h}_i} + \frac{1}{\eta_o \bar{h}_o} \tag{5.4}$$

In the above equation, the internal efficiency (η_i) is set equal to 1 since the channels with smooth internal surfaces have been assumed in the study. The finned heat transfer surface efficiency (η_o) is given by the equation below:

$$\eta_o = 1 - \left(\frac{A_{fin}}{A_o}\right)\left(1 - \eta_{fin}\right) \tag{5.5}$$

In addition, the internal heat transfer coefficients ($\bar{h}$) associated with the refrigerant in the heat exchangers are determined based on the correlation below (Dittus and Boelter, 1930):

$$\bar{h}_{evap,i} = \frac{3.6568k}{D_i} \qquad for\ 0 < Re < 2000 \qquad (5.6a)$$

$$\bar{h}_{cond,i} = \frac{4.3636k}{D_i} \qquad for\ 0 < Re < 2000 \qquad (5.6b)$$

$$\bar{h}_{evap\ or\ cond,i} = \frac{k}{D_i} \cdot \frac{0.5\ f\ (Re - 1000)Pr}{1 + 12.7\ (0.5\ f)^{0.5}\left(Pr^{\frac{2}{3}} - 1\right)} \qquad (5.6c)$$

where

$$f = 0.054 + 2.3 \times 10^{-8}\ Re^{3/2}\ for\ 2300 < Re < 4000 \qquad (5.6d)$$

$$f = 1.28 \times 10^{-3} + 0.1143\ Re^{-0.311}\ for\ 4000 < Re < 5 \times 10^{6} \qquad (5.6e)$$

In the above equations, Pr is the Prandtl number. On the air side, the heat transfer coefficients ($\bar{h}_o$) for the condenser and evaporator are calculated for forced convection by the correlation below (Churchill and Chu, 1975):

$$\bar{h}_0 = \frac{k}{D_o} \cdot \left[0.6 + \frac{0.387\ Ra^{\frac{1}{6}}}{\left(1 + (0.559/Pr)^{\frac{9}{16}}\right)^{\frac{8}{27}}}\right]^2 \qquad (5.7)$$

where Ra is the Rayleigh Number:

$$Ra = \Pr\ g\ \beta\ (T_0 - T_w)D_o^3/v^2 \qquad (5.8)$$

here, g is the gravitational acceleration, β is the coefficient of thermal expansion, D_o is the outer diameter of the tube and v is the specific heat of air.

The total pressure drop in the heat exchanger consists of frictional, acceleration and gravitational components. Assuming the flow is fully developed, the gravitational component is negligible. Moreover, the acceleration effects are significantly smaller than the frictional effects (up to 5 times less), thus only the frictional pressure drop is considered for the study. The pressure drop (in kPas) with respect to the heat exchangers is given below (Lee and Yoo, 2000):

$$\Delta P_{evap} = 6 \times 10^{-6}\, Re_g^{1.6387} \qquad for\ 4000 < Re_g < 12000 \qquad (5.9a)$$

$$\Delta P_{cond} = 6 \times 10^{-8}\, Re_g^2 + 0.0009\, Re_g - 6.049 \qquad for\ 3000 < Re_g < 3 \times 10^4 \qquad (5.9b)$$

where Re_g is the Reynolds number given below:

$$Re = \frac{\dot{m}_{ref}\, D_{in}}{\mu\, A_i} \qquad (5.10)$$

Here, $\dot{m}_{ref}$ is the mass flow rate of the refrigerant, D_{in} is the inner diameter of the tubes, μ is the dynamic viscosity and A_i is the tube cross-sectional area of the heat exchanger.

The air temperatures at the refrigerant evaporating/condensing exit states as well as superheating, desuperheating and subcooling states are determined based on the heating and cooling loads, associated mass flow rates and the respective temperature differences. The temperature differences are calculated based on the log mean temperature difference method (LMTD) for heat exchangers as given below:

$$LMTD = \frac{\left(T_{H,i} - T_{L,o}\right) - \left(T_{H,o} - T_{L,i}\right)}{\ln\left(\frac{T_{H,i} - T_{L,o}}{T_{H,o} - T_{L,i}}\right)} \qquad (5.11)$$

where the subscripts H and L represent high and low temperature sides and i and o refer to "in" and "out", respectively. The thermal performance of heat exchangers is calculated with respect to the effectiveness-NTU method, so the effectiveness is defined as

$$\varepsilon = \frac{\dot{Q}}{C_{min}(T_{hi} - T_{ci})} = 1 - \exp\left[\frac{1}{C^*} NTU^{0.22}(\exp(-C^* \times NTU^{0.78}) - 1\right] \quad (5.12a)$$

$$where\ \ C = \dot{m}C_p, \quad C^* = \frac{C_{min}}{C_{max}} \quad and \quad NTU = \frac{UA}{C_{min}} \quad (5.12b)$$

Here, C is the heat capacity rate, which is the mass flow rate times the specific heat, and C_{min} and C_{max} represents the smaller and larger heat capacity rates among the hot and cold sides, respectively. The heat transfer rates in the heat exchangers ($\dot{Q}$) are determined from the energy balance equations.

$$\varepsilon = \varepsilon_{max} = 1 - \exp(-NTU) \quad (5.13)$$

In the phase change regions of the evaporator and condenser, the effectiveness becomes maximum (ε_{max}) since C_{max} becomes considerably large. From the above equations, it can also be inferred that higher values of ε would require higher values of NTU which inherently means larger heat transfer coefficients on the hot and cold sides of the utilized heat exchangers.

5.1.1.3 Thermal Expansion Valve (TXV)

The thermal expansion valve controls the refrigerant flow into the evaporator via a capillary tube with a thermal bulb that controls the width of the valve by balancing the thermal bulb and refrigerant internal pressures (Kaynakli and Horuz, 2003). In the analysis, the expansion valve is modeled as an orifice through which the liquid is expanded from the condensing to evaporating pressures. The throttling process is assumed isenthalpic since the changes in the sum of potential and kinetic energies between the inlet and outlet are negligible and the heat transfer is relatively small. The associated flow rate (in terms of kg/s) can be correlated as follows:

$$\dot{m}_{ref} = C_{txv} A_{txv} \sqrt{(P_{txv,i} - P_{txv,o})/v_{txv,i}} \quad (5.14)$$

where $P_{txv,i}$ and $P_{txv,o}$ are the inlet and outlet valve pressures respectively. Also, A_{txv} is the flow area (in m^2) which can be calculated by the following equation:

$$A_{txv} = \frac{k_A}{\sqrt{2}C_{txv}} \tag{5.15}$$

where k_A is the thermal expansion valve characteristic parameter that relates to the evaporating temperature by the following correlation (Jabardo et al., 2002):

$$k_A = 5.637 \times 10^{-5} + 1.358 \times 10^{-7} T_{evaporating} \tag{5.16}$$

Moreover, C_{txv} is the valve flow coefficient that is correlated from experimental studies in the literature as follows (Tian and Li, 2005):

$$C_{txv} = 0.187 + 4.84 \times 10^{-7} P_{txv,i} - 0.579 x_{txv,o} \tag{5.17}$$

where $x_{txv,o}$ is the refrigerant quality at the valve exit.

5.1.1.4 Electric Battery

The electric battery plays a significant role on the overall vehicle performance and its efficiency is inherently linked to reducing the discrepancy between the optimum and operating conditions of the selected batteries, as regulated by the vehicle TMS. In this research, the battery is assumed to have a constant heat generation rate of 0.35 kW on average, based on 288 cells with 1.22 W of heat generation per cell (Pesaran, 2001). In addition, it is assumed that all of the heat generated is absorbed by the battery coolant.

5.1.2 System Parameters

For the analysis, each input is varied within certain ranges in order to understand the effects of each parameter on the overall system for different refrigerants. These ranges were constructed based on the common standards in the literature along with physical and economical limitations. In the refrigeration cycle, up to 10℃ of superheating and subcooling is utilized in order to improve the system efficiency. The evaporator and condenser air mass flow rates vary with respect to the vehicle speed and fan power. They are taken to be between 0.1 and 0.5 kg/s.

Moreover, initially relatively high ambient temperatures are used in order to observe the effects of cooling the electric battery under high temperatures, since hot weather conditions are a more significant concern than cold weather conditions due to the permanent effects of high temperatures on the battery performance as well as associated potential safety concerns. In addition, the heating is provided through several heaters placed in the vehicle such as the battery and the cabin core which have high efficiencies and very little room for improvement. Furthermore, a cooling capacity of up to 5 kW is used in order to provide adequate cooling to the vehicle cabin under these ambient temperatures. The list of all parameters and their selected ranges as observed is given in Table 5.1.

Table 5.1: Range of parameters used in the analysis

Parameter	**Range of variation**
Compressor speed (rev/min)	1,500-5,000
Compression Ratio	1 – 5
Evaporating Air Temperature (°C)	0 – 15
Superheating Temperature (°C)	0 – 12
Evaporator Air Mass Flow Rate (kg/s)	0.1 – 0.5
Cooling Capacity (kW)	1 – 5
Condensing Air Temperature (°C)	40 – 55
Condenser Air Mass Flow Rate (kg/s)	0.1 – 0.5
Subcooling Temperature (°C)	0 – 12

Moreover, since the use of R134a will be terminated in the near future by the European Community (due to the requirement of using refrigerants with GWP less than 150), the use of alternative refrigerants in the TMS is also considered for the analysis (European Union, 2006). One of the possible solutions to avoid R134a is the use of natural refrigerants, such as hydrocarbons, which attracted renewed interest during the past few decades due to being environmentally benign with negligible GWP and zero ODP. They also have various additional advantages such as availability, low cost, high miscibility with conventional mineral oil and compatibility with existing refrigerating systems. On the other hand, their main drawback is potential flammability and safety hazards. The characteristics of these refrigerants along with R134a can be seen in Table 5.2. Currently, hydrocarbons are already utilized in a few established applications around the world such as household refrigerators and small heat pump applications. It should be noted that R-744 (CO_2) is not considered among the prospective hydrocarbons even though it offers a number of desirable properties such as ready availability, low toxicity, low

GWP and cost, due to the need for implementing a transcritical cycle and additional safety standards that require significant modifications to the baseline system, based on its different thermophysical properties relative to R134a.

Table 5.2: Characteristics of R134a and various alternative refrigerants[1]

Code	Chemical Formula/ Common Name	Mol. Mass	NBP[2] (℃)	T_{crit} (℃)	P_{crit} (bar)	Latent Heat (kJ/kg)	Lower Flam. Limit (vol. %)[3]	ODP	GWP
R134a	CH_2FCF_3	44.1	-42.1	96.7	42.5	216.8	Non-flammable	0	1300
R290	$C_3H_{8/}$ Propane	44.1	-42.1	96.7	42.5	423.3	2.3-7.3	0	20
R600	C_4H_{10}/Butane	58.1	-0.5	152.0	38.0	385.7	1.6-6.5	0	20
R600a	C_4H_{10}/Isobutane	58.1	-11.7	134.7	36.4	364.2	1.8-8.4	0	20
R1234yf	$CF_3CF=CH_{2/}$ Tetrafluorpropene	N/A	-29.0	95	33.8	175[4]	6.2-13.3	0	4
RE170 (DME)	CH_3OCH_3/ Dimethylether	46.0	-24.7	126.9	53.7	410.2	3.4 – 17	0	< 3-5

[1]Data taken from Granryd, 2000; Somchai et al., 2006; Leck, 2009
[2]Normal Boling Point (NBP) is at 101.325 kPa (℃)
[3]Explosive limits in air % by volume
[4]Interpolated from Leck, 2009

In addition, there are also certain other refrigerants that could be utilized in EV TMSs, such as R1234yf and dimethyl ether (DME), and therefore included in the analysis. Among the fluorinated propene isomers, R1234yf is one of the major candidates as a replacement for R134a in automotive applications due to its ability to be used with compatible materials and oils as well as having a low GWP (about 4) and low normal boiling temperatures with respect to R134a. Moreover, several studies have shown that the environmental impact of R1234yf is significantly lower than R134a in most cases (Koban, 2009). However, it also has certain drawbacks such as additional costs, relative flammability, miscibility with oil as well as stability problems in the presence of small amounts of water and air in the TMS. DME is another good candidate due to being non-toxic during normal usage, widely available, environmentally safe, excellent material compatibility and better heat transfer properties as well as lower costs than R134a. The main drawback is its high flammability, which is about twice as high as the other hydrocarbons.

5.2 Energy and Exergy Analyses

5.2.1 Conventional Energy and Exergy Analyses

In the first step of the exergy analysis, the mass, energy, entropy and exergy balances are needed in order to determine the heat input, rate of entropy generation and exergy destruction as well as the energy and exergy efficiencies.

In general, a balance equation for a quantity in a system may be written as follows:

$$Input + Generation - Output - Consumption = Accumulation \tag{5.18}$$

where input and output terms refer to quantities entering and exiting through the system, respectively, whereas generation and consumption terms refer to quantities produced or consumed within the system, and the accumulation term refers to potential build-up of the quantity within the system (Dincer and Kanoğlu, 2010).

In steady-state conditions, however, all properties are unchanging with time and therefore, all the transient accumulation terms become zero. Thus, under the steady-state assumption, the balance equations for mass, energy, entropy and exergy can be written as follows:

$$\dot{m}_{in} = \dot{m}_{out} \tag{5.19a}$$

$$\dot{E}_{in} = \dot{E}_{out} \tag{5.19b}$$

$$\dot{S}_{in} + \dot{S}_{gen} = \dot{S}_{out} \tag{5.19c}$$

$$\dot{E}x_{in} = \dot{E}x_{out} + \dot{E}x_{D} \tag{5.19d}$$

where

$$\dot{S}_{gen} = \dot{m}\Delta s \tag{5.19e}$$

$$\dot{E}x_{D} = T_0\,\dot{S}_{gen} \tag{5.19f}$$

In the first two equations, $\dot{m}$ and $\dot{E}$ are associated with the mass flow rate and energy transfer rate and show that the respective total rates in / out across the boundary are conserved

(neglecting reactions). In the third equation, $\dot{S}$ is the entropy flow or generation rate. The amount transferred out of the boundary must exceed the rate in which entropy enters, the difference being the rate of entropy generation within the boundary due to associated irreversibilities. Similarly, in the equation (4.2d), $\dot{E}x$ is the exergy flow rate and it shows that exergy transferred out of the boundary must be less than the rate inwhich exergy enters, the difference being the rate of exergy destruction (or lost work) within the boundary due to associated irreversibilities which can be calculated by the dead-state temperature (T_0) multiplied by the entropy generation rate as given in equation (4.2f) (based on the Gouy-Stodola theorem)**.** Minimum exergy destruction, or minimum entropy generation, design characterizes a system with minimum destruction of available work, which in the case of refrigeration plants, is equivalent to the design with a maximum refrigeration load, or minimum mechanical power input (Bejan, 1997). In cooling systems, T_0 usually equals to the temperature of the high-temperature medium T_H.

In addition, the specific flow exergy associated with the coolant medium is given below:

$$ex_{coolant} = (h - h_0) + \frac{1}{2}V^2 + gZ - T_0(s - s_0) \tag{5.20}$$

Considering a system at rest relative to the environment, kinetic and potential terms can be ignored,

$$ex_{coolant} = (h - h_0) - T_0(s - s_0) \tag{5.21}$$

The exergy rate is determined as

$$\dot{E}x = \dot{m} * ex \tag{5.22}$$

Now that the TMS configuration and parameters are described and fundamental principles of the exergy are introduced, the TMS can be studied with respect to energy and exergy analyses based on the aforementioned system model.

Ideally, in the thermal management system, the refrigerant travels through the condenser at constant pressure by heat absorption and exits the condenser as a saturated liquid. Moreover, the refrigerant is compressed isentropically in the compressor before entering the condenser and

expanded isenthalpically in the thermal expansion valve before entering the evaporator. The refrigerant also flows through the evaporator at constant pressure by heat rejection and exits the evaporator as a saturated vapor. However, practical applications deviate from ideal conditions due to pressure and temperature drops associated with the refrigerant flow and heat transfer to/from the surroundings. During the compression process, entropy changes due to the irreversibilities and heat transfer to / from the surroundings. There is also some pressure drop as the refrigerant flows through the condenser and evaporator as modeled in the previous section. Furthermore, the refrigerant is subcooled as it is leaves the condenser (and may drop further before reaching the expansion valve) and slightly superheated (due to the pressure losses caused by friction) as it leaves the evaporator (and enters the compressor). The temperature of the refrigerant further increases as it flows to the compressor, increasing its specific volume, which increases the work of the compressor. On the coolant side, the coolant is pumped to the battery, where the pressure increases significantly with a slight increase on its temperature. The coolant then exchanges heat with the battery module without any phase change in the medium. Subsequently, the coolant enters the chiller in order to transfer the heat to the refrigerant cycle and enters the pump again to make up for the lost pressure before re-entering the battery.

For the compressor:

M.B.E
$$\dot{m}_1 = \dot{m}_2 = \dot{m}_r \tag{5.23a}$$

E.B.E
$$\dot{m}_1 h_1 + \dot{W}_{comp} = \dot{m}_2 h_2 \tag{5.23b}$$

En.B.E
$$\dot{m}_1 s_1 + \dot{S}_{gen,comp} = \dot{m}_2 s_2 \tag{5.23c}$$

Ex.B.E
$$\dot{m}_1 ex_1 + \dot{W}_{comp} = \dot{m}_2 ex_2 + \dot{E}x_{D,comp} \tag{5.23d}$$

$$\dot{E}x_{D,comp} = T_0 \dot{S}_{gen,comp} = \dot{m} T_0 (s_2 - s_1) \tag{5.23e}$$

Efficiency

$$\eta_{ex,comp} = \frac{(\dot{E}x_{2,act} - \dot{E}x_1)}{\dot{W}_{comp}} = 1 - \frac{\dot{E}x_{D,comp}}{\dot{W}_{comp}} \tag{5.23f}$$

where $\dot{W}_{comp}$ is the compressor power input in kW. Moreover, the isentropic efficiency of the adiabatic compressor is defined as

$$\eta_{comp} = \frac{\dot{W}_s}{\dot{W}} = \frac{h_{2,s} - h_1}{h_2 - h_1} \tag{5.24}$$

Here, $\dot{W}_s$ is the isentropic power and $h_{2,s}$ is the isentropic (i.e, reversible and adiabatic) enthalpy of the refrigerant leaving the compressor.

For the condenser:

M.B.E $$\dot{m}_2 = \dot{m}_3 = \dot{m}_r \quad (5.25a)$$

E.B.E $$\dot{m}h_2 = \dot{m}h_3 + \dot{Q}_{cond} \quad (5.25b)$$

En.B.E $$\dot{m}_2 s_2 + \dot{S}_{gen,cond} = \dot{m}_3 s_3 \quad (5.25c)$$

Ex.B.E $$\dot{m}_2 ex_2 = \dot{m}_3 ex_3 + Ex_{Q_H} + \dot{E}x_{D,cond} \quad (5.25d)$$

$$\dot{E}x_{D,cond} = T_0 \dot{S}_{gen,cond} = \dot{m}T_0\left(s_3 - s_2 + \frac{q_H}{T_H}\right) \quad (5.25e)$$

Efficiency

$$\eta_{ex,cond} = \frac{\dot{E}x_{\dot{Q}_H}}{\dot{E}x_2 - \dot{E}x_3} = 1 - \frac{\dot{E}x_{D,cond}}{\dot{E}x_2 - \dot{E}x_3} \quad (5.25f)$$

$$\dot{E}x_{\dot{Q}_H} = \dot{Q}_H\left(1 - \frac{T_0}{T_H}\right) \quad (5.25g)$$

where $\dot{Q}_H$ is the heat rejection from the condenser to the high-temperature environment.

For the thermal expansion valve before the evaporator (the expansion process is considered isenthalpic):

M.B.E $$\dot{m}_3 = \dot{m}_4 = \dot{m}_r \quad (5.26a)$$

E.B.E $$h_3 = h_4 \quad (5.26b)$$

En.B.E $$\dot{m}_3 s_3 + \dot{S}_{gen,TXV} = \dot{m}_4 s_4 \quad (5.26c)$$

Ex.B.E $$\dot{m}_3 ex_3 = \dot{m}_4 ex_4 + \dot{E}x_{D,TXV} \quad (5.26d)$$

$$\dot{E}x_{D,TXV} = T_0 \dot{S}_{gen,TXV} = \dot{m}T_0(s_4 - s_3) \quad (5.26e)$$

Efficiency

$$\eta_{ex,TXV} = \frac{\dot{E}x_4}{\dot{E}x_3} \quad (5.26f)$$

For the evaporator:

M.B.E $$\dot{m}_4 = \dot{m}_1 = \dot{m}_r \quad (5.27a)$$

E.B.E $$\dot{m}h_4 + \dot{Q}_L = \dot{m}h_1 \quad (5.27b)$$

En.B.E $$\dot{m}_4 s_4 + \dot{S}_{gen,evap} = \dot{m}_1 s_1 \quad (5.27c)$$

Ex.B.E $$\dot{m}_4 ex_4 + Ex_{Q_L} = \dot{m}_1 ex_1 + \dot{E}x_{D,evap} \quad (5.27d)$$

$$\dot{E}x_{D,evap} = T_0 \dot{S}_{gen,evap} = \dot{m}T_0 \left(s_1 - s_4 + \frac{q_L}{T_L}\right) \quad (5.27e)$$

Efficiency

$$\eta_{ex,evap} = \frac{\dot{E}x_{\dot{Q}_L}}{\dot{E}x_4 - \dot{E}x_1} = 1 - \frac{\dot{E}x_{D,evap}}{\dot{E}x_4 - \dot{E}x_1} \quad (5.27f)$$

$$\dot{E}x_{\dot{Q}_L} = -\dot{Q}_L \left(1 - \frac{T_0}{T_L}\right) \quad (5.27g)$$

where $\dot{Q}_L$ is the heat taken from the low-temperature environment to the evaporator.

For the chiller:

M.B.E $$\dot{m}_5 = \dot{m}_1 = \dot{m}_{ref,b} \quad \dot{m}_6 = \dot{m}_7 = \dot{m}_{cool} \quad (5.28a)$$

E.B.E $$\dot{m}_{ref,b} h_5 + \dot{Q}_{ch} = \dot{m}_{ref,b} h_{1''} \quad (5.28b)$$

En.B.E $$\dot{m}_{ref,b} s_5 + \dot{m}_{cool} s_6 + \dot{S}_{gen} = \dot{m}_{ref,b} s_{1''} + \dot{m}_{cool} s_7 \quad (5.28c)$$

Ex.B.E $$\dot{m}_{ref,b} ex_5 + \dot{E}x_{\dot{Q}_{ch}} \dot{m}_{ref,b} ex_{1''} + \dot{E}x_{D,ch} \quad (5.28d)$$

Efficiency

$$\eta_{ex,ch} = \frac{\dot{E}x_{\dot{Q}_{ch}}}{\dot{E}x_5 - \dot{E}x_{1''}} \quad (5.28e)$$

$$\dot{Q}_{ch} = \dot{m}_{cool}(h_7 - h_6) \ and \ \dot{E}x_{\dot{Q}_{ch}} = -\dot{Q}_{ch} \left(1 - \frac{T_0}{T_7}\right) \quad (5.28f)$$

The enthalpy and entropy changes in the water/glycol mixture of 50/50 by weight are calculated by assuming the specific heat remains constant as follows (Bornakke and Sonntag, 2009):

$$h_7 - h_6 = C_{wg}(T_7 - T_6) \ and \ s_7 - s_6 = C_{wg} \ln\left(\frac{T_7}{T_6}\right) \quad (5.29)$$

For the pump:

M.B.E $$\dot{m}_7 = \dot{m}_8 = \dot{m}_{cool} \quad (5.30a)$$

E.B.E $$\dot{m}_{cool} h_7 + \dot{W}_{pump} = \dot{m}_{cool} h_8 \quad (5.30b)$$

En.B.E $$\dot{m}_{cool} s_7 + \dot{S}_{gen} = \dot{m}_{cool} s_8 \quad (5.30c)$$

Ex.B.E $$\dot{m}_{cool} ex_7 + \dot{W}_{pump} = \dot{m}_{cool} ex_8 + \dot{E}x_{D,pump} \quad (5.30d)$$

Efficiency

$$\eta_{ex,pump} = \frac{(\dot{E}x_{8,act} - \dot{E}x_7)}{\dot{W}_{pump}} \quad (5.30e)$$

For the battery:

M.B.E $$\dot{m}_8 = \dot{m}_6 = \dot{m}_{cool} \quad (5.31a)$$

E.B.E $$\dot{m}_{cool} h_8 + \dot{Q}_{bat} = \dot{m}_{cool} h_6 \quad (5.31b)$$

En.B.E $$\dot{m}_{cool} s_8 + \dot{S}_{gen} = \dot{m}_{cool} s_6 \quad (5.31c)$$

Ex.B.E $$\dot{m}_{cool} ex_8 + \dot{E}x_{\dot{Q}_{bat}} = \dot{m}_{cool} ex_6 + \dot{E}x_{D,bat} \quad (5.31d)$$

For the entire cooling system, the energetic coefficient of performance (COP) becomes

$$COP_{en,system} = \frac{\dot{Q}_{evap} + \dot{Q}_{ch}}{\dot{W}_{comp} + \dot{W}_{pump}} \quad (5.32)$$

Actual cooling systems are less efficient than the ideal energy models due to irreversibilities in the actual systems. As given in the previous equations, a smaller temperature difference between the heat sink and heat source provides higher cooling system efficiency. Thus, the aim of the exergy analysis is to determine the system irreversibilities by calculating the exergy destruction in each component and to calculate the associated exergy efficiencies. This methodology helps to focus on the parts where the greatest impact can be achieved on the system since the components with larger exergy destruction also have more potential for improvements. The exergy destruction calculations and results for each component can be observed in Table 5.3. For the overall system, the total exergy destruction of the cycle can be calculated by adding the exergy destruction associated with each component that was previously calculated.

Table 5.3: Exergy destruction rates for each component in the TMS

Component	**Exergy Destruction Rates**
Compressor	$\dot{E}x_{D,comp} = T_0\dot{m}_r(s_2 - s_1)$
Condenser	$\dot{E}x_{D,cond} = T_0[\dot{m}_c(s_{c2} - s_{c1}) - \dot{m}_r(s_2 - s_3)]$
Evaporator TXV	$\dot{E}x_{D,evap,TXV} = T_0\dot{m}_{r1}(s_4 - s_3)$
Chiller TXV	$\dot{E}x_{D,ch,TXV} = T_0\dot{m}_{r2}(s_5 - s_3)$
Evaporator	$\dot{E}x_{D,evap} = T_0[\dot{m}_e(s_{e2} - s_{e1}) - \dot{m}_{r1}(s_4 - s_1)]$
Chiller	$\dot{E}x_{D,ch} = T_0\left[\dot{m}_{cool}\left(C_{wg}\ln(T_6/T_7)\right) - \dot{m}_{r2}(s_5 - s_1)\right]$
Pump	$\dot{E}x_{D,pump} = T_0\dot{m}_{cool}\left(C_{wg}\ln(T_6/T_0)\right)$
Battery	$\dot{E}x_{D,bat} = T_0\dot{m}_{cool}\left(C_{wg}\ln(T_6/T_8)\right)$

For the overall system, the total exergy destruction of the system can be calculated by adding the exergy destruction associated with each component that was previously calculated.

$$\dot{E}x_{D,system} = \dot{E}x_{D,comp} + \dot{E}x_{D,cond} + \dot{E}x_{D,evap,TXV} + \dot{E}x_{D,ch,TXV} + \dot{E}x_{D,evap} + \dot{E}x_{D,ch} + \dot{E}x_{D,pump} + \dot{E}x_{D,battery} \quad (5.33)$$

Finally, for the thermodynamic analysis, using the aforementioned exergy equations, the exergetic COP of the system can be calculated as

$$COP_{ex,system} = \frac{\dot{E}x_{\dot{Q}_{evap}} + \dot{E}x_{\dot{Q}_{ch}}}{\dot{W}_{comp} + \dot{W}_{pump}} \quad (5.34)$$

5.2.2 Advanced Exergy Analysis

In the previous section, the exergy analysis is conducted in order to determine the exergy destructions associated with each component as well as the overall system. However, the conventional exergy analysis does not evaluate the mutual interdependencies among the system components (Tsatsaronis, 2011). For this reason, the irreversibilities within the components are divided into two categories; the irreversibilities related to the specific entropy generation within the component ($s_{gen,k}$) and the ones related to the system structure and inefficiencies of the other components in the system (mainly with respect to the changes in the mass flow rate) (Kelly et al., 2009) by conducting so called advanced exergy analysis. For this reason, *endogenous* and *exogenous* exergy destruction concepts will be introduced as given below:

$$\dot{E}_{D,k} = \dot{E}_{D,k}^{EN} - \dot{E}_{D,k}^{EX} \tag{5.35}$$

The endogenous exergy destruction for a given component is associated only with the component itself and would still exist even if all the other components in the system would operate in an ideal way. On the other hand, exogenous exergy destruction is the remaining part of the entire exergy destruction within the component where it depends both on the inefficiencies associated with the component itself and the remaining components in the system. This distinction plays a key role in improving component design since the efforts spent on decreasing the endogenous exergy destruction in a component can often promote a decrease in exogenous part of the exergy destruction in other components. For the analysis conducted, the boundaries of all exergy balances are taken at the ambient temperature where the exergy loss is zero (for the individual components) and therefore all the thermodynamic inefficiencies are solely due to exergy destructions in the components.

In addition, the exergy destruction associated with a component may not be able to be reduced based on technological limitations (such as the availability and cost of materials and manufacturing processes). This portion of the exergy destruction in a component is called unavoidable part of exergy destruction ($\dot{E}_{D,k}^{UN}$), whereas the remaining part is called avoidable part of the exergy destruction ($\dot{E}_{D,k}^{AV}$). This distinction between the parts of exergy destructions can be useful in providing a realistic measure of the potential for improving the thermodynamic efficiency of a component (Morosuk and Tsatsaronis, 2008).

The combination of endogenous/exogenous and avoidable/unavoidable exergy destructions can be very helpful in determining the components needed to be focused on in order to reduce the exergy destruction of the overall system and the portion of this exergy destruction that can possibly be reduced. In this regard, endogenous avoidable part of the exergy destruction can be reduced through improving the efficiency of the component, whereas the exogenous avoidable exergy destruction can be reduced improving the efficiency of the remaining components as well as the efficiency of the analyzed component. Moreover, the endogenous unavoidable exergy destruction cannot be reduced due to technical limitations on the components, whereas

exogenous unavoidable exergy destruction cannot be reduced due to the technical limitations of the remaining components.

The thermal management system studied is a closed loop system, where compressor and pump works are used as the primary inputs and evaporator and chiller cooling loads are the primary outputs in a system where the output of one component is used as the input of the next component. In addition, the product for all the remaining components is the fuel of the component that follows them. Thus, the rates of exergy destruction should be calculated very carefully, since a part of the exergy destruction of each component is caused by inefficiencies of the remaining components. The exergy destruction in each component depends on the efficiency of the individual components along with the temperature and mass flow rates of the main and secondary working fluids (Tsatsaronis, 1999; Morosuk and Tsatsaronis, 2009).

In the studied system, the analysis can be conducted using either the total product ($\dot{E}_{P,TOT}$) or the total fuel ($\dot{E}_{F,TOT}$) to be constant in the system. This distinction does not affect any results in avoidable/unavoidable exergy destruction calculations since the components are considered in isolation during the analysis. However, it affects the endogenous/exogenous exergy destruction calculations since the mass flow rates of the working fluid changes based on the parameter that is considered to be constant (product or fuel). Since the analysis is trying to minimize the fuel consumption for a given system (with a fixed output), constant product assumption is used in the analysis.

In this regard, the exergy destruction of the evaporator is completely endogenous since $\dot{E}_{D,evap}$ is a function of the component's exergy destruction exclusively. On the other hand, $\dot{E}_{D,TXV}$ depends on the exergy efficiencies of the evaporator TXV and the evaporator. Similarly, $\dot{E}_{D,cond}$ depends on the exergy efficiency of condenser, evaporator TXV and evaporator, and $\dot{E}_{D,comp}$ depends on the exergy efficiency components compressor, condenser, evaporator TXV and evaporator in the refrigerant loop.

The studied thermal management system, in order to be able to split the exergy destruction into parts, a thermodynamic based approach (so called "Cycle method") is applied (Morosuk and Tsatsaronis, 2006). The exergy destruction in each component depends on the substance as well as the temperature/pressure and mass flow rates associated with the working fluids along with the efficiencies of each component. These fluids are composed of R134a for the refrigeration cycle, 50/50 water-glycol mix for the coolant cycle and air as the secondary fluids in the condenser and evaporator. The calculation of the exergy destructions associated with the TMS components are provided in Section 5.2.1.

In order to have a better understanding of the exergy destruction in each component and the associated interdependencies among them, the exergy destructions are split it into endogenous and exogenous components by analyzing the TMS under theoretical cycles (Morosuk and Tsatsaronis, 2009). This is achieved with respect to assuming minimum exergy destruction associated with each component (zero if possible). Based on this theoretical cycle, the compression process is considered isentropic($\dot{E}_{D,comp}^{th} = 0$). On the other hand, since the throttling process is always irreversible, it is replaced with an ideal expansion process for the theoretical cycle. Moreover, temperature difference of 0°C between the primary and secondary working fluids is used in the heat exchangers. However, the temperatures and mass flow rate associated with the evaporator and chiller secondary working fluids are kept the same in order to keep the cooling loads constant and therefore the associated exergy destructions within these components are considered only to be endogenous ($\dot{E}_{D,evap} = \dot{E}_{D,evap}^{EN}, \dot{E}_{D,chil} = \dot{E}_{D,chil}^{EN}$) (Kelly at al., 2009).

Additionally, only a part of the total thermodynamic inefficiencies can be avoided in each component while other parts cannot. The improvement efforts should be concentrated in the avoidable part of the irreversibilities, thus it becomes imperative to separate the avoidable and unavoidable parts of the exergy destruction for each component. In order to split the exergy destruction into avoidable and unavoidable parts, an additional cycle is developed where only unavoidable exergy destructions occur within each component. These unavoidable exergy destructions occur in the cycle as a result of unavoidable temperature differences in the heat exchangers, efficiencies in the compressor and pump and by the throttling processes. These

occur due to technological limitations (availability and cost of material and manufacturing) that prevent exceeding a certain upper limit of the component exergetic efficiency regardless of the amount of investment (Tsatsaronis and Park, 2002). In this analysis, the parameters to calculate the unavoidable cycle are selected as 0.5℃ for the heat exchangers and 0.95 for the compressor, regardless of the technological improvements in the system.

It should be noted that in order to assess the endogenous/exogenous and available/unavailable exergy destructions, simultaneous computations of the parallel cycles are needed to be calculated. This requires providing the system components with multiple inputs at once and obtaining multiple results where the differences among them could be evaluated. For this reason, EES is determined to be the most compatible software for the conducted analysis based on the ease of running alternative scenarios simultaneously in the software, and is used to develop the conventional and advanced exergy analyses.

5.3 Exergoeconomic Analysis

Even though the thermodynamic analyses (especially exergy analysis) can be used to improve the efficiencies of the components and corresponding systems, the feasibility of applying these improvements is generally constrained by the limitation of financial resources. Moreover, in many cases, the approaches taken by purely scientific motivation may not always be cost effective. Thus, in order to achieve the optimum design for energy systems, techniques combining scientific disciplines (mainly thermodynamics) with economic disciplines (mainly cost accounting) should be utilized.

Design of various thermal management systems is normally performed by conventional methods based on scientific analyses, experimental data and practical experience. Most of these systems are often operating outside of their optimum parameters which results in inefficient use of resources, increasing production costs and adverse environmental impact. The objective of exergoeconomic analysis is to determine the inefficiencies in the system and calculate the associated costs (Selbaş et al, 2006). In this section, an exergy costing method (SPECO method) is used for the analysis (Tsatsaronis and Lin, 1990; Lazzaretto and Tsatsaronis, 1999).

5.3.1 Cost Balance Equations

In order to conduct an exergoeconomic analysis, the cost flow rate, $\dot{C}$ ($\$/h$), is defined for each flow in a system, and a cost balance is written for each component to provide exergy costing as follows:

$$\dot{C}_{q,k} + \sum_{i} \dot{C}_{i,k} + \dot{Z}_k = \sum_{e} \dot{C}_{e,k} + \dot{C}_{w,k} \tag{5.36}$$

where

$$\dot{C}_j = c_j \dot{E}x_j \tag{5.37}$$

Exergy transfer by entering and exiting streams as well as by power and heat transfer rates are written respectively as follows:

$$\dot{C}_i = c_i \dot{E}x_i = c_i \dot{m}_i ex_i \tag{5.38a}$$

$$\dot{C}_e = c_e \dot{E}x_e = c_e \dot{m}_e ex_e \tag{5.38b}$$

$$\dot{C}_w = c_w \dot{W} \tag{5.38c}$$

$$\dot{C}_q = c_q \dot{E}x_q \tag{5.38d}$$

However, before the analysis can be conducted, the fuel and product exergies are needed to be defined for each component. The product exergy is defined according to the purpose of owning and operating a component under consideration, while the fuel represents the resources consumed in generating the product, where both are expressed in terms of exergy (Bejan et al., 1986). The fuel and products for each component can be seen in Table 5.4.

Table 5.4. Fuel and product definitions with respect to the system.

Component	***Fuel***	***Product***
Compressor	$\dot{W}_{comp}$	$\dot{E}x_2 - \dot{E}x_1$
Condenser	$\dot{E}x_2 - \dot{E}x_3$	$\dot{E}x_{10} - \dot{E}x_0$
Evaporator TXV	$\dot{E}x_{3a}$	$\dot{E}x_4$
Chiller TXV	$\dot{E}x_{3b}$	$\dot{E}x_5$
Evaporator	$\dot{E}x_4 - \dot{E}x_{1a}$	$\dot{E}x_9$
Chiller	$\dot{E}x_{1b} - \dot{E}x_5$	$\dot{E}x_7 - \dot{E}x_6$
Pump	$\dot{W}_{pump}$	$\dot{E}x_8 - \dot{E}x_7$
Battery	$\dot{W}_{bat}$	$\dot{E}x_6 - \dot{E}x_8$

By combining exergy and exergoeconomic balance equations, the following equation can be obtained as

$$\dot{E}x_{F,k} = \dot{E}x_{P,k} + \dot{E}x_{D,k} \tag{5.39}$$

The cost rate of exergy destruction is defined as follows:

$$\dot{C}_{D,k} = c_{F,k}\dot{E}x_{D,k} \tag{5.40}$$

Here, the component exergy destruction costs are determined by evaluating the exergy destruction rates associated with each component ($\dot{E}x_{D,k}$) with respect to the previously given exergy balance equations. Moreover, from Equation 5.36, the steady state form of the control volume cost balance can be written as given in Equation 5.41 below. The cost balances are generally written so that all terms are positive.

$$\sum_e \left(c_e \dot{E}x_e\right)_k + c_{w,k}\dot{W}_k = c_{q,k}\dot{E}x_{q,k} + \sum_i \left(c_i \dot{E}x_i\right)_k + \dot{Z}_k \tag{5.41}$$

Equation 5.41 states that the total cost of the exiting exergy streams equals the total expenditure to obtain them, namely the cost of the entering exergy streams plus the capital and other costs (Abusoglu and Kanoglu, 2009). In general, there are "n_e" exergy streams exiting the component, "n_e" unknowns and only one equation, the cost balance. Thus, "$n_e - 1$" auxiliary equations need to be formulated using F and P rules.

The F rule (fuel rule) refers to the removal of exergy from an exergy stream within the considered component when exergy differences between the inlet and outlet are considered in the fuel definition for this stream. Thus, this rule states that the specific cost (cost per exergy unit) associated with this fuel stream exergy removal must be equal to the average specific cost at which the removed exergy was supplied to the same stream in upstream components. This provides an auxiliary equation for each removal of exergy, which equals the number of exiting exergy streams and "$n_{e,F}$" that are associated with the definition of the fuel for each component. The P rule (product rule) refers to the supply of exergy to an exergy stream within the component and states that each exergy unit is applied to any stream associated with the product at the same average cost. Since this corresponds to an exiting stream, the number of auxiliary equations provided by this rule always equals $n_{e,P} - 1$, where $n_{e,P}$ is the number of exiting exergy streams that are included in the product definition. Thus, since each exiting stream is defined as either fuel or product, the total number of exiting streams is equal to "$n_{e,F} + n_{e,P}$", which provides "$n_e - 1$" auxiliary equations (Lazzaretto and Tsatsaronis, 2006).

5.3.2 Purchase Equipment Cost Correlations

On the economic side, the capital investment rate can be calculated with respect to the purchase cost of equipment and capital recovery as well as maintenance factor over the number of operation hours per year as given below:

$$\dot{Z}_k = \frac{Z_k \cdot CRF \cdot \varphi}{N} \tag{5.42}$$

where N is the annual number of operation hours for the unit and φ is the maintenance factor, generally taken as 1.06 (Bejan et al., 1996). CRF is the capital recovery factor which depends on the interest rate (i) and equipment life-time in years (n) as

$$CRF = \frac{i \times (1+i)^n}{(1+i)^n - 1} \tag{5.43}$$

Here, Z_k is the purchase equipment cost of the thermal management system components that should be written in terms of design parameters. The correlations for each component are given below (Valero, 1994):

$$Z_{comp} = \left(\frac{573\dot{m}_{ref}}{0.8996 - \eta_s}\right)\left(\frac{P_{cond}}{P_{evap}}\right)\ln\left(\frac{P_{cond}}{P_{evap}}\right) \tag{5.44}$$

where

$$\eta_s = 0.85 - 0.046667\,(\frac{P_{cond}}{P_{evap}}) \tag{5.45}$$

Here, $\dot{m}_{ref}$ is the refrigerant mass flow rate (kg/s) and η_s is the isentropic efficiency of a scroll compressor. For the heat exchangers the cost correlations developed by Selbas et al. (2006) are used. The fixed cost associated with the heat exchangers is neglected due to being insignificant relative to the variable costs as well as a lack of reliable data.

$$Z_{cond} = 516.621A_{cond} \tag{5.46}$$

$$Z_{evap} = 309.143A_{evap} \tag{5.47}$$

$$Z_{chil} = 309.143A_{chil} \tag{5.48}$$

where A_{cond}, A_{evap} and A_{chil} are the heat transfer areas associated with the condenser and evaporator respectively (Selbas et al., 2006).

$$Z_{pump} = 308.9\dot{W}_{pump}^{C_{pump}} \tag{5.49a}$$

$$C_{pump} = 0.25 \text{ for } 0.02 \text{ kW} < \dot{W}_{pump} < 0.3 \text{ kW} \tag{5.49b}$$

$$C_{pump} = 0.45 \text{ for } 0.3 \text{ kW} < \dot{W}_{pump} < 20 \text{ kW} \tag{5.49c}$$

$$C_{pump} = 0.84 \text{ for } 20 \text{ kW} < \dot{W}_{pump} < 200 \text{ kW} \tag{5.49d}$$

Here, $\dot{W}_{pump}$ is the pumping power in kW and C_{pump} is the pump coefficient with respect to the corresponding pumping power ranges, provided below (Sanaye and Niroomand, 1986):

$$Z_{evap,txv} = k_{txv}\dot{m}_{ref,a} \tag{5.50}$$

$$Z_{chil,txv} = k_{txv}\dot{m}_{ref,b} \tag{5.51}$$

where k_{txv} is the cost per mass flow rate of refrigerant which is taken to be \$5,000 (Al-Otaibi et al., 2004).

$$Z_{bat} = C_{bat}K_{bat} \tag{5.52}$$

Here, C_{bat} is the typical lithium-ion battery pack costs per kilowatt-hour, taken as \$500 (per Hensley et al., 2012) and K_{bat} is the battery pack energy that is associated with powering the thermal management system. The EV/HEV battery analyzed in the study has an energy storage capacity of 16 kWh, where only 12.9 kWh can be utilized for charging and driving in order to extend the life of the battery. Among this, only 9.6 kWh is used to propel the car and the accessories (Peterson, 2012). Of the remaining energy, the TMS can draw anywhere between 4% and 24% by just using the fans and turning the A/C all the way on a very hot day, respectively (Leibson, 2012).

5.3.3 Cost Accounting

Cost balances for each component are needed to be solved in order to estimate the cost rate of exergy destruction in each component. In the cost balance equations with more than one inlet or outlet flow, the number of unknown cost parameters exceeds the number of cost balances for that component. Thus, auxiliary exergoeconomic equations developed by F and P rules are used to equate the number of unknowns with the number of equations (Bejan et al., 1996). Implementing equation 5.41 for each component together with the auxiliary equations form a system of linear equations as follows:

$$\left[\dot{E}x_k\right] \times [c_k] = \left[\dot{Z}_k\right] \tag{5.53}$$

where the equation entails matrices of exergy rate (from exergy analysis), exergetic cost vector (to be evaluated) and the vector of $\dot{Z}_k$ factors (from economic analysis) respectively (Ahmadi et al., 2011). The matrix form of equation 5.53 is given below:

$$\begin{bmatrix}
1 & -1 & 0 & 0 & 0 & 0 & 0 & 0 & 0 & 0 & -\dot{W}_{comp} & 0 & 0 & 0 \\
0 & 1 & -1 & 0 & 0 & 0 & 0 & 0 & 0 & 0 & 0 & 0 & 1 & -1 \\
0 & \dot{E}x_3 & -\dot{E}x_2 & 0 & 0 & 0 & 0 & 0 & 0 & 0 & 0 & 0 & 0 & 0 \\
0 & 0 & 1 & -1 & 0 & 0 & 0 & 0 & 0 & 0 & 0 & 0 & 0 & 0 \\
-\dot{E}x_4 & 0 & 0 & \dot{E}x_1 & 0 & 0 & 0 & 0 & -1 & 0 & 0 & 0 & 0 & 0 \\
1 & 0 & 0 & -1 & 0 & 0 & 0 & 0 & 0 & 0 & 0 & 0 & 0 & 0 \\
0 & 0 & 1 & 0 & -1 & 0 & 0 & 0 & 0 & 0 & 0 & 0 & 0 & 0 \\
-1 & 0 & 0 & 0 & 1 & 1 & -1 & 0 & 0 & 0 & 0 & 0 & 0 & 0 \\
0 & 0 & 0 & 0 & 0 & 1 & -1 & 0 & 0 & 0 & 0 & 0 & 0 & 0 \\
0 & 0 & 0 & 0 & 0 & 0 & 1 & -1 & 0 & 0 & \dot{W}_{pump} & 0 & 0 & 0 \\
0 & 0 & 0 & 0 & 0 & 0 & 0 & 1 & 0 & -\dot{W}_{bat} & 0 & 0 & 0 & 0 \\
0 & 0 & 0 & 0 & 0 & 0 & 0 & 0 & 0 & 0 & 1 & 0 & 0 & 0 \\
0 & 0 & 0 & 0 & 0 & 0 & 0 & 0 & 0 & 0 & 0 & \dot{W}_{pump} & -\dot{W}_{comp} & 0 \\
0 & 0 & 0 & 0 & 0 & 0 & 0 & 0 & 0 & 0 & 0 & 0 & 1 & 0
\end{bmatrix} \times \begin{bmatrix}
\dot{C}_1 \\ \dot{C}_2 \\ \dot{C}_3 \\ \dot{C}_4 \\ \dot{C}_5 \\ \dot{C}_6 \\ \dot{C}_7 \\ \dot{C}_8 \\ \dot{C}_9 \\ \dot{C}_{10} \\ \dot{C}_{11} \\ \dot{C}_{12} \\ \dot{C}_{13} \\ \dot{C}_{14}
\end{bmatrix} = \begin{bmatrix}
-\dot{Z}_{comp} \\ -\dot{Z}_{cond} \\ 0 \\ -\dot{Z}_{etxv} \\ -\dot{Z}_{evap} \\ 0 \\ -\dot{Z}_{ctxv} \\ -\dot{Z}_{chil} \\ 0 \\ -\dot{Z}_{pump} \\ -\dot{Z}_{bat} \\ -c_{elect} \\ 0 \\ 0
\end{bmatrix}$$

The matrix is obtained based on the cost balance equations as given below:

$$\dot{C}_1 + \dot{Z}_{comp} + c_{elect}\dot{W}_{comp} = \dot{C}_2$$

$$\dot{C}_2 + \dot{C}_{13} + \dot{Z}_{cond} = \dot{C}_3 + \dot{C}_{14}$$

$$\dot{C}_2\dot{E}x_3 = \dot{C}_3\dot{E}x_2$$

$$\dot{C}_3 + \dot{Z}_{etxv} = \dot{C}_4$$

$$\dot{C}_4 + \dot{Z}_{evap} = \dot{C}_9 + \dot{C}_1$$

$$\dot{C}_4\dot{E}x_1 = \dot{C}_1\dot{E}x_4$$

$$\dot{C}_3 + \dot{Z}_{ctxv} = \dot{C}_5$$

$$\dot{C}_5 + \dot{C}_6 + \dot{Z}_{chil} = \dot{C}_1 + \dot{C}_7$$

$$\dot{C}_6 \dot{E}x_7 = \dot{C}_7 \dot{E}x_6$$

$$\dot{C}_7 + \dot{Z}_{pump} + c_{elect}\dot{W}_{pump} = \dot{C}_8$$

$$\dot{C}_8 + \dot{Z}_{bat} = \dot{C}_6 + \dot{W}_{bat}$$

$$\dot{C}_{11} = c_{elect}\dot{W}_{comp}$$

$$\dot{C}_{11}\dot{W}_{pump} = \dot{C}_{12}\dot{W}_{comp}$$

$$\dot{C}_{13} = 0$$

Here, c_{elect} is the unit cost of electricity, which is taken as $0.075\ \$/kWh$ (Toronto Hydro, 2012). By solving these equations, the cost rate of each flow can be calculated, which can be used to determine the cost rate of exergy destruction in each system component.

5.3.4 Exergoeconomic Evaluation

Moreover, certain additional variables can also provide useful exergoeconomic evaluation. Among these variables, the total cost rate provides the component with the highest priority in terms of exergoeconomic viewpoint and is the combination of the cost rate with respect to the exergy destruction and investment cost rates as given below:

$$\dot{C}_{TOT,k} = \dot{C}_{D,k} + \dot{Z}_k \tag{5.54}$$

The exergoeconomic relevance of a given component with respect to total cost rate is determined by the sum of the cost of exergy destruction $\dot{C}_{D,k}$ and the component-related cost $\dot{Z}_{D,k}$. Furthermore, an exergoeconomic factor is also used to determine the contribution of non-exergy related costs to the total cost of a component. It is defined as

$$f_k = \frac{\dot{Z}_k}{\dot{Z}_k + c_{f,k}\dot{E}_{D,k}} \tag{5.55}$$

where $c_{f,k}$ is the unit exergy cost of the fuel of any k component and $\dot{E}_{D,k}$ is the associated exergy destruction and the denominator forms the total cost rate. When a component has a low exergoeconomic factor value, cost savings in the entire system might be achieved by improving the component efficiency even if the capital investment for that component will increase. On the other hand, a high value might suggest a decrease in the investment costs at the expense of its exergetic efficiency (Sayyaadi and Sabzaligol, 2009).

In addition, relative cost difference can also be used as a useful thermoeconomic evaluation, where it shows the relative increase in the average cost per exergy unit is between the fuel and product of the component, and is defined as

$$r_k = \frac{c_{p,k} - c_{f,k}}{c_{f,k}} \tag{5.56}$$

5.3.5 Advanced Exergoeconomic Analysis

Exergoeconomic analysis is useful in understanding the relative cost importance of each system and the options for improving the overall system effectiveness (Tsatsaronis and Morosuk, 2007). Since cost of EVs and HEVs are one of the biggest road blocks for widespread commercialization of these technologies, where the thermal management is a significant portion of the total cost, it is worthwhile to further analyze the cost formation of the system, break it down into avoidable and unavoidable costs and determine the cost interactions among the components. Thus, the investment cost rates are also is split into endogenous/exogenous and avoidable/unavoidable parts (so called advanced exergoeconomic analysis).

The unavoidable investment cost $(\dot{Z}_k^{UN})$ for a component can be calculated by assuming a vastly inefficient version of this component which would not be used in real life applications due to very high fuel costs associated with it. This cost is determined based on arbitrary selection of a set of thermodynamic parameters for the components that would result in so inefficient solutions

that would be economically unpractical (Tsatsaronis and Park, 2002). These are composed of very low values for isentropic efficiencies of the compressor and small heat transfer area for the heat exchangers. For the analysis, the parameters to calculate the unavoidable investment costs are selected as temperature differences of 29℃ and 18℃ for the condenser and evaporator respectively, and an efficiency of 0.6 for the compressor (Tsatsaronis and Morosuk, 2007). The cost rates associated with unavoidable and avoidable exergy destruction along with unavoidable and avoidable investment costs are calculated as provided below:

$$\dot{C}_{D,k}^{UN} = c_{F,k}\, \dot{E}_{D,k}^{UN} \tag{5.57}$$

$$\dot{C}_{D,k}^{AV} = c_{F,k}\, \dot{E}_{D,k}^{AV} \tag{5.58}$$

where $c_{F,k}$ is the cost of fuel and $\dot{E}_{D,k}^{UN}$ and $\dot{E}_{D,k}^{AV}$ are the unavoidable and avoidable cost of exergy destruction associated with the individual components calculated in Section 5.22. $\dot{Z}_k^{UN}$ and $\dot{Z}_k^{AV}$ are the unavoidable and avoidable investment costs that are calculated by the aforementioned thermodynamic parameters as provided below:

$$\dot{Z}_k^{UN} = \dot{E}_{P,k} \left(\frac{\dot{Z}}{\dot{E}_P} \right)_k^{UN} \tag{5.59}$$

$$\dot{Z}_k^{AV} = \dot{E}_{P,k} \left(\frac{\dot{Z}}{\dot{E}_P} \right)_k^{AV} \tag{5.60}$$

Finally, the exergoeconomic factor can also be modified with respect to avoidable costs as given below:

$$f_k^* = \frac{\dot{Z}_k^{AV}}{\dot{Z}_k^{AV} + \dot{C}_{D,k}^{AV}} \tag{5.61}$$

where f_k^* shows the contribution of the avoidable investment cost on the total avoidable cost associated with the component. The use of avoidable exergy destruction and avoidable cost provide a more accurate representation with respect to the potential reductions that can be done

in the irreversibilities and cost of the components compared to the conventional exergoeconomic variables.

5.3.6 Enviroeconomic (Environmental Cost) Analysis

Most hybrid electric vehicles (HEVs) use electricity from the grid to power the TMS (thermal management system). The TMS has a significant role in reducing the associated GHG emissions compared to conventional vehicles. Even though these vehicles produce virtually zero GHG emissions through the tailpipe in all-electric mode during operation, there may still be indirect emissions associated with the generation of electricity (Samaras and Meisterling, 2008). These emissions, especially under a high carbon derived electricity generation mix, can be significantly high (possibly even higher than conventional vehicles) and therefore the associated CO_2 GHG emissions and corresponding environmental costs should be calculated.

For the studied model, various electricity generation mixes are considered from one that mainly utilizes a natural gas combined cycle to less environmentally friendly options that primarily use coal and steam (Yang and Maccarthy, 2009). The associated environmental assessment based on the corresponding CO_2 emissions can be calculated as given below (Caliskan et al., 2011):

$$x_{\mathrm{CO2}} = \frac{y_{\mathrm{CO2}} \times \dot{W}_{total} \times t_{total}}{10^6} \tag{5.62}$$

where x_{CO2} is the associated CO_2 emissions released in a year (tCO_2/year) and y_{CO2} is the corresponding CO_2 emissions for a coal fired electricity generator, $\dot{W}_{total}$ is the total power consumption of the TMS and t_{total} is the total working hours of the system in a year, which is assumed to be 1,460 based on 4 hours of daily driving.

In order to conduct an enviroeconomic analysis, a carbon price (or CO_2 emissions price) is needed to be established along with calculating the quantity of the carbon released. The carbon price is an approach imposing a cost on the emission of greenhouse gases which cause global warming. The international carbon price is typically between 13 and 16 $/tCO_2$ based on

different carbon scenarios (Den Elzen et al., 2011). The enviroeconomic parameter in terms of CO_2 emissions price in a year ($/year) can be calculated as given below:

$$C_{CO2} = (c_{CO2})(x_{CO2}) \tag{5.63}$$

where c_{CO2} is the CO_2 emissions price per tCO_2.

5.4 Exergoenvironmental Analysis

As mentioned in the previous sections, using exergy analysis to determine the exergy efficiencies and exergy destruction associated with each component can be used to make significant improvements on the system. However, improving the efficiencies of a system may often imply modifications in component design, which a lot of times lead to increasing a parameter (commonly an area, thickness or temperature) that results in an increase in the materials and energy needed for manufacturing the component. This in turn, may increase the consumption of natural resources to produce the component, pollutants generated during its operation or emissions associated with its disposal. Thus, the system should be evaluated with respect to the environmental impact associated with each component in addition to their thermodynamic efficiencies (Meyer et al., 2009).

Exergoenvironmental analysis reveals the environmental impact associated with each system component and the real sources of the impact by combining exergy analysis with a comprehensive environmental assessment method, such as life cycle assessment (LCA), which is an internationally standardized method that considers the entire useful life cycle of the components or overall systems with respect to their impact to the environment determined by the environmental models.

In the environmental analysis, LCA is carried out in order to obtain the environmental impact of each relevant system components and input streams. It consists of goal definition, inventory analysis and interpretation of results, which incorporates the supply of the input streams (especially fuel) and full life cycle of components. The quantification of environmental impact

with respect to depletion and emissions of a natural resource can be conducted using different methodologies. In this study, impact analysis using Eco-indicator 99 points along with previously determined impact analyses in the literature are used. For the LCA analysis, various damage categories are covered and the results are weighted and expressed in terms of Eco-indicator points (mPts) (Petrakopoulou et al., 2011) by using SimaPro 7.1 (Sima Pro, 2007).

SimaPro is a life cycle assessment software package that has the capability of collecting, analyzing and monitoring the environmental performance of products and services and can model and evaluate complex life cycles in a systematic and transparent way following the ISO 13030 series recommendations. The software is integrated with an ecoinvent database that is used for a variety of applications including carbon footprint calculations, product design/eco-design as well as assessing the environmental impact with respect to various parameters. The software can define non-linear relationships in the model, conduct analysis of complex waste treatment and recycling scenarios and allocate multiple output processes. Thus, it provides significant value in conducting LCA for the system components (Sima Pro, 2007).

5.4.1 Environmental Impact Balance Equations

Exergoenvironmental analysis is considered to be one of the most promising tools to evaluate energy conversion process from environmental point of view (Meyer et al., 2009 and Boyano et al., 2012). In order to be able to perform the analysis, the allocation of environmental analysis results to exergy streams is performed analogous to the allocation of exergy stream costs in exergoeconomics. Initially, an environmental impact rate $\dot{B}_j$ is expressed in terms of Eco-indicator 99 points which are determined through a combination of Sima Pro 7 analysis and available information on the literature. Subsequently, these points are converted into hourly rates (mPts/hour), based on 4 hours of driving for 15 years. Subsequently, these values along with the previously conducted exergy analysis are used to calculated specific environment impact b_j for the streams in the system.

$$b_j = \frac{\dot{B}_j}{\dot{E}x_j} \tag{5.64}$$

The environmental impact rates associated with heat and work transfers are calculated as follows:

$$\dot{B}_w = b_w \dot{W} \tag{5.65}$$

$$\dot{B}_q = b_q \dot{E}x_q \tag{5.66}$$

where,

$$\dot{E}x_q = \left(1 - \frac{T_0}{T_j}\right)\dot{Q} \tag{5.66}$$

The values for internal and output streams can only be obtained by considering the functional relations among system components, which are done through formulating environmental impact balances and auxiliary equations. The basis for formulating impact balances is that all environmental impacts entering a component have to exit the component with its output streams. In addition, there is also the component-related environmental impact that is associated with the life cycle of each component.

In order to conduct an exergoenvironmental analysis, an environmental impact balance is written for each component to provide environmental impact formation as follows:

$$\dot{B}_{q,k} + \sum_i \dot{B}_{i,k} + \dot{Y}_k = \sum_e \dot{B}_{e,k} + \dot{B}_{w,k} \tag{5.67}$$

In the above equation, $\dot{Y}_k$ is the component related environmental impact associated with the life cycle of the component, which is an indicator of the reduction potential of environmental impact of the component. The environmental balance equation states that the sum of all environmental impacts associated with all input streams plus the component-related environmental impact is equal to the sum of environmental impacts associated with all output streams.

5.4.2 Environmental Impact Correlations

In order to be able to solve the environmental balance equations, the environmental impacts associated with each component are determined with respect to Eco-indicator 99 points, which enable a fair comparison among different components. These impact points are approximated with respect to a combination of correlations developed from numerous studies conducted in literature, available data as well as the LCA developed for this study as provided in Table 5.5.

Table 5.5: Environmental impact correlations (Eco-indicator 99) developed based on the literature.

Component	$\dot{Y}$ $(mPts/h)$	$Criteria$
Compressor	0.89	m_{comp}
Condenser[1]	0.27	A_{cond}
Evaporator[1]	0.22	A_{evap}
Chiller[1]	0.15	A_{chil}
Evaporator TXV[2]	0.04	$\dot{m}_{ref,a}$
Chiller TXV[2]	<0.01	$\dot{m}_{ref,b}$
Pump	0.13	m_{pump}

[1]Tsatsaronis 2010; Buyano et al., 2011
[2]Matsunaga, 2002

For the heat exchangers, the eco-indicator points are rough estimations based on the area, and are calculated from scaling down various case studies performed in the literature. The component-related heat exchanger environmental impacts associated with the non-heat exchanging areas are neglected due to their relatively small size and unavailability of the data.

For the compressor and pump, the environmental impact is determined with respect to the weight of the components whereas for thermal expansion valves, it is based on the mass flow rate of the refrigerant. The thermal expansion valve component-related eco-indicator points per mass flow rate of the R134a refrigerant is calculated based on the correlations developed from LCA conducted for a 5000 Btu/h air conditioner by Matsunaga (2002).

5.4.3 LCA of the Electric Battery

Even though EVs and HEVs can form part of the solution to environmental concerns such as urban air pollution and global warming compared to the conventional vehicles with ICEs, when the EVs and HEVs are evaluated, there are still environmental concerns associated with the

electric battery itself (Matheys, 2009). Thus, determining the battery environmental impact plays a significant role in accurately assessing the overall environmental impact of the system.

In the environmental analysis, LCA is carried out in order to obtain the environmental impact of the battery assembly. It is a cradle to grave approach to study the environmental aspects throughout a product`s life from raw material acquisition through production, use and disposal and provides a quantitative data to identify the potential environmental impacts of the material and/or production on the environment (ISO 14040, 1997).

It consists of goal definition, inventory analysis and interpretation of results, which incorporates the supply of the full life cycle of the battery. The quantification of environmental impact with respect to depletion and emissions of a natural resource can be conducted using different methodologies. In this study, impact analysis method Eco-indicator 99 is used, an indicator especially developed to support decision making in design for the environment. For the LCA analysis, numerous damage categories are covered and the results are weighted and expressed in terms of eco-indicator points (Petrakopoulou et al., 2011) by using software package SimaPro 7.1 (Sima Pro, 2007).

The goal and scope of the analysis was to calculate the environmental impact associated with the lithium-ion battery in the TMS used and determine the parts/processes that have the largest contribution to the overall impact. For the analysis, the final environmental impact value is calculated as a single Eco-indicator 99 point based on 1 kg lithium-ion battery with European electric generation mix and weighting set belonging to the hierarchist perspective (H/H) provided in Table 5.6.

Table 5.6: Normalization used for eco-indicator 99 H/H.

Normalization	**Value**
Human Health[1]	114.1
Ecosystem Quality[2]	1.75×10^{-4}
Resources[3]	1.33×10^{-4}

[1]Unit: Disability adjusted life years
[2]Unit: Potential disappeared fraction of plant species
[3]Unit: MJ surplus energy

For the analysis, an eco-invent lithium-ion battery model (Ecoinvent, 2012) is modified and improved in order to calculate the environmental impacts of the components and processes associated with the production of the battery. Three stages of life cycle inventory (LCI) are used in the study. In stage 1, the initial mining of raw materials and metal production stages during which raw materials are extracted and transported are considered. The majority raw materials are determined to be the copper and aluminum used for the cathodes and anodes. Stage 2 included the conversion of materials to battery parts and associated machining processes. The main components are namely the electrodes, pastes, separators and electrolytes used in the battery cell along with the battery management system, module packaging, and the overall casing that are used to contain and protect the cells. The list of the major components considered for the analysis along with their corresponding weights (Majeau-Bettez et al., 2011) is provided in Table 5.7.

Table 5.7: Major components used in the LCA analysis and their corresponding weights per 1 kg of Li-ion battery.

Component	**Weight (kg)**
Electrode paste (+)	0.199
Electrode paste (-)	0.028
Cathode	0.034
Anode	0.083
Electrolyte	0.120
Separator	0.033
Casing	0.201
Module Packaging	0.170
BMS	0.029

Finally, stage 3 was composed of final assembly of the components to the battery. The analysis is conducted with respect to 1 kg of battery and later scaled up to the full size of the considered battery assembly (197 kgs). To be consistent with the rest of the analysis, the eco-indicator points are converted into hourly rates (mPts/hour), based on 4 hours of driving for 15 years.

5.4.4 Environmental Impact Accounting

Environmental impact balances for each component are needed to be solved in order to estimate the environmental impact rate of exergy destruction in each component. For the balance

equations with multiple inlet and outlet flows, auxiliary exergoenvironmental equations (analogous to exergoeconomic equations) are developed to match the unknown impact parameters with the number of environmental impact balance equations. Implementing equation 5.67 for each component together with the auxiliary equations form a system of linear equations as follows:

$$\left[\dot{E}x_k\right] \times [b_k] = \left[\dot{Y}_k\right] \tag{5.68}$$

where the equation entails matrixes of exergy rate (from exergy analysis), environmental impact vector (to be evaluated) and the vector of $\dot{Y}_k$ factors (from environmental analysis) respectively. The matrix form of the equation 5.68 can be seen below:

$$\begin{bmatrix}
1 & -1 & 0 & 0 & 0 & 0 & 0 & 0 & 0 & 0 & -\dot{W}_{comp} & 0 & 0 & 0 \\
0 & 1 & -1 & 0 & 0 & 0 & 0 & 0 & 0 & 0 & 0 & 0 & 1 & -1 \\
0 & \dot{E}x_3 & -\dot{E}x_2 & 0 & 0 & 0 & 0 & 0 & 0 & 0 & 0 & 0 & 0 & 0 \\
0 & 0 & 1 & -1 & 0 & 0 & 0 & 0 & 0 & 0 & 0 & 0 & 0 & 0 \\
-\dot{E}x_4 & 0 & 0 & \dot{E}x_1 & 0 & 0 & 0 & 0 & -1 & 0 & 0 & 0 & 0 & 0 \\
1 & 0 & 0 & -1 & 0 & 0 & 0 & 0 & 0 & 0 & 0 & 0 & 0 & 0 \\
0 & 0 & 1 & 0 & -1 & 0 & 0 & 0 & 0 & 0 & 0 & 0 & 0 & 0 \\
-1 & 0 & 0 & 0 & 1 & 1 & -1 & 0 & 0 & 0 & 0 & 0 & 0 & 0 \\
0 & 0 & 0 & 0 & 0 & 1 & -1 & 0 & 0 & 0 & 0 & 0 & 0 & 0 \\
0 & 0 & 0 & 0 & 0 & 0 & 1 & -1 & 0 & 0 & \dot{W}_{pump} & 0 & 0 & 0 \\
0 & 0 & 0 & 0 & 0 & 0 & 0 & 1 & 0 & -\dot{W}_{bat} & 0 & 0 & 0 & 0 \\
0 & 0 & 0 & 0 & 0 & 0 & 0 & 0 & 0 & 0 & 1 & 0 & 0 & 0 \\
0 & 0 & 0 & 0 & 0 & 0 & 0 & 0 & 0 & 0 & \dot{W}_{pump} & -\dot{W}_{comp} & 0 & 0 \\
0 & 0 & 0 & 0 & 0 & 0 & 0 & 0 & 0 & 0 & 0 & 1 & 0 & 0
\end{bmatrix} \times \begin{bmatrix} \dot{B}_1 \\ \dot{B}_2 \\ \dot{B}_3 \\ \dot{B}_4 \\ \dot{B}_5 \\ \dot{B}_6 \\ \dot{B}_7 \\ \dot{B}_8 \\ \dot{B}_9 \\ \dot{B}_{10} \\ \dot{B}_{11} \\ \dot{B}_{12} \\ \dot{B}_{13} \\ \dot{B}_{14} \end{bmatrix} = \begin{bmatrix} -\dot{Y}_{comp} \\ -\dot{Y}_{cond} \\ 0 \\ -\dot{Y}_{etxv} \\ -\dot{Y}_{evap} \\ 0 \\ -\dot{Y}_{ctxv} \\ -\dot{Y}_{chil} \\ 0 \\ -\dot{Y}_{pump} \\ -\dot{Y}_{bat} \\ -b_{elect} \\ 0 \\ 0 \end{bmatrix}$$

The matrix is obtained based on the environmental impact balance equations as given below:

$$\dot{B}_1 + \dot{Y}_{comp} + b_{elect}\dot{W}_{comp} = \dot{B}_2$$

$$\dot{B}_2 + \dot{B}_{13} + \dot{Y}_{cond} = \dot{B}_3 + \dot{B}_{14}$$

$$\dot{B}_2\dot{E}x_3 = \dot{B}_3\dot{E}x_2$$

$$\dot{B}_3 + \dot{Y}_{etxv} = \dot{B}_4$$

$$\dot{B}_4 + \dot{Y}_{evap} = \dot{B}_9 + \dot{B}_1$$

$$\dot{B}_4 \dot{E}x_1 = \dot{B}_1 \dot{E}x_4$$

$$\dot{B}_3 + \dot{Y}_{ctxv} = \dot{B}_5$$

$$\dot{B}_5 + \dot{B}_6 + \dot{Y}_{chil} = \dot{B}_1 + \dot{B}_7$$

$$\dot{B}_6 \dot{E}x_7 = \dot{B}_7 \dot{E}x_6$$

$$\dot{B}_7 + \dot{Y}_{pump} + b_{elect}\dot{W}_{pump} = \dot{B}_8$$

$$\dot{B}_8 + \dot{Y}_{bat} = \dot{B}_6 + \dot{W}_{bat}$$

$$\dot{B}_{11} = b_{elect}\dot{W}_{comp}$$

$$\dot{B}_{11}\dot{W}_{pump} = \dot{B}_{12}\dot{W}_{comp}$$

$$\dot{B}_{13} = 0$$

Here, b_{elect} is the unit environmental impact associated with the electricity generation mix used (from Eco-indicator 99), which is taken as 22 mPts/kWh. By solving these equations, the environmental impact rate of each flow can be calculated, which can be used to determine the environmental impact rate of exergy destruction in each system component.

5.4.5 Exergoenvironmental Evaluation

In order to evaluate the environmental performance of the TMS components and provide suggestions and recommendations, exergoenvironmental variables are defined for the system and are analogous to most exergoeconomic variables. The environmental impact rate associated with the exergy destruction of a component is defined as follows:

$$\dot{B}_{D,k} = b_{F,k}\dot{E}x_{D,k} \quad \text{(if } \dot{E}x_{P,k} \text{ is constant)} \tag{5.71}$$

Here, the environmental impact of component exergy destructions are determined by evaluating the exergy destruction rates associated with each component ($\dot{E}x_{D,k}$) with respect to the exergy balance equations along with the exergy based specific environmental impact calculated by the aforementioned environmental impact matrix. The total environmental impact of a component is calculated by adding the sum of the environmental impact of exergy destruction to the previously calculated component-related environmental impact.

$$\dot{B}_{TOT,k} = \dot{B}_{D,k} + \dot{Y}_k \tag{5.72}$$

The exergoenvironmental approach identifies the relevance from the environment point of view of a given component with respect to total environmental impact that is determined by the sum of the environmental impact of exergy destruction $\dot{B}_{D,k}$ and the component-related environmental impact $\dot{Y}_{D,k}$.

Moreover, the relative difference of specific environmental impacts $r_{b,k}$ is defined by

$$r_{b,k} = \frac{r_{P,k} - r_{F,k}}{r_{F,k}} \tag{5.73}$$

which is an indicator of reduction potential of the environmental impact associated with a component. In general, the higher the value of relative difference of specific environmental impacts of a component in a system, the smaller the effort it would be needed to reduce the environmental impact of that component. This variable represents the environmental quality, independently of the absolute value of environmental impact.

Furthermore, the sources for the formation of environmental impact in a component are compared using the exergoenvironmental factor $f_{b,k}$, which expresses the relative contribution of

the component-related environmental impact $\dot{Y}_k$ to the total environmental impact for the component.

$$f_{b,k} = \frac{\dot{Y}_k}{\dot{Y}_k + b_{f,k}\dot{E}_{D,k}} \tag{5.74}$$

In general, it is considered that $f_{b,k}$ higher than approximately 0.7 signifies that the component-related environmental impact $\dot{Y}_k$ is dominant, whereas $f_{b,k}$ lower than approximately 0.3 signifies that exergy destruction is the dominant source. Thus, the higher the exergoenvironmental factor, the higher the influence of the component-related environment impact to the overall performance of the system from the environmental perspective (Tsatsaronis, 2006).

Based on the exergoenvironmental variables above, an evaluation of the system can be conducted by examining the components with high total environmental impacts (indicated by $\dot{B}_{TOT,k}$) and selecting the ones with highest improvement potentials (indicated by $r_{b,k}$) and identifying the main source of the environmental impact (identified by $f_{b,k}$) associated with those components. Finally suggestions for reducing the overall environmental impact can be developed based on the results of the LCA and impact correlations if the component-related impact dominates the overall impact, or with the help of the exergy analysis, if the thermodynamics inefficiencies are the dominant source of the environmental impact being considered.

5.5 Multi-objective Optimization

In a world with finite natural resources and increasing energy demand and prices, developing systems that are efficient, cost-effective and environmentally benign is one of the most prominent challenges that many engineers face today. In the past decades, the energy prices have been increasing while the legislations that aim to mitigate environmental problems (such as ozone layer depletion and global warming) have become more stringent. In this regard, exergy analysis has been used to improve system component and system designs by determining the locations, types and true magnitude of inefficiencies in systems. However, exergy analysis does not provide any information on the financial and environmental aspect of the improvements.

Thus, an integrated procedure that combined all these concerns was developed to find a viable solution. For this reason, a multi-objective optimization is conducted through coupling the second law of thermodynamics with economics and environmental impact in order to develop a powerful tool for the systematic study of the TMS (Ahmadi and Dincer, 2010; Sayyaadi et al., 2011).

As shown in the previous sections, exergoeconomic analysis combines exergy analysis and economic principles, such as costs associated with purchase of equipment, input energy resources and maintenance, and incorporates the associated costs of the thermodynamic inefficiencies in the total product cost of the system. These costs can be used to find the most and least cost-effective components and improving the overall system design (Sayyaadi et al., 2009).

On the other hand, exergoenvironmental analysis combines exergy analysis and the environmental impact, associated with construction, operation and maintenance and disposal stages, and allocates the corresponding impacts to the exergy streams, in order to point out the components causing the highest environmental impact and suggesting possibilities and trends for improvement, based on the calculated exergoenvironmental variables.

Subsequently, multi-objective optimization with respect to these aforementioned analyses is utilized in order to compensate shortcomings of traditional single objective approaches (namely single objective exergy, exergoeconomic and exergoenvironmental optimizations) by allowing a larger perspective and determining a more complete spectrum of solutions that optimize the design according to more than one objective at a time. In most practical decision making problems, the objectives are conflicting in nature and a unique optimal solution cannot be identified. Thus, Pareto optimality is introduced to determine whether a solution is really one of the best possible trade-offs (Lazzaretto and Toffolo 2004; Sayyaadi and Babaelahi, 2011).

5.5.1 Objective Functions

A multi-objective optimization problem requires the simultaneous satisfaction of a number of different and usually conflicting objectives characterized by distinct measure of performance. It

should be noted that multi-objective optimization problems generally show a possible uncountable set of solutions which represents the best possible trade-offs in the objective function space and that no combination of decision variable values can minimize/maximize all the components of functions simultaneously (Sayyaadi and Babaelahi, 2011). In this study, the objective functions considered for multi-objective optimization are the combinations of exergy efficiency (to be maximized), the total cost rate of product (to be minimized) and environmental impact (to be minimized) and are compared against single-objective optimizations of these objectives. Consequently, the objective functions in the hybrid electric vehicle thermal management system analysis can be expressed in equations 5.75-5.77. Even though each objective function varies in terms of the objective it is optimizing, they all have the same underlying parameters which are affected by the changes in the selected decision variables. It should be noted that all the objectives in the multi-objective optimization are assumed to be equally important, and therefore no additional weighting criteria are assigned to the objectives in order to minimize subjectivity in the analysis. Instead, the LINMAP (linear programming technique for multidimensional analysis of preference) method is used where the point on the Pareto optimal frontier closest to an ideal unreachable point (where all selected objectives are optimized) is selected as the single best optimization point.

Exergy efficiency:

$$\psi_{system} = \frac{\dot{E}x_{\dot{Q}_{evap}} + \dot{E}x_{\dot{Q}_{ch}}}{\dot{W}_{comp} + \dot{W}_{pump}} \tag{5.75}$$

where the inputs are the work of the compressor and the pump and the outputs are the exergy of heat with respect to the evaporator and the chiller (refer to Section 5.2.1).

Total cost rate:

$$\dot{C}_{system} = \dot{Z}_k + \dot{C}_{D,k} \tag{5.76}$$

where the total cost rates of the system consists of the total investment cost and cost of exergy destruction respectively (refer to Section 5.3).

Environmental impact:

$$\dot{B}_{system} = \dot{B}_k + \dot{B}_{D,k} \tag{5.77}$$

where the total environmental impact of the system consists of the component-related environmental impact and the impact associated with exergy destruction respectively (refer to Section 5.4). The environmental impact points are determined from LCA conducted using SimaPro 7 along with various correlations developed from the data available in the literature.

5.5.2 Decision Variables and Constraints

In this study, the following six decision variables are chosen for the analysis:

- the condenser saturation temperature (T_{cond}),
- the evaporator saturation temperature (T_{evap}),
- the magnitude of superheating in the evaporator (ΔT_{sh}),
- the magnitude of subcooling in the condenser (ΔT_{sc}),
- the evaporator air mass flow rate ($\dot{m}_e$),
- the compressor efficiency (η_{comp}).

In engineering application of the optimization problems, there are usually constraints on the trade-off decision variables that arise from appropriate feasibility, commercial availability and engineering constraints (Sayyaadi and Nejatolahi, 2011). The limitations on the minimum and maximum ranges of decision variables are given in Table 5.8.

As can be seen from Table 5.8, the lower bound for the evaporator temperature is taken to be higher than 0℃ since lower temperatures would cause icing on the surface of the evaporator due to the formation of the water droplets. This reduces the volume of air flowing through the evaporator and in turn reduces the efficiency of the system (Daly, 2008). On the other hand, the upper bound of the evaporator is limited by the cabin cooling temperatures. For condenser, the lower temperature bound is based on the ambient temperature, whereas the upper bound is constraint with respect to the compression ratio of the compressor, since very high compression

ratios increase the probability of the high pressure vapor to leaking back to the low pressure side and even cause compressor failure. Moreover, constraints are provided between the evaporator and condenser temperatures and the incoming air temperatures in order to have feasible and adequate heat transfer in the heat exchangers. Furthermore, the compressor and pump efficiencies are limited to 0.95 due to previously mentioned technological limitations, whereas the air mass flow rates are limited with respect to the vehicle speed and fan power.

Table 5.8: Constraints associated with the decision variables selected for the TMS.

Constraints
$0℃ \leq T_{evap} \leq T_{cabin} - \Delta T_{evap.min}$
$T_0 + \Delta T_{cond.min} \leq T_{cond} \leq 65℃$
$T_{evap} < T_{evap,air,in} - \Delta T_{evap.min} - T_{sh}$
$T_{cond} > T_{cond,air,in} + \Delta T_{air.min} + \Delta T_{cond.\min} + \Delta T_{sc}$
$0℃ \leq \Delta T_{sh} \leq 10℃$
$0℃ \leq \Delta T_{sc} \leq 10℃$
$\eta_{comp} \leq 0.95$
$\eta_{pump} \leq 0.95$
$\dot{m}_{air} \leq 0.35\ kg/s$

5.5.3 Genetic Algorithm

Currently, there are many search techniques that are used to deal with multi-objective optimization problems. These include, but are not limited to, generic algorithm, simulated annealing, tabu and scatter search, ant system, particle swarm and fuzzy programing. Among these, there is no technique that provides the optimum results for all problems and thus the best method should be selected with respect to the current system. In this research, a generic algorithm is used since it requires no initial conditions, works with multiple design variables, finds global optima (as opposed to local optima), utilizes populations (as opposed to individuals) and uses objective function formation (as opposed to derivatives).

In the last decades, genetic algorithms (GAs) have been extensively used as search and optimization tools in various problem domains due to their broad applicability, ease of use and global perspective (Goldenberg, 1989). The concept of GAs was first conceived by Holland in

1970s (Holland, 1975) in order to simulate growth and decay of living organisms in a natural environment and various improvements were conducted ever since. GAs today apply an iterative and stochastic search strategy to drive its search towards an optimal solution through mimicking nature`s evolutionary principles and have received increasing attention by the research community as well as the industry to be used in optimization procedures.

Based on the inspired evolutionary process, the weak and unfit species are faced with extinction while the strong ones have greater opportunity to pass their genes to future generation via reproduction. Throughout this process, given long enough time line, the species carrying the suitable combination in their genes become the dominant population.

In the analysis, the GA terminology adopted by Konak et al. (2006) is used. Based on this terminology, a solution vector is called an individual or a *chromosome*, which consists of discrete units called *genes*. Each gene controls one or more features of the chromosome, which corresponds to a unique solution in the solution space. Moreover, the collection of these chromosomes are called a *population*, which are initialized randomly at first and includes solutions with increasing fitness as the search evolves until converging to a single solution. Furthermore, operators called *crossover* and *mutation* are used to generate new solutions from existing ones. Crossover is one of the key operators where two chromosomes, called *parents*, are combined together to form new chromosomes called *offspring*. Due to the having preference towards fitness, these offsprings will inherit good genes from the parents and through the iterative process, and therefore the good genes are expected to appear more frequently in the population, where they eventually converge to an overall good solution.

The mutation operator on the other hand introduces random changes into the characteristics of the chromosomes at the gene level. Usually the mutation rate (probability of changing properties of a gene) is very small and therefore the new chromosome produced will not be very different than the original one. The key here is that, while the crossover leads the population to converge (by making the chromosome in the population alike), the mutation reintroduces genetic diversity and assists to the escape from local optima (Konak et al., 2006).

Reproduction involves selection of chromosomes for the next generation, where the fitness of an individual usually determined the probability of its survival. The selection procedures can vary depending on how the fitness values are used (such as proportional selection, ranking and tournament). The basic schematic for the evolutionary algorithm for the case used in the study is given in Figure 5.2.

The GA has major advantages since constraints of any type can be easily implemented and that they can find more than one near-optimal point in the optimization space, which enables users to pick the most applicable solution for the specific optimization problem and therefore are widely used for various multi-objective optimization approaches. (Ghaffarizadeh, 2006; Ahmadi and Dincer, 2010; Ahmadi et al., 2011).

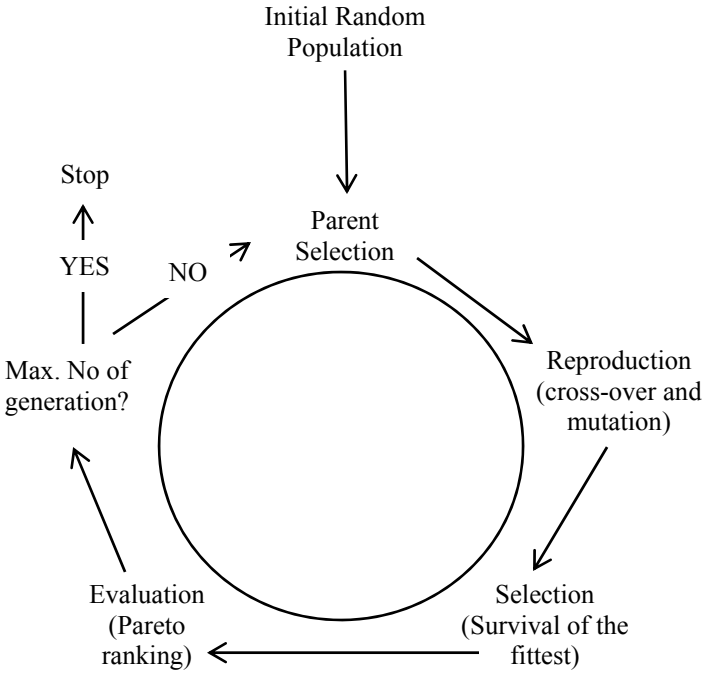

Figure 5.2: Sample schematic for the evolutionary algorithm used.

Even though maximizing/minimizing a criterion would be beneficial, many real-world problems involve multiple measures of performance, or objectives, which should be optimized simultaneously. Objectives that are optimized individually can provide optimal results with respect to their own criteria while providing very low performance in other objective functions. Thus, a trade-off is needed among the different dimensions in order to obtain a family of optimal

"acceptable" solutions for the problem (Fonseca and Fleming, 1995). This ability along with not requiring the user to prioritize, scale or weigh objectives makes them unique in solving multi-objective optimization problems.

The first real application of EAs for finding multiple trade-off solutions in one single simulation run was suggested and used by David Schaffer in 1984. (Schafer, 1984). He used vector-evaluated genetic algorithm (VEGA) to capture multiple trade-off solutions for a small number of iterations. This is followed by David Goldberg (Goldgberg, 1989) who suggested using 10-line sketch of a plausible multi-objective evolutionary algorithm optimization using the concept of domination. Consequently, many different implementations of MOEAs have been developed such as weight-based GA (Hajela, 1992), non-dominating sorting GA (Srinivas and Deb, 1994), Pareto-GA (NPGA) (Horn et al., 1994), fast non-dominating sorting generic algorithm (NSGA-II) (Deb et al., 2002) and multi-objective evolutionary algorithm (Sarker et al., 2002) along with different ways of using EAs to solve multi-objective optimization problems such as diploidy (Kursawe, 1990), weight-based (Hajela and Lin, 1992) and distance based (Osyczka and Kundu, 1995) approaches.

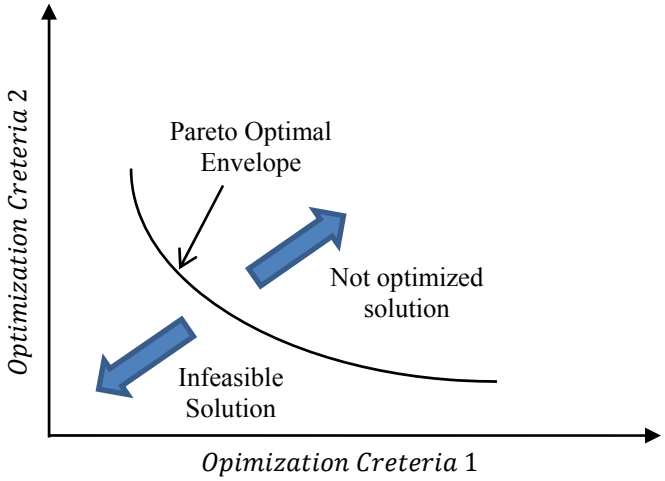

Figure 5.3: A general Pareto optimal curve.

One of the most prominent differences of classical search and optimization algorithms is that EAs use population of solutions in each iteration (instead of single solutions), which produces a final outcome of a population of multiple non-dominated solutions (that are in parallel) by taking

advantage of similarities in the family of possible solutions. Since usually, EAs usually do not converge in a single solution (due to conflicting criteria), EA captures multiple optimum solutions in its final population. These solutions are called “Pareto optimal”, where no other feasible solution can reduce some objective function without causing a simultaneous increase in at least no other objection function. The objective function values corresponding to these feasible non-dominating solutions are called “Pareto optimal frontier” (Fonseca and Fleming, 1995; Konak et al., 2006; Deb, 2011; Sayyaadi and Nejatolahi, 2011). The general concept of Pareto optimal frontier is illustrated in Figure 5.3.

Chapter 6: Results and Discussion

6.1 TMS comparison

In this section, before the detailed results of the exergy, exergoeconomic and exergoenvironmental analyses and the corresponding optimization are provided for the studied liquid thermal management system, a high level comparison of the cabin air, refrigerant and liquid based thermal management systems is introduced based on thermodynamic and heat transfer analyses.

6.1.1 Thermodynamic Analysis

The properties of air, refrigerant and the coolant are calculated in their associated circuits and used to conduct the exergy analysis based on the aforementioned balance equations. The energetic and exergetic COPs of each system are calculated with respect to Table 6.1. The same ambient and refrigerant circuit properties, as well as evaporator heat load are used in all TMSs in order to perform a consistent analysis.

Table 6.1: Energetic and exergetic COP equations used in the analysis.

TMS	**Coefficient of Performance (COP)**	
	Energetic	**Exergetic**
Passive cabin air cooling	$\frac{\dot{Q}_{Evap} + \dot{Q}_{bat}}{\dot{W}_{Comp}}$	$\frac{\dot{E}x_{QEvap} + \dot{E}x_{bat}}{\dot{W}_{Comp}}$
Active refrigerant cooling	$\frac{\dot{Q}_{Evap} + \dot{Q}_{bat\ evap}}{\dot{W}_{Comp}}$	$\frac{\dot{E}x_{QEvap} + \dot{E}x_{bat\ evap}}{\dot{W}_{Comp}}$
Active liquid cooling	$\frac{\dot{Q}_{Evap} + \dot{Q}_{chil}}{\dot{W}_{Comp} + \dot{W}_{Pump}}$	$\frac{\dot{E}x_{QEvap} + \dot{E}x_{chil}}{\dot{W}_{Comp} + \dot{W}_{Pump}}$

In passive cabin air cooling, the battery is cooled by the conditioned ambient air that is transferred through the evaporator into the cabin as shown in Figure 6.1. By using the battery fans, some of this air is used in order to cool the battery. Since the battery is cooled by using the available cabin air, it does not require any additional compressor work other than the work used to provide thermal management to the vehicle cabin. Moreover, the system is highly compatible due to the optimum cabin and battery temperatures being different by only 1.5℃ (cabin is kept at 20℃ and the battery desired temperature is 21.5℃). However, since the battery cooling solely relies on the cabin temperature, it can be significantly affected when cabin temperatures are high.

Moreover, a large fraction of the air flow rate is lost through its transition to the cabin. Therefore, significant fan power is required to increase the amount of air flow for the battery, which can increase the fan power consumption and noise level inside the cabin. This issue can be resolved by implementing independent air cooling with the help of a separate battery evaporator, but the trade-off will be the additional compressor power to flow the refrigerant through this evaporator.

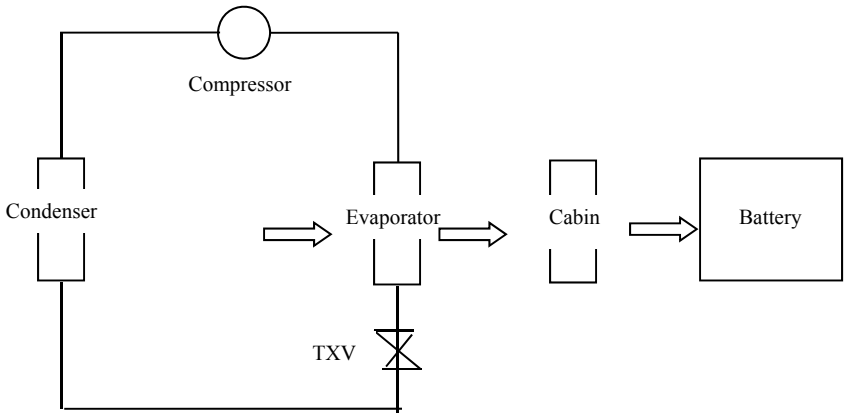

Figure 6.1: General schematic of cabin air TMS.

The exergy efficiency associated with this system is calculated to be 0.32. However this efficiency depends on the heat load applied to the evaporator and the battery heat dissipation rate. For relatively low battery heat dissipation rates, the TMS is highly effective due to usage of already available air in the vehicle cabin. However, due to the low exergy and flow rate of the cabin air, it would not be sufficient when the battery is operating in a harsh operating environment and extreme duty cycles (Sabbah et al., 2008). Therefore, this system is mainly utilized when the battery heat dissipation is low and ambient air conditions are within the desired battery operating ranges.

In active refrigerant cooling, the battery is cooled with the additional evaporator utilized specifically for the battery as shown in Figure 6.2. The exergy associated with the battery cooling is higher due to the use of the evaporator with a refrigerant, as opposed to just air flow in the previous TMS, but at the expense of the additional compressor work to pump the refrigerant to the battery evaporator. As a result, the total exergy efficiency of the system is determined to be 0.26, lower than the cabin air cooling TMS, since extra compressor work is needed to cool the battery via the refrigerant.

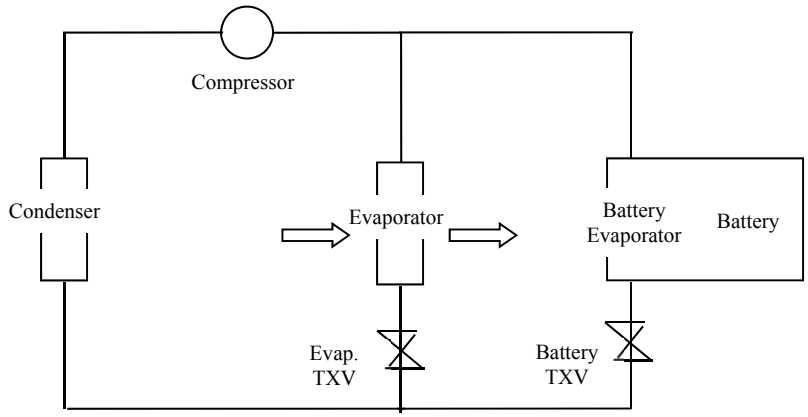

Figure 6.2: General schematic of refrigerant based TMS.

The active liquid cooling system on the other hand, incorporates the advantages of both the air cooling and refrigerant based cooling with the help of the additional battery cooler and chiller. This additional cooling loop is kept cool via different procedures depending on the cooling load and ambient conditions as discussed in Section 5.2.

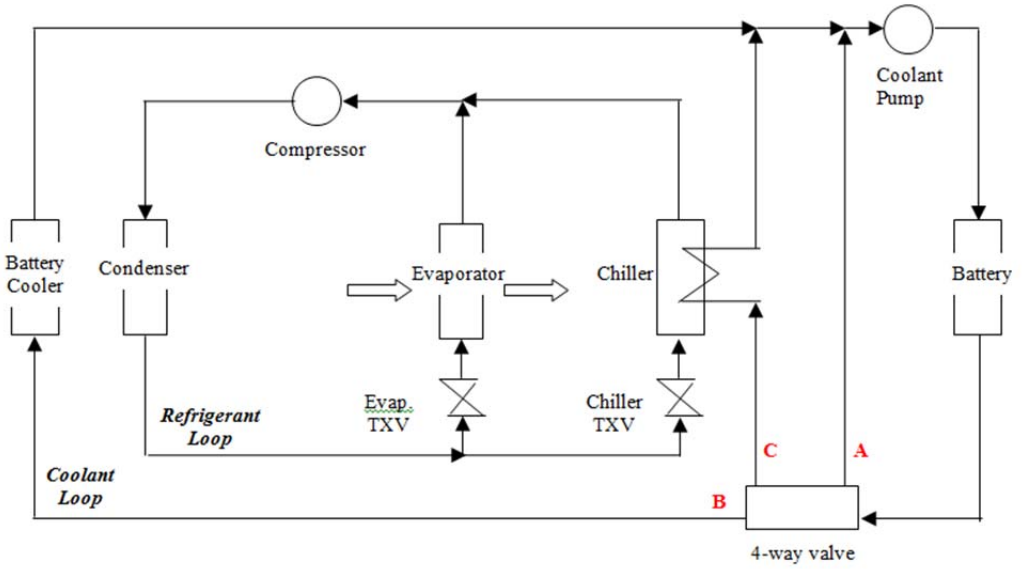

Figure 6.3: General schematic of liquid based TMS (A: bypass route, B: battery cooler route, C: chiller route).

In this system, the method of keeping the battery cooling medium at a low temperature depends on several factors such as the amount of heat generated in the battery, cabin heat load and ambient temperature. In the baseline model, since the ambient temperature is higher than the battery desired temperature target (21.5℃), the battery is cooled solely with the help of the

chiller which transfers heat from the coolant circuit to the refrigerant circuit. The coolant used (water/glycol mix) has high thermal capabilities, and the chiller is highly effective at cooling the battery to the optimal operating temperatures at high drive cycles. However, similar to the previous system, it uses additional compressor work associated with the chiller; therefore the exergy efficiency of the system is 0.29 with respect to the baseline model. Another important advantage of this system is the flexibility under various required cooling rates as well as battery and ambient temperatures. This can be seen when the ambient temperature is reduced below the 20℃. Below this temperature, some portion of the hot coolant that leaves the battery could be cooled with the help of the battery cooler that utilizes the ambient air flow, especially when the vehicle is travelling at high speeds. This cooling would be achieved by using a coolant pump in this circuit, which would consume negligible power compared to the compressor and thus increases the overall exergy efficiency of the system.

Even though the baseline refrigerant circuit model with different thermal management systems provides significant benefits in understanding the effectiveness of these systems based on the exergy analysis, the model neglects certain aspects which can have an important role when comparing these TMS. Among these aspects, the cost associated with manufacturing and maintenance has a significant role in selecting the appropriate thermal management system. Because of relatively recent widespread commercialization of these technologies in passenger vehicles, it is difficult to consistently compare each TMS based on cost. The passive air cooling TMS is in general considerably cheaper to install and maintain than active liquid cooling systems due to a significantly simpler design with less components and potential for leaks. Furthermore, passive air cooling systems utilize the already available cabin air to cool the battery and therefore, unlike most active liquid cooling TMSs, do not require any significant operating cost other than the power required for fan work. However, most passive air cooling TMSs are used on batteries that have lower cooling rate requirements than Li-ion (due to previously mentioned thermal capabilities in Section 2.3) and these batteries generally operate at higher temperatures. Since higher operating temperatures reduce the cycle life of the battery over the long term, especially under high drive cycles, the cost associated with replacing the battery increases the overall cost of the TMS drastically. Therefore, utilizing a TMS that is compatible with the

desired driving cycle, cooling load and operating conditions is a key factor in selecting an appropriate TMS to have a low cost over the long term.

In addition, another important factor is the entropy generation associated with each different TMS due to cooling the battery and/or the hot coolant. Entropy is generated due to the finite temperature differences as well as fluid friction associated with the TMS. In these systems, the majority of entropy generation is based on the corresponding heat transfer and frictional effects. The heat transfer effects are correlated to the difference of the coolant inlet and outlet temperatures. For the analysis, the average of the minimum and maximum inlet – outlet temperature differences are used. The same inlet temperatures are used in all systems in order to provide a consistent comparison. The second terms are taken with respect to the difference in the inlet and outlet pressure due to the irreversible losses caused by the fluid friction inside the tubes. For the cabin air cooling system, the entropy generation for cooling the battery is represented by the heat transfer irreversibility in external flow as given below (Bejan, 1996):

$$\dot{S}_{gen,external} = \left(\frac{(T_b - T_{c,in})}{T_{c,in}}\right)^2 \bar{h}A + \frac{1}{T_{c,in}} A_{tube} \Delta P \, V_c \tag{6.1}$$

The fluid velocity is calculated from the mass flow rate and the associated area of the tube. ΔP is the pressure drop of the flow inside the battery. For the refrigerant system, refrigerant is utilized in the system to cool the battery. The respective equation is

$$\dot{S}_{gen,refrigerant} = \frac{\dot{m}_r h_{fg}}{T_{evap}} + \frac{\dot{m}_c \Delta P}{\rho_{c,in} T_{c,in}} \tag{6.2}$$

For the refrigerant cooling system, the refrigerant goes through phase change when cooling the battery, and the heat transfer occurs from latent heat of vaporization (h_{fg}), where the temperature of the refrigerant remains constant. Therefore, the enthalpy difference is used for calculating the thermal entropy generation rate, which is significantly higher due to the phase change in the refrigerant. The liquid cooling system goes through a similar procedure in terms of entropy generation rate, except that the coolant does not change phase through the battery.

Therefore the thermal entropy generation is based on the temperature difference of the coolant as given below:

$$\dot{S}_{gen,coolant} = \frac{Q\ (T_{c,out} - T_{c,in})}{{T_b}^2} + \frac{\dot{m}_c \Delta P}{\rho_{c,in} T_{c,in}} \tag{6.3}$$

When different TMSs are analyzed with respect to these criteria, in order to provide the same amount of battery cooling (0.35 kW), the cabin air cooling system, refrigerant cooling system and liquid cooling system entropy generation rates are calculated to be 0.003 W/K, 1.190 W/K and 0.007 W/K, respectively, based on the average mass flow rates of each system. The refrigerant cooling system has significantly larger entropy generation rates due to phase change of the refrigerant in the system.

6.2.1 Battery Heat Transfer Analysis

6.2.1.1 Battery Temperature Distribution

In the TMS, the rate of heat transfer between the walls of the module and the fluid depends on various properties of the transfer medium. Air cooling is used for batteries that operate in relatively uniform operating conditions that do not require significant cooling. They are in general simpler and cheaper than liquid cooling with less components and potential for leaks. However, they have a significantly lower heat capacity and heat transfer coefficient. Direct contact fluids have relatively high heat transfer rates, especially compared to air, due to their boundary layer and thermal conductivity. Furthermore, they have the best packaging densities among the aforementioned TMSs. Indirect contact water also has significantly higher heat transfer coefficients because of its relatively low viscosity and thermal conductivity. Moreover, they do not require fans or air ducts in the vehicle or occupy a large space for proper cell arrangement. However, their effectiveness can decrease significantly as a result of the added thermal resistance such as a jacket wall or air gaps (Pesaran, 2001). As a result, even if the heat removal rates from the cells to the coolant are the same in the different thermal management systems, liquid coolants such as water (or water/glycol mix) would not be heated as fast as air due to a higher heat capacity. Moreover, the difference between the coolant mean temperature and the cell surface temperature would be significantly lower in liquid cooling systems due to

their larger heat transfer coefficient, which reduces both the maximum battery temperature and the temperature difference among the cells in the pack (Kim and Pesaran, 2006).

In order to calculate how fast each thermal management system cools the battery, first the battery heat generation needs to be determined. The heat in the battery is generated due to the internal resistance of the battery as follows:

$$Q_b = I^2 R \tag{6.4}$$

Here, I is the current and R is the resistance associated with the battery cells. The internal resistance is based on several factors such as ohmic resistance and kinetic and diffusion polarization losses in the cell and the electrical collector system. The present model incorporates 80A current and 66 mΩ resistance (Johnson and Pesaran, 2000), which corresponds to 0.35 kW of heat dissipation. Without any active heat dissipation, over time, this performance and cycle life of the battery will be reduced significantly. According to the Arrhenius approximation of the temperature dependence on the battery life, a 10-15 K increase in a Li-ion battery can result in 30% to 50% reduction in the battery's life endurance (Kuper et al., 2009, Bejan, 1996) Without any cooling system, the battery heat would be dissipated by natural convection with equation 6.5 given below:

$$m_b C_{P,b} \frac{dT}{dt} = \bar{h} A (T_b - T_0) \tag{6.5}$$

This equation can be solved in terms of time (t) as follows:

$$t = \frac{m_b C_{P,b}}{\bar{h} A} \; ln\left(\frac{T_b - T_0}{T_f - T_0}\right) \tag{6.6}$$

where m_b is the thermal mass of the battery, based on 288 cells with 0.45 kg each and $C_{P,b}$ is the heat capacity of the battery of 795 J/kg-K (Pesaran, 2001), $\bar{h}$ is the effective heat transfer coefficient of 6.4 W/m^2-K (Al-Hallaj, 2000) and A is the cell surface area that is assumed to be 8 m^2. Based on the battery characteristics assumed for the model and an ambient temperature of

25℃, the time required for the battery temperature to decrease from 55℃ to 30℃ by natural convection is determined to be approximately 1 hour. Since this time is unacceptable for most cycles in the battery, the need for a better designed TMS becomes evident. With the utilization of a TMS, the time it takes for the battery temperature to reach optimal levels while used in the vehicle can be calculated by the equation below:

$$m_b C_{P,b} \frac{\partial T}{\partial t} = I^2 R - \bar{h} A (T_b - T_0) - \dot{m}_c C_{P,c} \left(T_{c,out} - T_{c,in}\right) \tag{6.7}$$

For the majority of TMS, the natural convection term is usually negligible compared to the cooling provided by the system. In order for the model to be more representative of the actual case, the internal heat generation of the battery, natural convection and cooling rates are written as a function of time. The above differential equation is solved and sample results of the battery temperature with respect to time can be obtained for each thermal management system, as shown in Figure 6.4. For the refrigerant cooling system, the temperature rise varies significantly based on the mass flow rate of the refrigerant and is limited by the cost associated with the compressor work, and therefore a specific value is not provided in the figure. In order to provide an adequate comparison, the battery temperature rise is based on natural convection alone and it is also provided in Figure 6.4.

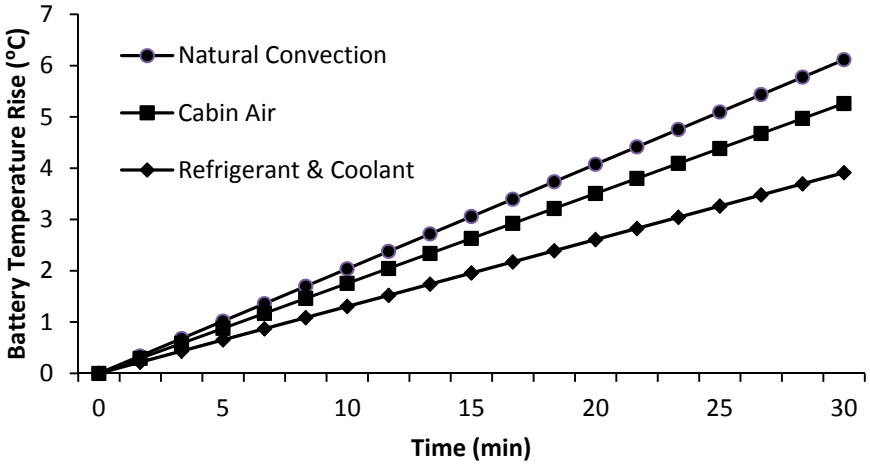

Figure 6.4: Temperature rise in the battery with time based on natural convection and various thermal management systems.

The heat generation and cooling rates are assumed to be linear for the analysis. From Figure 6.4, it can be seen that natural convection has the maximum temperature rise in the battery, significantly higher than the liquid cooling system. Thus, when the different TMSs are examined solely with respect to the minimum battery temperature rise, the liquid cooling system provides significantly better cooling than the cabin air system.

6.2.1.2 Battery Temperature Uniformity

The uniformity of the battery cells being cooled is just as important (if not more) as the maximum cell temperature, since it is one of the major causes of thermal runaway. Temperature variation between cells in the battery pack may result from ambient temperatures differences among the battery pack surface, non-uniform impedance distribution and heat transfer efficiency differences among cells in the pack (Al-Hallaj and Selman, 2002). Non-uniform impedance can result from defects in quality control or due to differences in the local heat transfer rate. Heat transfer efficiency differences are significantly related to the pack configuration since the cells along the edges are cooled by heat transfer to the environment while the ones in the center accumulate heat, which can magnify capacity differences among cells. The resultant excessive local temperatures rise in the cells, when not cooled down, may result in accelerating capacity fading and even thermal runaway in the battery pack. Even though the melting temperature for the battery is significantly high (e.g 180℃ for lithium-ion), if one or more internal cells in the stack is short-circuited, significant heat sources will exist locally, which is capable of raising the battery temperature from room temperature to above melting point of the battery in less than a minute (Yufei et al., 1996). Since most battery packs are closely packed in order to exploit the energy and power densities of the battery (especially Li-ion), thermal runaway of a single cell can propagate and cause an entire battery to fail violently (Sabbah et al., 2008). Therefore, the uniformity of the battery cells has a significant role when comparing different TMSs and can be calculated for the battery used in the model. It is directly related to the temperature difference of the cooling medium before and after cooling the battery. In order to keep the cell temperature differences within tolerable limits, the coolant temperature difference needs to be small (less than 3℃) (Kuper et al., 2009). In the TMS, this is limited by the specific heat of the medium and mass flow rate. The relationship can be written as follows:

$$\dot{Q}_b = \dot{m}_c C_{P,c}(T_{out} - T_{in}) \quad (6.8)$$

The model assumes the heat dissipation to be constant at 0.35 kW. In a cabin air cooling system, the maximum flow rate from the cabin to the battery is limited with respect to the cabin comfort and tolerable noise levels. It is typically between 1.9 kg/min and 4.8 kg/min (Kuper et al., 2009). This results in a cooling temperature difference variation between 4.5℃ and 11℃, approximately. In the refrigerant based cooling however, the cooling is provided with respect to latent heat instead, and the mass flow rate of the refrigerant depends on various factors, including the utilized compressor, and the cooling load of the evaporator and the battery, as is taken to be 0.07 kg/min to 0.7 kg/min. Moreover, the battery temperature uniformity will vary significantly based on the cooling parameters. In the liquid cooling system, the water flow rate is usually regulated around 1 kg/min to 10 kg/min which provides a cooling temperature difference of between 0.48℃ and 4.57℃. Thus, when the different TMSs are examined solely with respect to their ability to cool the battery cells without major temperature differences among them, the liquid cooling system provides significantly better cooling than a cabin air system. This is due to indirect-contact heat transfer liquids (such as water) having higher specific heat and thermal conductivity than air, resulting in higher heat transfer coefficients. Moreover, generally the mass flow rates of the coolants (such as water) are significantly higher than the mass flow rates of the refrigerants (such as R134a) since the cost associated with the electricity consumption of the pump is significantly lower than the compressor. However, the decrease in indirect contact effectiveness is also a significant factor, since the heat must be conducted primarily through the walls of the jacket/container.

6.2 Exergy Analysis of Liquid TMS

6.2.1 Baseline Model

A software code in EES was developed to analyze a baseline model, with respect to the balance equations and system parameters provided in Section 5.2. Based on the baseline analysis, the exergy efficiencies and exergy destruction rates associated with each component are provided in Figure 6.5. Throughout the exergy analysis; the exergy efficiencies and exergy destruction rates are calculated for each component in the thermal management system. Among these

components, the heat exchangers have the lowest exergy efficiencies with respect to the high temperature differences and phase change which results in more entropy generation between the refrigerant and coolants.

In the evaporator, the exergy losses are relatively high since (aside from the frictional losses) only part of the heat rejection occurs during the phase change process with large temperature differences between the working fluid in the evaporator and the vehicle cabin. Thus, reducing the mean temperature difference would reduce the exergy losses. One way of reducing the mean temperature difference is to increase the evaporator surface area, however, it should be weighed against the increase in the cost of installation (Hepbasli et al., 2009) (which is analyzed in the exergoeconomic analysis section).

The condenser is calculated to have a lower exergy efficiency than the evaporator and the chiller, mainly due to the relatively higher temperature difference between the condenser exit and ambient air (taken at 35ºC), when compared to the differences between the evaporator exit and vehicle cabin temperature as well as the refrigerant and coolant temperatures.

Among the remaining components, the compressor has high compression pressure ratio and change in temperature of the refrigerant passing through the compressor, which contributes to an increase in exergy destruction. The exergy loss in the compressor can be reduced by using a compressor with higher isentropic efficiencies. Moreover, since the compressor power is highly dependent of the inlet and outlet pressures, proper sealing inside the compressor, heat exchanger improvements (such has reducing ΔT) and the implementation of multistage compression would reduce the exergy losses, thus reducing the compressor power. Furthermore, since a part of the irreversibilities occurs with respect to the frictional losses inside the compressor, utilizing appropriate lubricating oil that is miscible with the refrigerant (such as Polyolester oil for R-134a) would reduce the respective exergy losses.

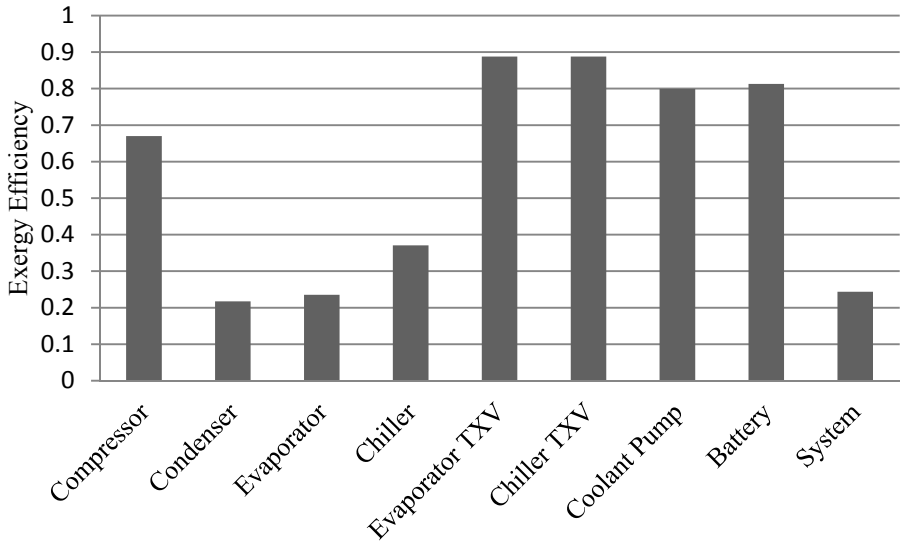

(a)

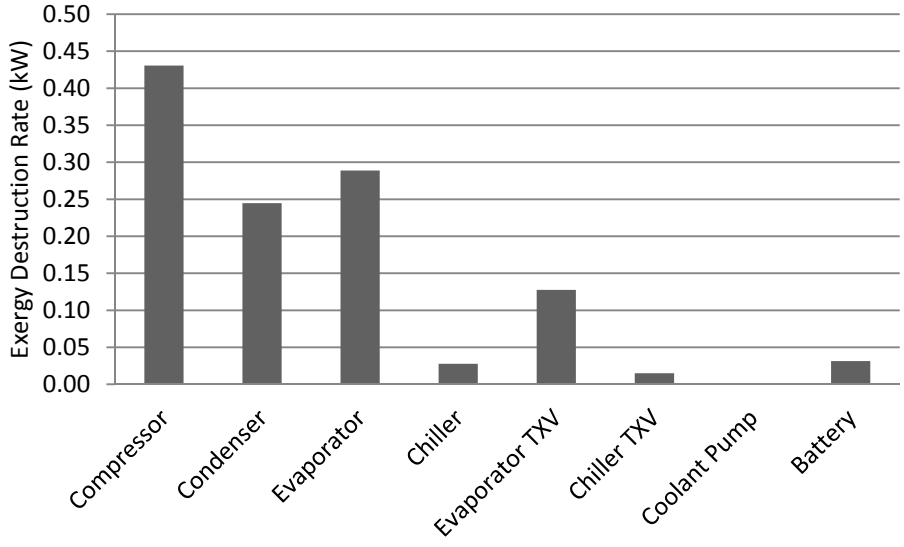

(b)

Figure 6.5: Baseline model (a) exergy efficiency and (b) exergy destruction rate of each component in the refrigerant and coolant cycles.

There is also significant research conducted (Lee at al., 2007, Kedzierski et al., 2009) on the effects of using additives with a high conductivity (certain lubricant based nanofluids) in the refrigerant in order to improve the heat transfer rate, thus reducing the difference in the operating temperatures, which also reduced the exergy losses. However, proper care must be taken in the utilization of the lubricant in order to prevent the deposition of the lubricant in the evaporator

wall. The interaction between the cooling and battery coolant cycles also helps in reducing the compressor requirements significantly. The transfer of excess heat from the battery coolant to the cooling cycle via the chiller helps allocate the thermal energy appropriately, since otherwise, the cooling cycle would need to supply the additional energy which uses a compressor. Therefore, further utilizing this interaction would also be beneficial. Moreover, irreversibilities in the system occur due to high temperature differences in heat exchangers, and therefore reducing these differences would reduce the associated irreversibilities (Behr, 2012).

The exergy efficiencies for the evaporator TXV and chiller TXV are higher (over 80%) since the processes are isenthalpic and have little or no heat loss. Therefore the exergy losses occur mainly due to a pressure drop in the expansion valve. The exergy losses in these TXVs can be reduced by lowering (or sub-cooling) the temperature of the refrigerant exiting the condenser, which can be feasible by utilizing the refrigerant vapor exiting the evaporator (Kumar et al., 1989; Arora 2008). The coolant pump also has a relatively higher efficiency (81%) since there is no significant heat loss from the pump.

It should be noted that the battery is modeled as a system and thus the internal efficiencies for the battery are not considered in this analysis. In this regard, the battery has high efficiencies within the target operating temperature range (up to 50ºC). However, the associated efficiency would decrease significantly as the battery is heated up beyond this range.

Moreover, TMS is analyzed with respect to theoretical thermodynamic and "unavoidable thermodynamic" cycles in order to split the exergy destructions associated with each component into endogenous/exogenous and avoidable/unavoidable parts. The normalized exergy destruction values for the major components can be seen in Figures 6.6 – 6.12. It should be noted that even though the total exergy destruction in a component cannot be negative, the exogenous portions can be negative, which would indicate a negative correlation between endogenous exergy destruction within a component and the exogenous exergy destruction within the remaining components.

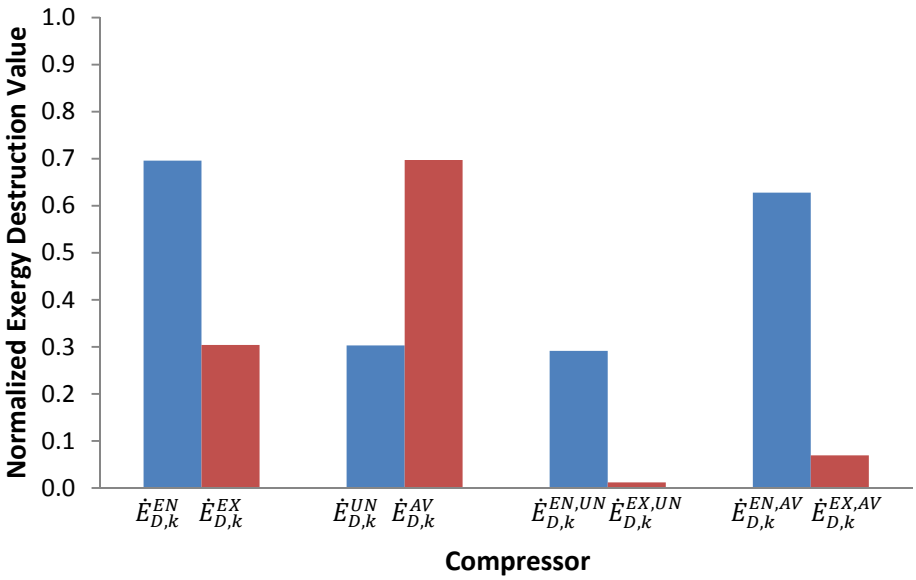

Figure 6.6: Normalized exergy destruction values associated with the compressor based on the conducted advanced exergy analysis.

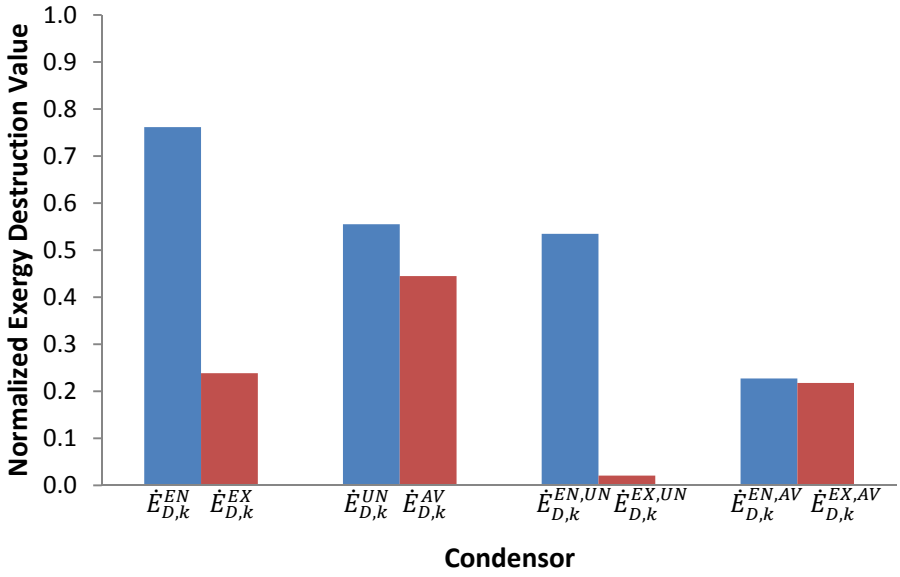

Figure 6.7: Normalized exergy destruction values associated with the condenser based on the conducted advanced exergy analysis.

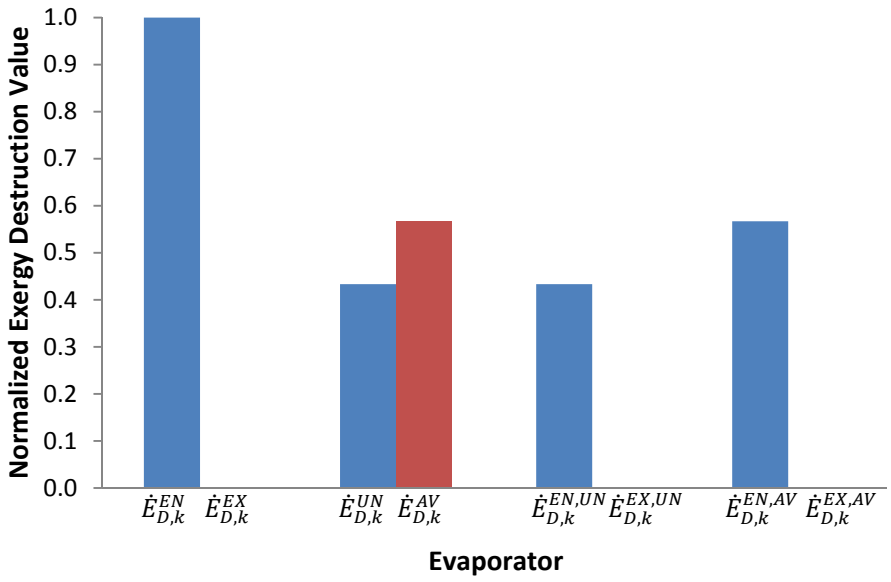

Figure 6.8: Normalized exergy destruction values associated with the evaporator based on the conducted advanced exergy analysis.

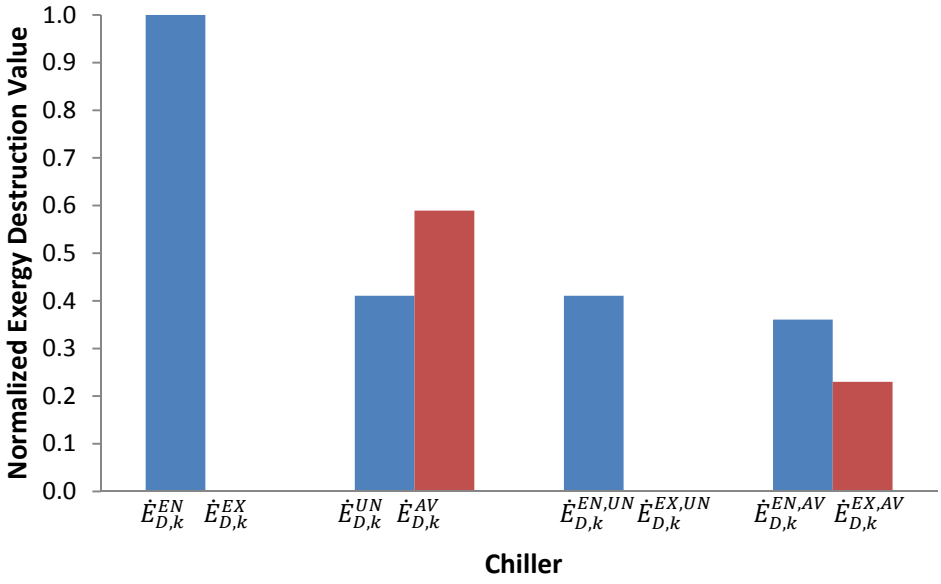

Figure 6.9: Normalized exergy destruction values associated with the chiller based on the conducted advanced exergy analysis.

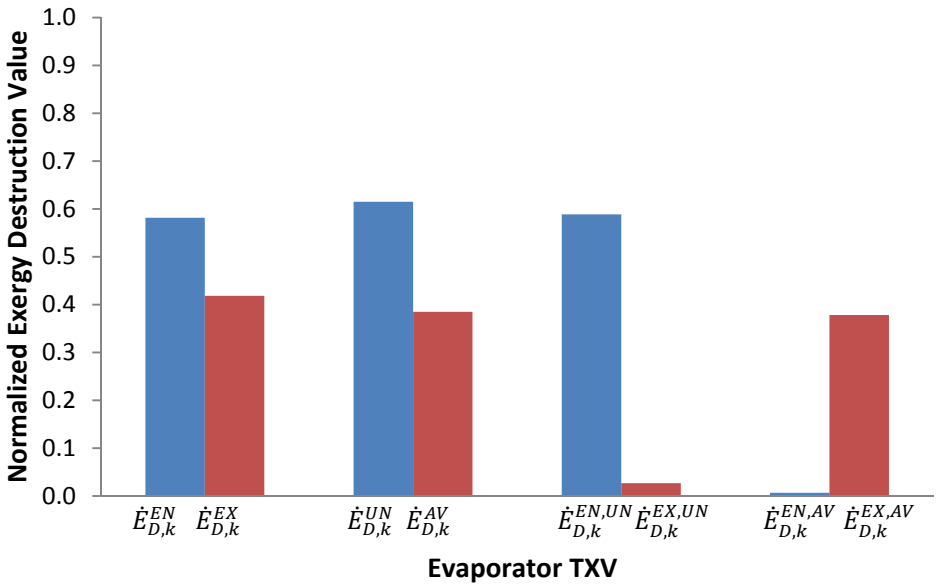

Figure 6.10: Normalized exergy destruction values associated with the evaporator TXV based on the conducted advanced exergy analysis.

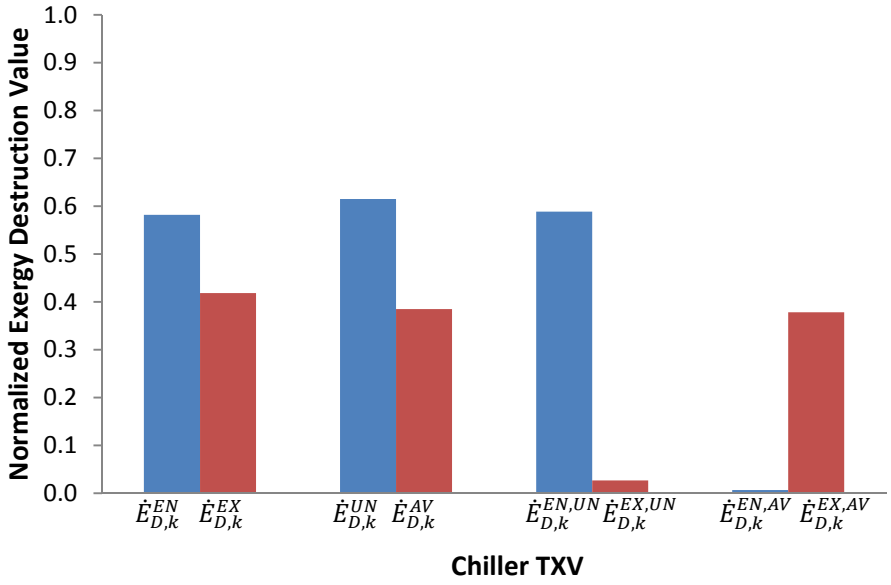

Figure 6.11: Normalized exergy destruction values associated with the chiller TXV based on the conducted advanced exergy analysis.

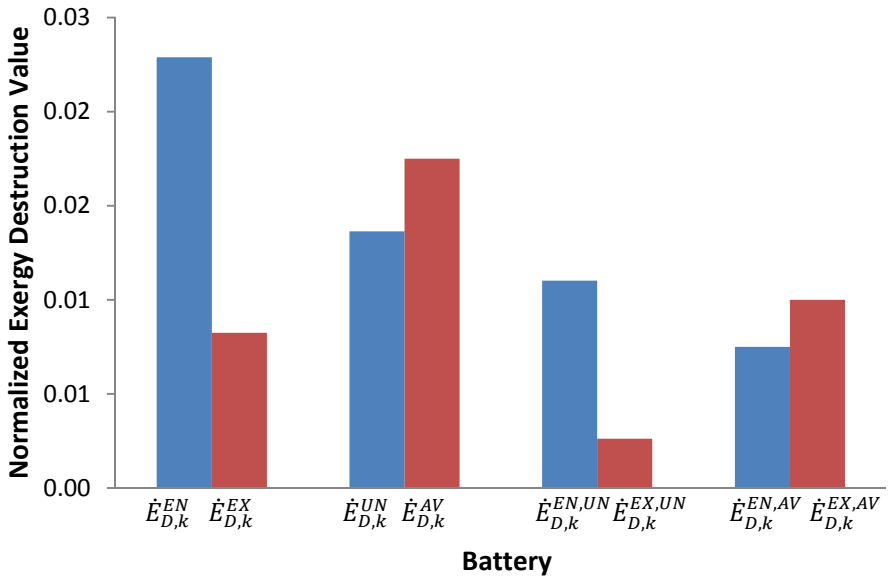

Figure 6.12: Normalized exergy destruction values associated with the battery based on the conducted advanced exergy analysis.

Based on the Figures 6.6 - 6.12, it can be seen that the exogenous exergy destruction is small but significant portion of the total exergy destruction in each component, which shows that there is a moderate level of interdependencies among the components. Furthermore the exogenous exergy destruction is lower than the total exergy destruction for each component ($\dot{E}_{D,k}^{EX}$ is positive), which indicates that a reduction in the endogenous exergy destruction within a component will yield a reduction in the exogenous exergy destruction within the remaining components.

6.2.2 Parametric Studies

The system model is also analyzed based on the effects of condensing and evaporating temperatures, as well as subcooling and superheating temperatures, compressor speed, heat exchanger pressure drop and battery heat generation rates. Baseline values are used for all non-varied parameters in the parametric studies. Moreover, the use of various alternative refrigerants such as R290 (propane), R600 (butane), R600a (isobutane), R1234yf (tetrafluorpropene) and dimethyl ether (DME) are also investigated under various conditions. Condensing and evaporating temperatures affect the compression ratio, cooling load, COP and volumetric heat capacity. Many studies in literature have considered the compression ratio as a useful parameter on which to predict the volumetric performance of the compressor (Guy, 1971; Stoecker and

Jones, 1982) since lower compression reduces the likelihood of the high pressure vapor to leak back to the low pressure side, which reduces the compressor volumetric efficiency. Figure 6.13 shows that the compression ratio is reduced by decreasing the condensing temperature or increasing the evaporator temperature.

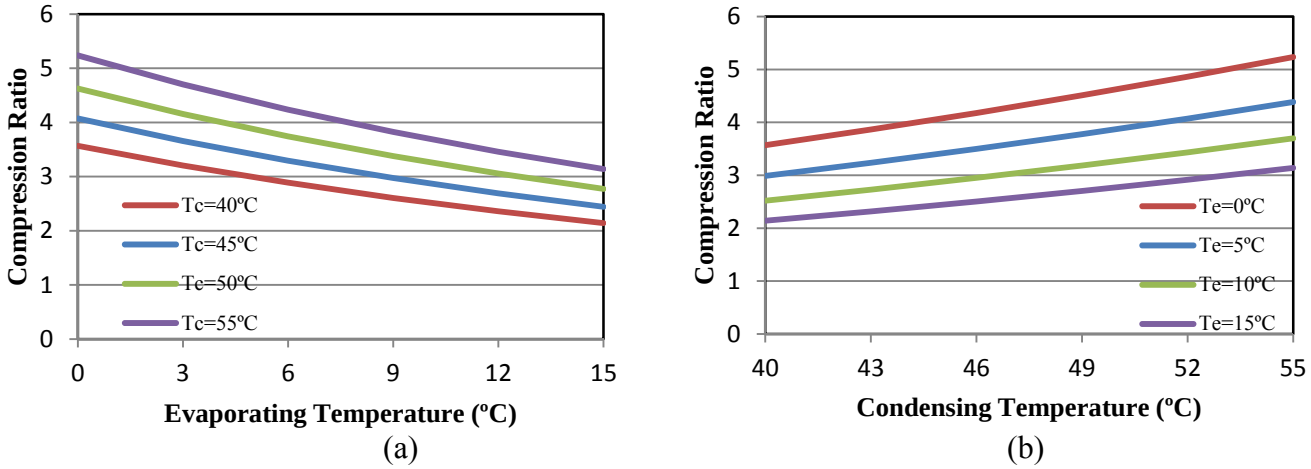

Figure 6.13: Compression ratio with respect to (a) evaporating and (b) condensing temperatures.

In addition, as the evaporator temperature increases, the temperature of the refrigerant vapor before entering the compressor also increases. The refrigerant vapor specific volume reduction increases the associated refrigerant mass flow rate, and therefore increases the system cooling output. On the other hand, an increase in the condensing temperature leads to an increase in the temperature of the refrigerant discharged from the compressor along with the compression ratio. However, the compression capacity of the compressor will be reduced. Moreover, the refrigerant circulated per unit of time will be lower, which reduces the cooling load as shown in Figure 6.14.

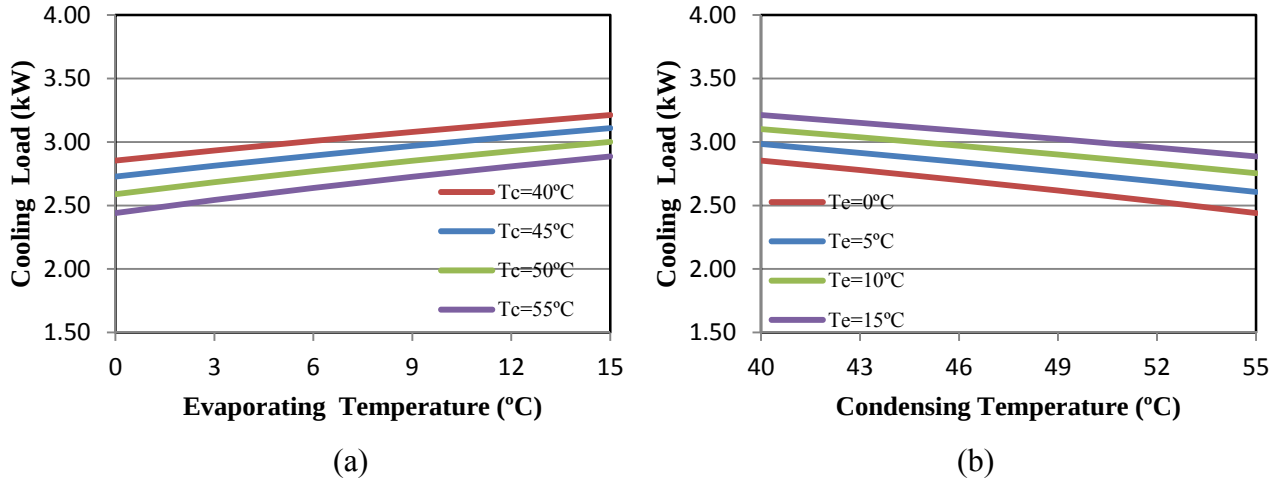

Figure 6.14: Cooling Load with respect to (a) evaporating and (b) condensing temperatures.

Moreover, since energy consumption of the compressor is also proportional to the pressure ratio, this reduction in the condensing temperature or increase in the evaporator temperature increases the COP of the system by reducing the compression ratio. This indicates that the required compressor power to a certain cooling capacity drops as the condensing temperature decreases or the evaporating temperature increases. Moreover, the throttling losses also decrease with decreasing temperature change, hence leading to an increase in the COP as shown in Figure 6.15.

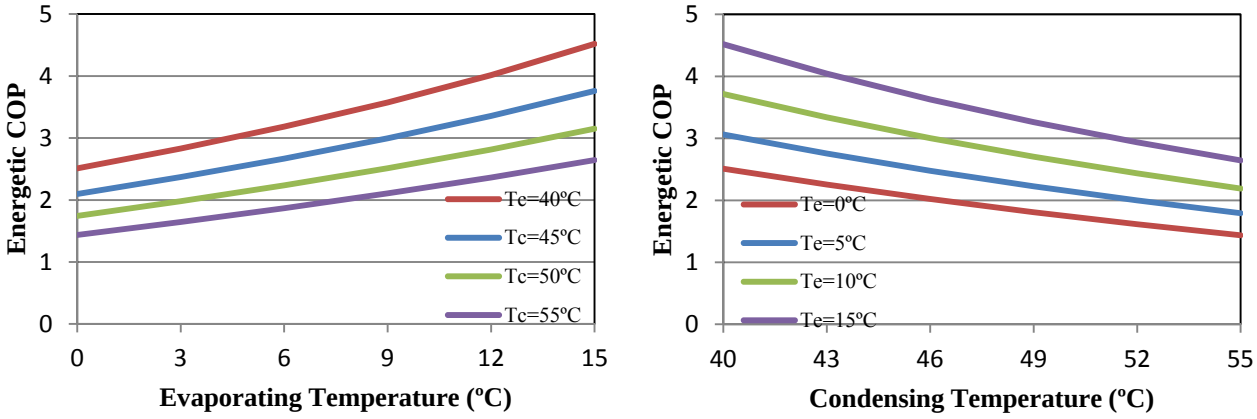

(a) (b)

Figure 6.15: Energetic COP with respect to (a) evaporating and (b) condensing temperatures

Furthermore, the exergetic COP of the system also increases since reducing the condensing temperatures reduces the mean temperature difference between the refrigerant and the ambient air. Increasing the evaporating temperatures reduces the mean temperature difference between the refrigerant and the cabin air, both reducing the associated exergy destruction as shown in Figures 6.16 and 6.17.

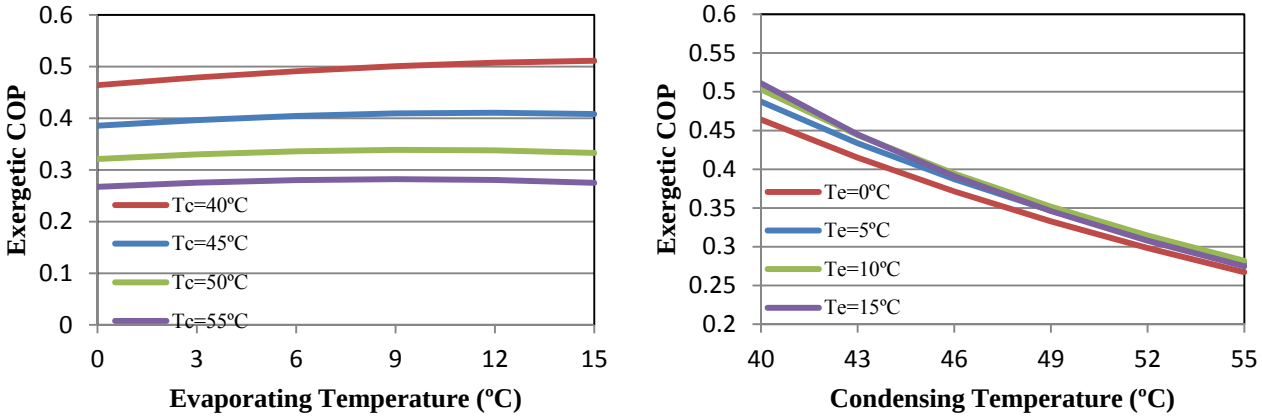

(a) (b)

Figure 6.16: Exergetic COP with respect to (a) evaporating and (b) condensing temperatures.

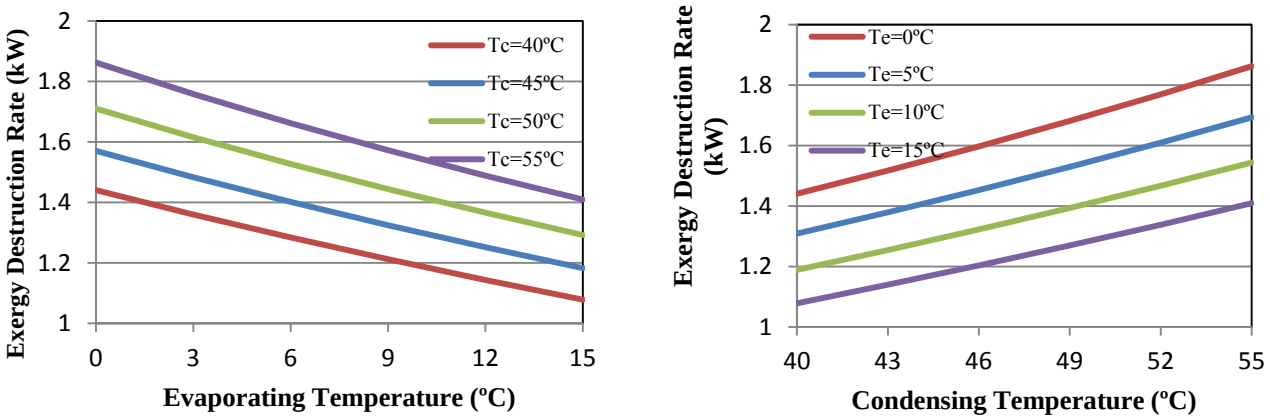

(a) (b)

Figure 6.17: Exergy destruction rate with respect to (a) evaporating and (b) condensing temperatures.

It is determined that increasing the degree of superheating can also lead to an increase in the refrigerant enthalpy, which results in extracting additional heat and increasing the refrigeration effect per unit mass of the evaporator. As a result of the larger refrigerating effect per unit mass of the superheated cycle, the associated mass flow rate of the refrigerant per unit capacity decreases. In addition, the specific volume of suction vapor as well as the work of compression per unit mass also increases. However, the increase in the refrigerating effect is slightly larger than that of the work of compression, thus the exergetic COP of the system increase is negligible (Dincer and Kanoglu, 2010) as shown in Figure 6.18.

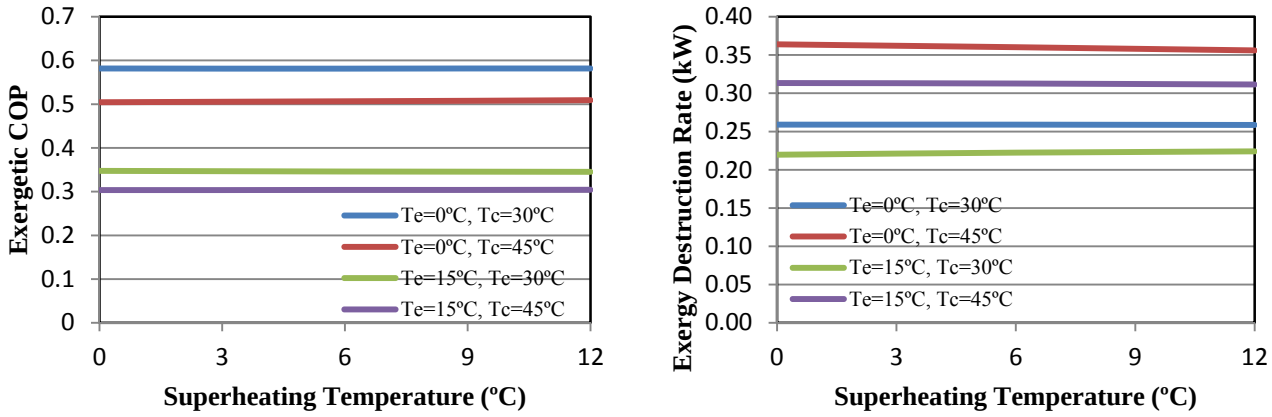

(a) (b)

Figure 6.18: (a) Exergetic COP and (b) exergy destruction rate with respect to superheating temperatures.

The refrigerating effect per unit mass can also be increased by subcooling the saturated liquid before it reaches the TXV, due to a lower mass flow rate of refrigerant per unit capacity compared to that of the saturated cycle. The volume of vapor that the compressor must handle per unit capacity decreases since the refrigerant vapor entering the suction line inlet (and thus the specific volume of the vapor entering the compressor) remains the same. Moreover, since the heat of compression per unit mass also remains the same, the increase in refrigerating effect per unit mass increases the heat absorbed in the refrigerated space without increasing the quantity of the energy input to the compressor, and thus increases the exergetic COP of the system as shown in Figure 6.19.

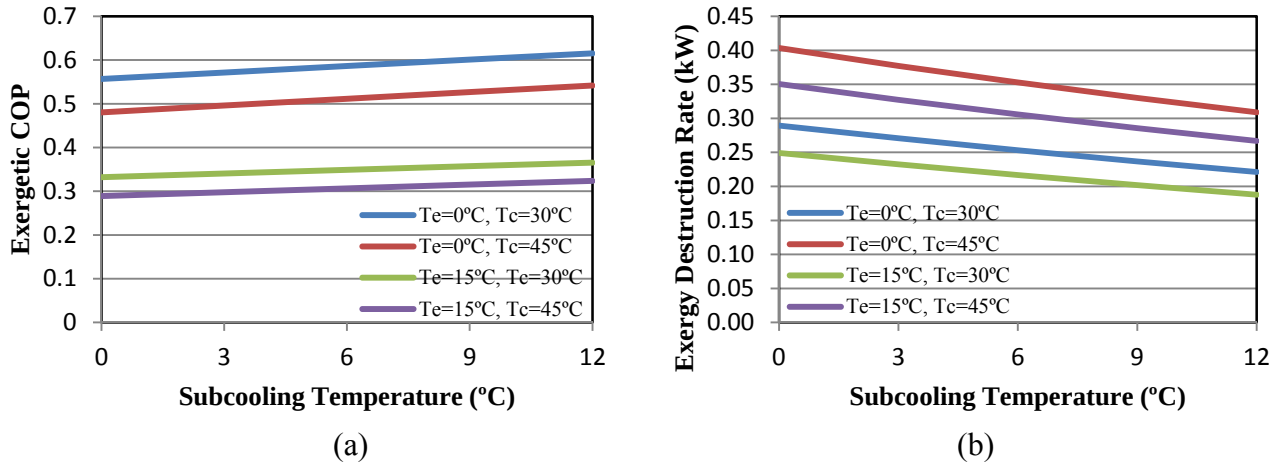

Figure 6.19: (a) Exergetic COP and (b) exergy destruction rate with respect to subcooling temperatures.

The pressure drop in the heat exchangers also has a certain effect in the system parameters. The increase in pressure drop decreases the cooling capacity due to the reduction in the specific refrigerating effect. In addition, the associated pressure ratio across the compressor increases, leading to an increase in the corresponding compressor work (Arora and Kaushik, 2008). Both of these effects assist in reducing the exergetic COP of the system while increasing the exergy destruction. The effects of the air mass flow rates on the pressure drops as well as the pressure drop on the exergetic COP and exergy destruction rate are shown in Figures 6.20 and 6.21.

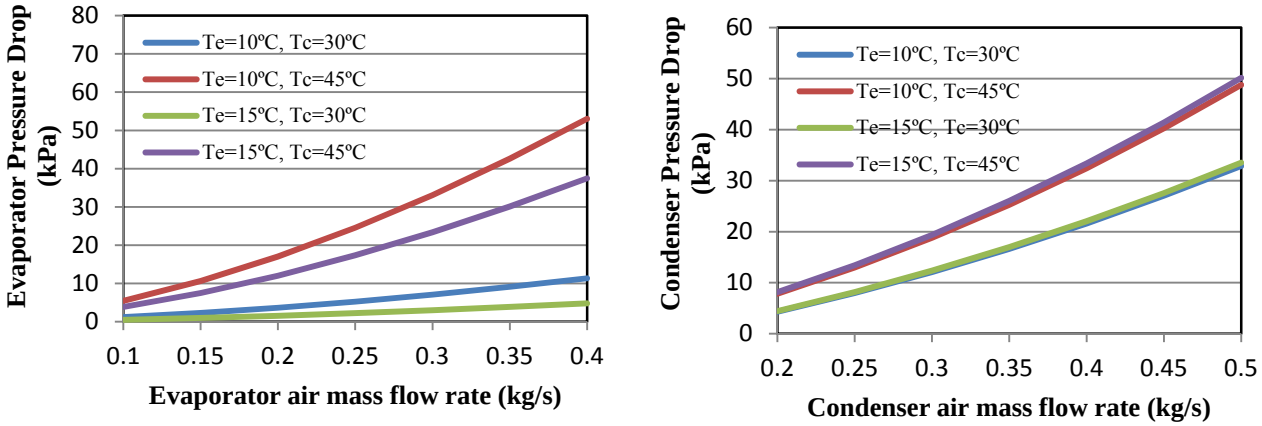

(a) (b)

Figure 6.20: Pressure drop with respect to (a) evaporator and (b) condenser air mass flow rates.

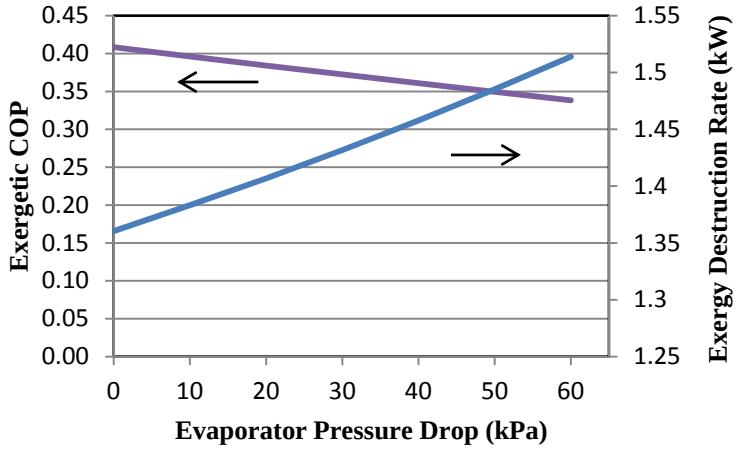

(a)

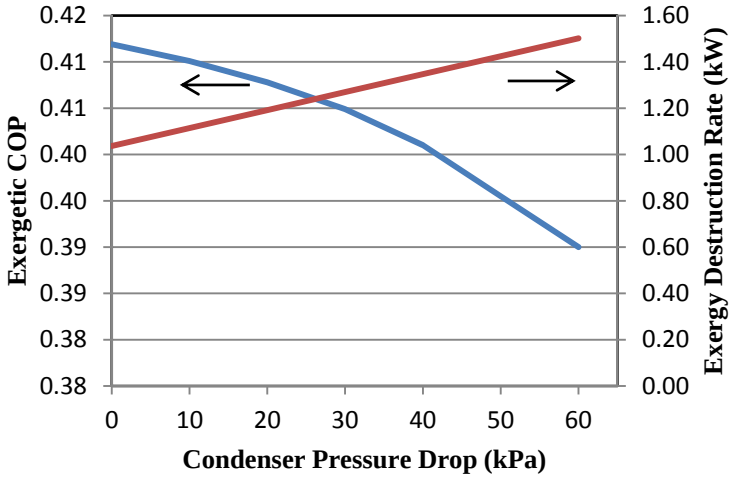

(b)

Figure 6.21: (a) Exergetic COP and (b) exergy destruction rate with respect to evaporator pressure drop.

The compressor ratio is another important parameter since it has a significant impact on compressor work, cooling capacity and energetic and exergetic COPs of the system. As the compressor speed increases, the average compressor work also increases, resulting in higher refrigerant mass flow rates, discharge pressure, compression ratio and lower suction pressure and volumetric efficiency. It is also found that the increase in the compressor ratio leads to an increase in the cooling capacity while decreasing the corresponding energetic COP of the system. The exergetic COP of the system also decreases since the associated pressure difference across the compressor and expansion valve increases the overall exergy destruction of the system (Hosoz and Direk, 2006). The effects of the resulting compression ratio on the system exergetic COP and exergy destruction rate are shown in Figure 6.22.

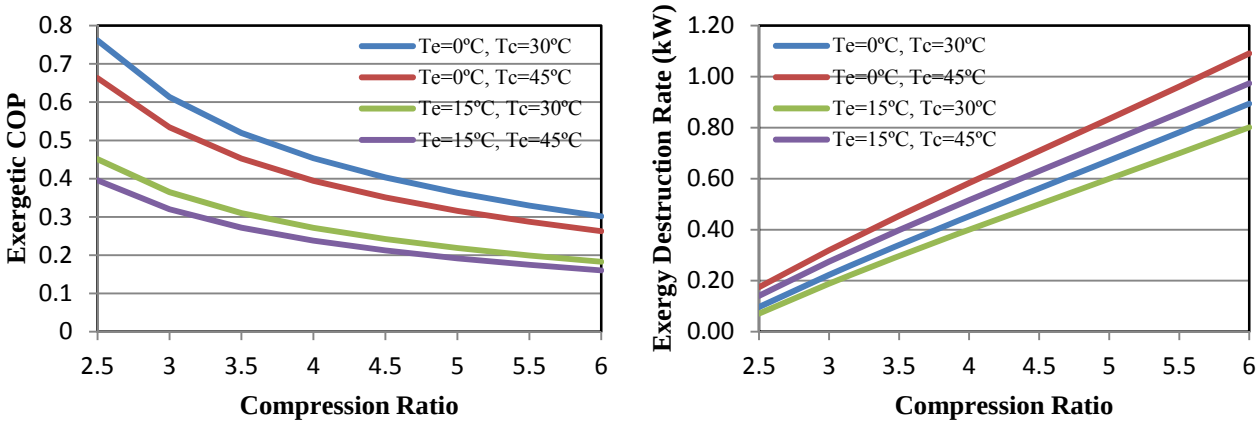

(a) (b)

Figure 6.22: (a) Exergetic COP and (b) exergy destruction rate with respect to compression ratio.

Moreover, parametric studies are conducted with respect to various refrigerants using EES and REFPROP software packages. In order to have a consistent comparison between these different refrigerants, the same cooling capacity (3 kW), condensing and evaporating temperatures (55 and 5°C, respectively), along with superheating and subcooling temperatures (5°C), are used in each model. The parameters for the model with different refrigerants are given in Table 6.2

Table 6.2 Operational parameters of a standard EV TMS for various refrigerants at baseline conditions.

Refrigerant	$\dot{m}_{ref,a}$ (kg/s) $\times 10^2$	$\dot{m}_{ref.b}$ (kg/s) $\times 10^2$	$\dot{W}_{comp}$ (kW)	x_{evap}	$T_{sat,dis}$ (°C)	P_{dis} (bar)	ΔP_{cond} (kPa)	ΔP_{evap} (kPa)
R134a	2.21	0.26	1.30	0.31	81.92	14.92	25.11	29.41
R290	1.18	0.14	1.27	0.32	77.93	19.07	24.60	32.97
R600	1.08	0.13	1.26	0.28	73.62	5.64	8.64	14.00
R600a	1.25	0.15	1.26	0.32	68.71	7.64	10.68	17.64
R1234yf	2.98	0.35	1.37	0.39	65.60	14.64	53.61	64.51
(DME)	0.92	0.11	1.21	0.25	95.33	12.97	6.28	13.25

In order for a refrigerant to be a suitable replacement for R134a, its compressor capacity should be similar to avoid a different size compressor in the cycle to accommodate the difference in capacity. For this reason, the vaporization temperature of the liquid in the evaporator (which is the suction or evaporating temperature) becomes one of the critical properties in considering a drop-in replacement refrigerant for the thermal management system, since refrigerants with similar vapor pressure evaporates and condenses at the same pressures. Thus, a refrigeration cycle designed with a particularly high and low side pressure would perform comparably for two refrigerants with comparable vapor pressures (Reasor et al., 2010). This would prevent a different size compressor in the cycle, since the compressor size decreases for fluids with higher vapor pressure and increases for ones with higher vapor pressure in order to provide the same cooling load. Moreover, since the expected capacities are proportional to the vapor pressure, the saturation pressure and temperature of the refrigerant alone would be good indicators of the compressor displacement volume (Kumar and Rajagopal, 2007). Thus, a convenient way to compare vapor pressure for multiple refrigerants is a saturation temperature - pressure plot as shown in Figure 6.23.

As shown in Figure 6.23, R290, R1234yf and Dimethylether have more compatible drop-in replacements (with the least changes in compressor physical dimensions) based on their compressor capacities, compared to R600 and R600a.

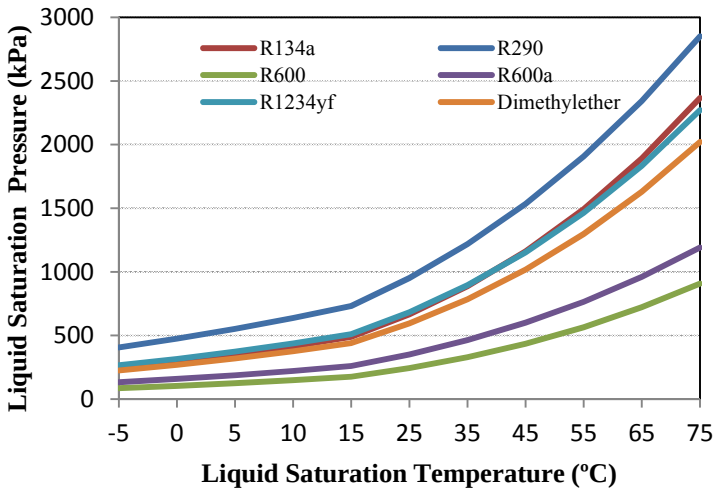

Figure 6.23: Liquid Saturation Temperature vs. Pressure for various refrigerants

The compression ratio is also a useful parameter on which to predict the volumetric performance of the compressor, since lower compression ratios can reduce the amount of potential leakage, and therefore can be used to compare the performance of the TMS using various refrigerants. Figure 6.24 shows that TMSs using R-600, R600a and R134a have higher compression ratios compared to the other systems. Systems utilizing R1234yf and Dimethylether exhibit the closest behavior to that of R134a with the compression ratio slightly lower than R134a system. Furthermore, the lowest compression ratio is achieved by TMS using R290, where it outperforms the system using R-134a up to 18% depending on the condensing and evaporating temperatures.

Moreover, the compressor work is also compared for the TMS using different refrigerants based on various evaporator and condenser temperatures, since it has a significant impact on the overall efficiency of the cycle. It can be seen that even though the TMS using R1234yf has a very low compression ratio among the refrigerants, it has the highest compressor work under baseline conditions due to its highest mass flow rate, as shown in Figures 6.24a and 6.24b. On the other hand, the TMS using Dimethylether has the lowest compressor work due to having the lowest mass flow rate as well as a relatively low compression ratio under baseline conditions. The systems using the rest of the studied refrigerants are calculated to have similar but slightly less compressor work, compared to R134a, due to lower compression ratios and significantly lower mass flow rates in the system as shown in Figures 6.24 – 6.26.

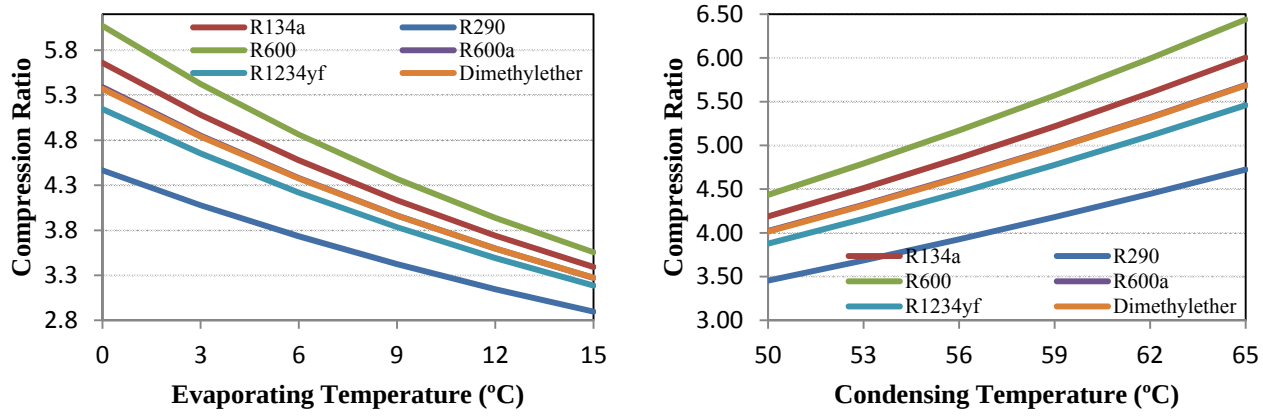

(a) (b)

Figure 6.24: Compression ratio of the TMS with respect to (a) evaporating and (b) condensing temperatures using various refrigerants.

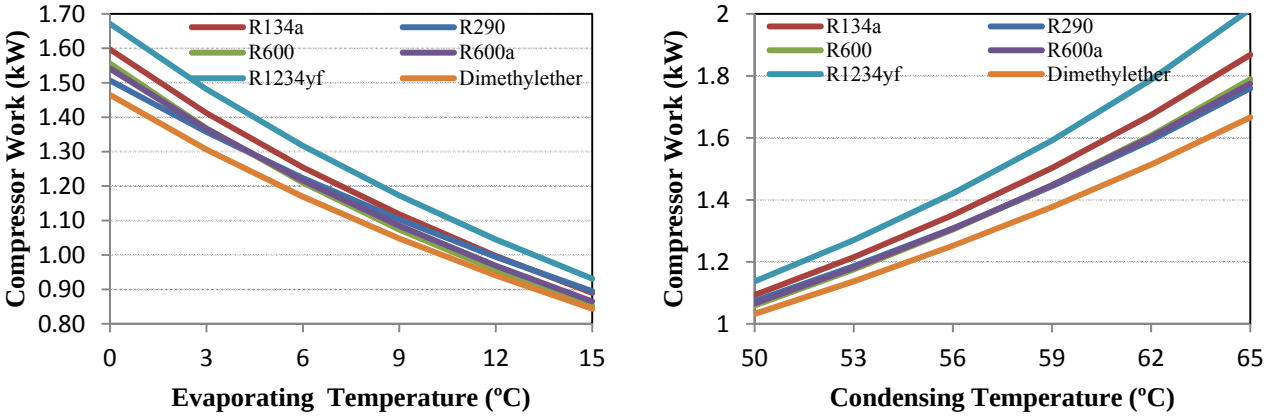

(a) (b)

Figure 6.25: Compressor work of the TMS with respect to (a) evaporating and (b) condensing temperatures using various refrigerants

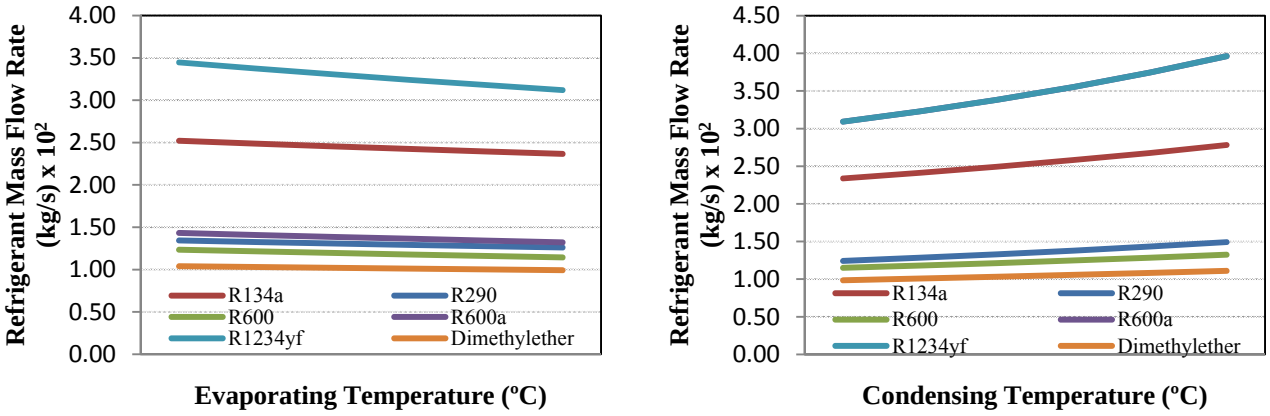

(a) (b)

Figure 6.26: Refrigerant mass flow rate with respect to (a) evaporating and (b) condensing temperatures using various refrigerants.

Moreover, since the energy consumption of the compressor is also proportional to the pressure ratio and refrigerant mass flow rate, the COP of the system also varies for the same cooling loads and different refrigerants. Among the TMS studied, all of the systems, except for the using R1234yf, have lower exergy destruction rates and higher energetic and exergetic COPs compared to the baseline R134a system for the range of evaporating and condensing temperatures. TMS using Dimethylether has the highest energetic and exergetic COPs with 7.3% and 7.7% higher than the baseline R134a system, respectively. However, due to the high flammability of this substance, in order to reduce the associated safety concerns, a secondary loop should be implemented to the thermal management system, where the conventional evaporator is replaced by a secondary fluid heat exchanger, which transfers heat between the primary and secondary loops. Thus, the overall efficiency of the system using this refrigerant may decrease for more practical applications. The energetic and exergetic COPs and exergy destruction of TMS with respect to evaporating and condensing temperatures using various refrigerants can be observed from Figures 6.27-6.29, respectively.

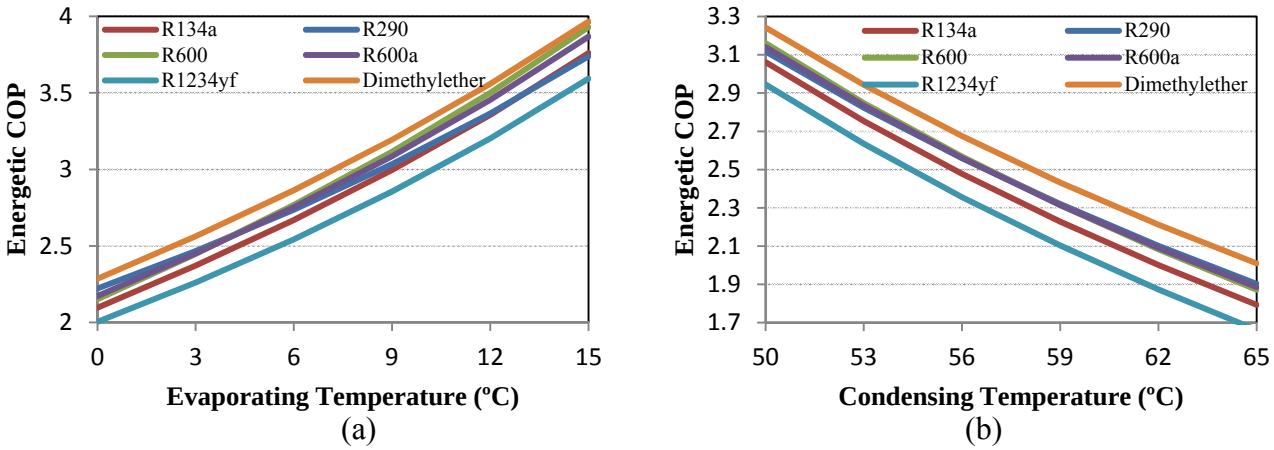

Figure 6.27: Energetic COP of the TMS with respect to (a) evaporating and (b) condensing temperatures using various refrigerants.

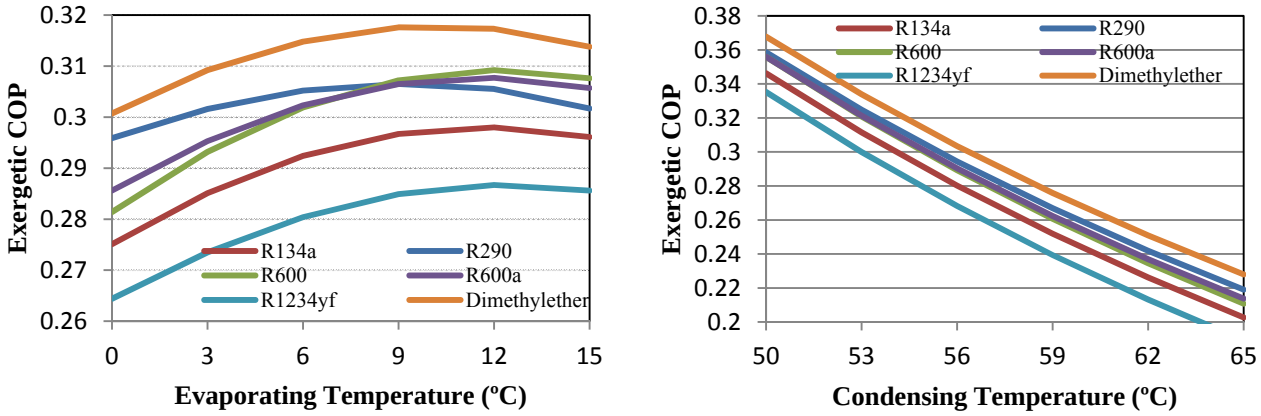

Figure 6.28: Exergetic COP of the TMS with respect to (a) evaporating and (b) condensing temperatures using various refrigerants.

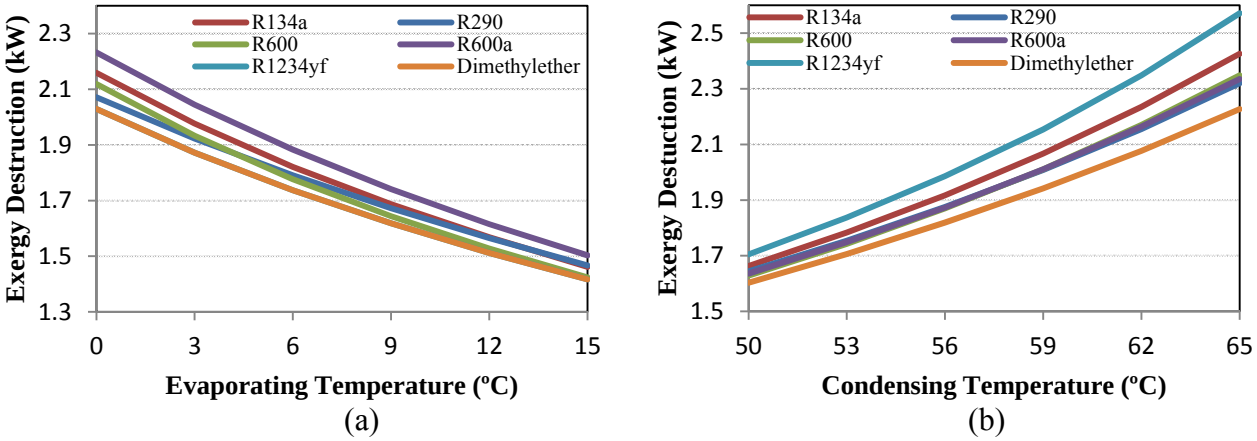

Figure 6.29: Exergy destruction of the TMS with respect to (a) evaporating and (b) condensing temperatures using various refrigerants.

Once the TMS COPs are calculated for various refrigerants, the corresponding indirect emissions and the sustainability indices are determined with respect to the system parameters of the baseline model. The sustainability index is a good indicator of how efficiently the resources are utilized in the TMS. Thus, it is therefore directly related to the exergetic COP and exergy destruction rates associated with each TMS. Moreover, the indirect GHG emissions are produced from electricity generation associated with the compressor and pump for the TMS. Figure 6.30 shows the GHG emissions and sustainability index with respect to the exergetic COP for the baseline TMS using R134a. In the figure, as the efficiency of the baseline TMS increases, the power input required for the TMS decreases under the same cooling loads. Hence, the

corresponding emissions decrease and the sustainability index increases. It should be noted that the emissions in Figure 6.30a are determined based on the U.S average energy generation mix composed of 49% coal, 20% natural gas, 20% nuclear, 7% hydro and 4% other renewables (Yang and Maccarthy, 2009) and therefore the associated indirect emissions will be different under other energy generation cases with different carbon intensities. Figure 6.30b shows that the emissions produced from electricity generation almost double under a high-carbon scenario, where the electricity is primarily generated using coal. This reduces significantly under a low-carbon scenario, where electricity is produced through a natural gas combined cycle.

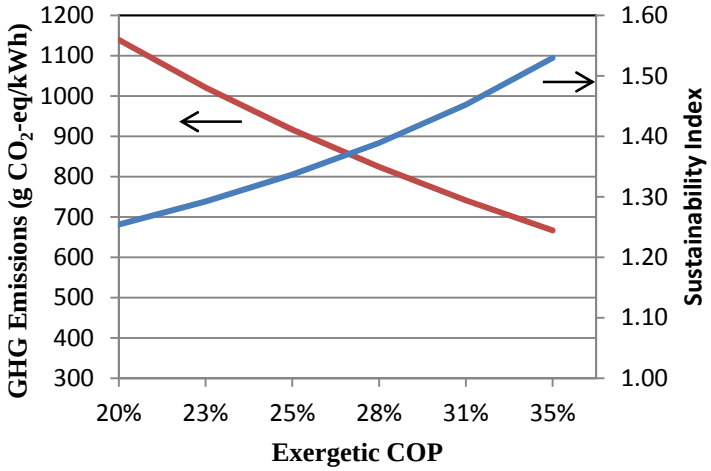

(a)

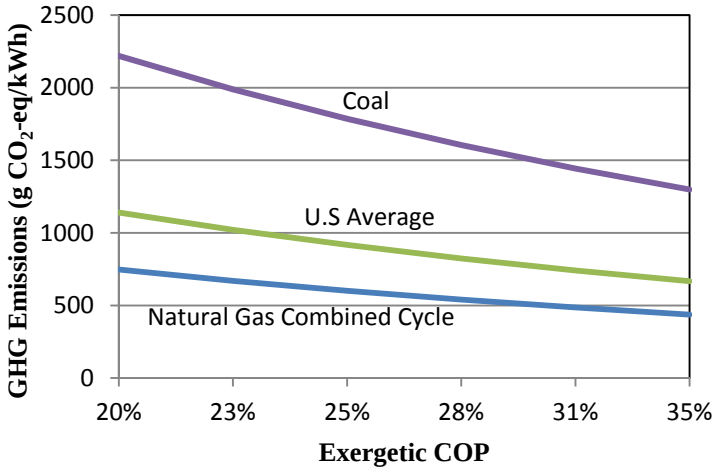

(b)

Figure 6.30: (a) GHG emissions and sustainability index with respect to baseline TMS exergetic COPs (b) under various carbon intensity of electricity generation.

Moreover, the calculated baseline TMS GHG emissions and sustainability indices are compared against TMSs using various refrigerants. Figures 6.31a and 6.31b show that the TMS using R1234yf generates the highest indirect emissions and lowest sustainability index (6% and -1.6% over the baseline TMS, respectively) due to having the lowest system efficiency. The case using dimethylether generates the lowest indirect emissions and highest sustainability index (-8.3% and 3.3% over the baseline TMS, respectively), among the studied TMSs based on high system efficiency.

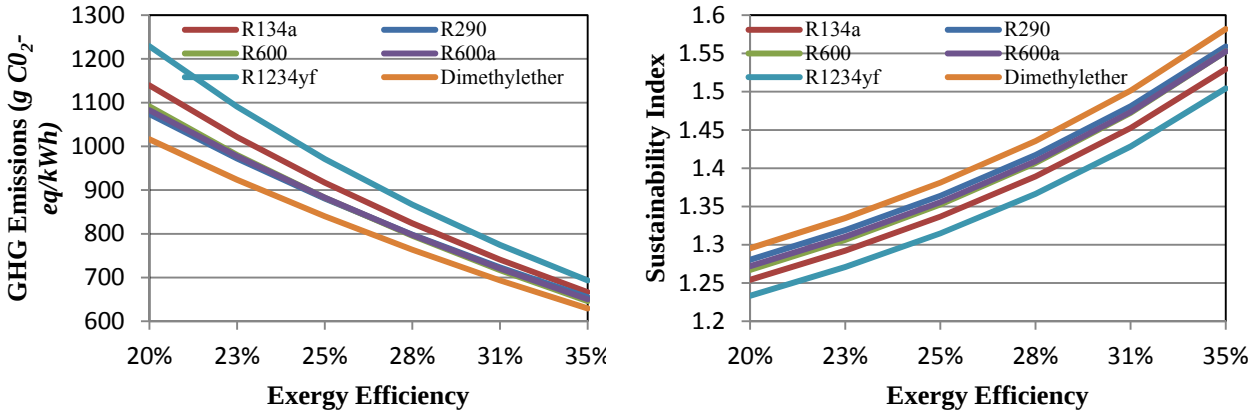

Figure 6.31: (a) GHG emissions and (b) sustainability index with respect to exergetic COPs of the TMSs using various refrigerants.

6.2.3 Model Validation

Through the conducted analysis, several models are developed for the studied thermal management system and exergy efficiencies are calculated with respect to the baseline model as well as various parameters and operating conditions. The conducted exergy analysis will provide the fundamentals behind the economic and environmental studies and optimizations that will be performed in the next sections. Thus, before going into further numerical models, the pre-established models are needed to be validated using experimental data and comparisons with respect to similar studies in the literature.

In order to determine the accuracy and reliability of the developed models, they are compared against the experimental studies conducted on the test bench and the production vehicle. Sample data obtained from these experiments are shown in Figures 6.32 – 6.41 and 6.42- 6.57 for the test bench and the production vehicle respectively. The instrumentations used, procedures taken and the parameters set for these data are provided in Chapter 4.

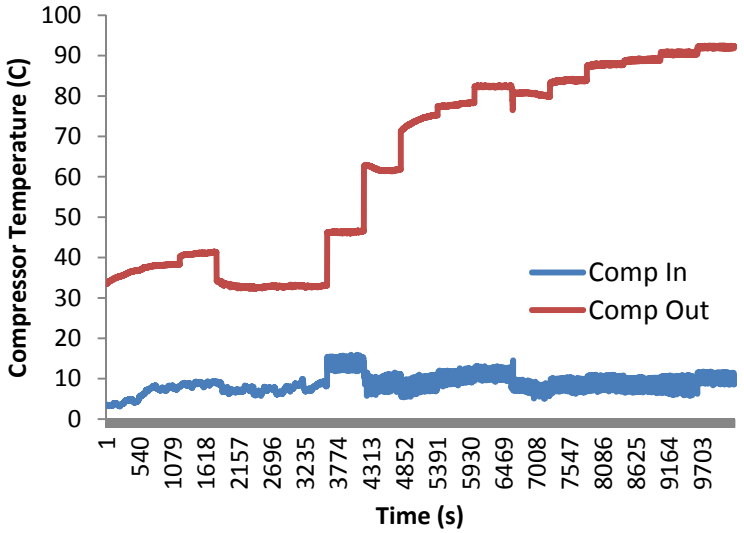

Figure 6.32: Refrigerant temperature before and after the compressor

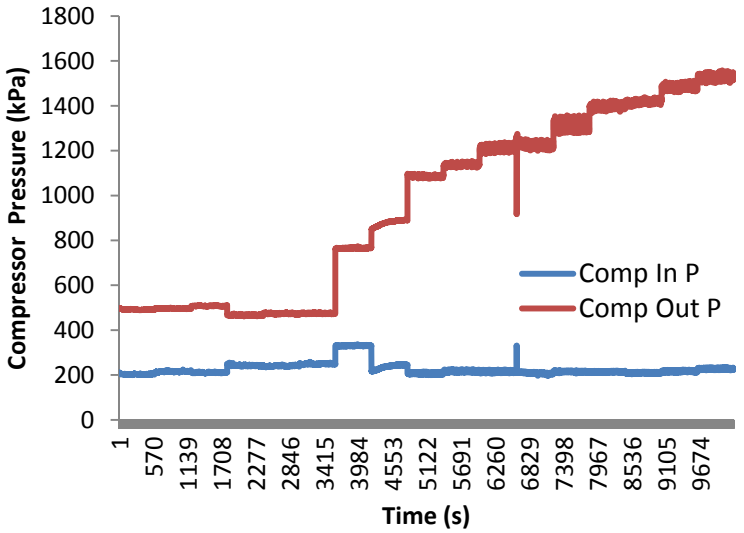

Figure 6.33: Refrigerant pressure before and after the compressor

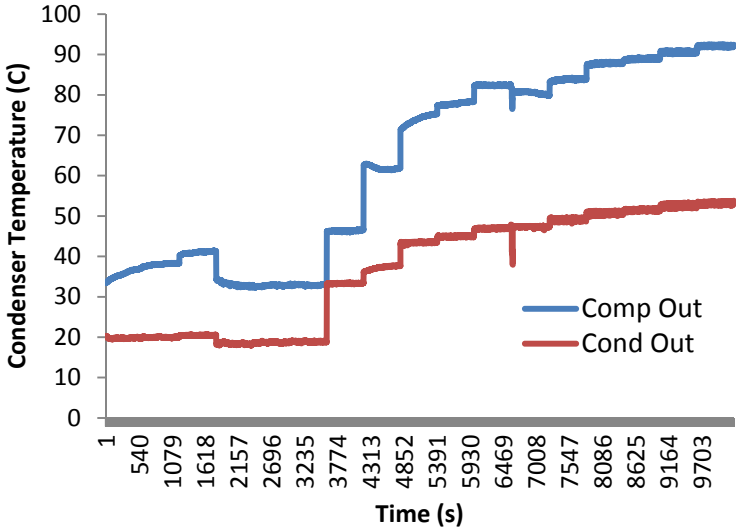

Figure 6.34: Refrigerant temperature before and after the condenser

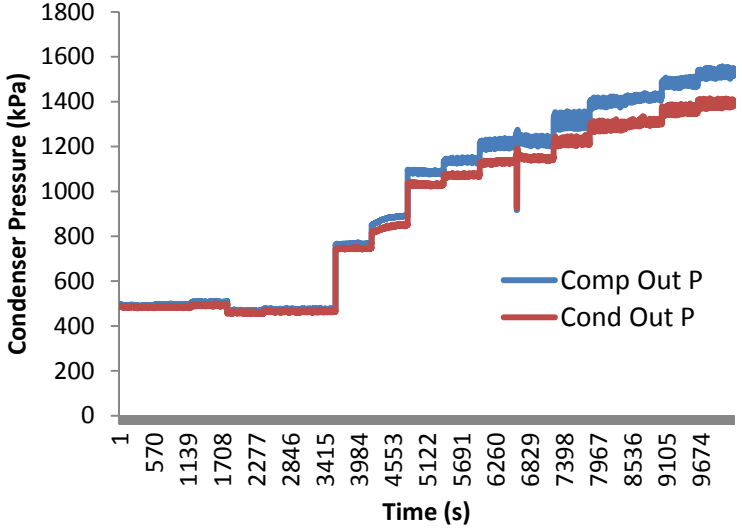

Figure 6.35: Refrigerant pressure before and after the condenser

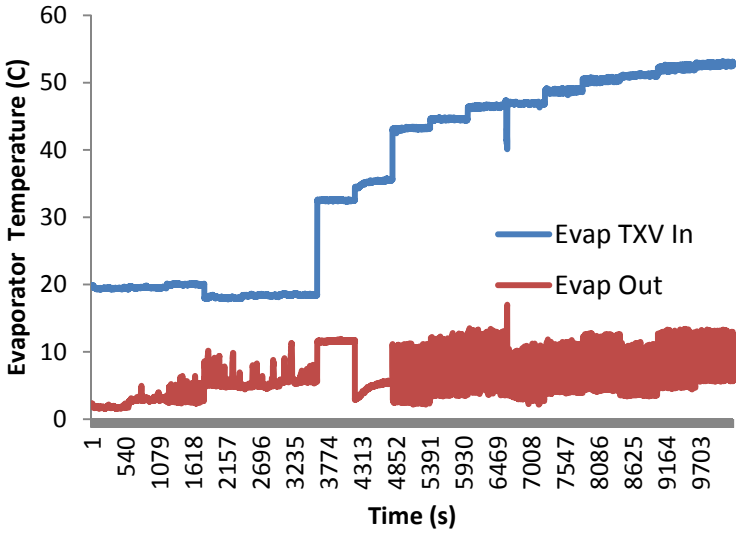

Figure 6.36: Refrigerant temperature before and after the evaporator

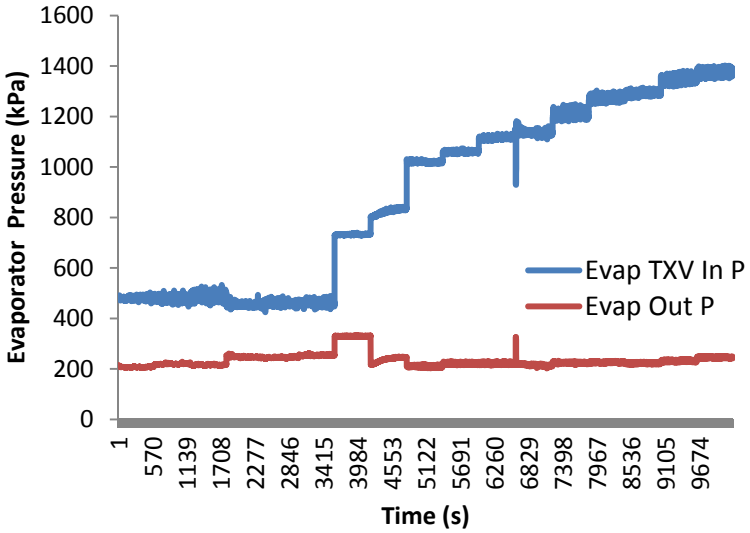

Figure 6.37: Refrigerant pressure before and after the evaporator

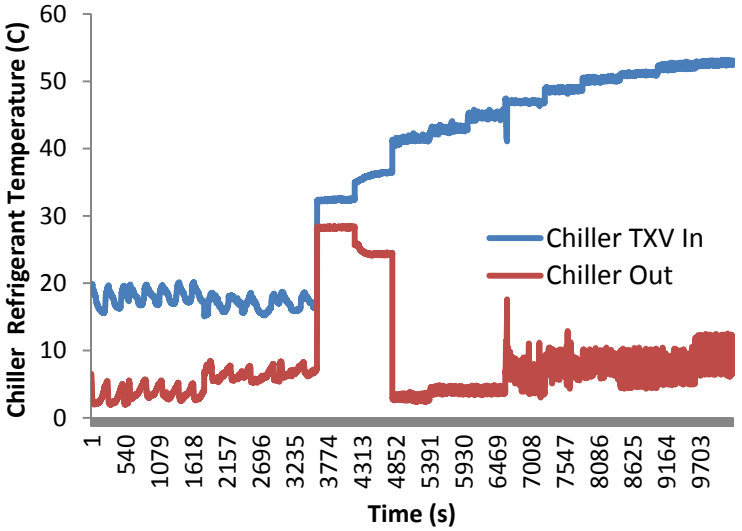

Figure 6.38: Refrigerant temperature before and after the chiller

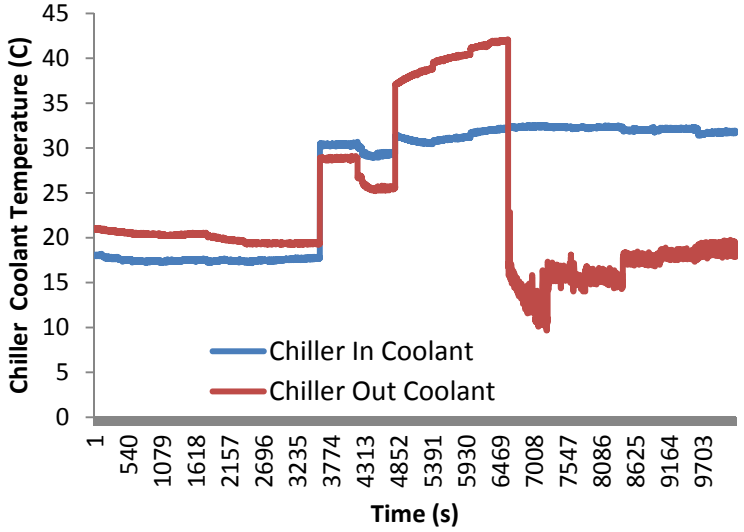

Figure 6.39: Coolant temperature before and after the chiller

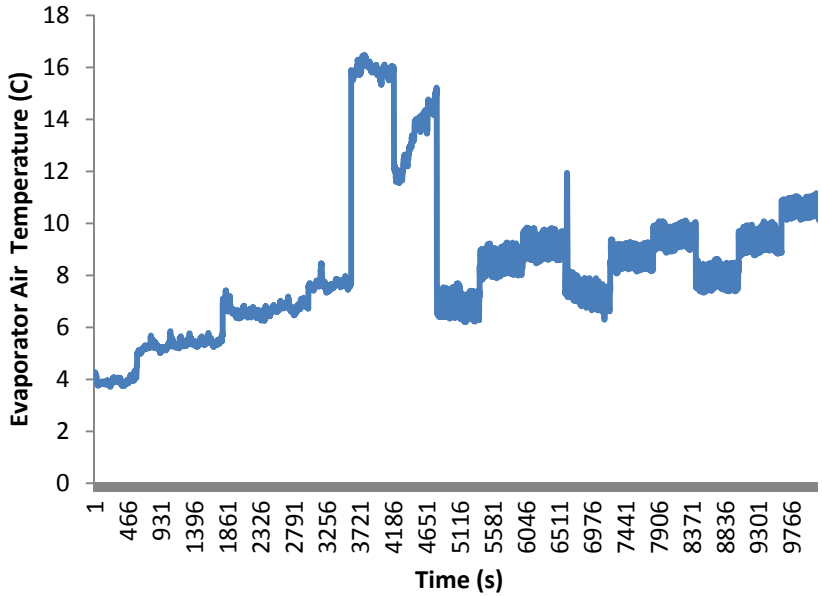

Figure 6.40: Refrigerant temperature before and after the compressor

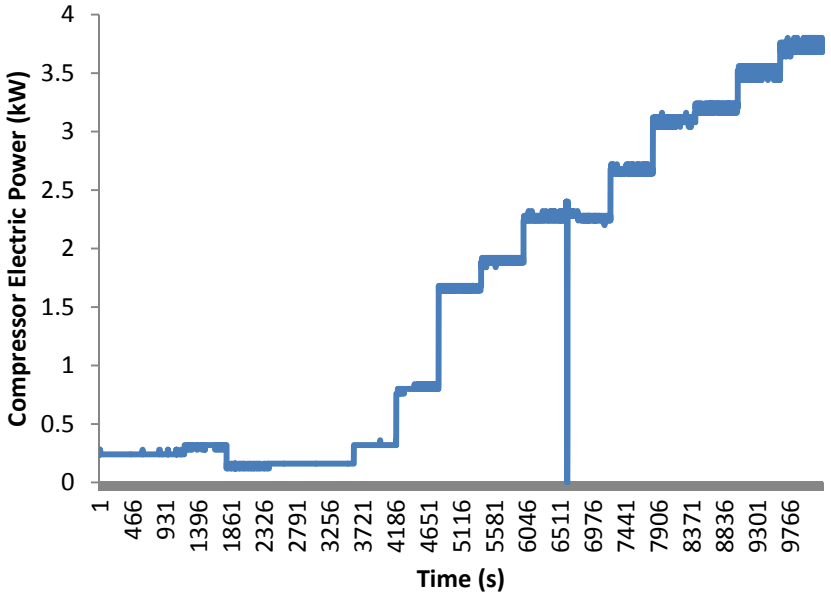

Figure 6.41: Compressor electric power

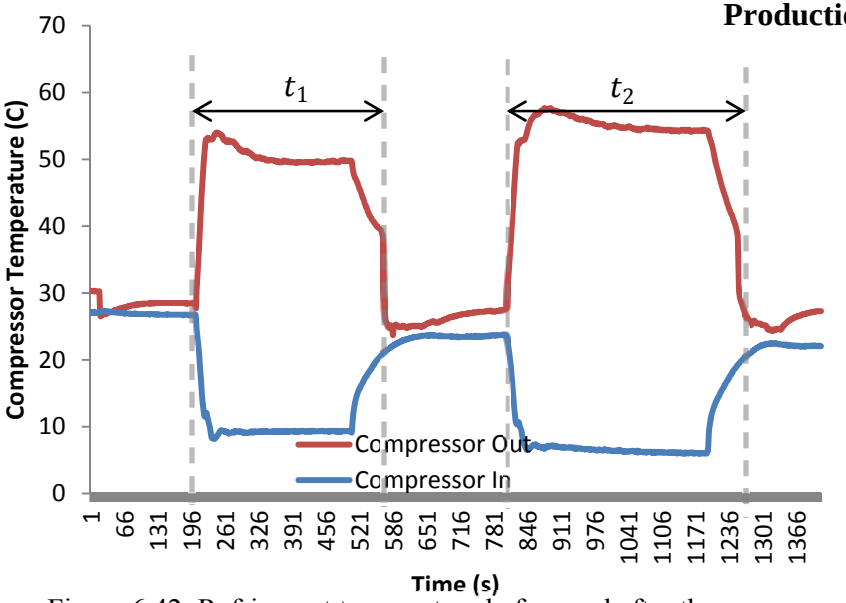

Figure 6.42: Refrigerant temperature before and after the compressor

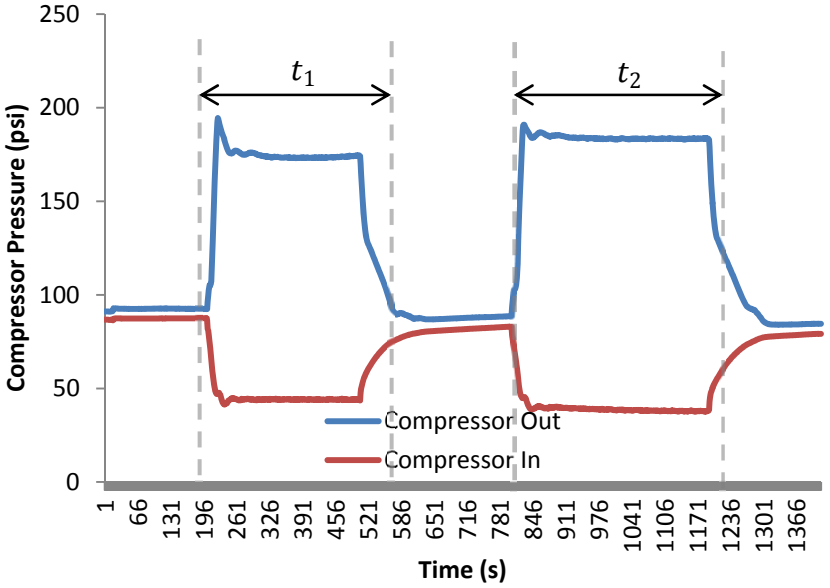

Figure 6.43: Refrigerant pressure before and after the compressor

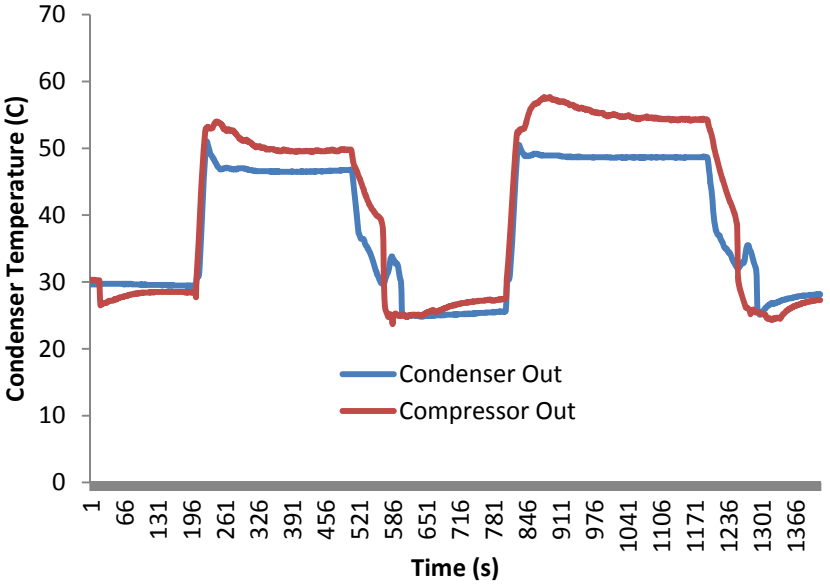

Figure 6.44: Refrigerant temperature before and after the condenser

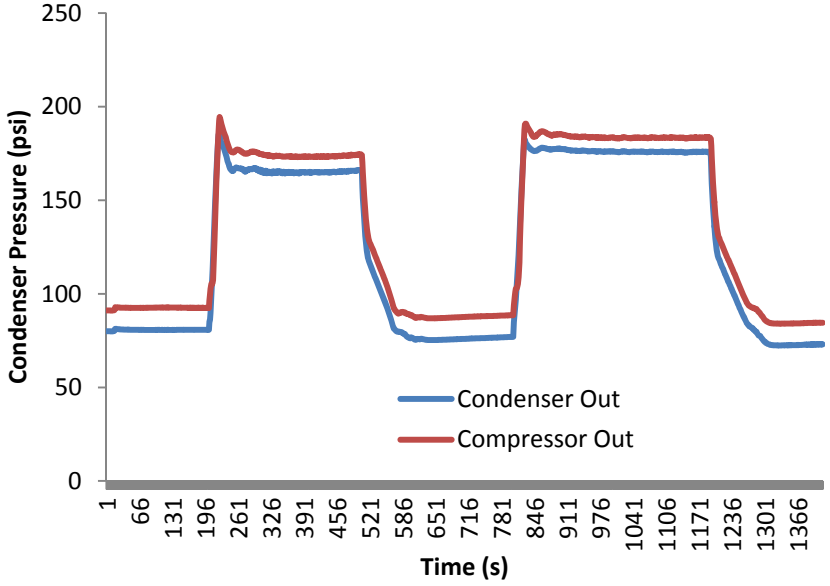

Figure 6.45: Refrigerant pressure before and after the condenser

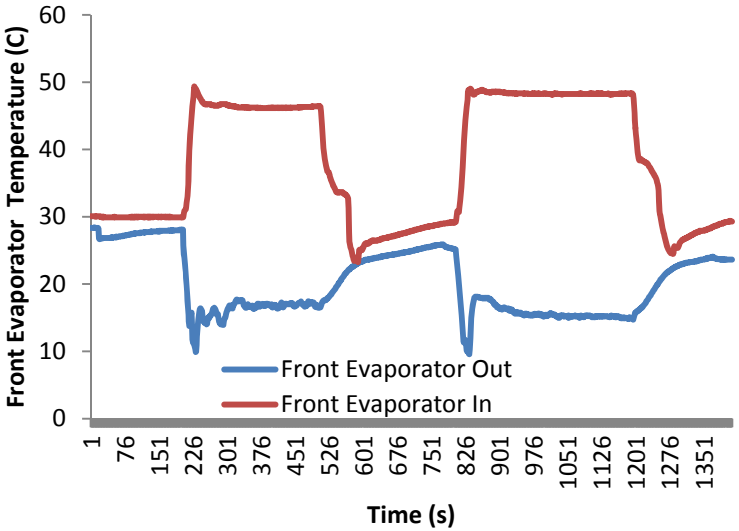

Figure 6.46: Refrigerant temperature before and after the evaporator

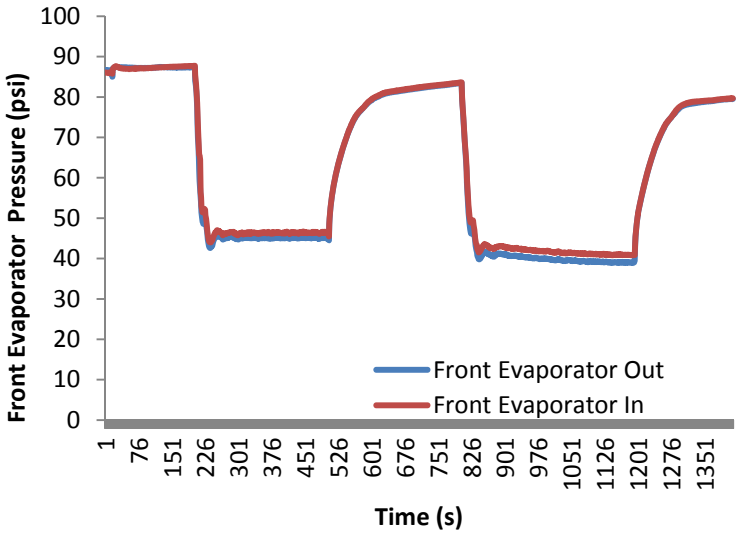

Figure 6.47: Refrigerant pressure before and after the evaporator

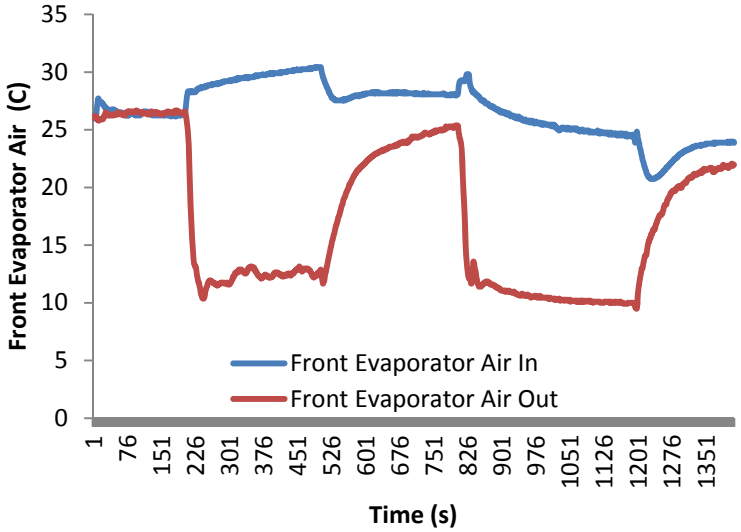

Figure 6.48: Air temperature before and after the evaporator

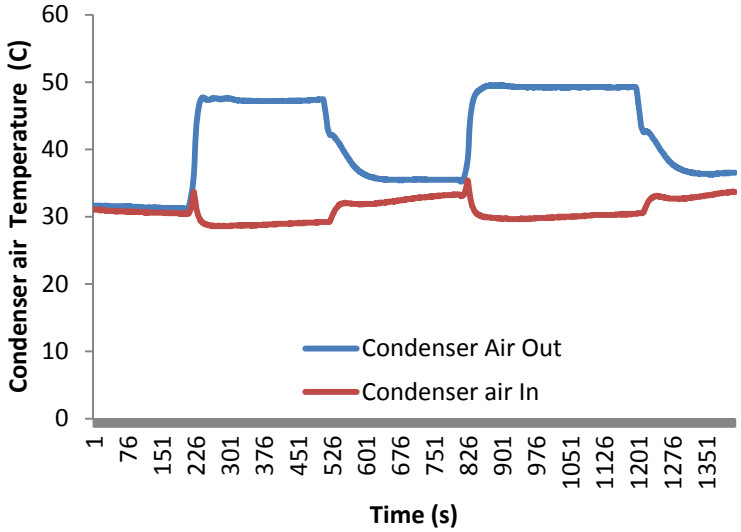

Figure 6.49: Air temperature before and after the condenser

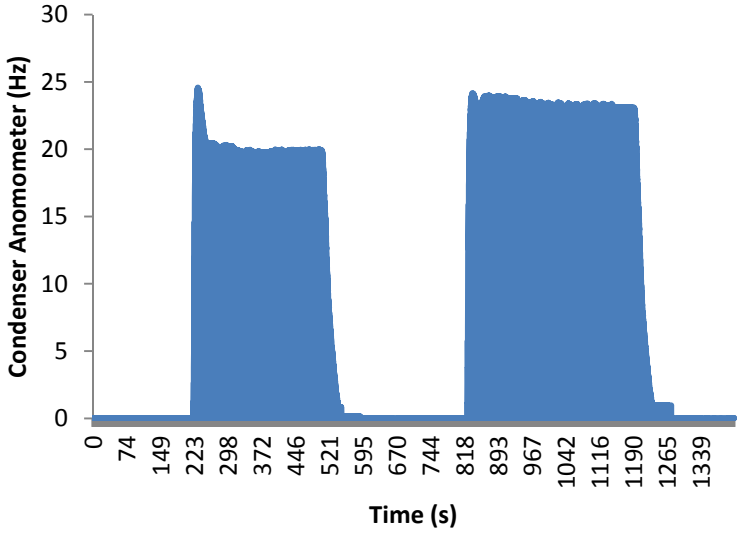

Figure 6.50: Anemometer readings of condenser fan

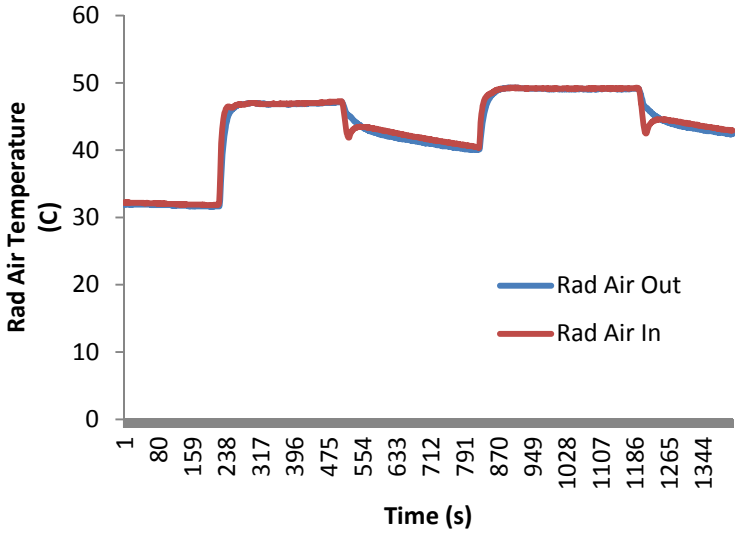

Figure 6.51: Air temperature before and after the radiator

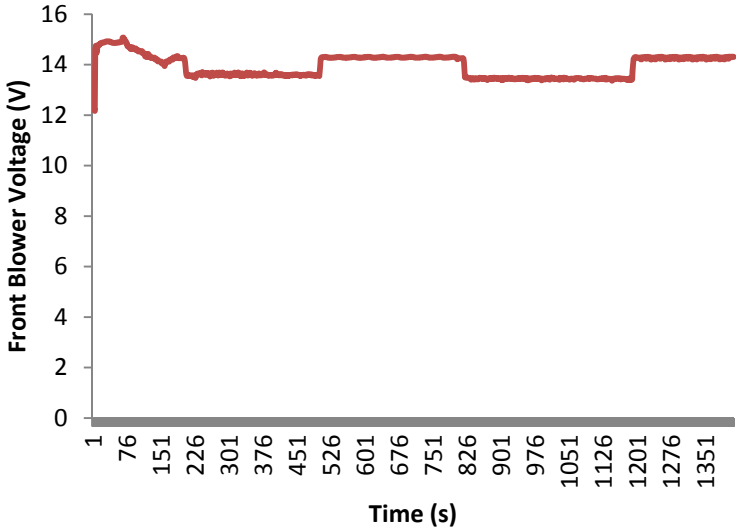

Figure 6.52: Front blower voltage

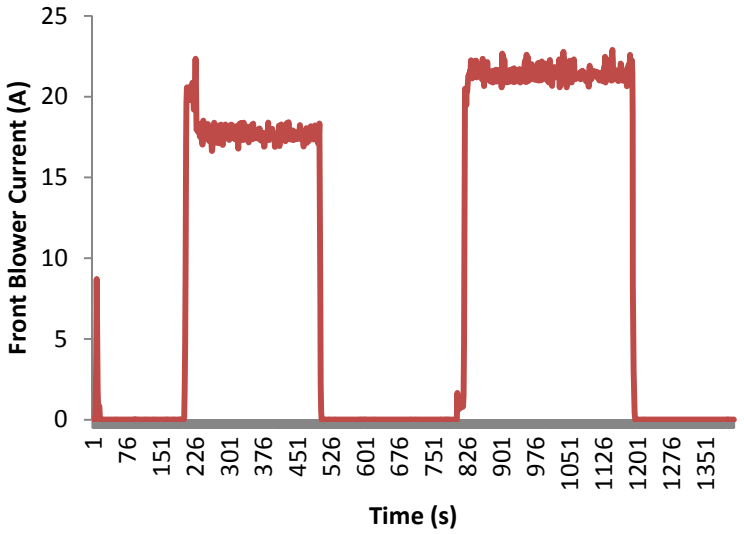

Figure 6.53: Front blower current

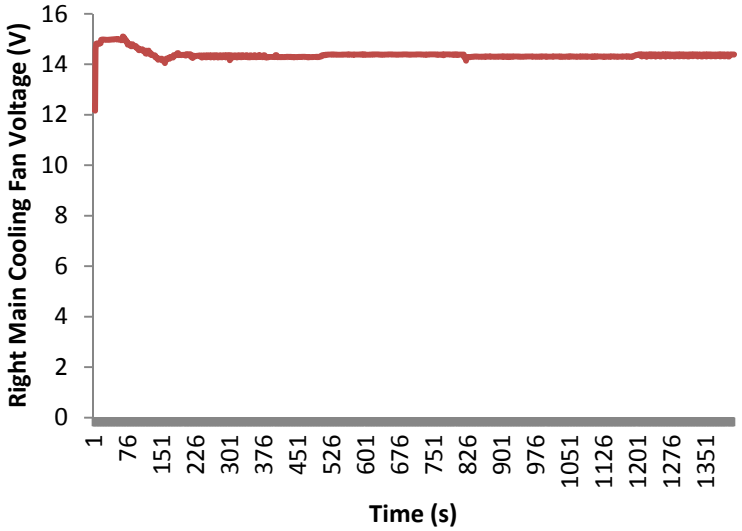

Figure 6.54: Right main cooling fan voltage.

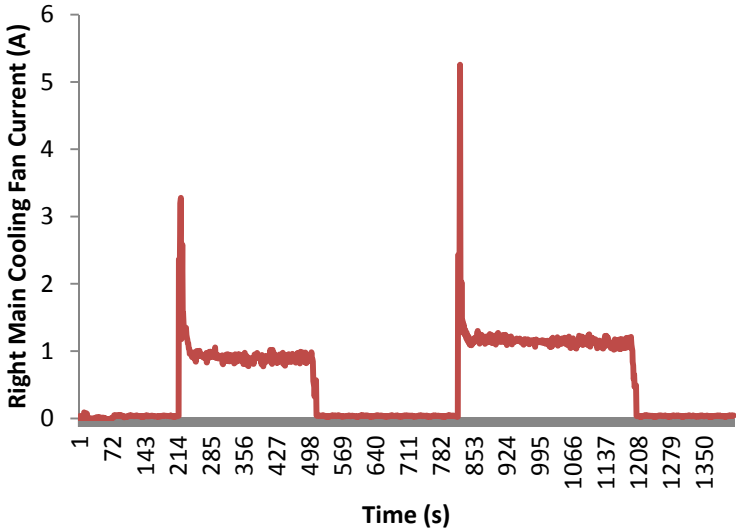

Figure 6.55: Right main cooling fan current.

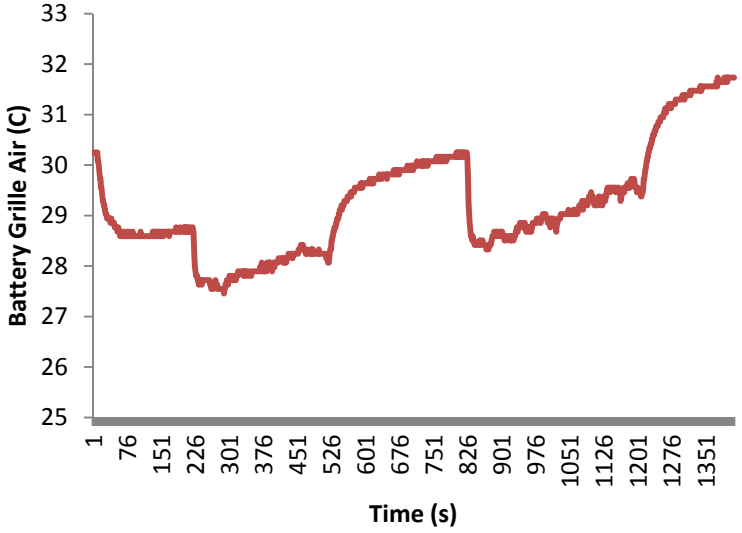

Figure 6.56: Battery grille air temperature.

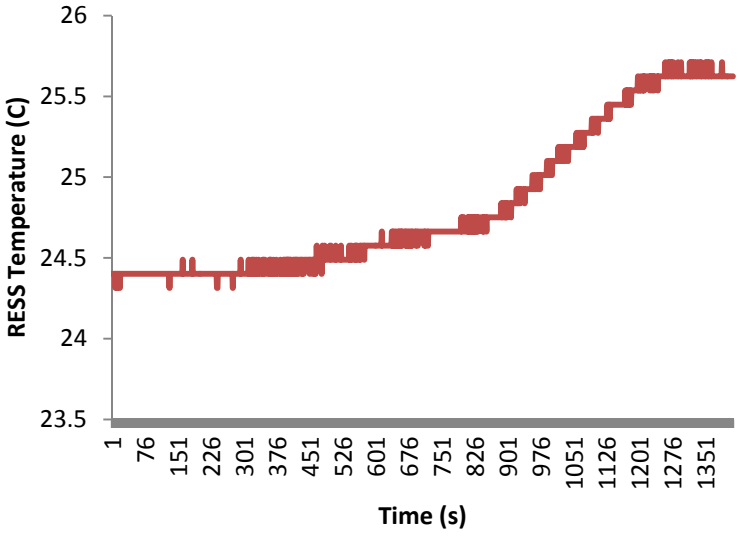

Figure 6.57: RESS temperature.

In order to provide a comparison, decision variable values for the model are retrieved from the experimental results taken from IPETRONIK and vehicle CAN bus; and the corresponding results calculated from the model are used to predict the remaining experimental outputs. The following data points, which are taken from various different states representing a wide range of operation parameters in the experimentation, are selected to compare with the model based

Table 6.3a: Refrigerant temperatures used to validate the model.

Time (s)	**Refrigerant Temperature (℃)**						
	Compressor IN	Compressor OUT	Condenser OUT	Front Evap. IN	Front Evap. OUT	Rear Evap. IN	Rear Evap. OUT
207	26.8	28.2	29.6	29.9	27.3	27.7	26.8
224	12.1	53.0	50.8	46.3	11.7	46.0	12.3
376	9.2	49.7	46.5	46.1	16.8	46.2	9.0
693	23.5	26.3	25.1	27.5	24.8	25.1	23.7
857	7.3	56.4	49.1	48.7	17.9	48.8	7.3
1092	6.2	54.4	48.7	48.2	15.3	48.3	6.1

Table 6.3b: Refrigerant pressures used to validate the model.

Time (s)	**Refrigerant Pressure (kPa)**						
	Compressor IN	Compressor OUT	Condenser OUT	Front Evap. IN	Front Evap. OUT	Rear Evap. IN	Rear Chiller OUT
207	87.4	92.6	80.7	87.1	87.2	87.2	87.2
224	47.6	193.8	183.6	52.2	49.3	49.6	49.1
376	304.7	1193.2	1135.6	320.1	311.8	313.8	311.8
693	560.9	602.6	522.2	566.0	564.8	563.4	564.0
857	40.4	186.7	177.8	43.3	41.4	41.8	41.4
1092	262.7	1263.3	1211.2	284.1	270.6	272.0	269.2

Table 6.3c: Air temperatures used to validate the model.

Time (s)	**Air Temperature (℃)**				
	Ambient Air	Condenser IN	Condenser OUT	Front Evap. IN	Front Evap. OUT
207	26.1	26.5	26.6	30.7	31.5
224	25.8	28.2	13.3	32.3	40.8
376	27.5	29.7	12.3	28.9	47.2
693	28.2	28.2	24.0	32.6	35.5
857	28.3	27.5	11.5	30.0	49.2
1092	27.5	24.9	10.2	30.2	49.3

Initially, the temperatures and mass flow rates of the air entering the heat exchanger are used from the experimental data along with the evaporating and condensing temperatures of the

refrigerant in the refrigeration cycle. In addition, the data acquired from the vehicle medium speed CAN bus is used to determine the battery heat dissipation rates to the coolant loop.

Based on these parameters, the thermodynamic states of the thermal management system, compression ratio and total work of the compressor as well as the heat load of the evaporator and chiller are predicted for each selected point in the experiment. The experimental results along with the ones developed from the model are provided in Table 6.4. In the table above, the first sub-columns in each parameter are obtained from the experimentations and the second sub-columns are calculated with respect to the developed model.

Table 6.4: Comparison of results between the experimentation and the model.

Time (s)	ΔP_{cond} (**kPa**)		ΔP_{evap} (**kPa**)		θ		$\dot{W}_{comp}$ (**kW**)		$\dot{Q}_{evap}$ (**kPa**)	
207	38.22	34.11	37.89	35.35	1.43	1.41	0.89	0.84	0.37	0.38
224	70.34	71.53	31.71	27.54	4.07	4.05	1.21	1.10	2.63	2.65
376	57.67	50.54	15.33	20.67	3.92	3.87	2.42	2.32	3.08	3.12
693	80.38	75.12	5.07	3.56	1.07	1.01	0.91	0.88	0.74	0.76
857	61.66	57.76	20.16	25.5	4.63	4.42	1.45	1.41	2.83	2.87
1092	52.09	54.62	21.41	17.43	4.81	4.76	1.52	1.47	2.60	2.63

Moreover, the outcomes of the exergy analysis are also compared to various studies conducted in the literature in order to compare the approaches and results obtained from these analyses. Even though currently there are no studies available in literature regarding exergy analysis of EV and HEV TMSs, there are numerous studies (based on energy analysis) that are conducted on conventional vehicle air conditioning and heat pump systems where the outcomes would be comparable. Furthermore, in order to be able to accurately compare the developed model with the literature, the electric battery heat dissipation rate is reduced to zero, where the entire refrigerant is forced to bypass the chiller unit and flow through the evaporator, thus operating similar to conventional vehicle air conditioning systems. Furthermore, the air mass flow rates, pressure drops, component efficiencies are adjusted according to the compared models.

It should be noted that not all the parameters used in these studies are provided and therefore deviations between these studies and the developed model may occur based on the parameters used; however same trends are concluded with the developed model. In addition, some of the results are obtained from various figures in these studies and therefore represent an approximation of the actual values. The inputs used and the corresponding results provided by these studies along with the ones predicted by the developed model are provided in Table 6.5.

Table 6.5: Comparison of model results with the literature data.

	T_{cond} (℃)	T_{evap} (℃)	**Compressor Speed (RPM)**	**COP calculated from literature**	**COP predicted from model**
Wongwises et al. (2006)	50	6	1500	2.1	1.9
	68	4	3000	1.1	1.0
Joudi et al. (2003)	50	0	3500	2.2	2.5
	70	10	3500	1.4	1.6
Kaynakli and Hosoz (2003)	50	0	1000	3.2	2.9
	60	7.5	750	2.5	2.2

Wongwises et al. (2006) conducted an experimental study on automotive air conditioners using R134a, R290, R600 and R600a refrigerants and a 3.5 kW capacity compressor. The air flowing through the condenser and evaporator is taken within 0.22 – 0.36 m^3/s and 0.036 – 0.097 m^3/s and the condensing and evaporating temperature ranges are taken to be 42℃ to 50℃ and 0℃ to 12 ℃ respectively. The study parameters are very similar to the research conducted since all the analyzed refrigerants are evaluated in this research using air flow rates and condensing and evaporating temperatures within these specified limits using a comparable size compressor. They have determined that the COP of the system increases with increasing evaporating temperatures as predicted by the developed model in Figure 6.15a.

Joudi et al. (2003) developed a computational model for simulating the performance of an ideal automotive air conditioning system using R134a, R-290, R600a and various other mixtures as refrigerants. They used condensing and evaporating temperature ranges of 30℃ to 80℃ and -5℃ to 15℃ respectively. In addition compressor speeds up to 3000 RPMs and cooling loads as much as 3.5 kW are used in the study. They used fixed compressor efficiency of 60% and fixed

pressure drops of 10% and 5% for evaporator and condenser respectively. They have determined that increasing the condensing temperatures increases the compression ratio and reduces the system COP as predicted by the developed model as shown in Figures 6.24 and 6.15.

Hosoz and Direk (2006) studied the performance characteristics of an automotive air conditioning system using R134a with condensing and operating temperature ranges of 10℃ to 50℃ and -2.5℃ and 12.5℃ respectively with respect to compressor speeds between 1500 rpms and 3500 rpms to analyze the changes in system parameters based on operating temperatures. They have determined that the cooling capacity and COP increases with increasing evaporating temperatures and that the rate of exergy destruction increases with compression ratio as predicted by the developed model in Figure 6.14 and Figure 6.22b.

In summary, a TMS of a hybrid electric vehicle composed of a refrigeration and battery coolant circuits is examined under various operating conditions. The heat exchanger exit temperatures are calculated with respect to the effectiveness-NTU method. The pressure drops in the heat exchangers are determined based on the Reynolds number correlations. For the analysis, the inlet air mass flow rate is increased up to 0.5 kg/s, the refrigerant is superheated and subcooled up to 10℃, and the evaporating and condensing temperatures are varied between 0-25℃ and 40-65℃, respectively. Moreover, the utilization of various alternative refrigerants such as R290 (propane), R600 (butane), R600a (isobutane), R1234yf (Tetrafluorpropene) and dimethyl ether (DME) are analyzed in terms of energetic and exergetic efficiencies. Finally, the calculated system efficiencies are validated using experimental data and studies conducted in the literature.

6.3 Exergoeconomic Analysis

6.3.1 Conventional Exergoeconomic Analysis

In the previous section, the exergy analysis is provided in order to gain a further understanding of the true efficiencies of each component and corresponding irreversibilities. However, this does not provide any information regarding the economic constraints on improving the efficiency of the components or the associated costs. Thus, an exergoeconomic analysis is also conducted where the cost formation can be determined for the thermal management system as provided in

Table 6.6. In the table, state 13 has 0 values, since it is available ambient air entering the condenser.

Table 6.6: Exergy flow rates, cost flow rates and the unit exergy cost associated with each state of TMS.

State	$\dot{E}x$ (kW)	$\dot{C}$ ($/h$)	c ($/kW$)
1	0.71	0.13	0.18
2	1.58	0.25	0.16
3	1.27	0.20	0.16
4	1.01	0.18	0.18
5	0.12	0.02	0.18
6	0.02	0.02	0.83
7	0.04	0.03	0.83
8	0.04	0.04	0.91
9	0.36	0.31	0.85
10	0.01	0.05	0.01
11	1.30	0.10	0.08
12	<0.01	<0.01	0.08
13	0.00	0.00	0.00
14	0.07	0.06	0.95

Based on the calculated costs, the exergy destruction costs are also determined for each component with respect to the selected baseline parameters. In Figure 6.58, it can be seen that the evaporator has the highest cost rate of exergy destruction, followed by the condenser, battery and compressor. The high exergy destruction cost of the battery is mostly associated with the high fuel cost, while the majority of the exergy destruction cost of the compressor, condenser and evaporator is associated with relatively high exergy destruction rates for these components.

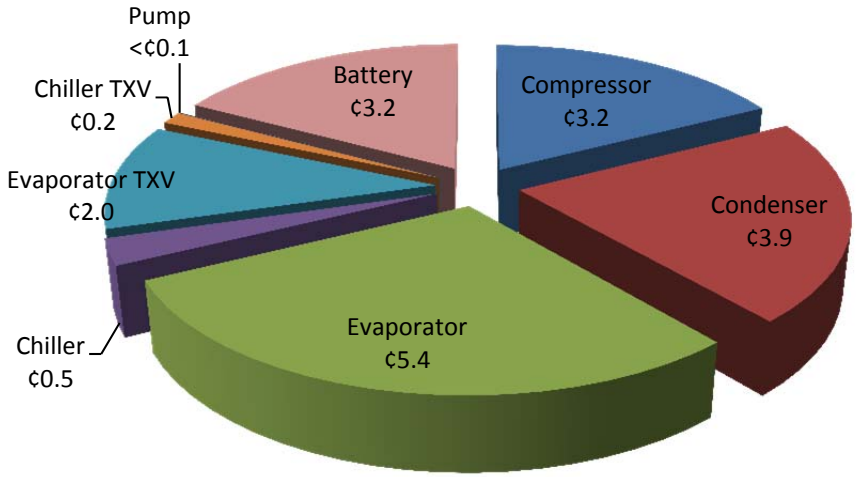

Figure 6.58: Cost rate of exergy destruction for thermal management system components.

However, before any remarks can be made regarding design or investment changes, the components should be analyzed with respect to the cost distribution, their exergoeconomic significance and the impact of improving the component efficiency on the total capital investment costs. The cost distribution among investment and exergy destruction rates can be seen in Figure 6.59.

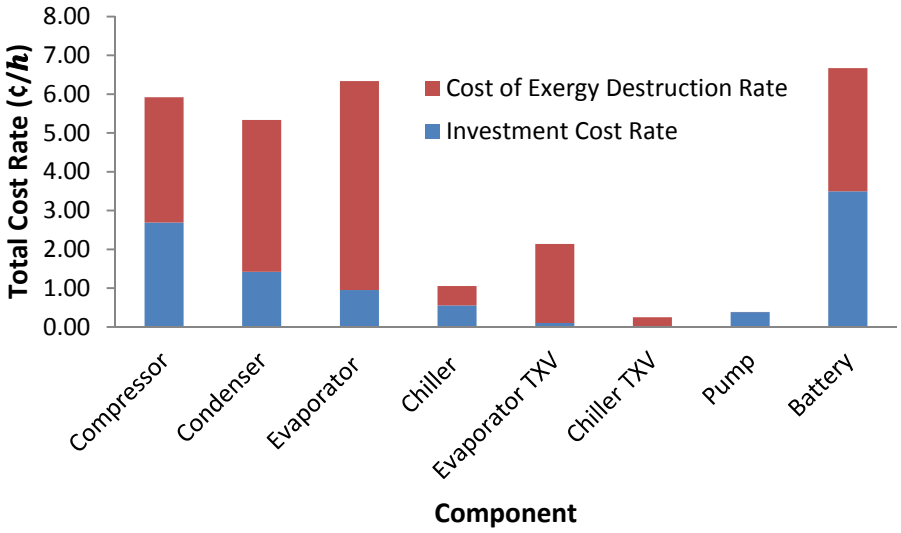

Figure 6.59: Cost distribution among investment and exergy destruction rates for the TMS components.

From an exergoeconomic viewpoint, the components that have the highest priority are the ones that have the highest sum of total capital investment and exergy destruction cost rate ($\dot{Z} + \dot{C}_D$). Among these components, the relationship between the exergy efficiency investment costs of the components is investigated with the help of the exergoeconomic factor. These values for each component are provided in Table 6.7.

Table 6.7: Investment cost rate, cost rate of exergy destruction, total cost rate, exergoeconomic factor and relative cost difference associated with the TMS components.

Component	$\dot{Z}_k$ (¢/h)	$\dot{C}_{D,k}$ (¢/h)	$\dot{Z}_k + \dot{C}_{D,k}$ (¢/h)	f_k (%)	r_k (−)
Compressor	2.7	3.2	5.9	45.4	0.9
Condenser	1.4	3.9	5.2	26.6	4.9
Evaporator	0.9	5.4	5.7	14.9	3.7
Chiller	0.6	0.5	1.2	52.4	3.6
Evaporator TXV	0.1	2.0	0.8	4.7	0.1
Chiller TXV	0.0	0.2	0.2	4.6	0.1
Pump	0.4	<0.1	0.4	99.6	25.1
Battery	3.5	3.2	6.4	52.4	2.7

When the components are analyzed with respect to $\dot{Z} + \dot{C}_D$, an electric battery has the highest total cost rate compared to the rest of the components, mainly due to having significantly larger investment costs, as provided in Table 6.7. After the battery, the highest sum of total capital investment rate and cost rate of exergy destruction are determined to be the compressor followed by the evaporator and condenser. These components are followed by the pump and thermal expansion valves which have relatively insignificant cost rates compared to the rest of the system components. In the battery, compressor and chiller, the non-exergy related costs and total cost of a component are divided rather equally, thus the current investment cost for this components are found to be reasonable. Condenser and evaporator are determined to have low exergoeconomic factors, where reducing the investment cost on this component should be investigated at the expense of their exergetic efficiencies to improve the effectiveness of the system. On the other hand, for the pump improving the component efficiency would be more cost effective even if the capital investment for that component will increase.

6.3.2 Advanced Exergoeconomic Analysis

In order to improve the accuracy and validity of the analysis, an advanced exergoeconomic study is also conducted for the thermal management system. Initially, the investment cost is split into avoidable and unavoidable parts in order to determine how much of the total investment can be actually eliminated as seen in Table 6.8.

Table 6.8: Comparison of total and avoidable cost rates of the respective exergoeconomic factors associated with the components of the TMS.

Component	$\dot{Z}_k + \dot{C}_{D,k}$ (¢/h)	$\dot{Z}_k^{AV} + \dot{C}_{D,k}^{AV}$ (¢/h)	$\dot{Z}_k^{AV} + \dot{C}_{D,k}^{AV} / \dot{Z}_k + \dot{C}_{D,k}$ (%)	f_k (%)	f_k^* (%)
Compressor	5.9	3.3	55.4	45.4	54.1
Condenser	5.2	2.7	52.0	26.6	35.5
Evaporator	5.7	3.1	53.7	14.9	23.7
Chiller	1.2	0.7	81.0	52.4	58.5
Evaporator TXV	0.8	0.7	36.7	4.7	9.2
Chiller TXV	0.2	0.1	36.7	4.6	9.2
Pump	0.4	<0.1	9.6	99.6	84.6
Battery	6.4	2.6	41.0	52.4	65.4

The total cost rates and exergoeconomic factor is also included in order to provide a comparison between the conventional and advanced exergoeconomic analysis. The ratio of available to total

cost rates indicates that up to 81% of the total cost rates could be theoretically avoided in the system. From the exergoeconomic factor based on the avoidable costs, it can be seen that the dominant factor in the total cost rate for the condenser, evaporator and thermal expansion valves are the cost of exergy destructions and therefore the exergy efficiency of these components should be increased, even at the expense of increased investment costs. On the other hand, the most prominent factor in the total cost rate for the chiller, pump and the electric battery is determined to be the investment costs and therefore the investment cost needs to be reduced for these components to improve the cost effectiveness of the system. Even though the similar trends are achieved using available cost rates (compared to the total cost rates), the use of avoidable costs revealed how far the components really are to the ideal parameters to optimize the cost distribution and provided a much realistic measure on what approach should be taken (and how much) to improve the effectiveness of each component and enabled comparison of dissimilar components with each other.

Moreover, the relationship between investment cost and exergy destruction for the compressor, condenser and evaporator is further examined in order to provide a more detailed information on their correlation since these components are the major contributor to the total cost and exergy destruction of the system and can be optimized accordingly. For the compressor, the compression ratio associated with the system is varied, which in turn changes the isentropic efficiency of the compressor and therefore effects the exergy destruction and investment cost associated with the compressor as seen in Figure 6.60. In the figures, the asymptotes in the X-axis and Y-axis provide the unavoidable cost and exergy destruction rates respectively.

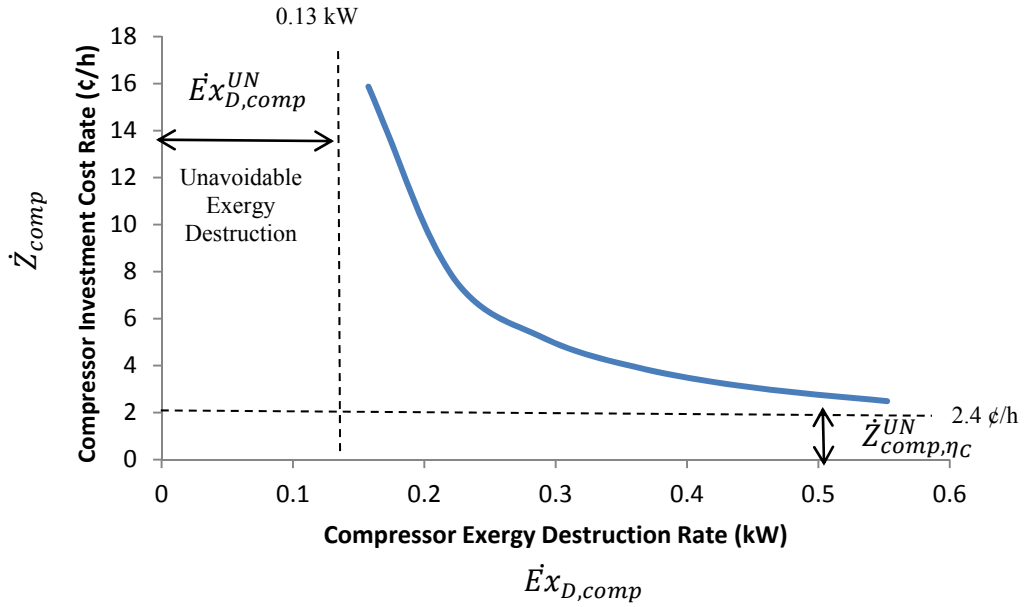

Figure 6.60: Relationship between compressor exergy destruction rate and investment cost rate.

Moreover, in order to further evaluate the heat exchangers, different evaporating and condensing temperatures are used which in turn varied the heat exchanging area associated with the system and thus altered the exergy destruction and investment costs for the condenser and evaporator as shown in Figures 6.61 and 6.62.

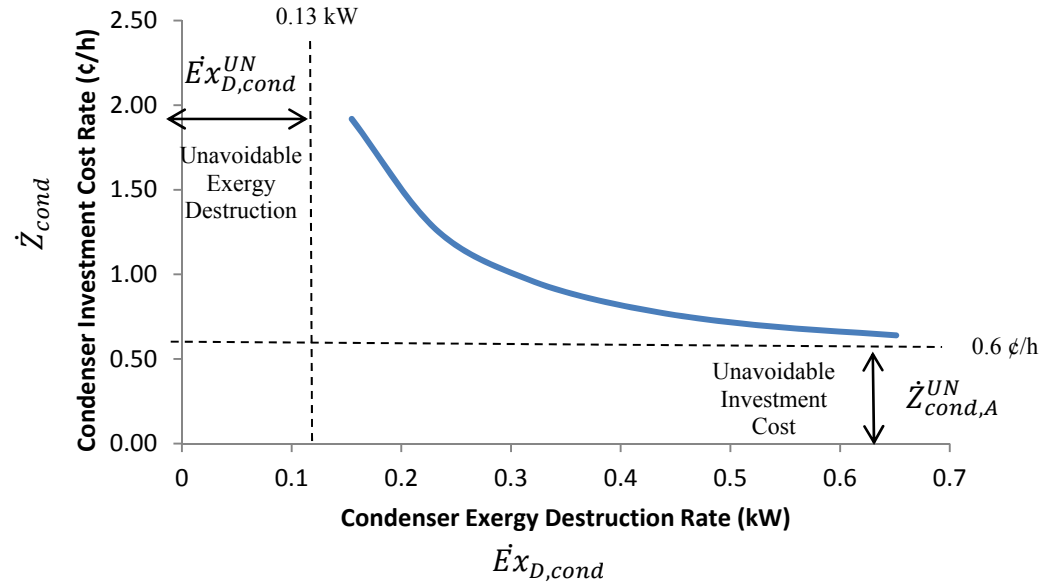

Figure 6.61: Relationship between condenser exergy destruction rate and investment cost rate.

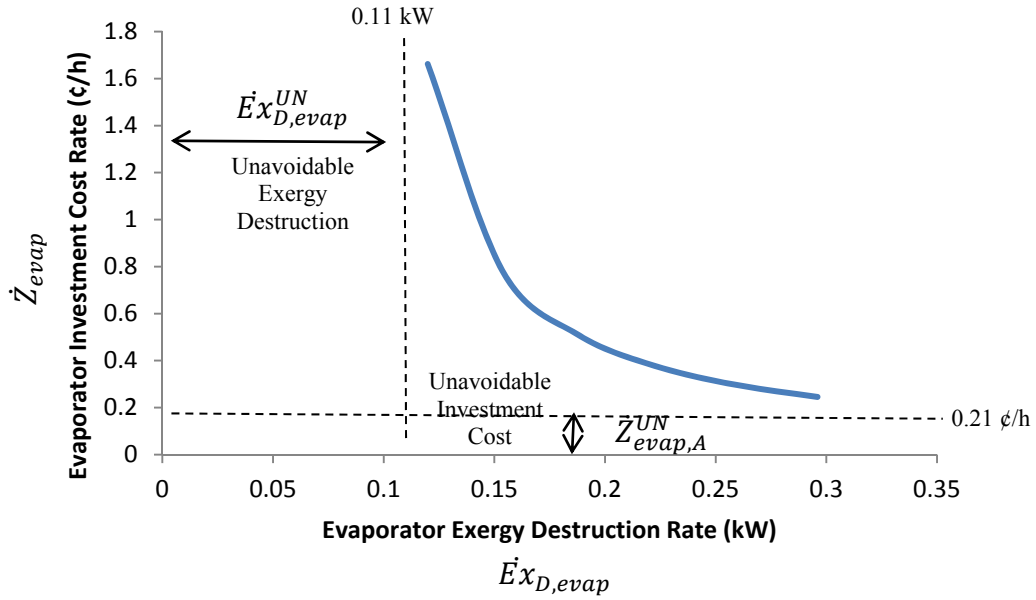

Figure 6.62: Relationship between evaporator exergy destruction rate and investment cost rate.

Furthermore, a sensitivity analysis is also conducted in order to determine the effects of the interest rates used in the analysis. Thus, the investment and exergy destruction rates with respect to various interest rates are shown in Figure 6.63 – 6.65. In order to provide a comparison among different components, exergy destruction rates and investment cost rates are provided in terms of "per product unit exergy".

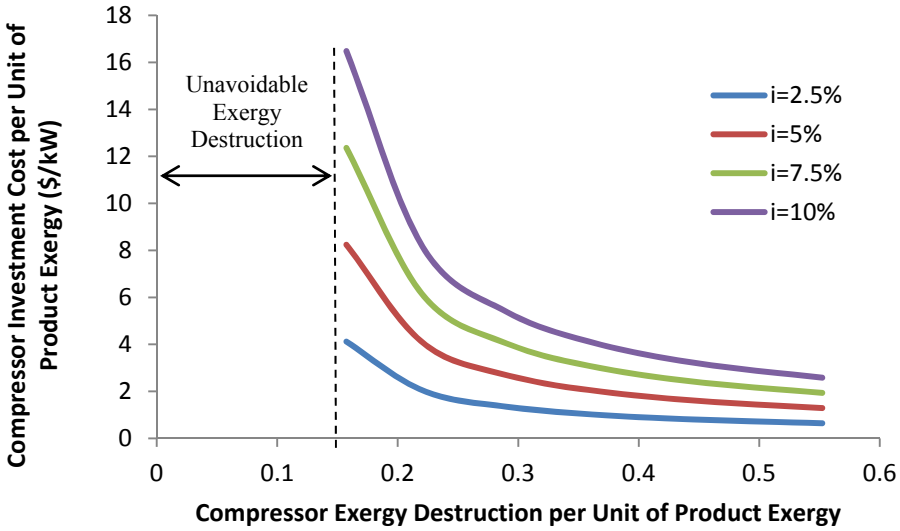

Figure 6.63: Relationship between compressor exergy destruction rate and investment cost rate per unit product exergy under different interest rates.

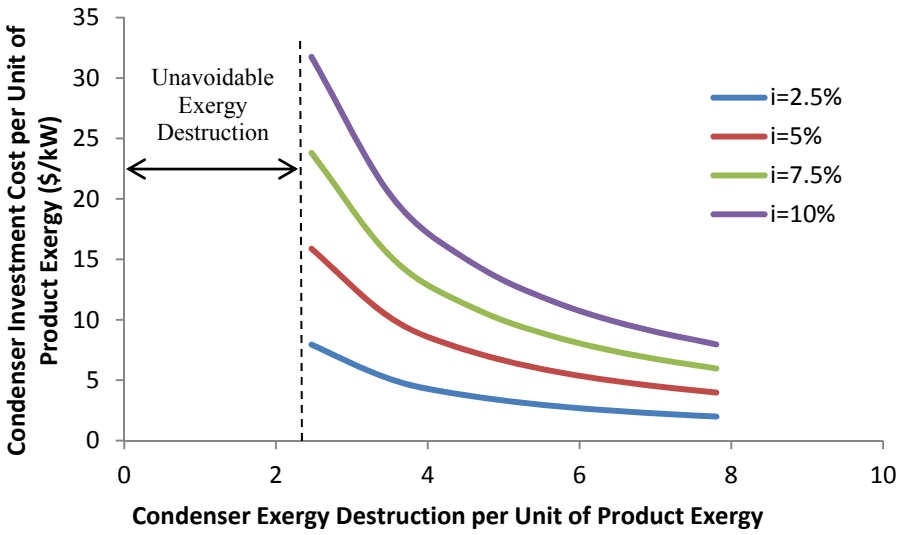

Figure 6.64: Relationship between condenser exergy destruction rate and investment cost rate per unit product exergy under different interest rates.

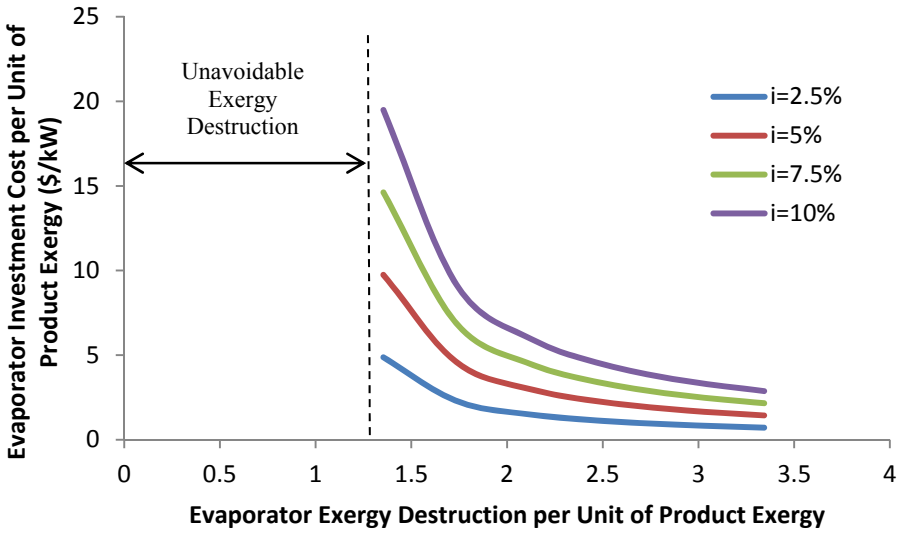

Figure 6.65: Relationship between evaporator exergy destruction rate and investment cost rate per unit product exergy under different interest rates.

In addition, parametric studies are also conducted based on different compressor efficiencies and condensing and evaporating temperatures in order to see their corresponding effects on investment and exergy destruction related costs which are shown in Figures 6.66-6.68.

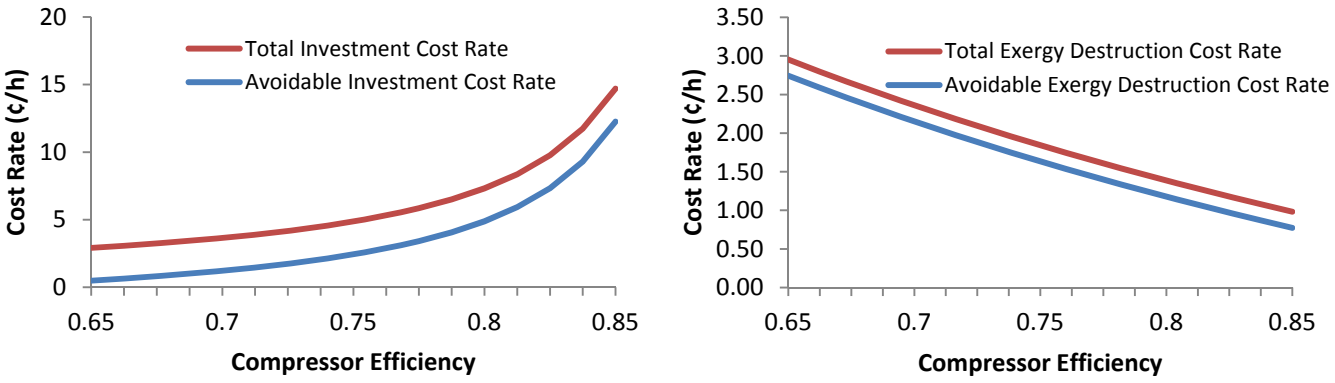

(a) (b)

Figure 6.66: Total and avoidable cost rates with respect to (a) investment and (b) exergy destruction for the compressor based on various compressor efficiencies.

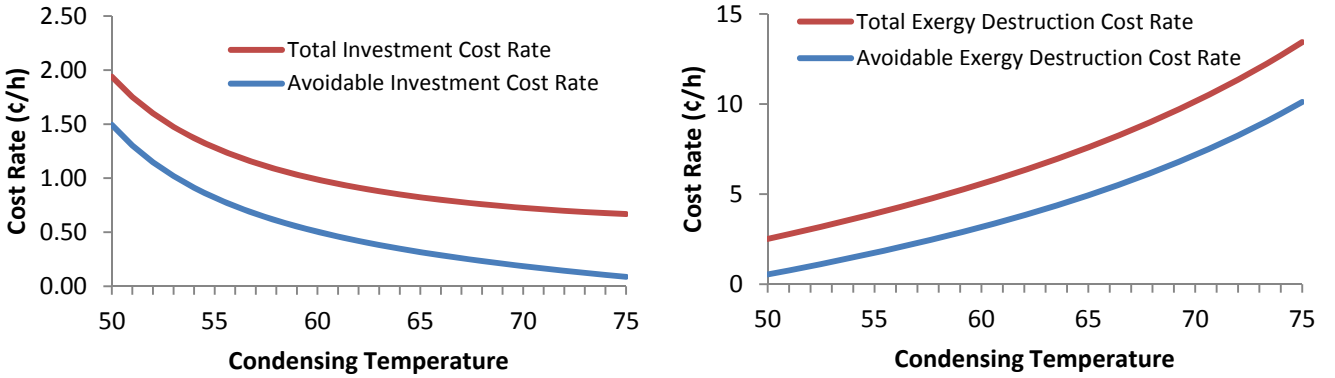

(a) (b)

Figure 6.67: Total and avoidable cost rates with respect to (a) investment and (b) exergy destruction for the condenser based on various condensing temperatures.

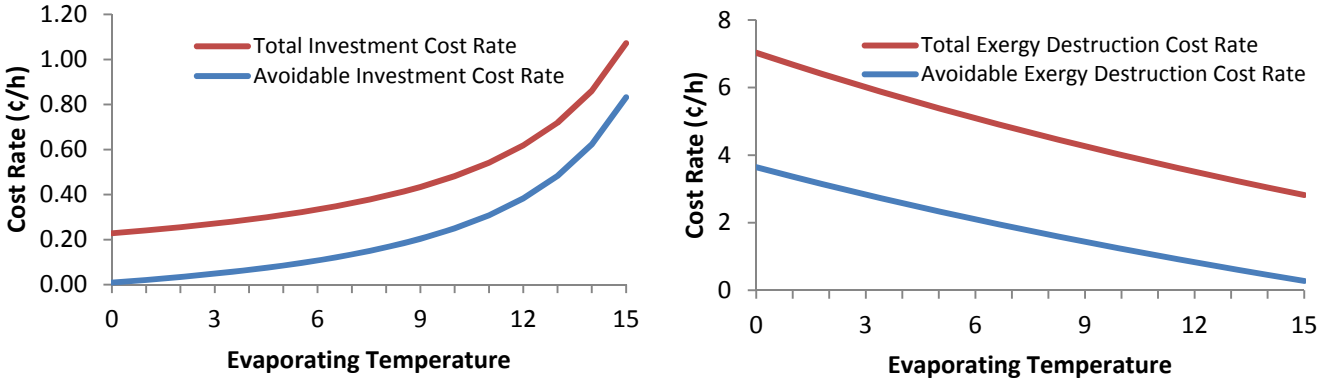

(a) (b)

Figure 6.68: Total and avoidable cost rates with respect to (a) investment and (b) exergy destruction for the evaporator based on various evaporating temperatures.

In addition, in order to provide the emissions associated with the system in terms of cost, the indirect amount of CO_2 emissions released to the environment as a result of the electricity consumed from the grid are also calculated in terms of a cost input. The emissions are calculated with respect to various electricity generation mixes, including one that utilizes a natural gas combined cycle to one that uses primarily coal / steam, with a range of 400 to 1,118 gCO_2eq/kWh including life cycle estimates for electricity production. The associated emissions with respect to various electricity generation mixes can be seen in Figure 6.69a. Subsequently, a carbon price is established and the associated cost of corresponding CO_2 emissions are determined accordingly under various carbon price ranges as shown in Figure 6.69b.

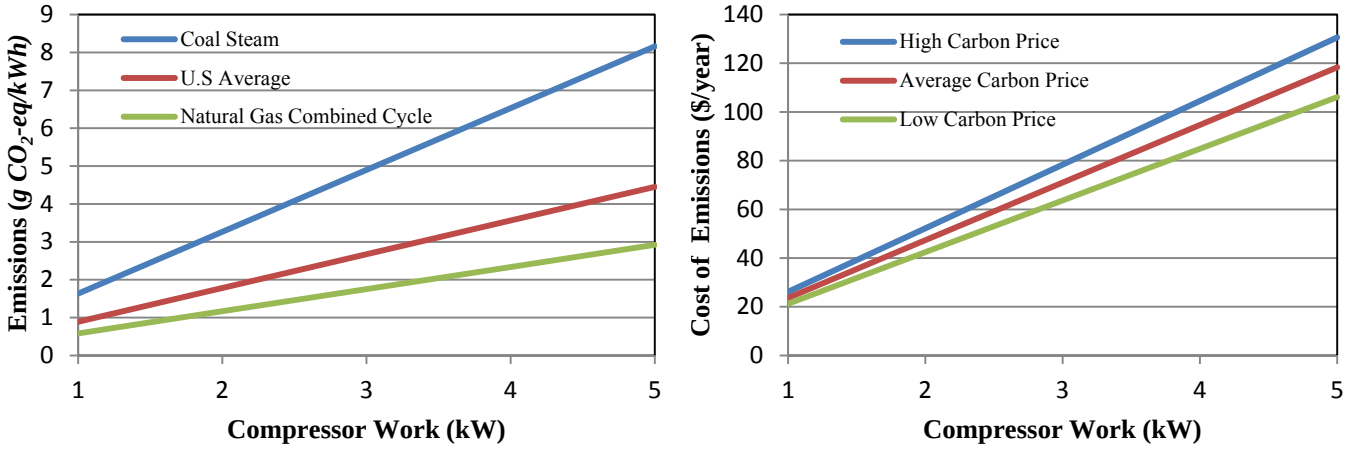

(a) (b)

Figure 6.69: (a) Amount of emissions released and (b) associated imposed cost with respect to varying compressor work under different electricity generation mixes.

In summary, exergoeconomic and enviroeconomic (environmental cost) analyses of hybrid electric vehicle thermal management systems are conducted in this section with respect to various system parameters as well as operating conditions. In the analysis, the investment cost rates are calculated with respect to equipment costs, which are determined by cost correlations for each system component, and capital recovery factors. Thus, by combining it with previously conducted exergy analysis (Section 5.2), an exergoeconomic model is developed whereby the exergy streams are identified, fuel and products are defined and cost equations are allocated for each component. The costs from the economic analysis are used to determine the unit cost of exergy, cost rate of exergy destruction as well as other useful exergoeconomic variables for each

component. Moreover, an enviroeconomical (environment cost) analysis is also conducted based on the established carbon price associated with the released CO_2 to the environment, corresponding to the indirect emissions from the electricity used in the TMS under varying carbon prices and electricity generation mixes.

6.4 Exergoenvironmental Analysis

In this study, the exergy analysis is provided in order to gain a further understanding of the true efficiencies of each component and corresponding irreversibilities. However, this does not provide any information regarding the environmental impact associated with the components. Thus, an exergoenvironmental analysis is also conducted where the associated environmental impacts can be determined for the thermal management system.

6.4.1 Battery Environmental Impact

Initially the LCA of battery is conducted in order to acquire environmental impact potential associated with the electric battery in terms of eco-indicator points. The battery assembly components and their respective environmental impacts are illustration in Figure 6.70.

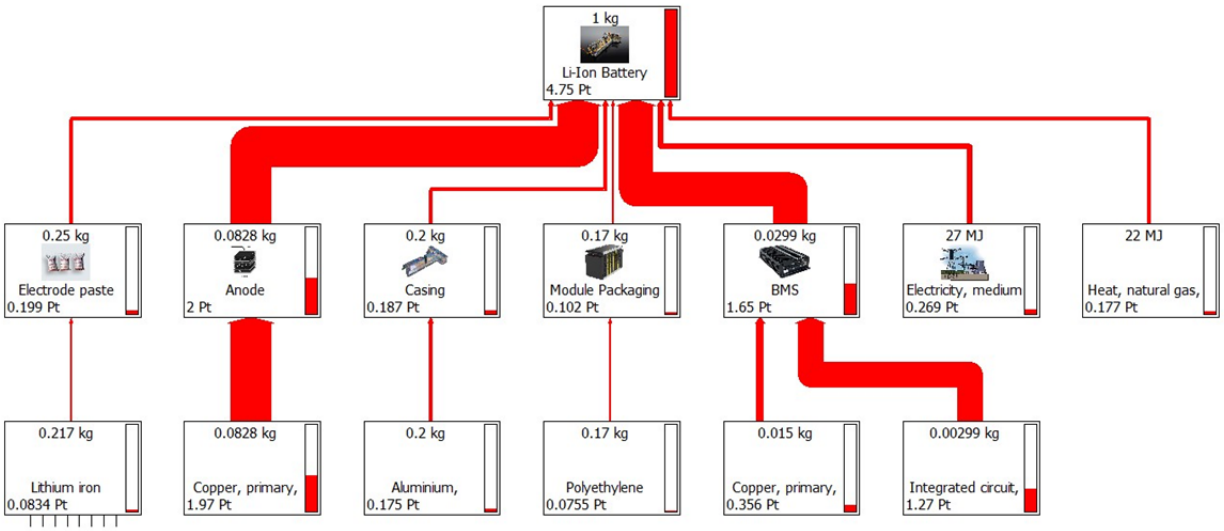

Figure 6.70: Illustration of the lithium-ion battery using SimaPro 7.

From Figure 6.70, it can be seen that anode has the highest impact in the battery due to the high amount of copper used, followed by the battery thermal system with respect to the gold used in the integrated circuits which accounts for over 40% and 26% of the total impact score

respectively. Electrode paste on the other hand, has a relatively small contribution to the total environmental impact even though it encompasses a significant portion of the battery weight. In addition, other auxiliary components such as the module packaging and the battery case also add to the battery impact along with the electricity, heat and natural gas used to produce the battery. The impacts associated with the battery are also provided in Figure 6.71.

Moreover, Figure 6.71 is divided into production, energy and transportation categories in order to provide their contributions to the total environmental impacts as shown in Figure 6.72. From the analysis, it can be seen that up to 90% of the total emissions come from the direct production of the battery while majority of the remaining impact corresponds to that of the energy used during the production. In addition, the battery components are also investigated in terms of various environmental impact potentials as shown in Figure 6.73.

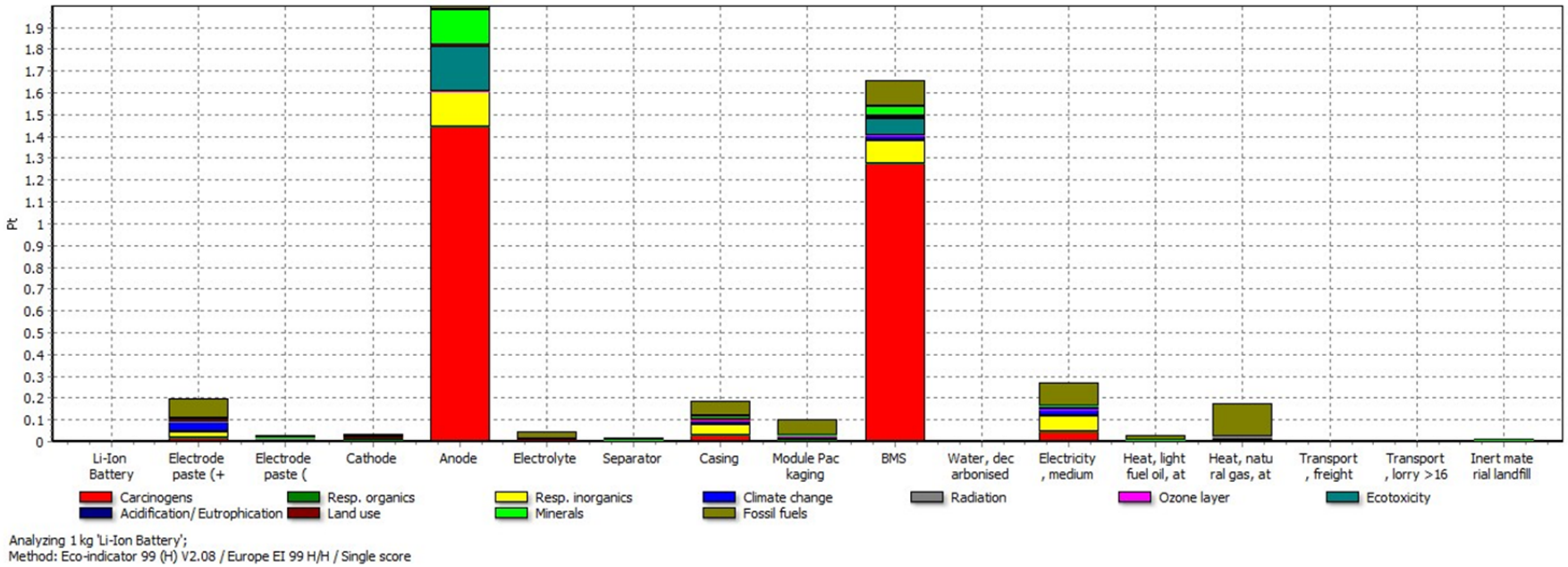

Figure 6.71: Various environmental impact potentials associated with each battery sub-component.

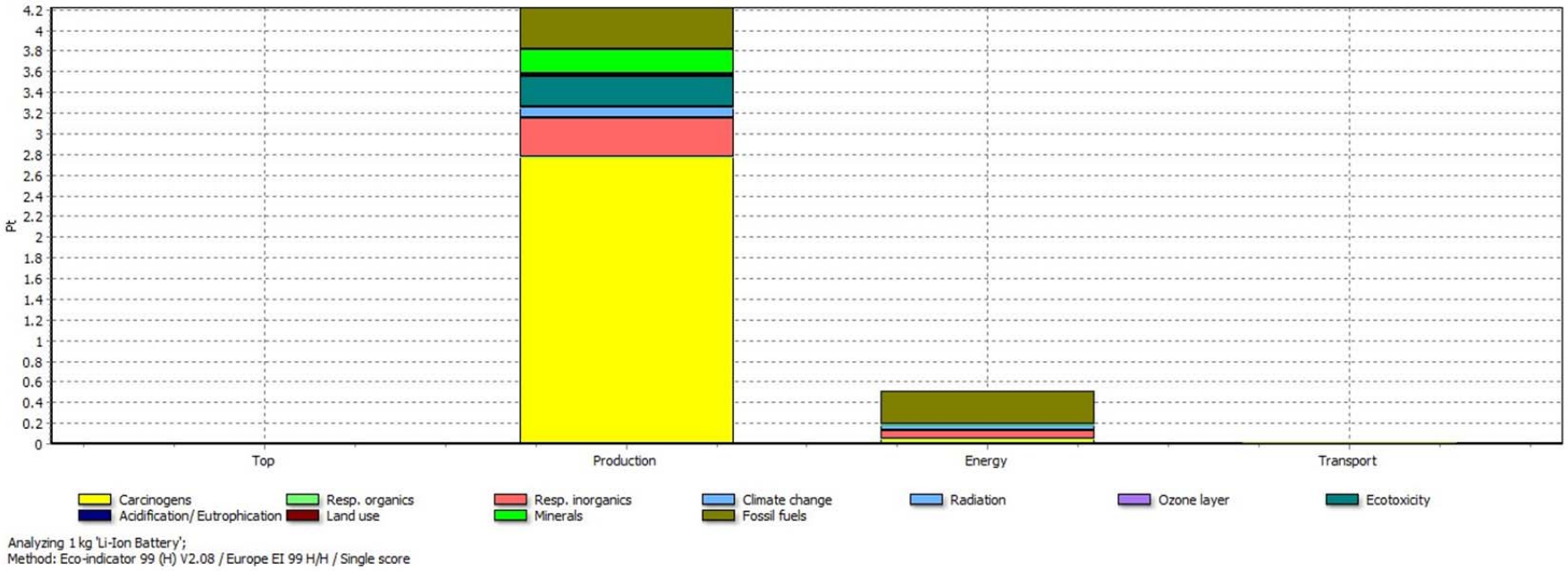

Figure 6.72: Eco-indicator points associated with production, energy usage and transport of the battery.

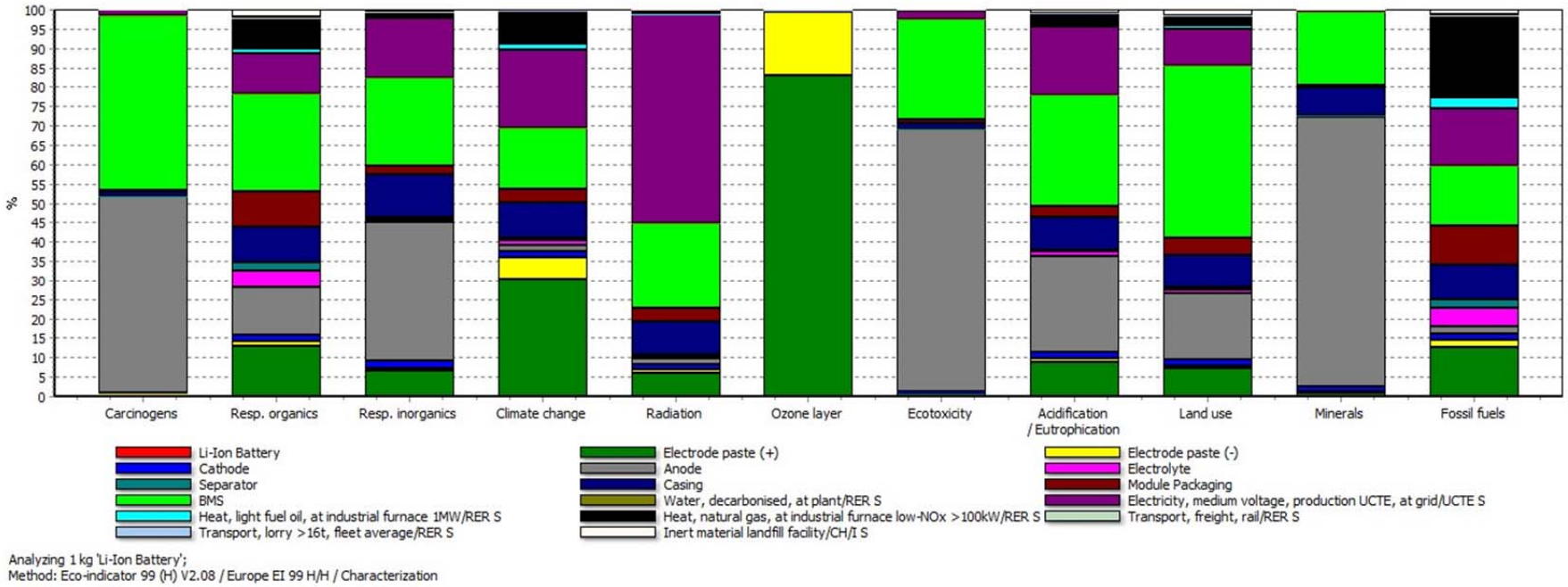

Figure 6.73: Percentage contribution of each component to the environmental impact with respect to Eco-indicator 99 points.

6.4.2 Conventional Exergoenvironmental Analysis

Once the environmental impact associated with the battery is calculated and combined with that of the remaining TMS components (provided in Section 5.4.3), it is used to determine the environmental impact formation of the system. In Table 6.9, it can be seen that the highest environmental impact rate is achieved at state 10, which is the exit state of the electric battery and the lowest environmental impact rate is associated with the pump input. In the table, state 13 has a value of zero, since it is available ambient air entering the condenser.

Table 6.9. Exergy flow rates, environmental impact due flow rates and the unit environmental impact cost associated with each state of TMS.

State	$\dot{E}x\ (kW)$	$\dot{B}\ (mPts/h)$	$b\ (mPts/kJ)$
1	0.71	30.21	42.67
2	1.58	59.84	37.83
3	1.27	48.15	37.88
4	1.01	43.17	42.62
5	0.12	5.01	42.69
6	0.02	2.74	123.34
7	0.04	4.77	123.32
8	0.04	4.92	124.92
9	0.36	64.15	178.27
10	0.01	35.98	7.20
11	1.30	28.76	22.05
12	<0.01	<0.10	22.04
13	0.00	0.00	0.00
14	0.07	12.01	177.91

Moreover, based on the environmental impact associated with component flow and the exergy destruction rates, the environmental impact due to exergy destruction rates are also determined for each component. In Figure 6.74, it can be seen that the evaporator has the highest environmental impact due to exergy destruction rates, followed by the condenser, compressor and the battery. The environmental impact of the battery is determined to be mostly component-related, while the environmental impact of the compressor, condenser and evaporator is associated with relatively high exergy destruction rates for these components.

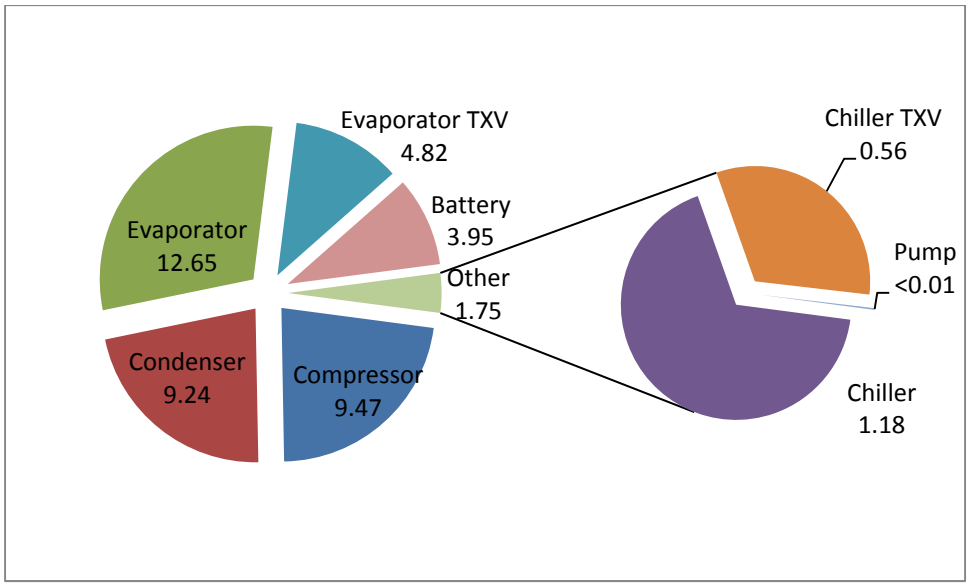

Figure 6.74: Environmental impact Eco-indicator 99 points associated with exergy destruction for thermal management system components.

When evaluated from an exergoenvironmental point of view, the most important component would be the one with the highest sum of component-related environmental impact and environmental impact due to exergy destruction rate ($\dot{Y} + \dot{B}_D$). Moreover, exergoenvironmental factor and relative difference of exergy-related environmental impacts are also calculated to provide the relationship between these two factors. The capital environmental impact, exergy destruction impact rate and exergoenvironmental factor for each component is provided in Table 6.10.

Table 6.10. Total environmental impact, exergoenvironmental factor and relative difference of exergy-related environmental impacts associated with the TMS components.

Component	$\dot{Y}_k$ $(mPts/h)$	$\dot{B}_{D,k}$ $(mPts/h)$	$\dot{Y}_k + \dot{B}_{D,k}$ $(mPts/h)$	f_b (%)	r_b $(-)$
Compressor	0.90	9.47	10.37	8.64	0.55
Condenser	0.28	9.24	9.514	2.91	6.54
Evaporator	0.22	12.65	12.87	1.72	4.05
Chiller	0.13	1.18	1.31	10.13	4.10
Evaporator TXV	0.02	4.82	4.83	0.36	0.14
Chiller TXV	<0.01	0.56	0.56	0.36	0.13
Pump	0.13	<0.01	0.13	96.94	8.19
Battery	33.78	3.95	37.72	89.54	2.02

When the components are analyzed with respect to $\dot{Y} + \dot{B}_D$, the electric battery by far has the highest environmental impact mainly due to the high copper mass used in the lithium-ion battery anodes. Moreover, the battery is also determined to have a high exergoeconomic factor (f), which suggests that the environmental impact of the entire system could be improved by reducing the component-related environmental impact. The evaporator, compressor and condenser have the next highest environmental impacts respectively, where the environmental impact related with the exergy destruction associated with these components should be reduced even if it would mean increasing the environmental impact during production of the components. This is followed by the evaporator TXV and the chiller where the environmental impact is significantly lower. Finally, the chiller TXV and the pump impacts are found to be exergoenvironmentally insignificant compared to the aforementioned components.

Moreover, due to the significance of the electricity generation mix on the overall environmental impact, a sensitivity analysis is also conducted where the environmental impact related to the exergy destruction rate of the system is determined with respect to the electricity generation mixes for various countries as shown in Table 6.11.

Table 6.11: Environmental impact related to the exergy destruction rate for TMS components using electricity generation mixes for various countries.

Component	**U.S**	**Europe Average**	**Switzerland**	**Italy**
	$(\boldsymbol{mPts/h})$			
Compressor	9.47	11.19	3.62	20.60
Condenser	9.24	10.86	3.70	19.76
Evaporator	12.65	14.88	5.07	27.05
Chiller	1.18	1.39	0.47	2.53
Evaporator TXV	4.82	5.66	1.93	10.30
Chiller TXV	0.56	0.66	0.23	1.21
Pump	<0.01	0.01	<0.01	0.01
Battery	3.95	4.55	1.87	7.91

In summary, exergoenvironmental analysis for the TMS is conducted with respect to the environmental impact from LCA along with literature review are used in order to obtain the impact of each relevant system components and input streams in terms of Eco-indicator 99 points which are assigned to the corresponding product exergy streams. Subsequently, exergoenvironmental variables (such as environmental impact of product, fuel and components,

environmental impact rate of exergy destruction as well as relative difference of specific environmental impacts and exergoenvironmental factor) are calculated and exergoenvironmental evaluation is performed in order to identify the environmentally most relevant system components and provide information about possibilities and trends for design improvements.

6.5 Multi-objective Optimization

Multi-objective optimization with aforementioned objective functions (Equations 5.75-5.77), constraints (Table 5.9) and six decision variables are performed with the help of genetic algorithms. In the analysis, five optimization scenarios with the objective functions of exergy efficiency (single-objective), total cost rate (single-objective), environmental impact rate (single-objective), along with exergoeconomic (multi-objective) and exergoenvironmental (multi-objective) optimizations are performed. The corresponding optimization scenarios can be seen in Figures 6.75-6.79.

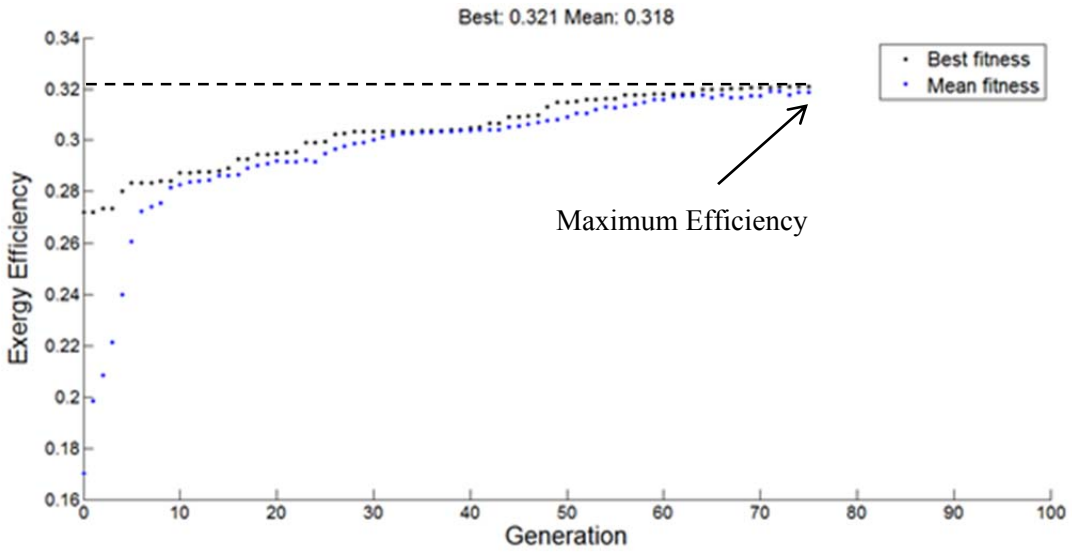

Figure 6.75: Single objective optimization of TMS over generations with respect to exergy efficiency.

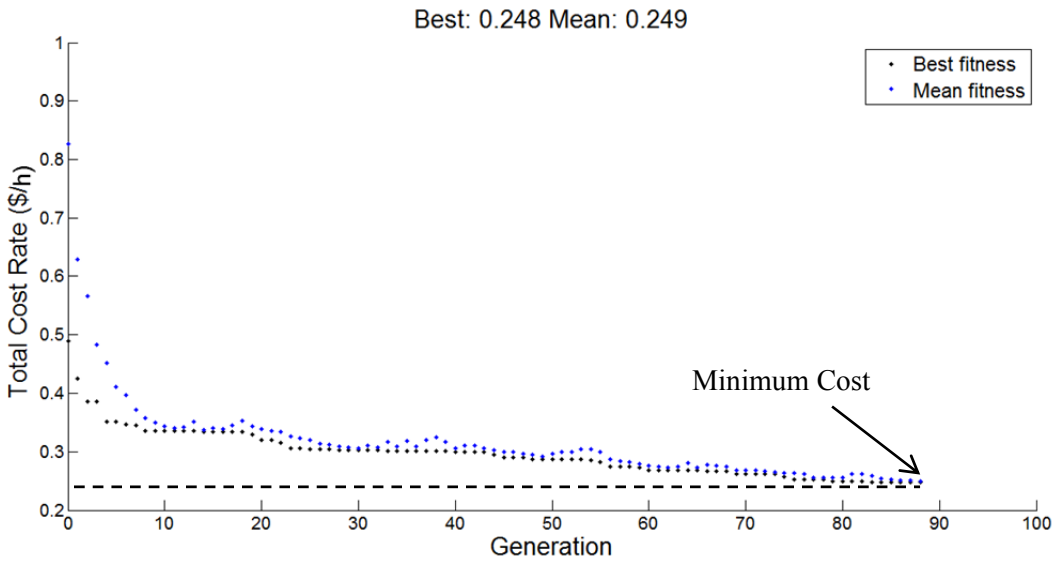

Figure 6.76: Single objective optimization of TMS over generations with respect to product cost rate.

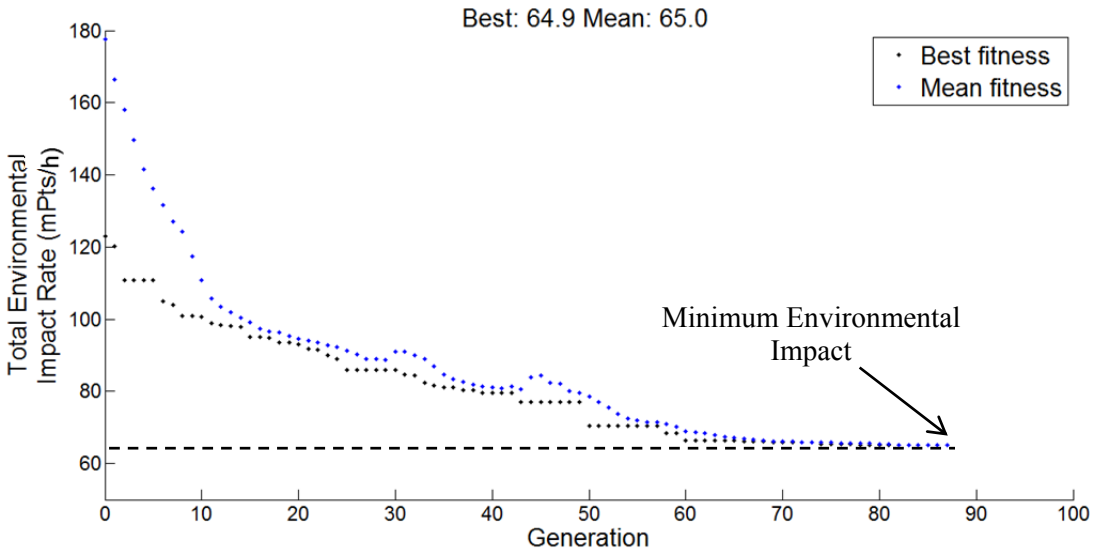

Figure 6.77: Single objective optimization of TMS over generations with respect to product cost rate.

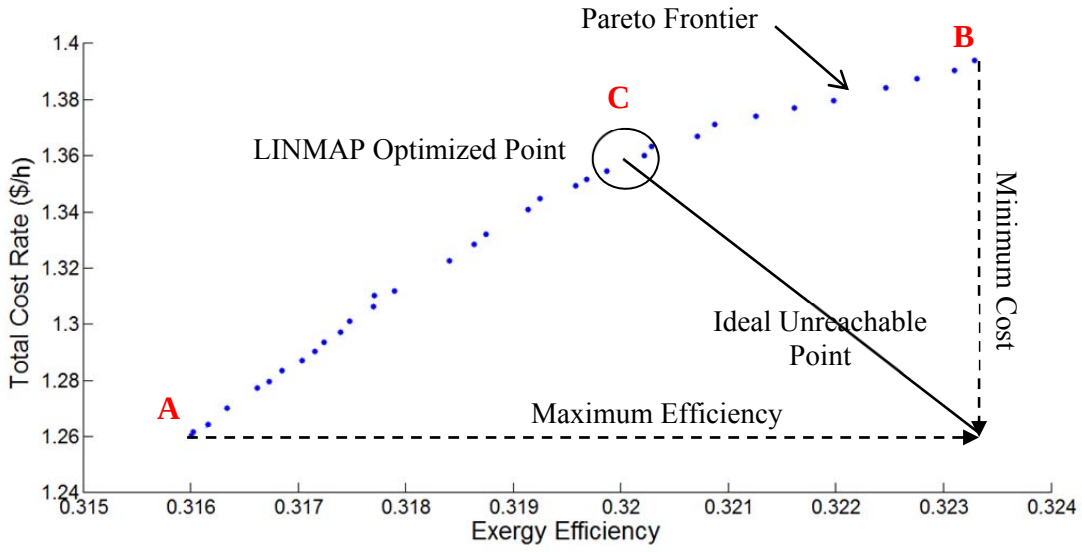

Figure 6.78: Multi-objective optimization of TMS with respect to exergy efficiency and total cost rate.

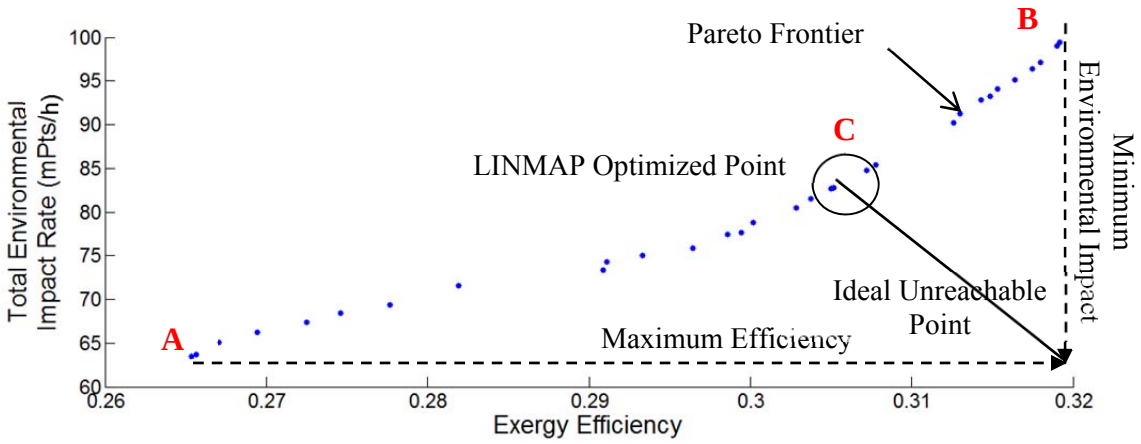

Figure 6.79: Multi-objective optimization of TMS with respect to exergy efficiency and total environmental impact rate.

As previously mentioned, all the points on the Pareto optimum frontier are potentially an optimum solution for the analysis and therefore a weighting factor is needed to be assigned for each objective and/or decision is needed to be made (often based on experience or importance of each objective) in order to select a single final solution among them. In this selection process, a traditional method called LINMAP decision-making (Yu, 1985) is used to select a desirable final solution as shown in Figures 6.78 and 6.79. This method creates a hypothetical ideal point in which all objectives have their corresponding optimum values independent of each other and would stay below the Pareto optimum frontier. Even though this point would be impossible in

reality, it would serve a useful purpose by assisting the decision makers to select the point on the Pareto optimum frontier that has the closest distance to this ideal point as the desirable final solution (Sayyaadi and Babaelahi, 2011).

Table 6.12 shows the values for the decision variables in the base case design along with the four different optimization criteria. In addition, the results of exergy, economic and environmental analyses for each optimization criteria are shown in Tables 6.12-6.15. It should be noted that the values for the decision variables are considered to be continuous over the determined constraints for the multi-objective optimization problem. However, usually parameters associated with some of these variables (especially size and efficiency) are only available in discrete units. Therefore, in a case where the determined parameter values are not available, the closest available values should be utilized in the system for most optimal results.

Table 6.12: Decision variables for the base case design under various optimization criteria.

Decision Variable	Base Case Design	Single-Obj. Exergetic	Single-Obj. Economic	Single-Obj. Environmental	Multi-Obj. Exergo-economic	Multi-Obj. Exergo-Environmental
T_{cond} (℃)	55	55.23	54.20	55.18	56.01	55.25
T_{evap}(℃)	5	0.40	8.94	8.92	8.93	8.82
ΔT_{sh}(℃)	5	4.75	3.86	2.40	9.69	0.96
ΔT_{sc}(℃)	5	9.94	9.68	4.90	9.99	1.71
$\dot{m}_e(kg/s)$	0.17	0.35	0.19	0.18	0.21	0.25
η_{comp}	0.63	0.80	0.66	0.79	0.72	0.79

Table 6.13: Exergetic analysis results for the base case design under various optimization criteria.

Decision Variable	Base Case Design	Single-Obj. Exergetic	Single-Obj. Economic	Single-Obj. Environmental	Multi-Obj. Exergo-economic	Multi-Obj. Exergo-Environmental
$\eta_{ex,comp}$	0.67	0.82	0.69	0.81	0.75	0.81
$\eta_{ex,cond}$	0.22	0.24	0.26	0.21	0.23	0.20
$\eta_{ex,evap}$	0.24	0.21	0.27	0.27	0.26	0.28
$\eta_{ex,chil}$	0.37	0.32	0.43	0.42	0.43	0.42
$\eta_{ex,etxv}$	0.89	0.88	0.92	0.91	0.92	0.88
$\eta_{ex,ctxv}$	0.89	0.89	0.92	0.91	0.92	0.89
$\eta_{ex,pump}$	0.80	0.83	0.84	0.80	0.78	0.77
$\eta_{ex,bat}$	0.81	0.83	0.85	0.83	0.84	0.83

Table 6.14: Economic analysis results for the base case design under various optimization criteria.

Decision Variable ($\$/h$)	Base Case Design	Single-Obj. Exergetic	Single-Obj. Economic	Single-Obj. Environmental	Multi-Obj. Exergo-economic	Multi-Obj. Exergo-Environmental
$\dot{Z}_{comp}$	5.90	20.38	5.10	6.87	5.57	9.80
$\dot{Z}_{cond}$	5.32	10.96	5.08	5.31	5.46	7.27
$\dot{Z}_{evap}$	6.32	18.39	5.75	6.44	6.39	9.23
$\dot{Z}_{chil}$	1.06	1.38	0.92	1.01	0.91	1.04
$\dot{Z}_{etxv}$	2.13	5.56	1.47	2.15	1.53	3.68
$\dot{Z}_{ctxv}$	0.25	0.33	0.16	0.25	0.15	0.30
$\dot{Z}_{pump}$	0.38	0.38	0.38	0.38	0.38	0.38
$\dot{Z}_{bat}$	6.67	7.45	6.38	6.66	6.37	6.74

Table 6.15: Environmental analysis results for the base case design under various optimization criteria.

Decision Variable ($mPts/h$)	Base Case Design	Single-Obj. Exergetic	Single-Obj. Economic	Single-Obj. Environmental	Multi-Obj. Exergo-economic	Multi-Obj. Exergo-Environmental
$\dot{B}_{comp}$	9.34	9.13	8.58	4.93	9.11	6.61
$\dot{B}_{cond}$	8.48	12.62	8.77	7.10	9.61	8.64
$\dot{B}_{evap}$	12.83	24.05	10.49	9.09	14.06	12.54
$\dot{B}_{chil}$	1.31	1.29	0.98	0.92	0.90	0.95
$\dot{B}_{etxv}$	4.82	7.56	3.22	3.55	5.12	6.01
$\dot{B}_{ctxv}$	0.57	0.44	0.35	0.41	0.31	0.49
$\dot{B}_{pump}$	0.14	0.14	0.14	0.14	0.14	0.14
$\dot{B}_{bat}$	37.73	37.42	37.01	36.79	36.77	35.67

In the above tables, it can be seen that each single objective optimization approach pays attention only to its own criterion without taken others into consideration. Exergetic single-objective optimization scenario maximizes the exergy efficiencies for each component; however no attention is paid to economic or environmental objectives. Similarly, exergoeconomic single-objective optimization scenario has the lowest unit costs for each component at the expense of exergy efficiency and environmental impact. And finally, exergoenvironmental single-objective optimization has the lowest Eco-indicator 99 points for each component at the expense of exergy efficiencies and cost. In multi-objective optimization scenario however, these objectives are considered simultaneously, which provided optimized solutions with values in between the extremes yielded by the single-objective approaches as a result of the trade-offs made between the solutions of the two conflicting objectives. Normalized value of the objectives with respect to each optimization criteria is provided in Figure 6.80. Moreover, when the exergoeconomic and exergoenvironmental optimizations are compared against the ones using energy efficiencies, the selected values for the decision variables in the LINMAP optimization points are determined to

have 4.8% lower cost and 3.9% lower environmental impact rates than the one calculated by the energy approach, which yields total cost and environmental impact rates of 1.41 $/h and 87.27 mPts/h respectively.

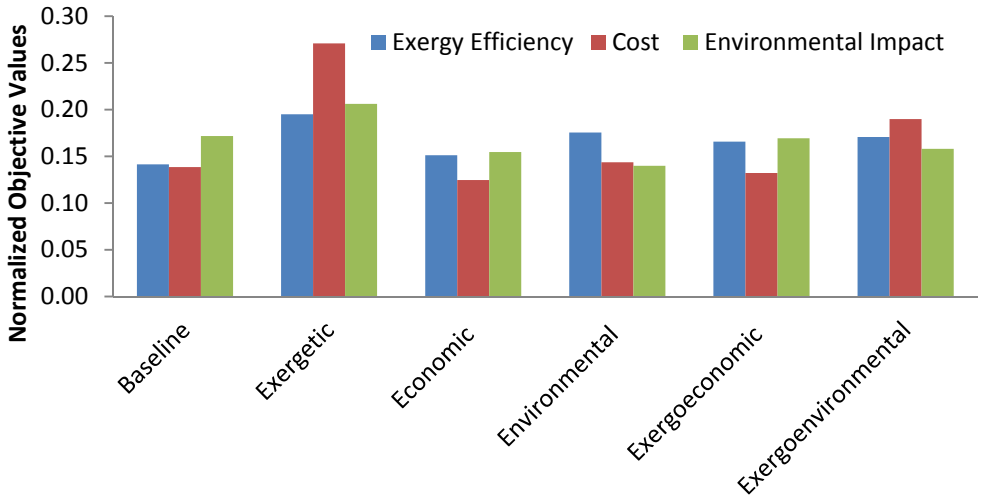

Figure 6.80: Normalized values of different objectives with respect to various optimization functions.

In summary, the TMS of a hybrid vehicle is optimized using a multi-objective evolutionary algorithm using exergoeconomic and exergoenvironmental objectives. The optimization is performed in order to maximize the exergy efficiency (based on exergetic efficiency), minimize the unit exergy cost (based on cost of unit exergy destruction and investment costs) and unit environmental impact (based on Eco-Indicator 99 impact points). Condensing and evaporating, superheating and subcooling temperatures, evaporator air mass flow rate and compressor efficiency are selected as the decision variables for the analyses and various constraints are applied based on appropriate feasibility and engineering constraints. The decision variables along with exergy efficiency, total cost and environmental impact (for each component) are compared under each optimization approach. In the multi-objective optimization, a Pareto frontier is obtained and a single desirable optimal solution is selected based on LINMAP decision-making process. The corresponding solutions are compared against each exergetic, exergoeconomic and exergoenvironmental single objective optimization results. Even though the single-objective approaches provided optimal solutions for their objectives, they have provided very poor solutions for the remaining objectives. Thus, the multi-objection optimization approach provided a solution set within the extremes of the single-objective results by evaluating two objectives simultaneously and providing trade-off between them to obtain desirable solution sets.

Chapter 7: Conclusions and Recommendations

7.1 Conclusions

Energy related problems are one of the most important issues we face in the 21th century and, undoubtedly, transportation sector is one of the biggest contributors of this problem. In order to mitigate the energy usage as well as the petroleum demand and associated environmental impact, various sustainable technologies have emerged over the past decades, where EV and HEVs has been the leading alternative to conventional vehicles.

In electric and hybrid electric vehicles, battery performance has a key role in providing a long driving range, fast acceleration, long life and even low overall costs. Even though the battery technology is becoming more and more capable of meeting the demands to compete with conventional vehicles in many areas, its performance, efficiency and life cycle are highly dependent on operating temperatures. Furthermore, the peak temperatures and temperature uniformity have significant impact on the life cycle of the battery and possibility of thermal runaway propagation. Therefore, selecting the right thermal management system and input parameters are important to keep the battery operating within optimal temperature ranges.

In this thesis, a numerical model was described for active liquid thermal management systems based on exergy analysis. Results are obtained with respect to battery temperature increase, uniformity and entropy generation associated with the system. Moreover, the active liquid management system is compared against passive cabin cooling (via air) and active moderate liquid circulation (via refrigerant) to understand the benefits and drawbacks associated with each system.

Subsequently, the liquid thermal management system is analyzed with respect to exergy efficiencies under various system parameters and operating conditions. The major thermal management system components are modeled in detail, heat transfer coefficients in the heat exchangers are calculated and the pressure drops are determined with respect to Reynolds

Number correlations to provide a more accurate representation of the system. The thermodynamic analyses of the system are conducted under various operating conditions including evaporating and condensing temperatures, subcooling and superheating, compressor speed, heat exchanger pressure drop and battery heat dissipation rates. Moreover, alternative refrigerants such as R600 (butane), R600a (isobutene), R1234yf (Tetrafluorpropene) and Dimethyl ether (DME) are investigated in terms of compatibility with the existing system and overall exergy efficiencies. In addition, an advanced exergy analysis is conducted where the avoidable and unavoidable as well as endogenous and exogenous parts of exergy destructions are determined in order to advance our understanding of the interactions among the TMS components, establish priorities on which components should be improved first and assist in further optimization of the overall system. Finally, recommendations are provided to improve the exergy efficiencies of the components as well as the overall system under the studied operating conditions and parameters.

Moreover, conventional exergoeconomic analysis is also conducted in order to analyze the investment costs associated with the system components and assess the economic feasibility of the suggested improvements. In the economic portion of the analysis, the investment cost rates are calculated with respect to equipment costs and capital recovery factors. Subsequently, by combining it with previously conducted exergy analysis, an exergoeconomic analysis is conducted and exergoeconomic variables are determined. Using these variables, suggestions were made on which components should be focused more and which ones should be neglected from an exergoeconomic viewpoint, and increase the cost effectiveness of the system by calculating the cost of thermodynamic inefficiencies on the important components and compare them with the required investment cost at the component level. In addition, advanced exergy and exergoeconomic analyses are also conducted by dividing the exergy destruction and cost into endogenous/exogenous and avoidable/unavoidable parts for each component in order to enhance our understanding of the interdependencies among the TMS components and provide information on how much of the cost can be avoided for each component. Moreover, an enviroeconomical (environmental cost) analysis is also conducted with respect to the indirect emissions by imposing a carbon price to the released CO_2 to the environment from the electricity

consumed by the system under varying carbon prices and electricity generation mixes in order to identify and keep track of system`s "cost" of environmental impact.

Furthermore, an exergoenvironmental analysis is also conducted in order to determine the environmental impact associated with the system. Exergy streams are determined for each relevant component. Environmental impact correlations are determined from the available data in the literature for each component in order to understand the effects of changing different parameters on the component-related environmental impact. Moreover, a life cycle assessment (LCA) is also carried on in order to determine an environmental impact (in terms of eco-indicator points) of the electric battery since it is expected to have significantly higher impact than the rest of the components. Next, the impact points are assigned to these exergy streams in the system in order to point out the components causing the highest environmental impact and suggesting possibilities and trends for improvement, based on the calculated exergoenvironmental variables. In addition, an environmental assessment for the operation stage is also conducted to determine the corresponding changes in CO_2 emissions for various cooling loads, battery heat dissipation rates and alternative refrigerants under different carbon dioxide scenarios.

A multi-objective optimization study is carried on where the results from exergy, exergoeconomic and exergoenvironmental analyses are used according to the developed objective functions and system constraints in order to optimize the system parameters under different operating conditions with respect to these criteria using Pareto Optimal optimization techniques.

In addition, a test bench, which consists of the vehicle thermal management system along with auxiliary components, are assembled in UOIT laboratories The test bench is instrumented with temperature sensors, pressure gauges and flow meters before and after each major change in the flow properties. Finally, a production vehicle (Volt Gen 1) is also equipped with various measurement instrumentations and data is collected under various parameters and operating conditions using IPETRONIK data acquisition system. The models developed are used to optimize the system and conduct vehicle level demonstration.

The following concluding remarks are drawn from this study:

- The exergetic performance results indicate that the pump and thermal expansion valves have very high exergy efficiencies (0.79 and 0.88 respectively), while the heat exchangers (evaporator, condenser and chiller) have much lower efficiencies in the system (0.22, 0.23 and 0.37 respectively), which can be improved by reducing the mean temperature difference between the working fluids.
- Among the studied refrigerants, R290, R1234yf and Dimethylether are the most compatible drop-in replacements for R134a and all of the refrigerants, except for R1234yf, are determined to have lower exergy destruction rates and higher energetic and exergetic COPs compared to R134a, where Dimethylether has the highest energetic and exergetic efficiencies.
- The exergy destruction associated with each component is split into endogenous/exogenous and avoidable/unavoidable parts and determined that the exogenous exergy destruction is small but significant portion of the total exergy destruction in each component (up to 40%), which shows that there is a moderate level of interdependencies among the components of the TMS and that up to 70% of the exergy destruction and up to 81% of the total cost rate within the components could be potentially avoided.
- Based on the exergoeconomic analysis, the electric battery is determined to have the highest total cost rate due to its significantly higher initial investment rates. In addition, it is determined that the investment costs of the condenser and evaporator should be reduced to improve the cost effectiveness of the system while keeping the compressor and the chiller the same.
- Based on the exergoenvironmental analysis, the electric battery is determined to have the highest environmental impact as well, and the total system impact could be improved by reducing the component-related environmental impact of the battery and improving the component efficiency of all the remaining components in the system.
- The exergy efficiency, total cost rate and environmental impact for the baseline system is determined to be 0.29, ¢28/h and 77.3 mPts/h respectively. The exergy efficiency could be increase by up to 27% (by single objective exergy) and the cost and environmental

impact can be reduced by 10% (by single objective cost) and 19% (by single objective environmental impact) respectively, at the expense of the non-optimized outputs.

- Based on the exergoeconomic optimization, the exergy efficiency is still 14% higher and the total cost is 5% lower than the baseline parameters at an expense of 14% increase in the environmental impact. Moreover, with exergoenvironmental optimization, the exergy efficiency is 13% higher with 5% lower environmental impact than the baseline model at the expense of 27% increase in the total cost.

7.2 Recommendations

The results obtained from this thesis research also suggest several areas for future studies, as summarized below:

- The conducted analyses could be employed to compare thermodynamic performance, cost and environmental impact of the current TMS with any other alternative thermal management systems (such cabin air and refrigerant TMS) or auxiliary units (PCMs or thermoelectrics).
- The presented study could help to expand the knowledge of, and be applied to various applications in different fields requiring thermal management systems (such as any form of vehicle or residential TMSs) that strive to provide a better understanding of the system.
- The presented analysis could be used to prioritize the components in terms of the adjusted objectives and determine the necessary amount of investment for the required improvements for thermal management system applications.
- The obtained results could be used to justify the cost of installing (or not installing) insulation and/or heat shields in various locations of a vehicle TMSs.
- The developed numerical model could be used as a criterion for designing new heat exchangers based on minimizing the corresponding endogenous unavoidable exergy destruction in order to improve the overall exergy efficiency of the system.
- The model can also be used to help decision makers in selecting the optimum size and/or efficiency of the components when purchasing thermal management system components.

- Database regarding product costs (along with avoidable/unavoidable portions) could be improved in the future in order to better represent the current prices of electric vehicle thermal management components.
- Enviroeconomics (environmental cost) is determined to be a useful tool for assigning a cost on the greenhouse gas emissions, where it can later be implemented as a part of the exergoeconomic evaluation.
- The conducted LCA of the electric battery can be used as a guideline to improve the battery structure in order to reduce the associated environmental impact of the battery.
- Most component-related environmental impacts are interpolated from large scale plants in the literature, thus LCA of the remaining thermal management system components could be conducted in order to improve the accuracy and reliability of the exergoenvironmental analysis of the system. In addition, the methods presented in advanced exergoeconomic model could be used as a guideline to implement advanced exergoenvironmental analysis.
- The developed model can be extended to incorporate a weighting scale among the exergy efficiency, cost and environmental impact where the presented multi-objective optimization Pareto optimal envelope could be adjusted based on the relative importance of these objectives.

References

1. Abusoglu A. Kanoglu M., 2009, "*Exergetic and thermoeconomic analyses of diesel engine powered cogeneration: Part 1 – Formulations*", Applied Thermal Engineering **29**,234–241.

2. Abusoglu A. and Kanoglu M., 2009, "*Exergetic and thermodynamic analyses of diesel engine powered cogeneration: Part 2 – Application*", Applied Thermal Engineering, **29**,242-249.

3. Ahamed J. U., Saidur R. and Masjuki H. H., 2011, "*A review on exergy analysis of vapor compression refrigeration system*", Renewable and Sustainable Energy Reviews **15**, 1593-1600.

4. Al-Hallaj S., Prakash J. and Selman J.R., 2000, *"Characterization of commercial Li-ion batteries using electrochemical–calorimetric measurements",* Journal of Power Sources **87,** 186–194.

5. Al-Hallaj S. and Selman J. R., 2002, "*Thermal modeling of secondary lithium batteries for electric vehicle/hybrid electric vehicle applications"*, Journal of Power Sources **110**, 341–348.

6. Al-Otabi D. A., Dincer I. and Kalyon M., 2004, "*Thermoeconomic optimization of vapor-compression refrigeration systems*", International Communications in Heat and Mass Transfer. **31**, 95-107.

7. Ahmadi P., Dincer I. and Rosen M. A. 2011, "*Exergy, exergoeconomic and environmental analyses and evolutionary algorithm based multi-objective optimization of combined cycle power plants*", Energy **36**, 5886-5898.

8. Arcaklioglu E., Çavuşoglu A. and Erisen A., 2005, "*An algorithmic approach towards finding better refrigerant substitutes of CFCs in terms of the second law of thermodynamics*", Energy Conversion and Management **46**, 1595-1611.

9. Aropra A., Arora B. B., Pathak B. D. and Sachdev H. L., 2007, "*Exergy analysis of Vapour Compression Refrigeration system with R-22, R407C and R-410A*", International Journal of Exergy **4**, 441-454.

10. Arora A. and Kaushik S. C., 2008, "*Theoretical analysis of a vapour compression refrigerant system with R502, R404a and R507a*", International Journal of Refrigeration **31**, 998-1005.

11. ASPEN Plus, version 2006. Aspen Technology Inc., 200 Wheeler Road Burlington, MA, USA.

12. ASHRAE, 1989, "*Handbook-fundamentals*", Atlanta (GA): American Society of Heating, Refrigerating and Air-Conditioning Engineers, Inc.

13. Asif M., Muneer T., 2007, "*Energy supply, its demand and security issues for developed and emerging economies*", Renewable and Sustainable Energy Reviews **11**, 1388–1413.

14. Bakan K., Dincer I. and Rosen M.A, 2008, "*Exergoeconomic analyses of glycol cold thermal energy storage systems*", International Journal of Energy Research **32**, 215-225.

15. Behr GmbH & Co. KG, Press Official Website, "*Technical Press Day*". http://www.behrgroup.com/Internet/behrcms_eng.nsf, accessed October 01, 2012.

16. Bejan A, 1996, "*Entropy Generation Minimization: The Method of Thermodynamic Optimization of Finite-Size Systems and Finite-Time Processes"*, CRC Press LLC, Florida, U.S.

17. Bejan A., 1997, "*Thermodynamic optimization of heat transfer and fluid flow processes*" Developments in the design of thermal systems, Cambridge University Press, Cambridge U.K.

18. Bejan A, Tsatsaronis G, Moran M. 1986, "*Thermal design and optimization*", New York: Wiley.

19. Bhatti M. S., 1999, "*Enhancement of R134a Automotive Air Conditioning System*", International Congress and Exposition, Detroit, Michigan.

20. Bilgen E. and Takahashi H., 2002, "*Exergy analysis and experimental study of heat pump systems*", Exergy, an international Journal **2**, 259-265.

21. Bornakke C., and Sonntag R. E., 2009, "*Fundemantals of Thermodynamics*", 7th ed, Wiley, Hobooken, NJ.

22. Bossche P. V., Vergels F., Mierlo J. V., Matheys J. and Autenboer W. V., 2006, "*SUBAT: An assessment of sustainable battery technology*", Journal of Power Sources **162**, 913-919.

23. Boyano A., Morosuk T., Blanco-Marigota A.M., Tsatsaronis G., 2012, "*Conventional and advanced exergoenvironmental analysis of steam methane reforming reactor for hydrogen production*", Journal of Cleaner Production **20**, 152-160.

24. Bradley T. H. and Frank A. A., 2009, "*Design, demonstrations and sustainability impact assessments for plug-in hybrid electric vehicles*", Renewable and Sustainable Energy Reviews **13**, 115-128.

25. Bram S., and Ruyck J., 1997, "*Exergy analysis tools for ASPEN applied to evaporative cycle design*", Energy Conversion Management **38**, 1613-1624.

26. Brooke L., 2010, *"2011 Chevrolet Volt Development Story"*, Vehicle Electrification Magazine, November Issue.

27. Brown J. S., Yana-Motta S. F., and Domanski P. A., 2002, "*Comparative analysis of an automotive air conditioning systems operating with CO_2 and R134a*", International Journal of Refrigeration **25**, 19-32.

28. Caliskan H., Dincer I., and Hepbasli A., 2011, "*Exergoeconomic, Enviroeconomic and sustainability analyses of a novel air cooler*", International Green Energy Conference, Eskisehir, Turkey.

29. Caliskan H. and Hepbasli A., 2011, "*Exergetic cost analysis and sustainability assessment of an Internal Combustion Engine*", International Journal of Exergy **8**, 310-324.

30. Camargo J. R., Ebinuma C. D. and Silveira J. L., 2003, "*Thermoeconomic analysis of an evaporative desiccant air conditioning system*", Applied Thermal Engineering **23**, 1537-1549.

31. Chau K. T. and Wong Y. S., 2002, "*Overview of power management in hybrid electric vehicles*", Energy Conversion and Management **43**, 1953–1968.

32. Churchill S. W., and Chu H. H. S., 1975, "*Correlating Equations for Laminar and Turbulent Free Convection From a Vertical Plate*", International Journal of Heat Mass Transfer **18**, 1323 – 1329.

33. Conte F. V., 2006, "*Battery and battery management for hybrid electric vehicles: a review*" Elektrotechnik & Informationstechnik **123**, 424–431.

34. Cooper A. and Moseley P., 2009, "*Advanced Lead-Acid Batteries-the Way forward for Low-Cost Micro and Mild Hybrid Vehicles*", EVS24, Stavanger, Norway.

35. D'accadia M. D. and Sasso M., 1997, "*Exergetic cost and exergoeconomic evaluation of vapour-compression heat pumps*", Energy **23**, 937-942.

36. D'accadia M. D and Rossi F., 1998, "*Thermoeconomic optimization of a refrigeration plant*", International Journal of Refrigeration **21**, 42-54.

37. Daly S., 2008, "Automotive Air-Conditioning and Climate Control Systems", 1st ed. Elsevier Ltd. Burlington, 01803.

38. Den Elzen M. G. J., Hof A. D., Beltran M., Grassi G., Roelfsema M., van Ruijven B., et al., 2011, "*The Copenhagen accord: Abatement costs and carbon prices resulting from the submissions*", Environmental Science and Policy **14**, 28-39.

39. Diamond D., 2009, "*The impact of government incentives for hybrid-electric vehicles: Evidence from US states",* Energy Policy **37**, 972-983.

40. Dincer I., 2000, "*Renewable energy and sustainable development: a crucial review*", Renewable and Sustainable Energy Reviews **4**, 157-175.

41. Dincer I. and Kanoglu M, 2010, "*Refrigeration Systems and Applications*", 2nd Edition, John Wiley and Sons, West Sussex, UK.

42. Dincer I. and Rosen M. A., 2007, "*Exergy: Energy, Environment and Sustainable Development*", Elsevier, Oxford, UK.

43. Dingec H. and Ileri A., 1999, "*Thermoeconomic optimization of simple refrogerators*", International Journal of Energy Research **23**, 949-962.

44. Dittus S. J., and Boelter L. M. K., 1930, "*University of California Publications in Engineering*" **2**, 443.

45. DOE, 2009, "*Annual Energy Outlook-Early Release*", Washington DC.

46. Doucette R. T. and McCulloch M. D., 2001, "*Modeling the prospects of plug-in hybrid electric vehicles to reduce CO_2 emissions*", Applied Energy **88**, 2315-2323.

47. Ecoinvent, "*Ecoinvent Centre Database*", www.ecoinvent.org/database, accessed on October 2012.

48. EIA, 2008a, "*Annual Energy Review 2007*", US Department of Energy http:// www.eia.doe.gov/emeu/aer/elect.htmlS.

49. El-Sayed, Y. M. and R. B. Evans, 1970, "*Thermoeconomics and the design of heat systems*", Trans ASME Journal of Engineering Power **92**, 27–34.

50. EPA, 2008, "*Inventory of US Greenhouse Gas Emissions and Sinks: 1990–2006*". Office of Global Warming, Washington D.C.

51. EPRI, 2007, "*Environmental assessment of plug-in hybrid electric vehicles. Volume 1: Nationwide greenhouse gas emissions*", Electric Power Research Institute, Palo Alto, CA.

52. Faiz A., Weaver C. S. and Walsh M. P., 1996, "*Air pollution from motor vehicles: standards and technologies for controlling emissions*" World Bank Publications, Washington D.C., U.S.

53. Fartaj A., Ting D. S.-K., and Yang W. W., 2004, "*Second law analysis of the transcritical CO_2 refrigeration cycle*", Energy conversion and Management **45**, 2269-2281.

54. Frangopolous C., Caralis Y., 1997, "*A method for taking into account environmental impacts in the economic evaluation of energy systems*", Energy Conversions Management **38**, 1751-63.

55. Gutmann G., 1999, "*Hybrid electric vehicles and electrochemical storage systems - a technology push–pull couple*", Journal of Power Sources **84**, 275–279.

56. Guy R., 1971, "*Modern refrigeration practice",* 1st ed. McGraw-Hill.

57. Hensley R., Newman J., and Rogers M., 2012, "Battery technology charges ahead", McKinsey Quarterly.

58. Hepbasli A., 2007, "*Thermoeconomic analysis of household refrigerators*", International Journal of Energy Research **31**, 947-959.

59. Hepbasli A., and Akdemir O., 2004, "*Energy and exergy analysis of a ground source (geothermal) heat pump system*", Energy Conversion and Management **45**, 737-753.

60. Hepbasli A., Erbay Z., Icier F., Colak N., and Hancioglu E., 2009, "*A review of gas engine driven heat pumps (GEHPs) for residential and industrial applications*" Renewable and Sustainable Energy Review **13**, 85-99.

61. Hosoz M. and Direk M., 2006, "*Performance evaluation of an integrated automotive air conditioning and heat pump system*" Energy Conversation and Management **47**, 545-559.

62. ISO14040, 2006, "*Environmental Management – Life cycle assessment – Principals and Framework*" International Organization for Standardization Geneva, Switzerland.

63. Jabardo J. M. S., Mamani W. G., and Ianekka M. R., 2002, "*Modeling and experimental evaluation of an automotive air conditioning system with a variable capacity compressor*", International Journal of Refrigeration **25**, 1157-1172.

64. Johnson V. and Pesaran A., 2000, *"Temperature-Dependant Battery Models for High-Power Lithium-Ion Batteries"*, 17th Electric Vehicle Symposium, Montreal, Canada.

65. Joudi K., Mohammed A. S. K., and Aljanabi M. K., 2003, "*Experimental and computer performance study of an automotive air conditioning system with alternative refrigerants*", Energy Conversion and Management **44,** 2959-2976.

66. Kabul A., Kizilkan Ö. and Yakut A. K., 2008, "*Performance and exergetic analysis of vapor compression refrigerant system with an internal heat exchanger using a hydrocarbon, isobutene (R600a)*", International Journal of Energy Research **32**, 824-836.

67. Kedzierski M.A. and Gong M., 2009, "Effect of CuO nano-lubricant on R134a pool boiling heat transfer" International Journal of Refrigeration **32**, 791-799.

68. Keller A. S., and Whitehead G., 1991, "*Thermal Characteristics of Electric Vehicle Batteries",* Passenger Car Conference & Exposition, Nashville, TN, USA.

69. Kelly S., Tsatsaronis G., Morosuk R., 2009, "*Advanced exergetic analysis: Approaches for splitting the exergy destruction into endogenous and exogenous parts*", Energy **24**, 384-391.

70. Khateeb S. A., Farid M. M., Selman J. R. and Al-Hallaj S., 2004, *"Design and simulation of a lithium-ion battery with a phase change material thermal management system for an electric scooter",* Journal of Power Sources **128**, 292–307.

71. Kim G. H., Pesaran A., 2006, "*Battery Thermal Management System Design and Modeling*", 22nd International Battery, Hybrid and Fuel Cell Electric Vehicle Conference and Exhibition, Yokohama, Japan.

72. Kizilel R., Lateefa A., Sabbaha R., Farid M. M., Selman J. R. and Al-Hallaj S., 2008, "*Passive control of temperature excursion and uniformity in high-energy Li-ion battery packs at high current and ambient temperature*", Journal of Power Sources **183,** 370–375.

73. Kobylecky M., 2011, "*Personal Communication*", General Motors, Oshawa, Canada.

74. Kotas, T. J.. 1985, "*The Exergy Method of Thermal Plant Analysis*". Anchor Brendon Ltd, Tiptree, Essex, Great Britain.

75. Kristoffersen T. K, Capion K. and Meibom P., 2011, "*Optimal charging of electric drive vehicles in a market environment*" Applied Energy **88**, 1940-1948.

76. Kaynakli O., and Horuz I., 2003, "*An experimental analysis of automotive air conditioning system*", International Communication Heat and Mass Transfer **30**, 273 – 284.

77. Kumar S., Prevost M. and Bugarel R., 1989, "Exergy *Analysis of a Compression Refrigeration System",* Heat Recovery Systems & CHP **9**, 151-157.

78. Kuper Ch., Hoh M., Houchin-Miller G. and Fuhr J., 2009, *"Thermal Management of Hybrid Vehicle Battery Systems",* 24th International Battery, Hybrid and Fuel Cell Electric Vehicle Conference and Exhibition, Stavanger, Norway.

79. Lazzaretto A. and Tsatsaronis G., 2006, "*SPECO: A systematic and general methodology for calculating efficiencies and costs in thermal systems*", Energy **31**, 1257-1289.

80. Lee G. H., and Yoo J. Y., 2000, "*Performance analysis and simulation of automobile air conditioning system*", International Journal of Refrigerant **23**, 243 – 254.

81. Lee C.G, Cho S.W, Hwang Y., Lee J.K., Lee B.C., Park J.S., Jung J.S., 2007,"*Effects of nano-lubricants on the friction and wear characteristics at thrust slide bearing of scroll compressor*", 22nd international congress of refrigeration, Beijing, China.

82. Leibson S., 2012, "*Driving the Chevy Volt*", Low-Power Design Forums. http://low-powerdesign.com. Posted on August 4, 2012.

83. Mi C., Li B., Buck D. and Ota N., 2007, "*Advanced electro-thermal modeling of lithium-ion battery system for hybrid electric vehicle applications*", IEEE Vehicle Power and Propulsion Conference, Arlington TX, USA.

84. Magnetto D., Mola S., DaCosta D. H., Golben M. and Rosso M., 2006, *"A metal hydride mobile air conditioning system"*, SAE International 115, 1150-1159.

85. Majeau-Bettez G., Hawkins T. R. and Strømman A. H., 2011, "Life Cycle Environmental Assessment of Lithium-Ion and Nickel Metal Hydride Batteries for Plug-in Hybrid and Battery Electric Vehicles", Environmental Science and Technology **45**, 4548-4554.

86. Matheys J., Timmermans J-M., Van Mierlo J. Meyer S., Van den Bossche P., 2009, "*Comparison of the Environmental impact of 5 Electric Vehicle Battery technologies using LCA*" , International Journal of Sustainable Manufacturing **1**, 318-329.

87. Matsunaga K., 2002, "*Comparison of Environmental Impacts and physical properties of refrigerants*". Thesis. Columbia University.

88. Meyer L., Tsatsaronis G., Buchgeister J., Schebek L., 2009, "*Exergoenvironmental analysis for evaluation of the environmental impact of energy conversion systems*", Energy **34**, 75-89.

89. Moran, M. J., 1999, "*Engineering thermodynamics, in Mechanical Engineering Handbook*", CRC Press LLC, Boca Raton.

90. Morosuk T., Tsatsaronis G., 2006, "*The "Cycle Method" used in the exergy analysis of refrigeration machines: from education to research*", Proceedings of the 19th international conference on efficiency, cost, optimization, simulation and environmental impact of energy systems, July 12-14, National Technical University of Athens, Greece **1**, 157-63.

91. Morosuk T., Tsatsaronis G., 2008, "*A new approach to the exergy analysis of absorption refrigeration machines*", Energy, **33**, 890-907.

92. Morosuk T., Tsatsaronus G., 2009, "*Advanced exergetic evaluation of refrigeration machines using different working fluids*," Energy, **34**, 2248-2258.

93. Nelson P., Dees D., Amine K. and Henriksen G., 2002, "*Modeling thermal management of lithium-ion PNGV batteries*", Journal of Power Sources **110**, 349-356.

94. Nelson R. F., 2000, "*Power requirements for batteries in hybrid electric vehicles*", Journal of Power Sources **91**, 2-26.

95. Nikolaidis, C. and Probert S. D., 1992, "*Exergy Method for Analysis and Optimising Refrigeration Processes*", Applied Energy **43**, 201-220.

96. Noboru S., 2001, *"Thermal behavior analysis of lithium-ion batteries for electric and hybrid vehicles",* Journal of Power Sources **99**, 70-77

97. Ozgener O. and Hepbasli A., 2005, "*Exergo-economic analysis of a solar assisted ground-source heat pump greenhouse heating system*", Applied Thermal Engineering **25**, 1459-1471.

98. Ozgener O., Hepbasli A. and Ozgener L., 2007, "*A parametric study on the exergoeconomic assessment of a vertical ground-coupled (geothermal) heat pump system*", Building and Environment **42**, 1503-1509.

99. Ozkaymak M., Kurt H and Recepli Z., 2008, "*Thermo-economic optimization of superheating and sub-cooling heat exchangers in vapor-compressed refrigeration system*", International Journal of Energy Research **32**, 634-647.

100. Petrakopoulou F., Boyano A., Cabrera M., Tsatsaronis G., 2011, "*Exergoeconomic and exergoenvironmental analyses of a combine cycle power plant with chemical looping technology*", International Journal Greenhouse Gas Control **5**, 475-482.

101. Pasquier A. D., Plitz I., Menocal S., and Amatucci G., 2003, "*A comparative study of Li-ion battery, supercapacitor and nonaqueous asymmetric hybrid devices for automotive applications*", Journal of Power Sources **115**, 171-198.

102. Patil P., 2008, "*Developments in Lithium-Ion Battery Technology in People's Republic of China*", Energy Systems Division, National Argon Laboratory Report, Oak Ridge, TN, USA.

103. Pesaran A. A., 2002, "*Battery thermal models for hybrid vehicle simulations*", Journal of Power Sources **110**, 377-382.

104. Pesaran A. A., 2001, *"Battery Thermal Management in EVs and HEVs: Issues and Solutions",* Advanced Automotive Battery Conference, Las Vegas, Nevada, USA.

105. Pesaran A. A., Burch S., and Keyser M., 1999,*"An Approach for Designing Thermal Management Systems for Electric and Hybrid Vehicle Battery Packs",* The Fourth Vehicle Thermal Management Systems Conference and Exhibition, London, UK.

106. Pesaran A. A., Kim G. and Keyser M., 2009, *"Integration Issues of Cells into Battery Packs for Plug-in and Hybrid Electric Vehicles",* EVS 24 Stavanger, Norway.

107. Pesaran A. A., Vlahinos A., and Stuart T., 2003, *"Cooling and preheating of batteries in hybrid electric vehicles"*, 6th ASME-JSME Thermal Engineering Conference, Hawaii.

108. Peterson R., 2012, "*Chevrolet Volt Math Everybody Can Understand*", Chevrolet Volt Communications. http://www.chevroletvoltage.com. Posted on February 23, 2012.

109. Phuan Z. Y., Gan G. D., Leong C. K., Cheah B. K., Yoong M. K., Gan Y. H. and Chew K. W., 2010, "*Design of battery pack for electric vehicle based on lithium-ion technology*", Proceeding of Malaysian Universities Transportation Research Forum and Conferences, Putrajaya, Malaysia.

110. Querol E., Gonzalez-Regueral B., Ramos A., and Perez-Benedito J. L., 2011, "*Novel application for exergy and thermoeconomic analysis of processes simulated with Aspen Plus*", Energy **36**, 964-974.

111. Rosen M.A. 1999, "*Second law analysis: Approaches and implications*". International Journal of Energy Research **23**, 415–429.

112. Rosen M. A., 2009, "*Energy Sustainability: A Pragmatic Approach and Illustrations*", Sustainability **1**, 55-80.

113. Rosen M. A. and Dincer I., 2003, "*Exergoeconomic analysis of power plants operating on various fuels*", Applied Thermal Engineering **23**, 643-658.

114. Rosen M. A. and Dincer I, 2003, "*Thermoeconomic analysis of power plants: an application to a coal fired electrical generation station*", Energy Conversion and Management **44**, 2743-2761.

115. Ross, M., 1994, "*Automobile fuel consumption and emissions: efects of vehicle and driving characteristics*" Annual Review of Energy and the Environment **19**, 75-112.

116. Sabbah R., Kizilel R., Selman J. R. and Al-Hallaj S., 2008, *"Passive Thermal Management System for Plug-in Hybrid and Comparison with Active Cooling: Limitation of Temperature Rise and Uniformity of Temperature Distribution"*, ECS Transactions **13,** 41-52.

117. Samaras C. and Meisterling K., 2008, "*Life Cycle Assessment of Greenhouse Gas Emissions from Plug-in Hybrid Vehicles: Implications for Policy*" Environmental Science and Technology **42**, 3170-3176.

118. Sanaye S., Malekmohammadi H. R., 2004, "*Thermal and economical optimization of air conditioning units with vapor compression refrigeration system*", Applied Thermal Engineering **24**, 1807-1825.

119. Sanaye, S., Niroomand, B., 2009, "*Thermal-economic modeling and optimization of vertical ground-coupled heat pump*", Energy Conversion. Management **50**, 1136-1147.

120. Sayyaadi H. and Nejatolahi M., 2011, "*Multi-objective optimization of a cooling tower assisted vapor compression refrigeration system*", International Journal of Refrigeration **34**, 254-256.

121. Sayyaadi H., and Sabzaligol T. 2009, "*Exergoeconomic optimization of a 1000MW light water reactor power generation system*", International Journal of Energy Research **33**, 378–395.

122. Schmidt, W. P., Dahlqvist, E., Finkbeiner, M., Krinke, S., Lazzari, S., Oschmann, D., Pichon, S. and Thiel, C., 2004, "*Life cycle assessment of lightweight and end-of-life scenarios for generic compact class passenger vehicles*", The International Journal of Life Cycle Assessment **9**, 405-416.

123. Sciubba E. 2005, "*Exergo-economics: thermodynamic foundation for a more rational resource use",* International Journal of Energy Research **29**, 613–636.

124. Selbaş R., Kizilkan Ö. and Şencan A., 2006, "*Thermoeconomic optimization of subcooled and superheated vapor compression refrigeration cycle*", Energy **31**, 2108-2128.

125. Shafiee S. and Topal E., 2008, "*An econometrics view of worldwide fossil fuel consumption and the role of US*", Energy Policy **36**, 775-786.

126. Shah R. K., and Sekulic D. P., 2003, "*Fundamentals of Heat Exchanger Design*", Wiley, Hobooken, NJ.

127. Shiau C. N., Samaras C., Hauffe R. and Michalek J. J., "*Impact of battery weight and charging patterns on the economic and environmental benefits of plug-in hybrid vehicles*", Energy Policy **37**, 2653-2663.

128. Shilliday J. A., Tassou, S. A and Shilliday N., 2009, "*Comparative energy and exergy analysis of R744, R404a and R290 refrigeration cycles*" International Journal of Low-Carbon Technologies **4**, 1-4-111.

129. Siddique A. K., Farid M. M., Selman J. R. and Al-Hallaj S., 2004, "*Design and simulation of a lithium-ion battery with a phase change material thermal management system for an electric scooter*", Journal of Power Sources **128**, 292-307.

130. Sima Pro, 2007, "*Users Manual*", Pre Consultansta BV, Amersfoot, Netherlands.

131. Somers C., 2011, "*Simulation of absorption cycles for integrating into refining processes*" Master's thesis, University of Maryland, College Park.

132. Somers C., Mortazavi A., Hwang Y., Radermacher R., Rodgers P., Al-Hashimi S., 2011, "*Modeling water/lithium bromide absorption chillers in ASPEN Plus*", Applied Energy **88**, 4197-4205.

133. Stegou-Sagia A. and Paignigiannis N. 2005, "*Evaluation of mixtures efficiency in refrigerating systems*", Energy Conversion and Management **46**, 27887-2802.

134. Stoecker F, and Jones W., 1982 "*Refrigeration and air conditioning*", 2nd ed. McGraws-Hill.

135. Suganthi L., and Samuel A. A., 2012, "*Energy models for demand forecasting—A review*", Renewable and Sustainable Energy Reviews **16**, 1223–1240.

136. Şencan A., Selbaş R., Kizilkan Ö. and Kalogirou S. A., 2005, "*Thermodynamic analysis of subcooling and superheating effects of alternative refrigerants for vapour compression refrigeration cycles*", International Journal of Energy Research **30**, 323-347.

137. Tian C., and Li X., 2005, "*Numerical simulation on performance bad of automotive air conditioning system with a variable displacement compressor*", Energy Conversion and Management **46**, 2718 – 2738.

138. Tichy R., 2009, *"Li-lon Batteries Offer High-Density and Small Size Necessary to Drive Electric Vehicles"*, Power Electronics Technology Magazine, October.

139. Toronto Hydro, "*Electricity Rates and Charges*", www. Torontohydro.com, accessed on October 2012.

140. Tsatsaronis G., 1987, "*A review of exergoeconomic methodologies, in Second Law Analysis of Thermal Systems*", New York: American Society of Mechanical Engineers, pp.81–87.

141. Tsatsaronis G., 2007, "*Definitions and nomenclature in exergy analysis and exergoeconomics*", Energy **32**, 249-53.

142. Tsatsaronis G., 2011, "*Exergoeconomics and exergoenvironmental analysis*", in Bakshi B. R., Gutowski, T. G., Sekulic (Eds), D.P, Thermodynamics and destruction of resources, Cambridge University Press, New York, 377 – 401.

143. Tsatsaronis G., 2012, "*Minimization of Costs and Environmental Impact Using Exergy-Based Methods*". The Future for Sustainable Built Environments with High Performance Energy System Conference, 21 October 2012, Munich, Germany.

144. Tsatsaronis G., Kelly S. O., Morosuk T.V., 2006, "*Endogenous and exogenous exergy destruction in thermal systems*", In the Proceedings of ASME IMECE, November 5-10, Chicago, IL, USA.

145. Tsatsaronis G., Lin L., 1990, "*On Exergy Costing in Exergoeconomics, Computer-Aided Energy Systems Analysis*", American Society of Mechanical Engineers, AES **21**, 1-11.

146. Tsatsaronis G., Morosuk T., 2007, "*Advanced exergoeconomic evaluation and its application to compression refrigeration machines*". In the Proceedings of IMECE2007, November 11-15, 2007, Seattle, Washington, USA.

147. Tsatsaronis G., Morosuk T., 2008, "*A General Exergy-Based Method for Combining a Cost Analysis With an Environmental Impact Analysis: Part I — Theoretical Development*". In Proceedings of the ASME International Mechanical Engineering Congress and Exposition, November 2-6. Boston, Massachusets, USA, file IMECE2008-67218

148. Tsatsaronis G., Morosuk T., 2008, "*A General Exergy-Based Method for Combining a Cost Analysis With an Environmental Impact Analysis: Part II — Application to a Cogeneration System*". In Proceedings of the ASME International Mechanical Engineering Congress and Exposition, November 2-6. Boston, Massachusets, USA, file IMECE2008-67219

149. Tsatsaronis G., Pisa J., 1994, "*Exergoeconomic evaluation and optimization of energy system; application to the CGAM problem*", Energy **19**, 287-321.

150. Tsatsaronis G., Park M., 2002, "*On avoidable and unavoidable exergy destructions and investment costs in thermal systems*", Energy Conversion. Management, **43**, 1259-1270.

151. Ucar A. and Inalli M., 2006, "*Exergoeconomic analysis and optimization of a solar-assisted heating system for residential building*", Building and Environment **41**, 1551-1556.

152. U.S. Department of Transportation, 2004, "*2001 National Household Travel Survey*" DOT: Washington, DC.

153. Valero, A., 1994, "*CGAM problem: definition and conventional solution*", Energy **19**, 268- 279.

154. Valero, A., M. A. Lozano and M. Munoz, 1986, "*A general theory of exergy savings, in Computer-Aided Engineering of Energy Systems*", New York: American Society of Mechanical Engineers AES **2**, 1–21.

155. Wall G., 1991, "*Optimization of refrigeration machinery*", International Journal of Refrigeration **14**, 336–340.

156. Wang S. J., and Gu J. J., 2004, "*Experimental Analysis of an Automotive Air Conditioning System With Two-Phase Flow Measurements*", International Refrigeration and Air Conditioning Conference.

157. Wang S. W., Gu J., Dickson T., Dexter T., and McGregor I., 2005, "*Vapor quality and performance of an automotive air conditioning system*", Experimental Thermal Fluid Science **30**, 59 – 66.

158. Weiller C., 2011, "*Plug-in hybrid electric vehicle impacts on hourly electricity demand in the United States*", Energy Policy **39**, 3766-3778.

159. Wongwises S., Kamboon A., and Orachon B., 2006, "*Experimental investigation of hydrocarbon mixtures to replace HFC-134a in an automotive air conditioning system*", Energy Conversion and Management **47**, 1644–1659.

160. Wood E, Alexander M. and Bradley T. H., 2011, "*Investigation of battery end-of-life conditions for plug-in hybrid electric vehicles*", Journal of Power Sources **196**, 5147-5154.

161. Yang C., Maccarthy R., 2009, "*Electricity Grid: Impacts of Plug-In Electric Vehicle Charging, Recent Work*", Institute of Transportation Studies (UC Davis).

162. Yap W. K. and Karri V., 2010, "Performance simulation and predictive model for a multi-mode parallel hybrid electric scooter drive", International Journal of Energy Research **34**, 67-83.

163. Yeh, S., 2009, "*Reducing long-term transportation emissions: electricity as a low carbon fuel",* Presentation at the EPRI Conference, Long Beach, California.

164. Yufei C., Li S. and Evans J.W., 1996, "*Modeling studies on battery thermal behavior, thermal runaway, thermal management, and energy efficiency*," 31st Intersociety Energy Conversion Engineering Conference **2**, 1465 – 147.

165. Yumrutas R., Kunduz M. and Kanoglu M., 2002, "*Exergy analysis of vapor compression refrigeration systems*", Exergy, an International Journal **2**, 266-272.

166. Zubair S. M., Yaqub M. and Khan S. H., 1996, "*Second-law-based thermodynamic analysis of two-stage and mechanical-subcooling refrigeration cycles*", International Journal of Refrigeration **19**, 506-516.